Rotational Spectroscopic and Theoretical Investigations of Non-conventional Hydrogen Bonds

A Thesis

Submitted for the Degree of

Doctor of Philosophy

in the Faculty of Science

by

Aiswarya Lakshmi P.

Department of Inorganic and Physical Chemistry

INDIAN INSTITUTE OF SCIENCE

Bangalore – 560012, India

December, 2011

Dedicated to

my

Grandfather

DECLARATION

I hereby declare that the work presented in this thesis entitled "**Rotational Spectroscopic and Theoretical Investigations of Non-conventional Hydrogen Bonds**" has been carried out by me at the Department of Inorganic and Physical Chemistry, Indian Institute of Science, Bangalore, India under the supervision of Professor E. Arunan.

Date: Aiswarya Lakshmi P.

CERTIFICATE

I hereby certify that the work presented in this thesis entitled "**Rotational Spectroscopic and Theoretical Investigations of Non-conventional Hydrogen Bonds**" has been carried out by Ms. Aiswarya Lakshmi P. at the Department of Inorganic and Physical Chemistry, Indian Institute of Science, Bangalore, India under my supervision.

Date:

Professor E. Arunan

(Research Supervisor)

Acknowledgements

I take this opportunity to thank each and everyone who have supported, encouraged and helped me to carry out the research work. First and foremost I thank my research supervisor ***Prof. E. Arunan*** *for introducing me into the field of non-covalent interactions and microwave spectroscopy. I would like to take the opportunity to express my gratitude for his active involvement in all aspect of my research work and the valuable discussions we have has. His support and guidance has helped me through the challenging times.*

I thank the former and present chairmen of the department, Prof. A. R. Chakravarty, Prof. K. L. Sebastian and Prof. A. G. Samuelson for their encouragement and the departmental facilities. I am thankful to all the faculties, students and staff members of the department for their help and encouragement.

I would like to acknowledge the valuable discussions I have had with Prof. K. L. Sebastian, Prof. P. K. Das and Prof. S. Umapathy and all the Chemical Dynamics Group members during the saturday group meetings. The chemical dynamics group seminars were a great learning experience.

Special thanks to Prof. G. N. Patwari, IIT Bombay for the discussions regarding experiment with iron pentacarbonyl.

I thank Supercomputer Education and Research Center (SERC) for the computational facility and IISc for providing the infrastructure and facilities. I am thankful to IISc for the fellowship and CSIR, DST and IISc for providing the funds for research.

I thank IPC Dept and IISc for the travel grant to attend the International Symposium on Molecular Spectroscopy held at Ohio State University.

It would not have been possible to complete my thesis without the support of people around me. I would like to take the opportunity to thank my laboratory colleagues. I thank Pankaj, Mausumi, Raghavendra, Harish, Devendra, Abhishek, Kiran and Kunal. I thank Mausumi and Raghavendra for their valuable advice. It has also been a joy working with my junior colleagues Devendra and Abhishek. I thank Dr. Rajendra Parajuli for the valuable discussions we have shared. I thank Sanjeev, Narasimhan, Manju and Lavanya for their help and support. It was also a pleasurable experience to work with, Atisha, Arghya, Sajesh, Manikavally, Aparna, Seshagiri, Indu and Dilna, our short term students.

I would like to thank all my batch mates, Akshai, Babita, Debjyoti, Prasanta, Dipak, Vikrant, Deepa, Sangeeta, Sovan, Mithun, Selvi, Ramkumar and Viswanath for the wonderful time I had with them from the very beginning of my stay in IISc.

Very special thanks to Aditi, Lalit, Rekha and Rajarshi for their support. I thank Deepika, Soni, Garima, Pratibha, Jasbeer, Sandeep, Bhabatosh and Sudanshu for the joyous times we have shared together.

Above all I would like to thank my parents, Mr. K. Ramachandran Nair and Dr. Prabha Ramakrishnan and my brother, Ashok, for their love, unequivocal moral support and patience. Last but not the least I thank my husband, Naveen Kartha, for his love, patience and encouragement throughout :)

Aiswarya Lakshmi P.

Contents

Synopsis

The nature of interactions within a molecule, i.e. chemical bonding, is well understood today. However, our understanding about intermolecular interactions, which has great relevance in nature, is still evolving. Historically there are two types of intermolecular interactions, van der Waals interaction and hydrogen bonding. However, there has been an upsurge of interest in the halogen bonding and lithium bonding during the last decade. The main emphasis of our research is to understand these interactions in detail, in particular non-conventional hydrogen bond acceptors. In this work, weakly bound complexes are studied using Pulsed Nozzle Fourier Transform Microwave Spectrometer, which has been fabricated in our laboratory and various theoretical methods. FTMW spectroscopy in the supersonic beam provides accurate structural information about the near-equilibrium geometry of small dimers and trimers in isolation. The home-built Pulsed Nozzle Microwave spectrometer, having a spectral range of 2-26.5 GHz has been used to record the microwave spectrum of these complexes. The spectrometer consists of a Fabry-Perot cavity, electronic circuit and pumps. Fabry-Perot cavity is the interaction zone of the molecules and radiation. The electronic circuit is used for the polarization and detection of the signal. Mechanical and diffusion pumps are used to maintain the vacuum inside the cavity. The gas molecules of interest are then mixed with a carrier gas and pulsed supersonically inside the cavity through a nozzle of 0.8 mm diameter. The emission from the complexes formed during the expansion is detected by super-heterodyne detection technique and then Fourier transformed.

The first chapter of the thesis gives a brief introduction to intermolecular interactions, hydrogen bonding, halogen bonding, lithium bonding and molecular

π clusters. The chapter also includes a brief introduction to rotational spectroscopy.

The second chapter of the thesis discusses the experimental and theoretical methods. It includes a detailed discussion of the mechanical and electrical parts of the spectrometer and the software used, which is developed in Labview 7.1. The various theoretical methods (*ab initio* and DFT) and the basis sets are discussed along with Atoms In Molecules Theory and the criteria used to characterize hydrogen bond.

In the third chapter, to understand the ability of saturated hydrocarbons to act as hydrogen bond donor and acceptor, interaction of CH_4 with H_2S is studied using rotational spectroscopy as well as theoretical methods such as *ab initio* and Atoms In Molecules theory. Three progressions were obtained for the CH_4•••H_2S complex using microwave spectroscopy. The progressions were independently fitted to a linear top Hamiltonian. Absence of $J_{1\leftarrow 0}$ transition in Progression II confirms the presence of higher internal angular momentum state, m=1. This also confirms the internal rotation of the monomers in the complex. Progressions II and III have negative centrifugal distortion constants. Hence both the states are from some excited internal rotation/torsional motion with strong vibrational-rotational coupling. The moment of inertia obtained from the experimental rotational constant confirms the structure in which sulphur of H_2S is close to CH_4. This also supports the structure in which CH_4 is the hydrogen bond donor, if such an interaction is present. AIM analysis and the potential energy barrier for internal rotation show orientational preference and hence hydrogen bonding. The *ab initio* results show that CH_4•••HSH interaction is more favorable than CH_3H•••SH_2. *Ab initio* and AIM studies also gave a structure where there is direct interaction between C and S. This is interesting since the electronegativities of C and S are comparable. Experimentally obtained negative

distortion constants for the other two states, confirm excited state rotational-vibrational coupling. The experimental data give a floppy structure having internal rotation.

In the fourth chapter the complex chosen for investigation is benzene-ethylene. Experiments in condensed phase and theoretical works show evidence of π-stacking in benzene dimer, but there is no gas phase spectroscopic evidence available for the same. The lack of permanent dipole moment in the π-stacked geometry of benzene dimer is the hindrance in the experimental observation of the same using microwave spectroscopy. Substitution of one of the benzene with ethylene in the π-stacked structure will result in a complex having permanent dipole moment. C_6H_6•••C_2H_4 complex can have, in addition to π-stacking, C-H/π interaction. There could be a competition between C_6H_6 and C_2H_4, either of which can act as H-bond donor. Experiments show the evidence of C-H/π interaction, where C_2H_4 is the hydrogen bond donor. To ascertain hydrogen bond interaction AIM analysis has been carried out. The results show C-H/π interaction, where one of the C_2H_4 hydrogen interacts with the benzene. Even though the aim was to get the π-stacked geometry, it could not be obtained. However theory and AIM supports the formation of π-stacked complex.

In the fifth chapter using theoretical methods the ability of radicals as acceptor of hydrogen, lithium and chlorine bonds are examined with CF_3 radical as the model system. As hydrogen bonds are highly sensitive to the environment, the effect of substitution of hydrogen by fluorine is also analyzed. It is found that, even though CH_3 and CF_3 radicals are topologically different, they interact in a similar fashion. AIM analysis of CF_3•••HY satisfies all the eight criteria proposed by Koch and Popelier for hydrogen bonding. Here the hydrogen bond formed is charge transfer

assisted. The interaction energies of the complexes are inversely proportional to the dipole moment of hydrogen bond donors and are proportional to the charge transfer occurring in the complex. Interaction energies from *ab initio* calculations confirm complexation of CF_3 radical with LiY(Y=F, Cl, Br) and ClF. AIM analysis of CF_3●●●LiY and CF_3●●●ClF complexes show a bond critical point between Li/Cl and the C of CF_3 and the condition of mutual penetration is also met. In CF_3●●●LiY complexes the interaction energies and charge transferred are directly proportional to the dipole moment of the Li bond donor.

In the sixth chapter in order to extend the concept of non-conventional hydrogen bond acceptors to transition metals, complexes of Fe ($Fe(CO)_5$) with HX (X=F,Cl,Br) have been studied theoretically. DFT calculations show that the structure in which the hydrogen of HX interacting with Fe through the sixth co-ordination site is a stable geometry. AIM analysis shows the presence of a bond critical point between the iron and the hydrogen of HX and hence bond formation. ΔQ obtained from NBO analysis shows that there is charge transfer from the organometallic system to the hydrogen bond donor. However the interaction energies of the complexes are proportional to the dipole moment of hydrogen bond donors and are inversely proportional to the charge transfer for these complexes. H-bonding leads to the stabilization of square pyramidal geometry. 'Hydrogen bond radius' of iron has also been defined. Studies on the interaction of $Fe(CO)_5$ with ClF and ClH showed that Fe can also act as a chlorine bond acceptor.

Seventh chapter provides the overall conclusion and also discusses future direction.

CHAPTER I

Introduction

I. 1. An Introduction to Intermolecular Interactions:

Understanding of the interactions between molecules is still one of the most challenging topics in chemical literature[1]. A lot of interest is on the nature of relatively weak interactions between atoms, molecules, ions, radicals etc, which do not lead to the formation of a chemical bond[2-4]. It is very difficult to characterise the intrinsic nature of noncovalent bonds since these bonds are floppy and are more sensitive to environment than covalent bonds. Even though intermolecular interactions are much weaker than the intramolecular interactions, the former play a significant role in nature. Intermolecular interactions occur between molecules and hence they are mainly responsible for the properties of the condensed states of matter, solids and liquids. The physical properties both at the molecular and bulk level are enormously influenced by these interactions. A classic example is a comparison of H_2O and H_2S. Both oxygen and sulphur belong to the same group but H_2O is a liquid and H_2S a gas at room temperature.

Supramolecular chemistry is a highly active interdisciplinary field having important implications in biology, chemistry, physics and engineering[5, 6]. Knowledge of intermolecular potential is required to obtain solutions for these wide ranges of problems. The very fact that biomolecules such as DNA and proteins are largely the results of these interactions, which are responsible for different conformations and orientations, indicate that life on earth would not be possible without these interactions. Interactions such as π stacking, C-H/π, S-H/π, S/π etc contribute to the energy stability and structure of proteins. Noncovalent interactions play a major role also in molecular crystal packing, solvent phenomena etc.

In 1834 Clapeyron[7] derived the ideal gas law assuming molecules as point masses and that there is no interaction between gas molecules. Later van der Waal accounted for non ideality, showed that molecules have finite volume and there is intermolecular interaction between the molecules. It was J. D. van der Waals, who first recognized the existence of noncovalent interactions and the van der Waals' equation of state dates back to 1867[8,9]. A classic example which has helped to understand the importance of intermolecular interactions and the forces responsible for it is the liquefaction of helium by Kamerlingh-Onnes in 1908. All intermolecular forces were called van der Waals forces. But the existence liquid state of H_2O and gaseous state of H_2S at room temperature cannot be explained only on the basis of van der Waals force. Further classification of intermolecular forces apart from van der Waals force is required. The crystal structures of H_2O and H_2S also exhibit remarkable differences. In ice, each of the H_2O molecules is coordinated to four H_2O molecules in a tetrahedral arrangement. H_2S, under ambient pressure, has been found to crystallize (freezing point -60°C) in a close-packed fashion where each hydrogen sulfide molecule is in contact with twelve equidistant neighbours. This disorder in the crystal structure of H_2S is attributed to the isotropic nature of the interaction among the neighbors, which are essentially spherical. To explain this further classification of intermolecular forces is essential.

Huggins in 1919[10], Latimer and Rodebush in 1920[11] and Pauling in 1930[1] came up with a new concept, hydrogen bonding. Hydrogen bonding is defined as an interaction where two atoms which are not bound by a conventional chemical covalent bond, are linked by a hydrogen atom. Volumes of work have been done on the two types of intermolecular interactions, van der Waals interaction and hydrogen

bonding. During last decade halogen bonding and lithium bonding have gained immense popularity. The noncovalent interactions between two molecules involve the interplay of different effects. A correct knowledge of the physical forces that contributes to the intermolecular interaction is necessary to develop an exact potential energy function[12,13,14].

Based on the nature of forces involved, intermolecular interactions can be broadly classified as long-range and short-range interactions. Intermolecular forces have contributions from electrostatic forces (dipole-dipole, dipole-quadrupole, quadrupole-quadrupole etc), inductive forces and London Dispersion forces. Dipole-dipole attraction is the electrostatic attraction between molecules having permanent dipole moment. Molecules line up so that the positive and negative ends are close to each other. Dipole–dipole forces are very weak compared to covalent or ionic bonds and they rapidly become weaker as the distance between the dipoles increases. At low pressure in the gas phase, where the molecules are far apart, these forces are relatively unimportant. The first explanation of the attraction between noble gas atoms was given by Fritz London in 1930. London dispersion forces exist among nonpolar molecules or noble gas atoms. The source is the instantaneous quantum mechanical fluctuation of the electron density of the molecule. Hence a momentary electric moment is created on a nonpolar moiety which in turn polarizes the neighboring nonpolar molecule or an atom giving rise to an interatomic or intermolecular attraction that is relatively weak and short-lived. The long range contribution is due to the instantaneous dipole - induced dipole interaction.

The van der Waals interaction, which has major contribution from dispersion and repulsion energies, defines the size and shape specificity of non covalent

interactions. Specificity on recognition events are conferred by electrostatic interaction between the static molecular charge distributions. Other important contribution comes from induction energy, charge transfer etc. The total interaction energy can be decomposed as[12]

$$E^{total} = E^{ele} + E^{ind} + E^{ere} + E^{disp}$$

Where E^{ele}, E^{ind}, E^{ere} and E^{disp} represents the electrostatic, induction, exchange-repulsion and dispersion energies. Contribution from electrostatic energy is more in strong, directional intermolecular interactions like hydrogen bond and halogen bond. Induction energy comes into picture when the nature of interaction is dipole-induced dipole interaction. The exchange energy is a repulsive term and arises due to Pauli Exclusion Principle which prevents the mutual penetration of electron cloud of the monomers. Dispersion is weak and non-directional and is the dominant force in weak van der Waals complexes. These interactions are instantaneous dipole – induced dipole interactions.

I. 2. van der Waals Interactions:

van der Waals force act between neutral atoms and molecules. van der Waals' equation of state is

$$\left(P + \frac{a}{n^2V^2}\right)(V - nb) = nRT$$

P, V, T, R and n are pressure, volume, temperature, gas constant and number of moles of a gas respectively. The constant 'a' takes into account the attraction between the molecules of a gas. That is, at constant volume and temperature, the pressure decreases with increasing "a", in agreement with the fact that the attraction between

the molecules must reduce the pressure on the vessel walls. This equation tells us that the actual pressure exerted by the gas molecules on the container would be less than what would be predicted if the gases were ideal. van der Waals interaction can generally be accounted for in terms of permanent, induced and instantaneous multipole moments of the molecules involved. van der Waals interaction is much weaker compared to covalent interaction and it leads to the formation of molecular clusters, liquids and solids.

I. 3. Hydrogen bond interaction:

Among non covalent interactions hydrogen bond occupies a central position. It is because of its strength and directionality. High directionality of hydrogen bond finds many applications in biology and crystal engineering. Hydrogen bonding was identified between a H atom bonded to an electronegative element X and another electronegative element Y which has a lone pair of electrons, and it was usually represented as X-H···Y. Conventional hydrogen bond acceptors were electronegative atoms like fluorine, oxygen, nitrogen etc. Volumes of work have been done on the nature of hydrogen bonds[15, 16.] Progress in the experimental and theoretical studies on hydrogen bonding have led to a number of unusual hydrogen bonds. σ electrons, unpaired electrons, π electrons, C-H bond, hydride ions, metal hydrides[17-25] etc act as hydrogen bond acceptor. H_2O···HF, HF···HF etc are classical examples of conventional hydrogen bonds. Coming to non conventional hydrogen bonds, C_2H_4···HF, C_2H_4···H_2O etc are example of non conventional hydrogen bonds where the hydrogen bond is formed between π electrons and the hydrogen atom. Both experimental and theoretical studies on these systems show that the hydrogen of HX

is directed towards the π electrons. Another form of non conventional hydrogen bonding is the one formed between hydrogen atom and an unpaired electron from a radical. Example is HX interacting with CH_3 radical[24] ($H_3C\cdots HF$). Hydrogen bond formed between sigma electrons and hydrogen of HX forms another type. In this case HX can interact with σ electrons of H_2 molecule to give a hydrogen bonded complex, e.g. $H_2\cdots HF$. HX also interacts with inert gas like Ar. Dihydrogen bonds are another type of hydrogen bond, X-H···H-M, where X is N or O and M is any metal like B, Ir, Re etc, i.e. interaction between a metal hydride bond and an OH or NH group or another proton donor[26]. Taking into account the non conventional hydrogen bond acceptors, IUPAC task group has come up with a modern definition of hydrogen bonding[27]. According to the new definition, the hydrogen bond is an attractive interaction between a hydrogen atom from a molecule or fragment X–H in which X is more electronegative than H, and an atom or a group of atoms in the same or a different molecule or fragment in which there is evidence of bond formation.

It is difficult to decide an interaction to be H-bonded or van der Waals from the structure just on the basis of the presence of hydrogen as one of the interacting element. Geometric parameters, interaction energy, frequency shifts, energy decomposition analysis, potential energy surface, Atoms In Molecules theory etc are used to ascertain a given interaction to be H-bond. The strength of hydrogen bond is in between that of chemical bond and non-bonding interactions (van der Waals interaction). The nature and strength of hydrogen bond varies with the substituent on the hydrogen bond donor. Very strong hydrogen bonds resemble covalent bond and weak hydrogen bonds resemble van der Waals interaction. The infrared frequency

shift of X-H bond, $\Delta\nu = (\nu_{X-H})_{free} - (\nu_{X-H})_{complex}$ and the change in the X-H bond length on complexation are treated as the experimental and theoretical evidence for the existence of H-bond. Also the distance between the hydrogen atom and the acceptor atom should be less than the sum of the van der Waals radii of hydrogen and the acceptor atom.

I. 4. Halogen bond interactions:

Halogen bonds are similar to hydrogen bonds except that instead of hydrogen it is the halogen atom that is taking part in bonding. Hydrogen needs one more electron to attain the noble gas configuration. This is the case with halogens too and hence there can be some similarity in the behaviour of hydrogen and the halogens. Here the halogen atoms, chlorine, bromine and iodine act as Lewis acids. It can be represented as Z—X--Y, ie, a halogen atom, X, is shared between a donor Z and an acceptor Y. This interaction is referred as halogen bonding[28,29,30] and the topic has recently gained attention[31,32,33]. Halogen bonding may involve dihalogens, X_2 and X-Y as well as organic halides. With atoms having lone pairs, such as nitrogen, oxygen etc, halogen atom gets engaged in electron donor-acceptor interaction. Halogen bonding can be well understood on the basis of σ-hole concept. σ-hole is a region of positive electrostatic potential on the outermost portion of the halogen's surface, centered on the Z–X axis. Halogen bonds are strong, specific and directional; hence give rise to well-defined structures. This property has good application in biology and supramolecular chemistry to direct molecular conformation[34,35].

I. 5. Lithium bond interactions:

Lithium bonding is analogous to hydrogen bonding[36]. Lithium atom has one electron in its valence shell like hydrogen atom. On bonding with a more electronegative atom X, Li can produce a polar molecule. Li bonding can be represented as X-Li···Y. The existence of Li bond was theoretically predicted by Kollman *et al*.[37] and first experimental evidence for the formation of lithium bonded complex was given by Pimentel et al.[38]. Li interacts with σ-electrons, lone pair, pi electron cloud etc[25]. π-Li bonds formed between lithium and unsaturated hydrocarbons has got much attention[39,40]. The concept of single electron lithium has recently been introduced[25,41].

I. 6. Molecular clusters of π system :

In aromatic molecules, among the various factors governing noncovalent interaction, van der Waals and electrostatic interactions are the two major participants. Noncovalent interaction of π systems with different moieties results in various novel types of molecular clusters having π-π , cation-π, anion-π, C-H - π, N-H - π, O-H - π interactions[42]. The nature of the interaction varies depending on the interacting partner. Molecules having both unpaired and π electrons often interact through the unpair electron. However, the molecules which have nonpolar π cloud like ethylene and benzene, the interaction of the hydrogen happens through the π cloud. Among these much discussed are the complexes formed due to π-π and cation-π interactions. Hunter and Sanders[43] have shown that the π-π interactions are not due to an attractive electronic interaction between the two π-systems but occur when the

attractive interactions between π-electrons and the σ -framework outweigh unfavorable contributions such as π-electron repulsion. The cation–π effect arises from favourable interactions between the electron-rich π system of an aromatic molecule and a positively charged species[44,45]. Electrostatic interaction and cation induced polarization are responsible for this. Anion-π interaction is a recently developed branch of supramolecular chemistry where non-covalent force between electron deficient aromatic systems and anions results in a molecular cluster. This interaction is dominated by contribution from electrostatic component and anion-induced polarization. In case of anion-π interaction where the aromatic ring is not electron deficient, the interaction is assisted by the presence of a cation. i.e. the aromatic ring is simultaneously interacting with the anion on one side of the ring and with a cation on the other side[46]. An overview of the theoretical and experimental investigations on anion-π interaction is given by Dunbar et al.[47].

Interaction of O-H group with π cloud is a widely studied area, both theoretically and experimentally. Non-covalent interaction of benzene and H_2O gives a π hydrogen bonded complex[48,49]. In a similar way O-H group forms π hydrogen bonded complex with aromatic and aliphatic π clouds. A few examples are phenol···H_2O[50,51], pyridine···H_2O[52], C_2H_4···H_2O [53,54] etc. S-H bond also interacts with the C cloud similar to O-H/π interaction, e.g. C_6H_6···H_2S[55]. N-H/π interaction is a less experimentally explored area[56].

Turning the attention towards yet another category of molecular cluster formed by π systems, let us look into the interaction of aromatic systems with C-H group[57]. Interaction between a C-H bond and a π system can be grouped under both

hydrogen bond complex and molecular clusters of π systems. Kim, Tarakeshwar and Lee pointed out that Dewar was the first to suggest that π complexes can act as a proton acceptor, in 1946[58]. However, Jatkar and co-workers presented the evidence of hydrogen bonding in benzene in 1943[59]. Considering C-H/π interaction as a hydrogen bond interaction, it is the weakest among the hydrogen bonds. Polarisation and dispersion are the dominant factors governing the C-H/π interaction. In spite of being a weak interaction, it plays important role in determining the physical, chemical and biological properties. A classic example of C-H/π interaction is the benzene dimer. The T-shape of benzene dimer, obtained using microwave spectroscopy by Arunan et al.[60] is a result of the interaction of the C-H bond of one benzene with the π cloud of the other monomer. C-H/π interaction has great contribution in protein folding and the three dimensional structure of proteins, DNA etc are stabilized by the C-H/π interaction[61,62].

I. 7. Different experimental methods for studying noncovalent interactions:

Noncovalent interactions, as the name implies, lead to the formation of molecular clusters which are not chemically bound. Even though the strength of noncovalent interactions can be said to range from strong to weak, they are much weaker than the chemical bonds. In majority of the cases these molecular clusters will be floppy. Determination of the structure of these complexes is the major step in the investigation of the nature of the complex. Among this study of dimers, trimers etc i.e.

cluster having less number of moieties is much more difficult since we need to produce them in isolation to avoid long range interactions. Here preparation of molecular clusters using supersonic jet expansion becomes very important. Investigation of the structure and dynamics of these molecular clusters are done using spectroscopic analysis and mass selective detection.

Mass spectroscopy, rotational spectroscopy, vibrational rotational tunnelling spectroscopy, vibrational spectroscopy, REMPI and hole burning spectroscopy, ZEKE spectroscopy, Raman spectroscopy etc are the spectroscopic techniques widely used to study noncovalent molecules and their interactions. Mass spectroscopy[63] is a widely used technique. Deduction of molecular structure from the rotational constants is a popular method. Molecular beam electric resonance (MBER)[64] and Pulsed nozzle fourier transform microwave (PNFTMW)[65] spectrometer are used to obtain the pure rotational spectrum of molecular clusters. Rotational coherence spectroscopy, using ultrafast laser pulse is another technique which can give rotational constants. It is based on rotational coherence and the measurement of its recurrence[66,67]. Introduction of Terahertz spectroscopy and far-infrared fourier transform spectroscopy opened the way to explore the vibrational-rotational tunnelling states[68-71]. Multidimensional potential energy surfaces of molecular clusters can be obtained using IR spectroscopy[72,73]. Similarly structure and dynamics of nonbonded systems can be studied using UV spectroscopy[74]. Low frequency intermolecular vibrations, identification of isomers, exploring structural changes upon electronic excitation and ionization or properties of van der Waals complexes in general can be well understood by the aid of resonance enhanced multi photon ionization (REMPI)[75-77] and Hole-burning spectroscopy[78,79]. Zero Electron Kinetic Energy spectroscopy

(ZEKE)[80-82] and mass-analyzed threshold ionization (MATI)[83] are the two other techniques used for investigating weakly bound complexes..

I. 8. Pulsed Nozzle Fourier Transform Microwave (PNFTMW) spectrometer:

A detailed study of intermolecular and intramolecular interaction is essential to understand the nature around us. As discussed in the previous section, due to the floppy nature of most of the noncovalent clusters, highly sensitive technique is required to explore the structure and dynamics of these molecular clusters. In many cases the direct measurement of structural parameters may not be possible. Obtaining the structural data from the rotational constant is the most popular method. The technique of "Pulsed Nozzle Fourier Transform Microwave spectrometer" is used to obtain the rotational spectrum. Pulsed Nozzle Fourier Transform Microwave Spectroscopic (PNFTMW) technique was developed by Flygare and co-workers in 1979[65]. It combines the technique of cavity Fourier transform microwave spectrometer and the supersonic expansion. Supersonic expansion provides a collision-free environment and hence the complexes formed during expansion are effectively isolated. Cooling of the rotational and vibrational degrees of freedom provides spectral simplicity. Weakly bound complexes involving van der Waals and hydrogen bonding interactions are being studied in our laboratory by the PNFTMW spectrometer[84].

I. 9. Introduction to Microwave Spectroscopy:

Microwave spectroscopy is a classical method of spectroscopy widely regarded as an accurate tool for the determination of structure of molecules in the gas phase. High spectral resolution is the greatest advantage of this technique. Rotational spectrum can be obtained only for molecules or molecular clusters having permanent dipole moment. Accurate determination of structure is possible by this technique since the rotational constants which have inverse dependence on the moment of inertia depends on the mass distribution, i.e., the mass and the distance of each of the atom from the molecular centre of mass. The frequencies corresponding to transitions between different rotational energy levels depend on the molecule's moment of inertia about the three principal axes of inertia. Thus by measurement of transition frequencies one can calculate the principal moment of inertia for the molecule. Depending on the symmetry of the molecule or the molecular cluster and hence the symmetry of the moment of inertia ellipsoid, the observed spectral pattern varies. Molecules are divided into four classes according to the principal moment of inertia[85,86]: 1) Linear Top 2) Symmetric Top 3) Asymmetric Top and 4) Spherical Top.

The distortion constants which can be obtained along with the rotational constants by fitting the observed rotational transitions to a suitable rotational Hamiltonian have information about the force field of the molecule about different internal axes. For a simple diatomic molecule, the centrifugal distortion constant, D_j is related to the vibrational frequency and hence from the rotational spectrum one could determine the vibrational frequency[87]. Molecules containing one or more nuclei with nuclear spin I $\geq$ 1 show nuclear hyperfine structure in their rotational spectrum[85,86,88]. The non-

spherical distribution of nuclear charge gives rise to nuclear quadrupole moment and an electric field gradient at the nucleus. The quadrupole moment of the nucleus interacts with the electric field gradient at the nucleus. Electric field gradients within the molecules can be obtained from the nuclear hyperfine structure from which information about electronic structure and chemical bonds can be obtained. Molecules having internal rotation give a more complicated rotational spectrum than the one having no internal rotation. It is because the internal rotation within a molecule can couple with the overall rotation of the molecule. This coupling leads to the splitting of the rotational transitions. The observed splitting depends on both the symmetry of the potential as well the barrier height for internal rotation. Thus by getting the value of splitting due to internal motions the nature of the potential and the barrier height can be determined for several molecules[89,90]. Application of electric field, the stark effect, lifts the $(2J+1)$ degeneracy associated with M_J values (M_J=-J to +J including zero) for each J level. The extent of splitting depends on the dipole moment of the molecule and thus the measurement of this splitting leads to experimental determination of the permanent dipole moment of the molecule, in the ground state [91,92].

I. 10. Present Investigations:

In this thesis, some non-conventional hydrogen bond acceptors have been characterised using microwave spectroscopic and various theoretical methods. Home made Pulsed Nozzle Fourier Transform Microwave Spectrometer (PNFTMW)[84] is used to obtain the rotational spectrum. *Ab initio*, density functional theory (DFT) and Atoms In Molecules (AIM) calculations are used for theoretical

analysis of all the hydrogen bond complexes studied. Chapter II briefly discusses the experimental and theoretical techniques. To understand the ability of saturated hydrocarbons to act as hydrogen bond donor and acceptor, the interaction of CH_4 with H_2S is studied in the chapter III using rotational spectroscopy as well as theoretical methods such as *ab initio*, AIM and NBO analysis. *Ab initio* and AIM studies gave a structure where there is direct interaction between C and S. The next complex chosen for investigation, chapter IV, is benzene-ethylene. Experiments in condensed phase and theoretical works show evidence of π-stacking, but there is no gas phase spectroscopic evidence available. In addition to π-stacking, C_6H_6●●● C_2H_4 complex can have C-H/π interaction where there can be a competition between C_6H_6 and C_2H_4 about which of the two moieties will act as H-bond donor. The ability of radicals as acceptor of hydrogen, lithium and chlorine bonds is examined in the next chapter, chapter V with CF_3 radical as the model system. As hydrogen bonds are highly sensitive to the environment, the effect of substitution of hydrogen with fluorine is also analyzed. In order to extend the concept of non conventional hydrogen bond acceptors to transition metals, in chapter VI complexes of Fe, ($Fe(CO)_5$) with HX (F,Cl,Br) have been studied using theoretical methods. A 'hydrogen bond radius' for iron has also been defined. Studies on the interaction of $Fe(CO)_5$ with ClF and ClH showed that Fe can also act as a chlorine bond acceptor. The possibility of using the hydrogen and halogen bond to stabilize the square pyramidal geometry of iron pentacarbonyl is further analyzed.

I. 11. References:

1) L. Pauling, "*The Nature of Chemical Bond*", Cornell University Press, Ithaka, **1960.**

2) van der Waals molecules I, special issue, *Chem. Rev.* **1988**, *88(6).*

3) van der Waals molecules II, special issue, *Chem. Rev*. **1994**, *94(7).*

4) van der Waals molecules III, special issue, *Chem. Rev*. **2000**, *100(11).*

5) J. Steed , J. L. Atwood, *Supramolecular Chemistry*, John Wiley, New York, **2001**.

6) Special issue dedicated to Supramolecular Chemistry, *Chem. Soc.Rev.,* **2007**, *36(2).*

7) Source: Wikipedia http://en.wikipedia.org/wiki/Ideal_gas_law

8) J. D. van der Waals, Doctoral Dissertation, Leiden, 1873.

9) J. D. Van der Waals, Physical Memoirs, Physical Society of London, vol I, Longmans Green, London **1890.**

10) M. L. Huggins, M. S. Thesis, University of California at Berkeley, **1919**.

11) W. M Latimer, W. H Rodebush, *J. Am. Chem. Soc*.**1920**, *42*, 1419.

12) H. Umeyama, K. Morokuma*, J. Am. Chem.* Soc, **1977**, *99*, 1316.

13) O. Enkvist, P. Åstrand, G. Karlström, *Chem. Rev,* **2000,** *100*, 4087.

14) A. J. Stone, *Science*, **2008**, *321*, 787.

15) S. Scheiner, *Hydrogen Bonding*: *A TheoreticalPperspecitive*; Oxford University Press: Oxford, NY, **1997**.

16) G. R. Desiraju, T. Steiner, *The Weak Hydrogen Bond: In Structural Chemistry and Biology*; Oxford University Press: Oxford, NY, **1997**.

17) E. Y. Misochko, V. A. Benderskii, A. U. Goldshleger, A. V. Akimov, A. F. Shestakov, *J. Am. Chem. Soc,* **1995**, *117*, 11997.

18) I. Alkorta, I. Rozas, J. F. Elguero, *Ber. Bunsen.-Ges. Phys. Chem,* **1998**, *102*, 429.

19) J. J. Szymczak, S. J. Grabowski, S. Roszak, J. Leszczynski, *Chem. Phys. Lett.* **2004**, *393*, 81.

20) S. J. Grabowski, W. A. Sokalski, J. Leszczynski, *Chem. Phys. Lett.* **2006**, *432*, 33.

21) D. Wu, Z-R. Li, X. Y. Hao, A. F. Jalbout, L. Adamowicz, R. J. Li, C-C. Sun, *J. Chem. Phys.* **2004**, *120*, 1330.

22) I. Alkorta, I. Roza, J. Ekguero, *Chem. Soc. Rev.* **1998**, *27*, 163.

23) T. F. Koetzle, O. Eisenstein, A. L. Rheingold, R. H. Crabtree, *Angew. Chem., Int. Ed. Engl.* **1995**, *34*, 2507.

24) B. Raghavendra, E. Arunan, *J. Phys. Chem. A.* **2007**, *111*, 9699.

25) B. Raghavendra, E. Arunan, *Chem. Phys. Lett.* **2008**, *467*, 37.

26) R. H. Crabtree, *Journal of Organometallic Chemistry*, **1998**, *577*, 111.

27) E. Arunan, G. R. Desiraju, R. A. Klein, J. Sadlej, S. Scheiner, I. Alkorta, D. C. Clary, R. H. Crabtree, J. J. Dannenberg, P. Hobza, H. G. Kjaergaard, A. C. Legon, B. Mennucci, D. J. Nesbitt, *Pure Appl. Chem.,* **2011**, *83*,1637. ;
http://ipc.iisc.ernet.in/_arunan/iupac/

28) J-M. Dumas, H. Peurichard, M . Gomel, *Chem Res (S),* **1978**, 54.

29) A. C. Legon, *Chem.-Eur. J.* **1998**, *10*, 1890.

30) A. C. Legon, *Angew. Chem., Int. Ed*. **1999**, *38*, 2686.

31) A. C. Legon, *Phys. Chem. Chem. Phys*., **2010**, *12*, 7736.

32) P. Metrangolo, G. Resnati, *Chem.-Eur. J*., **2001**, *7*, 2511.

33) P. Politzer, P. Lane, M. C. Concha, Y. Ma, J. S. Murray, *J. Mol. Model*., **2007**, *13*, 305.

34) A. Brisdon, *Annu Rep Prog Chem Sect A.* **2002**, *98*, 107.

35) A. R. Voth, F. A. Hays, P. Shing Ho, *PNAS*. **2007**, *104*, 6188.

36) A. M. Sapse , P. V. Schleyer, "*Lithium chemistry: A theoretical and experimental overview"*, John Wiley & Sons Inc., New York, **1995**.

37) P. A. Kollman, J. F. Liebman, L. C. Allen. *J. Am. Chem. Soc*., **1970**, *92*, 1142.

38) B. S. Ault, G. C. Pimentel, *J. Phys. Chem*., **1975**, *79*, 621.

39) K. N. Houk, N. G. Rondan, P. v. R. Schleyer, E. Kaufmann, T. Clark, *J. Am. Chem. Soc*., **1985**, *107*, 2821.

40) S. S. C. Ammal, P. Venuvanalingam, *J. Chem. Phys*., **1998**, *109*, 9820.

41) Y. Li, D. Wu, Z-R. Li, W. Chen, C-C. Sun, *J. Chem. Phys*., **2006**, *125*, 084317.

42) R. K. Castellano, F. Diederich, E. A. Meyer, *Angew. Chem. Int. Ed*., **2003**, *42*, 1210.

43) C. A. Hunter, J. K. M. Sanders, *J. Am. Chem. Soc*., **1990**, *112*, 5525.

44) D. A. Dougherty, *Science*, **1996**, *271*, 163.

45) J. C. Ma, D. A. Dougherty, *Chem. Rev.* **1997**, 97, 1303.

46) C. Garau, D. Quin˜ onero, A. Frontera, P. Ballester, A. Costa, P. M. Deya`, *New J. Chem*., **2003**, *27*, 211.

47) B. L. Schottel, H. T. Chifotides, K. R. Dunbar, *Chem. Soc. Rev*., **2008**, *37*, 68.

48) S. Suzuki, P. G. Green, R. E. Bumgarner, S. Dasgupta, W. A. Goddard III, G. A. Blake, *Science*, **1992**, *257*, 942.

49) H. S. Gutowski, T. Emilsoon, E. Arunan, *J. Chem. Phys.,* **1993**, *99*, 4883.

50) M. Gerhards, M. Schmitt, K. Kleinermanns, W. Stahl, *J. Chem. Phys.,* **1996**, *104*, 967.

51) S. Melandri, A. Maris, P. G. Favero, W. Caminati, *Chem. Phys.,* **2002**, *283*, 185.

52) S. Schlücker, R. K. Singh, B. P. Asthana, J. Popp, W. Kiefer, *J. Phys. Chem. A.,* **2001**, *105*, 9983.

53) K. I. Peterson, W. Klemperer, *J. Chem. Phys*., **1986**, *85*, 725.

54) A. M. Andrews, R. L. Kuczkowski, *J. Chem. Phys.,* **1993**, *98*, 791.

55) E. Arunan, T. Emilsson, H. S. Gutowski, G. T. Fraser, G. de Oliveria, C. E. Dykstra, *J. Chem. Phys.,* **2002**, 117, 9766.

56) D. A. Rodham, S. Suzuki, R. D. Suenram, F. J. Lovas, S. Dasgupta, W. A. Goddard III, G. A. Blake, *Nature,* **1993**, *362*, 735.

57) M. Nishio, M. Hirota and Y. Umezawa, The CH/π interaction,Wiley-VCH, New York, **1998**.

58) K. S. Kim, P. Tarakeshwar, J. Y. Lee*, Chem. Rev.,* **2000**, 100, 3891. and references therein

59) N. S. Rao, S. K. K. Jatkar, *Quart. J. Indian Inst. Sci.,* **1943,** 6, 1.

60) E. Arunan, H. S. Gutowsky*, J. Chem. Phys*., **1993**, *98*, 4294.

61) M. Nishio, Y. Umezawa, M. Hirota, Y. Takeuchi, *Tetrahedron*, **1995**, *51*, 8665.

62) M. Brandl, M. S. Weiss, A. Jabs, J. Sühnel, R. Hilgenfeld, *J. Mol. Biol*., **2001** , *307*, 357.

63) J. F. Garvey, W. J. Herron, G. Vaidyanathan, *Chem. Rev*., **1994**, *94*, 1999.

64) S. J. Harris, S. E. Novick, W. Klemperer, *J. Chem. Phys*., **1974**, *60*, 3208.

65) T. J. Balle, W. H. Flygare, *Rev. Sci. Instrum*., **1981**, *52*, 33.

66) P. M. Felker , A. H. Zewail*, J. Chem. Phys*., **1987**, *86*, 2460.

67) J. S. Baskin, P. M. Felker, A. H. Zewail, *J. Chem. Phys*., **1987**, *86*, 2483.

68) R. J. Saykally*, Acc. Chem. Res*., **1989**, *22*, 295.

69) M. C. Beard, G. M. Turner, C. A. Schmuttenmaer, *J. Phys. Chem. B*., **2002**, *106*, 7146.

70) C. A. Schmuttenmaer, *Chem. Rev*., **2004**, *104*, 1759.

71) N. Pugliano, R. J. Saykally, *Science*, **1992**, *104*,1937

72) D. J. Nesbitt, *Chem. Rev*., **1998**, *88*, 843

73) S. Djafari, H.-D. Barth, K. Buchhold, B. Brutschy. *J. Chem. Phys*. **1997**, *107*, 10573.

74) H. J. Neusser, K. Siglow, *Chem. Rev*. **2000**, *100*, 3921.

75) X. Tong, J. C˘ erny´, K. Muller-Dethlefs, *J. Phys. Chem. A* **2008**, *112*, 5872.

76) M. Kim, S-S Kim, H. Kang, Y. D. Park, *Journal of Molecular Spectroscopy*, **2010**, *263*, 51.

77) C. E. H. Dessent, K. Muller-Dethlefs, *Chem. Rev*., **2000**, *100*, 3999.

78) S. Volker, *Annual Review of Physical Chemistry*, **1989**, *40*, 499.

79) G. N. Patwari, S. Doraiswamy, S. Wategaonkar, *Chem. Phys. Lett*., **1998**, *289*, 8.

80) K. Muller-Dethlefs, O. Dopfer, *Chem. Rev.,* **1994**, *94*, 1845.

81) S. Y. Ketkov, H. L. Selzle, F. Geoffrey, N. Cloke, G. V. Markin, Y. A. Shevelev, G. A. Domrachev, E. W. Schlag, *J. Phys, Chem. A*., **2010**, *114*, 11298.

82) . Schlicht, M. Entfellner, U. Boesl, *J. Phys, Chem. A*., **2010**, *114*, 11125.

83) S. Y. Ketkov, H. L. Selzle, F. G. N. Cloke,G. V. Markin,Y. A. Shevelev,G. A. Domrachev, E. W. Schlag, *J. Phys. Chem. A*, **2010**, *114*, 11298.

84) E. Arunan, A. P. Tiwari, P. K. Mandal, P. C. Mathias, *Curr. Sci.,* **2002**, *82*, 533.

85) W. Gordy, R. L. Cook, *Microwave Molecular Spectra*, Wiley, New York, **1984.**

86) C. H. Townes, A. L. Schawlow, *Microwave Spectroscopy*, Dover Publications, INC. New York, **1975.**

87) J. Kraitchman, *Am. J. Phys.,* **1953**, *21*, 17.

88) H. A. Fry, S. G. Kukolich, *J. Chem. Phys.*, **1982**, *76*, 4387.

89) E. Tannenbaum, R. J. Myers, W. D. Gwinn, *J. Chem. Phys.*,**1956**, *25*, 42.

90) J. Nakagawa, M. Imachi, M. Hayashi, *J. Mol. Struct.*, **1984**, *112*, 201.

91) S. A. Marshall, J. Weber *Phys. Re,* **1957**, *105*, 1502.

92) O Desyatnyk, L Pszczolkowski et al., *Phys. Chem. Chem. Phys*, **2005**, *7*, 1708.

CHAPTER II

Experimental and Theoretical Methods

II. 1. Introduction:

Microwave spectroscopic studies can provide accurate structural data of molecules and complexes. The technique of "Pulsed Nozzle Fourier Transform Microwave Spectrometer" is used to study the structure and dynamics of the complexes. It combines the technique of cavity Fourier transform microwave spectrometer and supersonic expansion. Supersonic expansion provides a collision-free environment and hence the complexes formed during expansion are effectively isolated. Cooling of the rotational and vibrational degrees of freedom provides spectral simplicity. Pulsed Nozzle Fourier Transform Microwave Spectroscopic (PNFTMW) technique was developed by Flygare and co-workers in 1979[1]. Invention of PNFTMW technique enhanced the sensitivity and resolution. Many modifications which have been introduced into the technique have increased the range of the molecular systems which can be studied by this technique[2]. In our laboratory, a Balle-Flygare type spectrometer has been set up and its details and performance can be found elsewhere[3,4].

II. 2. Design of PNFTMW Spectrometer

II. 2. A. Mechanical design

The mechanical design of the Fourier Transform Microwave spectrometer is shown in Figure. II. 1. The unique feature of this spectrometer is the Fabry-Perot cavity. It is housed by a vacuum chamber which is cylindrical in shape and made of stainless steel, SS 304. The vacuum chamber is 1000 mm long and has a diameter of 850 mm. The chamber is directly seated on top of the 20" diffusion pump (Vacuum Techniques, Bangalore, India). The pumping speed of the diffusion pump is 10,000 l

s^{-1}. The diffusion pump is backed by a roots blower (Boc Edward, EH 250) and a belt-less rotary mechanical pump (Boc Edward, E2M80). The combined pumping speed of the backing pumping system is ~4000 l min^{-1}. The chamber can be evacuated to 10^{-6} Torr. The working of the diffusion pump produces enormous amount of heat. To prevent overheating the diffusion pump is water-cooled. A closed circuit water circulation facility includes a water circulation pump, a cooling tower cum water reservoir to keep the water at room temperature. Inside the chamber at both ends two spherical Aluminium mirrors are mounted co-axially on 3 SS guide rods. The mirrors are made of 65 mm thick Aluminium disks with a diameter of 500 mm. The radius of curvature of both the mirrors is 800 mm and the surface roughness and the radius were good to 1 micron. The distance between the mirrors could be varied in steps of microns between 630 and 730 mm with the help of a stepper motor driver. The low frequency cut-off for the spectrometer is about 3.8 GHz which is determined by the radius of the mirror (a) and its radius of curvature (R). The low frequency limit of the spectrometer is the one at which the Fresnel number is unity:

$$a^2/R\lambda = 1$$

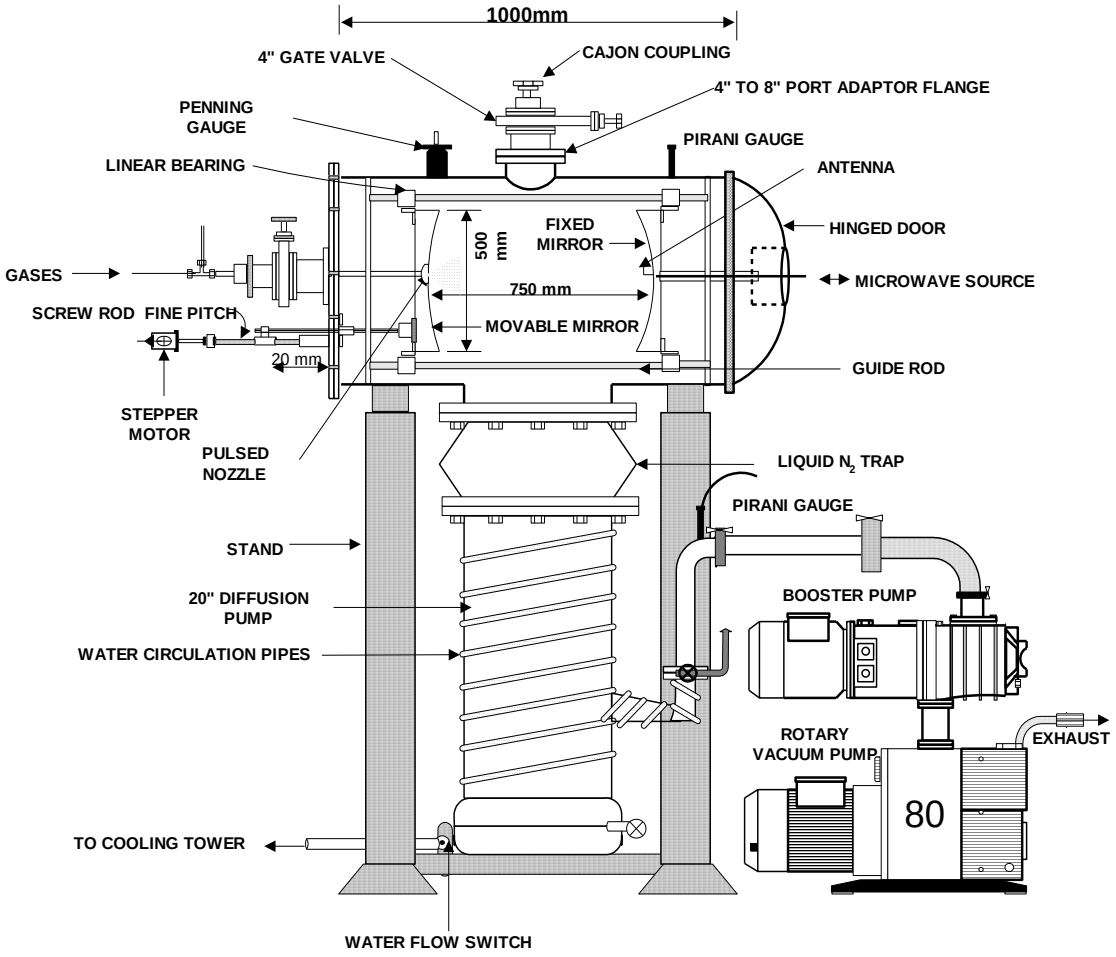

Figure. II. 1: *Mechanical design of the PNFTMW spectrometer*

The lower frequency limit is important while studying larger clusters since it would have many low *J* transitions below 4 GHz. The spectrometer operates well within the range 2-26 GHz. In our laboratory for $Ar_2 \bullet\bullet\bullet H_2S$[5] complex, a transition has been observed at 2447.8427 MHz. The movable mirror which is fixed with a micrometer controlled fine pitch screw rod is driven by a synchronized stepper motor (103H8221-5041, Sanyo Denki, Japan). The linear screw rod has a pitch of 5 mm i.e. the linear distance covered by the mirror for a 360° rotation is 5 mm. The stepper motor, in high-resolution mode, takes 4000 steps for a complete rotation and thus the mirror

moves in steps of 1.25 μm. The original design used the stepper motor driver (PMM-BA-4803), during the course of the work.

For injecting the sample into the chamber a pulsed nozzle is used. The center of the movable mirror has a 10 mm hole. A pulsed nozzle (General Valve, USA, Series 9) of 0.8 mm diameter is connected with a stainless steel tube of ¼ inch OD and is placed at the movable mirror. A trigger to open and close the nozzle is fed through a pin connector, which is sealed with an 'O' ring and a clamp.

A coaxial cable runs through the supporting tube with an SMA female connector at the mirror end. This cable has a hermetically sealed SMA connector at the other end so that the microwave power can be coupled in and out of the cavity at vacuum. The SMA connector goes through a small hole at the center of the fixed mirror and an antenna (L-shaped bent wire made from the central wire of the coaxial cable) can be placed at the connector. Antennas of different lengths are used for different frequency range. The length (L) of the antenna and the wavelength (λ) of the radiation are related as

$$L \approx \lambda/4$$

This is a good enough approximation to make antenna for a particular frequency region having the range extended by few GHz on both side of central frequency corresponding to λ. Using 3-4 antennas of different lengths one could cover the entire range of the spectrometer, 2-26.5 GHz.

II. 2. B. Electrical design

The polarization of the molecular cluster by microwave pulse, the detection of the emitted signal and its digitization involve many electrical and electronic

components. The electrical design of the spectrometer is shown in Figure. II. 2. The major steps involved in the electrical part are the production of the microwave pulse having optimum power to excite the molecular cluster, a device to send and receive the pulse and a technique to digitize the output. The microwave source is a frequency synthesizer from Agilent Technologies (#1 in Figure.2, N5 183A). The synthesizer can generate any frequency between 10 MHz and 26.5 GHz to 1 Hz accuracy. The output from the synthesizer (at ν) is routed to a single pole double throw (SPDT) switch (#7, Sierra Microwave Technology, SFD0526-001, Isolation 60 dB), from which the output either goes through a single side band generator (#5 Miteq, SM-0226-LC1A) or an image rejection mixer (#11 Miteq, IR-0226-LC1A). The single side band mixer (SSBM) mixes the synthesizer output at ν with a synchronous 30 MHz signal (Stanford Research Systems DS345) and generates ν+30 MHz signal. This signal is amplified by a medium power amplifier (#6, Miteq, JS3-02002600-5-7A) with a gain of 24 dB. The amplified signal goes through another SPDT switch (#7'). Both switches work synchronously connecting the polarization and detection parts (top and bottom of the SPDT switches in the Figure. II. 2), alternatively. During the polarisation, the SPDT output goes through a directional coupler (#8, Narda, 4227-16) and a DC block (#18, HP 11742 A) to the antenna inside the chamber. The antenna couples radiation inside the cavity. The microwave pulse has a bandwidth associated with it (typically 1 MHz for 1 μs pulse). If there is any molecular transition within this bandwidth, the molecules will absorb this frequency and will emit $\nu+30\pm\Delta$. The same antenna couples the molecular signal out of the cavity to the detection circuit. The molecular signal is detected by super heterodyne

technique. This signal is amplified by a low noise amplifier (#10, Miteq JS4-02002600-3-5P, noise 2.8 dB, gain 28 dB) and mixed with the synthesizer signal at ν in an image rejection mixer (#11, Miteq, IRO-0226-LC1A). The IRM gives only the $30\pm\Delta$ signal, which passes through a band pass filter (#12, Minicircuits BBP 30) and a low noise amplifier (#13, Minicircuits, ZFL-500LN). The $30\pm\Delta$ signal is down converted to Δ by the RF mixer (#14, Minicircuits ZAD-1) and a low pass filter (#15, Minicircuits, BLP-5). This signal (Δ), generally in kHz range, is amplified and digitized by the scope card (National Instrument, PCI 5112) and transferred to the computer for further processing. Thus digitising the <1 MHz signal is much easier as it does not need a high speed digitiser and does not need storage of large amount of data. The typical sampling speed is 5MHz.

The Fabry-Perot cavity is tuned to the particular frequency, ν+30 MHz, during polarization. If the cavity is not tuned, most of the microwave power gets reflected. To monitor whether the cavity is tuned to a particular frequency, 2.5 % of this reflected signal is fed to the oscilloscope (#27, Tektronix, TDS 2022) by the directional coupler via a diode detector (#9, Narda, 4507). The moving mirror is moved in steps of micron until the reflected power shows a dip in the scope. Figure. II. 3 shows the two conditions, cavity not tuned and the cavity tuned to the polarization pulse. The resonant frequencies,ν, of Fabry-Perot resonator for the TEM_{mnq} modes are:[3]

$$\nu = c/2d\,[(q+1) + (1/\pi)(m+n+1)\cos^{-1}(d/R)]$$

Here, d is the distance between the mirrors and R is the radius of curvature;

m, n and q are the number of nodes in the three perpendicular axes. For a particular frequency there will be several distances between the mirrors which satisfy the resonance condition. As the mirror moves the reflected signal is monitored in the oscilloscope. It is preferable to do the experiment with the cavity tuned to the TEM_{00q} mode at a particular frequency. All the components in our spectrometer are ultra wide-band and the experiment can be performed from 2 GHz to 26.5 GHz without changing any component. Inside the cavity due to reflection by both the mirrors the radiation travels back and forth. The molecular beam travels only in one direction and hence it faces two relative velocities of the radiation. This causes a splitting of the signals obtained from the spectrometer or the observed transitions appear as a doublet due to Doppler splitting. The spectrometer has resolution in sub kHz.

Figure. II. 2: *Electrical design of the spectrometer*

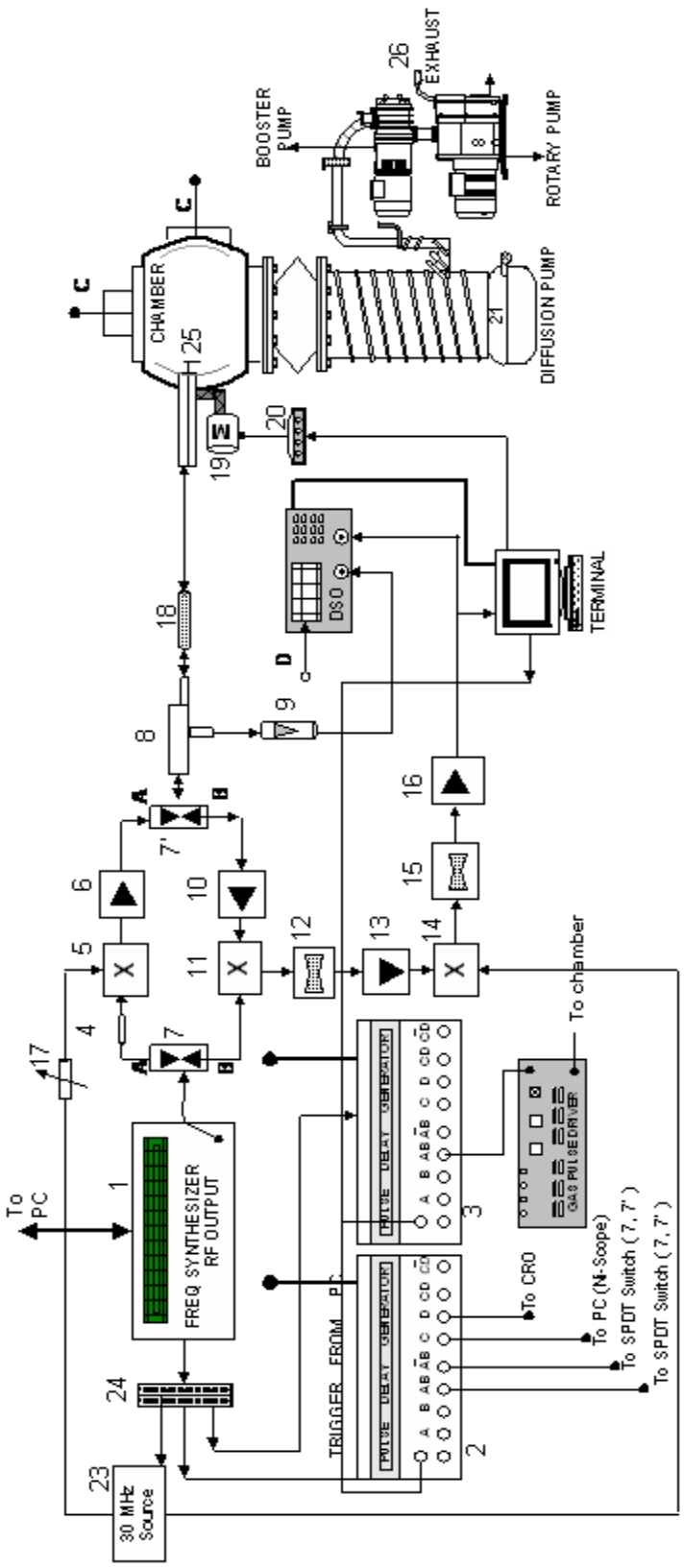

Figure. II.F 2. Electrical design of the spectrometer. [(1) Frequency Synthesizer (Agilent Technologies); (2) & (3) Delay generator; (4) Microwave Attenuator (HP, 8493C, 3dB); (5) SSB Mixer (Miteq, SMO-226LC1A); (6) Medium Power Amplifier (Miteq, JS3-02002600-5-7A); (7) MW SPDT Switch (Siarra MW, 0.5-26.5 SFD0526-000); (8)Direction Coupler (Narda, 1.7-26.5--4227-16); (9) Diode Detector (Narda, 0.01-26.5--4507); (10) Low noise Amplifier (Miteq, JS4-02002600-3-5P); (11) Image Rejection Mixer (Miteq, IRO-0226LC1A); (12) Band Pass Filter (Mini Circuits, BBP-30); (13) RF Amplifier (Mini Circuits, ZFL-500LN); (14) RF Mixer (Mini Circuits, ZAD-1); (15) Low Pass Filter (Mini Circuits, BLP-5); (16) RF Amplifier (HD Communications Corp., HD 17153BB); (17) Attenuator (Mini Circuits, ZAFT-51020); (18) Blocking Capacitor (HP, 11742A); (19)

Figure. II. 3: (A)

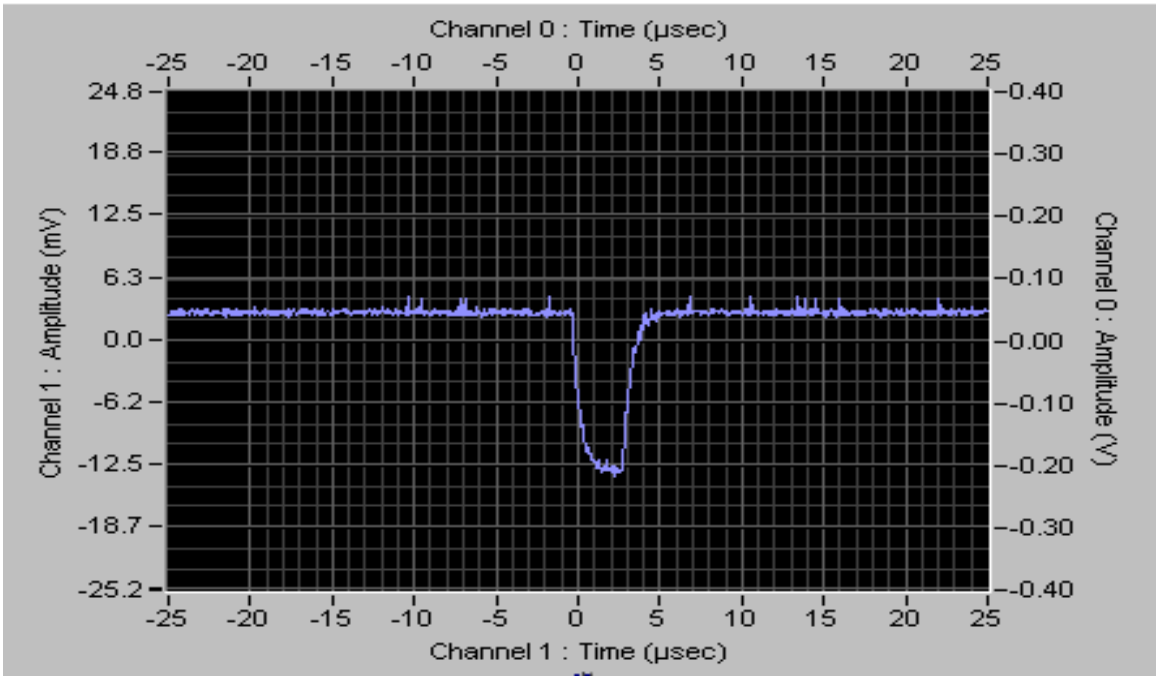

(B)

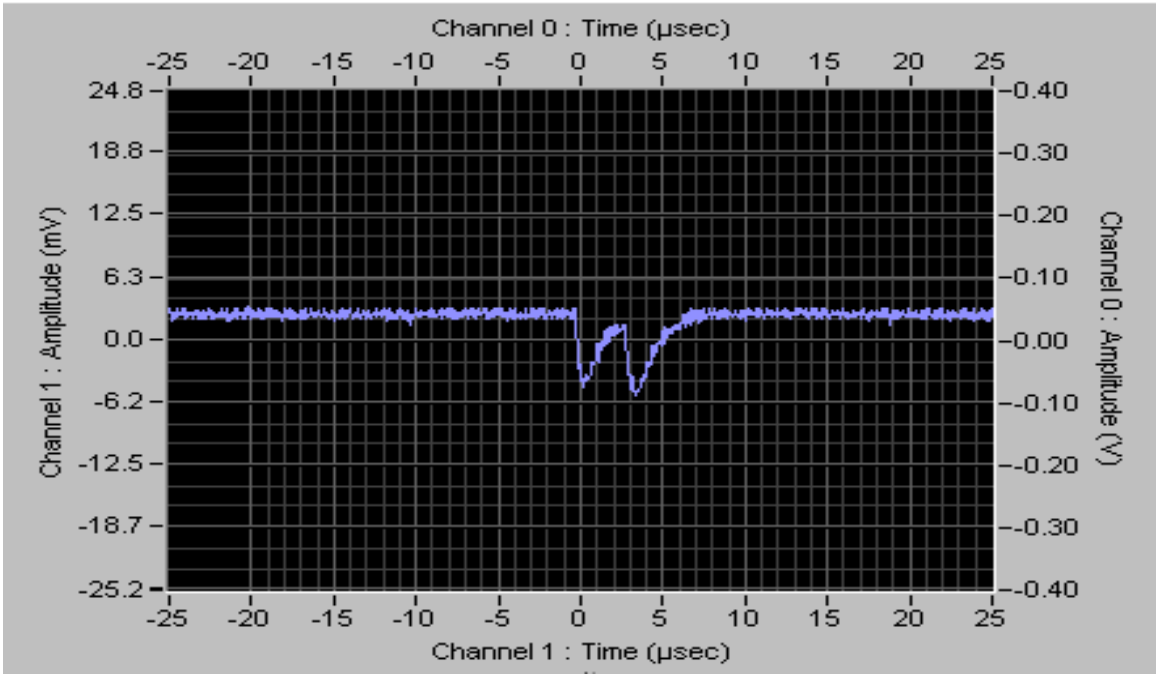

Reflected signal from the cavity: (A) Cavity is not in tune; the amplitude of the reflected signal is maximum. (B) Cavity is in tune; amplitude of the reflected signal is minimum

II. 2. C. Time sequence of the pulses:

The microwave pulse used to polarize the gas sample is sent to the cavity at the beginning of the cycle. The width of the microwave pulse generally varies from 0.3-3 μs depending on the dipole moment of the sample under analysis. The microwave pulse forms a standing wave inside the cavity and the decay time of this pulse is a few microseconds, typically 25-30μs. Rarely it goes up to 40 μs. The molecular emission lasts for hundreds of microseconds. To avoid the overlapping of the polarizing pulse with the emitted signal, a delay called 'record delay' is introduced. The record delay is set such that polarizing pulse and the ringing completely die off before the digitizing process starts. The peak to peak amplitude of the standing wave formed by the microwave pulse is 6-8 V and to digitize a mV amplitude signal in presence of such a high background is not feasible. This is the reason why a delay is introduced. After the digitization process is over, the data is stored as noise. The gas pulse of typically 1 ms duration is fed into the cavity. The microwave pulse of typically 0.3-3 μs follows this. There is typically a delay of a few microseconds before the microwave pulse is send so that the gas molecule comes within the interaction zone of the cavity. However, this delay is taken care of by the processing time of the programme. After sending the microwave pulse, the process of digitization starts again. The gas pulse resides within the cavity for 2 ms, whereas typical time of acquisition is 100 μs. Hence, multiple radiation pulses can be sent for a single gas pulse. This process can be repeated for the N number of gas pulses to improve the signal to noise ratio. Each record collected before sending the gas pulse is subtracted from the corresponding record after sending the gas pulse and is called

signal and this signal is stored. The Fourier transform of this time domain signal gives the frequency domain spectrum. The time sequences for the microwave pulse and gas pulse is shown in Figure. II. 4.

Figure. II. 4: *The MW pulse and gas pulse sequences of PNFTMW spectrometer*

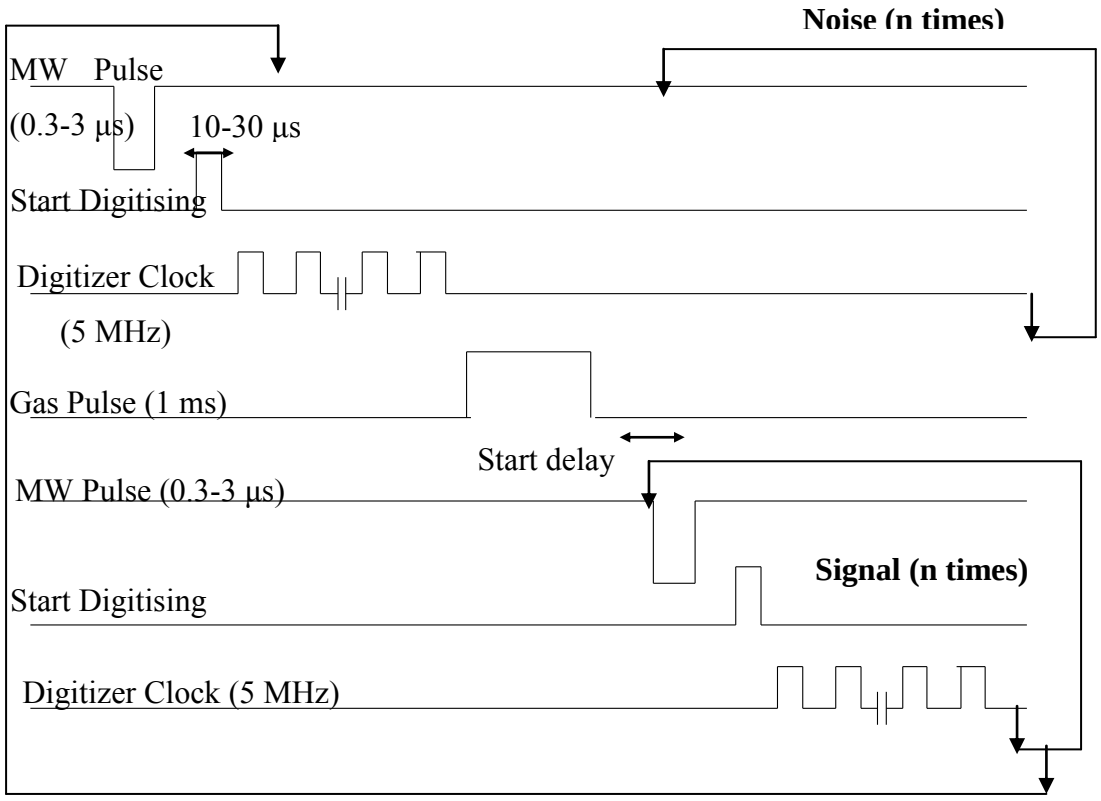

II. 3. Operation and control:

II. 3. A. Software for the PNFTMW Spectrometer:

The PNFTMW spectrometer in our laboratory uses a code based on Lab View 7.1 from National Instruments. It has a very user friendly environment. Labview is a graphical development programme provided by the National Instruments. It provides built-in functions which can be used to create different applications depending on the needs. Labview programs are called virtual instruments (VIs). The VI has three main

parts i) Front Panel, ii) Block diagram and iii) Connectors. The Front panel can be regarded as the interface between the user and the VI. The controls (inputs) and indicators (outputs) are displayed in the front panel. Every control and indicator has a corresponding terminal in the Block Diagram. Block Diagram contains the graphical source code that controls the programme. The synonym of the subroutine in Labview is SubVI. When the run command is given to the VI, the values from controls flow through the Block Diagram. The Block diagram contains different nodes e.g. control and indicator terminals, functions, SubVIs, structures etc. These nodes are connected through the wires. The data flow through the wires and it determines the direction of data flow. The nodes will execute when data is available to all the input terminals and it supplies data to the outputs when done. These results are passed onto other functions or indicators.

The main functionalities of the code, FTMWfinal.vi, the software used for the PNFTMW spectrometer are: i) GPIB control of two SRS delay generators and the frequency synthesiser, ii) Controlling the stepper motor driver via the parallel port of the PC to automate the mirror movement, iii) Programming the NI PCI-5112 card for multiple record acquisition and iv) Processing and presenting the data for the user. The front panel of this programme is shown in Figure. II 5. The programme mainly uses five other subVIs apart from the Lab view inbuilt VIs. These subVIs are i) frequencygpib.vi ii) mwpulsegpib.vi, iii) record-delaygpib.vi , iv) gaspulsegpib.vi, v) freqdom.vi . each one of the sub VIs perform different tasks.

i) frequencygpib.vi: This VI is used to set the frequency in the frequency synthesiser. The frequency synthesiser (N5 183A) is interfaced via GPIB (General

Purpose Interface Bus). The function 'GPIB Write' provided by the Lab view is used to write the value to the synthesiser.

ii) mwpulsegpib.vi: This VI is used to communicate with the delay generator which is used to send the radiation pulse. The communication is via GPIB. This delay generator can generate nine outputs T_0, A, B, C, D, AB, -AB, CD and –CD, five delays and four pulses. T_0 defines the start of the timing cycle. The delay generator can be triggered internally or externally. Once triggered, the timing cycle starts according to the delays set in different channels. AB and -AB are two pulses of opposite polarity and are generated as specified by the intervals between delays of two channels A and B. Similarly, the delays set for C and D define the pulse duration of CD. The outputs AB and AB- from the delay generator is connected to two SPDT switches which open for the specified amount of time to allow the signal to pass into the polarising circuit or the detection circuit. This VI sets the delay value for the channel A to the desired value. The same function 'GPIB write' is again used

iii) record-delaygpib.vi: This VI is used to set the delay of channel C, the record delay, of the first delay generator with respect to the channel A via GPIB communication. The digitizer card gets the trigger to start the digitisation from the output C of the delay generator. Another output of the delay generator, D triggers the oscilloscope which monitors the reflected signal. This external trigger occurs via the parallel port of the computer and is done by the software.

iv) gaspulsegpib.vi: This VI is used to communicate with the delay generator which is used to send the gas pulse. The output AB from the second delay generator goes to

the pulse driver which drives the nozzle. The VI writes the value of the delays of channels A with respect to T_0. B is preset as 'zero' with respect to T_0. This VI is similar to mwpulsegpib.vi.

v) freqdom.vi: This subVI is used to open an existing data file. It displays the existing time-domain plot and performs Fourier Transform to read and display the frequency domain information. It also displays the frequency at which the spectrum was collected, duration of gas pulse and microwave pulse, record delay, start delay, number of shots averaged, number of points and the sampling rate of the acquisition in their respective text boxes.

II. 3. B. Execution of the programme:

The main body of the current programme FTMW_final.vi uses all the five sub VI s described above. Apart from these, it also has different subparts which can execute in parallel. These subparts involve the programming which control the mirror movements and data acquisition by NI scope digitizer card (PCI 5112). All of these parts use several subVIs provided by the Lab View.

The mirror distance can be varied from 63 to 73 cm in order to tune the cavity for a particular frequency. The movement of the mirror is controlled by the stepper motor driver. The stepper motor driver is controlled by the software through the parallel port.

The programme can acquire data in two modes 1) average and 2) autoscan.

In average mode at a particular frequency, several FIDs are collected per gas pulse. Then the average of all the FIDs is taken. This is repeated for a finite number of gas pulses. Here a good signal to noise ratio is obtained. The number of FIDs to be

collected and the number of FIDs to be averaged can be specified in the front panel of the Labview programme. In autoscan mode the FIDs are collected for a particular frequency and the data are saved in a file. Then the frequency is changed automatically according to the step size specified in the front panel. To keep the cavity tuned, the mirror is moved accordingly. The data acquisition and then averaging is repeated for the new frequency. This process i.e. changing the frequency, tuning the cavity to the particular frequency and collecting the signal is continued for a certain search length specified in the front panel. Figure. II. 6 shows time domain and frequency domain signal.

Figure. II. 5: *Front panel of the Labview programme*

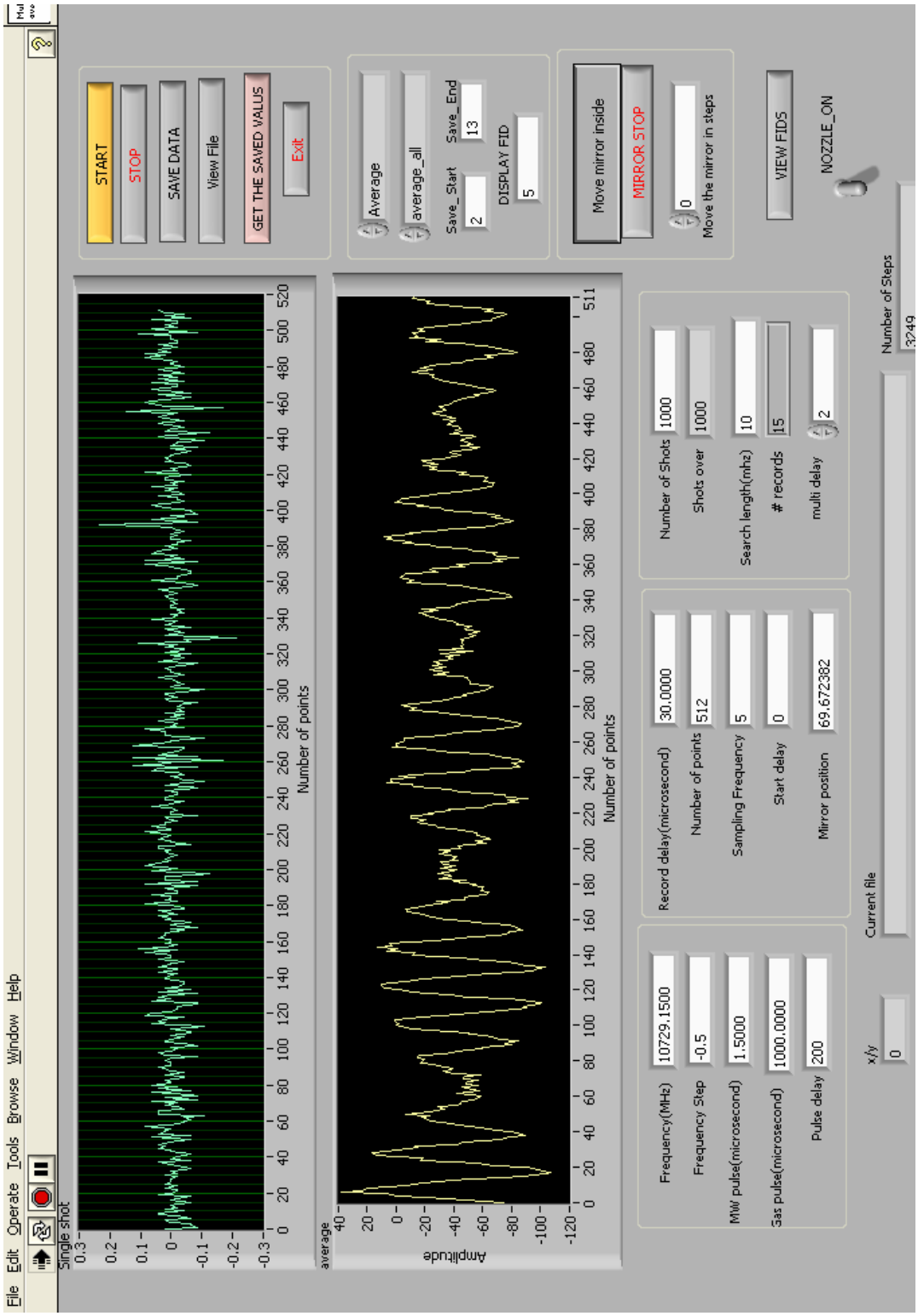

Figure . II. 6: *The time domain and frequency domain signal*

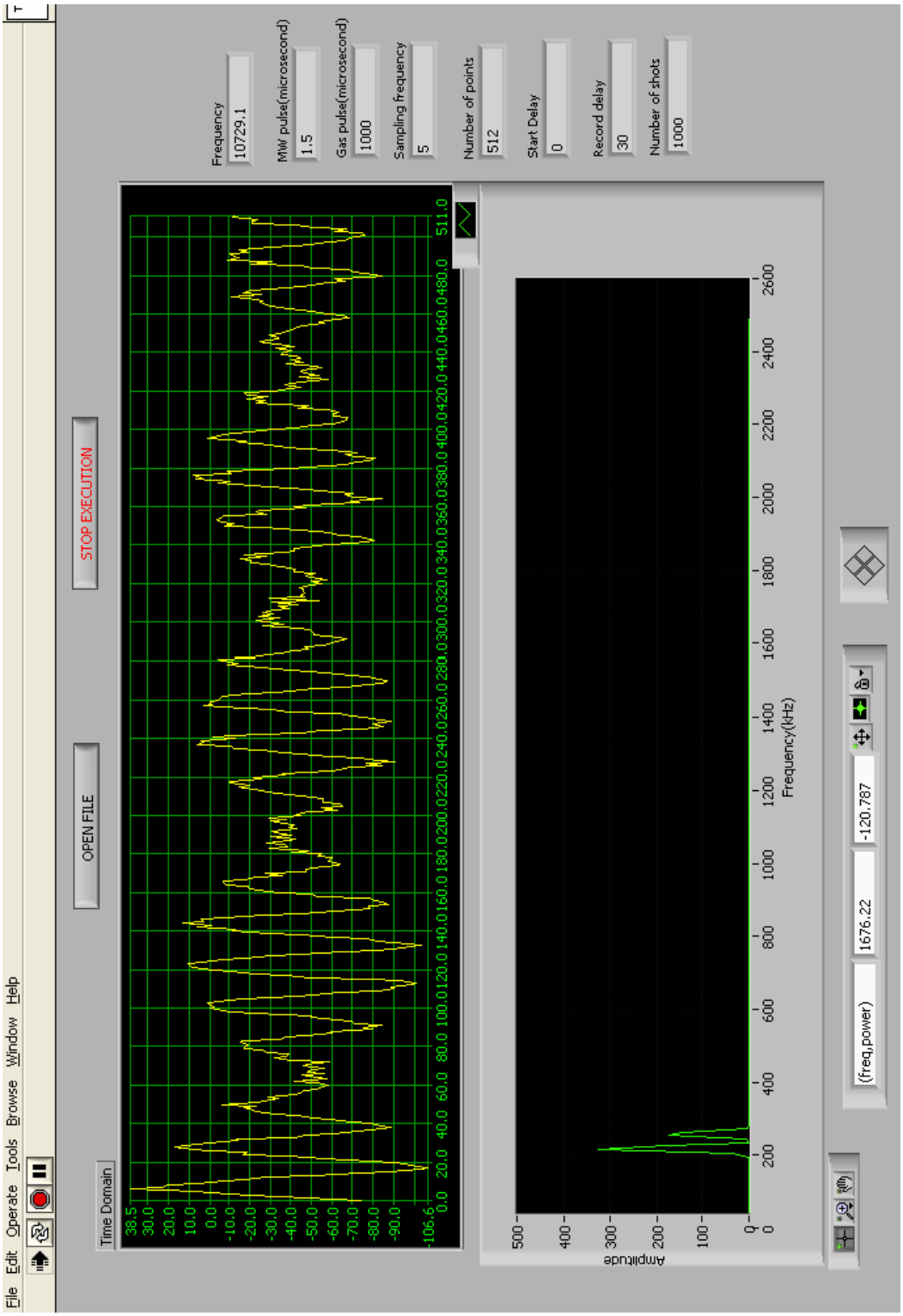

II. 4. Sample preparation:

Pulsed Nozzle Fourier Transform Microwave Spectrometer combines the technique of cavity Fourier transform microwave spectrometer and the supersonic expansion. Supersonic expansion provides a collision-free environment and the molecules can be studied in isolation. Here the sample gas is seeded in a carrier gas. The typical carrier gases used in the experiment are argon and helium. Typically 1-3% of the monomers are mixed with the carrier gas and the ratio varies according to the size of the molecular cluster under investigation. For the purpose of injecting the required concentration of the sample and to maintain the flow of the gases, four mass flow controllers (MKS, 1179A) are used. The unit to measure the flow rate is Standard Cubic Centimetre per Minute (SCCM) or Standard Litter per Minute (SLM).Two of the mass flow controllers are having a range of 0-1000 SCCM are used for the carrier gases. The other two are used to flow the reagents and they have a range of 0-20 SCCM. Two numbers of 2 channel mass flow meters are used for setting and reading the input flow rate. The samples are mixed with argon or helium in a four-way junction. The gaseous reagents are directly flown to the mixer and for the liquids the carrier gas is bubbled through a glass reservoir containing the liquid. The 3-way valves could be selected either for direct flow or through the liquid bubbler. The pulse valve feed through has a 3-way valve through which the excess gases can be pumped out with a separate mechanical pump. This bleed line goes through a needle valve to control the outflow so that the back pressure at the nozzle could be maintained at the required level. At the nozzle, the gas mixture expands from a pressure 0.5-1 bar to 10^{-6} mbar through the nozzle orifice of 0.8 mm diameter to

undergo supersonic expansion. Before the expansion, the gas may be described as having a Maxwellian velocity distribution. After the expansion, there is a highly directional mass flow. The translational, rotational and vibrational degrees of freedom of the molecules get cooled due to the collision in the nozzle during expansion. The translational energy equilibrates at a faster rate than do the rotational and the vibrational energies. The translational temperature attained during this expansion is 0.02-0.03 K whereas the rotational and the vibrational temperatures are 2-3 K and 50-100 K respectively. The random translational energy of the molecules are converted to directional mass flow, which means the velocity distribution narrows and the central peak of the distribution moves towards right. Thus, when the molecules emerge from the nozzle, they are effectively in the collisionless expansion and the weakly bound complexes which are formed during the expansion stabilise in that condition and can be studied.

II. 5. Kraitchman Analysis:

Microwave spectroscopy is very accurate and can obtain moment of inertia to six or more significant figures. From these inertia, structure can be determined. However, even in the ground state molecules have vibrational energy. This will affect the molecular structure determination. Hence to obtain meaningful structural information different geometric parameters are introduced. They are, i) r_e, the equilibrium bond length: deduced by the correction for the effects of vibrations including the zero point vibrations. ii) r_0, the effective bond lengths: obtained for the ground vibrational state calculated from fitting the vibrationally averaged rotational constants to an effective structure. iii) r_s, the substitution bond lengths: can be derived from isotopic

substitution method. iv) <r> (or <r_z>), the average bond length: evaluated by a partial correction for the effects of vibration. v) r_m, the mass dependent bond lengths: derived from a large number of isotopic species by a first-order treatment of isotopic effects.

The substitution method would be a preferred one when only limited set of isotopic data are available. By the help of the Kraitchman equations[6], one can calculate the position of the substituted atom from the center of mass. For a linear molecule and for a symmetric top molecule with a substitution on the symmetry axis, the distance of the particular atom from the center of mass is given by:

$$|z| = \left[\frac{1}{\mu}(I_x' - I_x)\right]^{1/2} = \left[\frac{1}{\mu}(I_y' - I_y)\right]^{1/2}$$

Here, I_x' and I_x are the moment of inertia of the substituted species and the parent species respectively.

Kraitchman equations to find the co-ordinates of the substituted atoms from the center of mass for symmetric top and asymmetric top molecules are given in reference 6.

II. 6. Theoretical methods:

Modern computational chemistry has proven to be a useful tool in a variety of chemical problems and have gained immense popularity. Computational chemical methods find a variety of applications in structure, spectroscopy and dynamics. These methods are classified as (a) Molecular mechanics method, (b) *ab initio* methods, (c) Semi-empirical methods and (d) density functional methods. In the following chapters computational calculations have been used to get the optimized geometries, frequencies, rotational constants and the interaction energies of various

complexes studied. Moreover the wave functions from these calculations have been used to analyse the electron density topology using Atoms In Molecules theory. These methodologies are described in this section.

II. 6. A. *Ab initio* methods:

German physicist, Shrödinger, laid a strong foundation for the development of quantum chemistry. The Shrödinger equation $H\Psi = E\Psi$, gives the solution to atomic and molecular structures. Here Ψ is a wave function, E is the energy of the system and H, the Hamiltonian of the system.

The goal of calculations on a particular molecular system is to solve the n-particle time-independent Shrödinger equation. Many-body problems of this kind cannot be solved exactly. As a simplification the independent particle model is introduced and thereby the problem reduced to solving an n-single particle equation. Thus an effective one electron Hamiltonian is applied to a set of single-particle wave functions, expanded in a suitable basis and the total energy is minimized using variation principle. Various *ab initio*[7] methods include Hartree-Fock formulation (HF), Second Order Møller-Plesset (MP2(FULL)) Method, Configuration Interaction (CI), QCISD Method, Multi configuration Self-Consistent Field (MC-SCF), Coupled Cluster (CC) etc.

While determining the wave function, electron correlation has profound importance since it influences the various chemical and physical properties derived from them. The main drawback of HF method is that it does not take into account the electron correlation. Unlike HF, Møller-Plesset method[8] incorporates electron

correlation. Here again there is a choice, depending on how the inner electrons are considered. The MP2 method assumes that the inner electrons are frozen and hence do not affect the correlation energy. The MP2(FULL) method the correlation energy is estimated considering the inner electrons too. Perturbation theory is applied to take into account the electron correlation.

II. 6. B. Density Functional Theory:

Ab initio method was based on the many electron wavefunction which dependents on 3N variables i.e., three spatial variable for each of the N electrons The main objective of density functional theory is to replace the many-body electronic wavefunction with the electron density as the basic quantity. The density is only a function of three variables and is a simpler quantity to deal with. So in DFT[7], electron density is the vibrational parameter. B3LYP is a DFT method which is a hybrid functional, i.e. functions of another function. In B3LYP the exchange energy, in this case Becke's exchange functional, is combined with the exact energy from the Hartree-Fock theory.

II. 6. C. Basis Sets:

Within the LCAO-MO approximation, molecular orbitals, MOs are expanded as linear combinations of atomic orbitals, AOs. However, since it is not possible to obtain the exact AOs for many-electron atoms, Slater type orbitals (STOs) were used to mimic AOs in early days. Due to the difficulty in computing two and other multi-center integrals using STOs, Boys suggested the use of standard Gaussian functions

centered on atoms (GTO). A Cartesian Gaussian function used in electronic structure calculations has the form:

$$g(\alpha, l, m, n; x, y, z) = N_{lmn}(x - x_A)^l (y - y_A)^m (z - z_A)^n e^{-\alpha |r - r_A|^2}$$

where, α is the orbital exponent and *l, m, n* are the powers of cartesian components *x*,*y* and *z* respectively. The center of a Gaussian function is denoted by $r_A = (x_A, y_A, z_A)$. the computational advantage of GTOs over STOs is primarly due to the Gaussian product theorem which states that the product of two GTOs is also a Gaussian function centered at the weighted midpoint of the two functions. In addition, the resulting integrals can be evaluated analytically. For computational convenience, a set of GTOs are bunched together with fixed coefficients, d_i. Such a linear combination is termed the contracted GTO (CGTO).

$$g^{CGTO}(l, m, n, x, y, z) = \sum_i d_i g(\alpha_i, l, m, n, x, y, z)$$

This orbital exponents and contraction coefficients are determined from appropriate atomic calculations.

There are varieties of Gaussian basis sets available[7], which have been continuously improved over the years. The single-zeta Gaussian basis set, also known as minimal basis set are the simplest GTOs. The STO-nG, n=3, basis set which has been used extensively is the most popular single-zeta basis set. For reliable qualitative results, it is essential to use double-zeta basis functions that contain two CGTOs per shell. Recently most of the calculations make use of triple-zeta basis functions. In

addition, the extended basis sets include an atomic shell of higher angular momentum than those present in the basis. This ensures adequate representation of polarization of the electronic charge density. Similarly, it is essential to add the diffuse functions to the basis set when the region of low electron density in the system is of great interest. The polarization functions are denoted by asterisk '*' and '**'. Double star indicates that the polarization function to be added to light atoms (hydrogen and helium), i.e. when polarization is added to this basis set, a p-function is also added to the basis set. Similarly, d-type functions can be added to a basis set with valence p-orbitals, and f-functions to a basis set with d-type orbitals, and so on. Another, more precise notation (p,d) is used to indicate exactly which and how many diffuse functions are added to the basis set. It can also be denoted by '+' and '++'. Two plus signs indicate that diffuse functions are also added to the light atoms (hydrogen and helium).

Apart from the minimal basis sets, there are three more different type of basis sets, (a) Split-valence basis sets (Pople basis sets), (b) Correlation consistent basis sets and (c) Plane wave basis sets. Split-valence basis sets or Pople basis set is denoted as *X-YZg*, where, *X* represents the number of primitive Gaussians comprising each core atomic orbital basis function. The *Y* and *Z* indicate that the valence orbitals are composed of two basis functions each, the first one composed of a linear combination of *Y* primitive Gaussian functions, the other composed of a linear combination of *Z* primitive Gaussian functions. In this case, the presence of two numbers after the hyphens implies that this basis set is a split-valence double-zeta basis set. eg. 6-31G(d,p), 6-311++G(2d,2p) etc. Dunning and co-workers have developed the Correlation consistent basis sets. Using Correlation consistent basis sets, the complete

basis set (CBS) limit can be obtained by extrapolation. Dunning basis sets are represented as cc-pVNZ where N=D,T,Q,5,6.. (D=double, T=triples, etc.). The 'cc-p', stands for 'correlation consistent polarized' and the 'V' indicate they are valence only basis sets. To introduce diffuse function, the term 'aug' (augumented) is used. eg. cc-pVDZ, cc-pVTZ etc

II. 6. D. Interaction energy:

The main objective of computational chemistry is to obtain the minima energy structure. This is achieved by geometry optimization and the frequency calculation. Frequency calculation is used to ascertain whether the optimized geometry corresponds to a minimum energy structure or not. In case of weak clusters, its formation can be easily detected by measuring its intermolecular vibrational frequencies. Interaction energy is the important parameter used to classify different type of interaction. Supramolecular approach is used to calculate the intermolecular interaction energy. In this approach, the interaction energy is given by

$$\Delta E_c = E_c - \sum (E_M)$$

Here, E_c is the absolute energy of the complex and E_M are the constituent monomers energies in the complex. The interaction energy thus calculated will have some error due to basis set superposition. Basis set superposition error has been calculated for the dimer A•••B formed by the monomers A and B following the Boys Bernardi[9] counterpoise procedure.

$$E_{BSSE} = E_A + E_B - (E_A(AB) + E_B(AB))$$

E_A and E_B are the energies of the monomers A and B at the same basis set as that of AB. These calculations also use structure of A and B as observed in AB. $E_A(AB)$ is

the energy of the monomer "A" calculated by taking its geometry in AB at the same level as that of AB. $E_B(AB)$ is the energy of the monomer "B" calculated by taking its geometry in "AB" at the same level as that of "AB".

The basis set corrected interaction energy, ΔE_{BSSE} is calculated as follows.

$$\Delta E = E_{AB} - (E_A + E_B)$$

$$\Delta E_{BSSE} = \Delta E + E_{BSSE}$$

All the calculations were done using Gaussian 03 programme[10].

II. 6. E. Atoms In Molecules Theory (AIM):

Much of the chemical meaning derived from the analysis of molecular electron density (ρ) is due to the pioneering work by R.F.W. Bader[11,12] and P. Popelier[13]. Since molecular electron density is a scalar field, to analyze and understand its properties, it is useful to have the aid of 3D-graphical visualization tools. In general, molecular electron density is evaluated over a 3D-grid encompassing the molecule and the analyses are carried out in terms of iso-valued contour and surface plots. Alternatively, the topology of molecular electron density can be used to analyze its salient features. Bader pioneered the topological concept to study molecular electron density and its Laplacian. Bader and co-workers employed the electron density to build a rigorous QM basis for the definition of an atom in a molecule (AIM). The AIM theory looks at the distribution (variation) of electron density at every point around the nuclei of a molecule. Based on the electron density distribution, the theory also calculates volume of the atom, electronic population of

the atom, atomic first moments, atomic energy and electronic population of the atoms in a molecule. The AIM theory is able to predict the nature and properties of the bond based on the electron densities at the bond critical points.

II. 6. E. 1. <u>Critical Points:</u> Consider a 3D-scalar field, f. in each direction; f can be a local maximum or minimum. These results in four types of topological features: maxima, minima and two types of saddle points. Any point in space where all the first-order partial derivatives of a function vanishes ($\frac{\partial f}{\partial x} = 0$) is termed as a critical point (CP) of f. the topological feature of such a point, P is characterized in terms of the rank and the signature of its Hessian matrix, defined as $H_{ij} = \left.\frac{\partial^2 f}{\partial x_i \partial x_j}\right|_P$

The rank is defined as the number of non-zero Eigen values of the Hessian matrix and signature as the algebraic sum of the signs of non-zero eigenvalues. Thus a CP is characterized as (ω,σ) where, ω is the rank and σ is the signature of the critical point. Hence 3D scalar function can have four types of non-degenerate critical points:

1) (3, +3) → All curvatures are positive and ρ is a local minimum at P

2) (3, +1) → Two curvatures are positive and "ρ" is a minimum at P in the plane defined by their corresponding axes. ρ is a maximum at P along the third axis which is perpendicular to this plane.

3) (3, -1) → Two curvatures are negative and "ρ" is a maximum at P in the plane defined by their corresponding axes. ρ is a minimum at P along the third axis which is perpendicular to this plane.

4) (3, -3) → All curvatures are negative and "ρ" is a local maximum at P

Any two atoms that falls within moderate distance, indicating a strong or weak bonding interaction between them, exhibit a (3, -1) saddle point. A set of bonded atoms forming a ring possess a (3, +1) critical point at the centre of the ring, while a closed cage formed by bonded atoms has a minimum (3, +3) at the centre. Nuclear positions behave topologically as do (3, -3) critical points in the charge distribution. The curvature of the electron density at the bond critical point gives insight into the nature of bond and explains features of π-bond, bent bond etc. the bond can also be characterized in terms of the ellipticity , ε given by

$\varepsilon = \left[\lambda_1 / \lambda_2 - 1 \right]$ where, λ_1 and λ_2 are the principal eigenvalues of the Hessian of electron density at the bond criticalpoint., the former being higher in magnitude than the latter.

II. 6. E. 2. AIM Criteria for Hydrogen Bonding

On the basis of AIM theory Koch and Popeiler[14] has suggested a set of eight criteria to decide an intermolecular interaction as H-bonded. The eight criteria are

1). Consistent Topology: There should be a bond critical point between interacting hydrogen atom and the acceptor atom and this should be of (3, -1) type to be called

this bond as hydrogen bond. Other topological requirement such as bond path (the path connecting two interacting atoms) and interatomic surface should be consistent with the chemical bond nature.

2). Electron Density at the Bond Critical Point: The value of the electron density at the bond critical point will be different for different bonds and hence it determines the nature of a chemical bond. For hydrogen bond, this value lies between 0.002 to 0.04 au. It is pointed out here that the electron density values at the bcp of few covalent bonds C-H, O-H, H-F and H-S for example are 0.286, 0.366, 0.364 and 0.222 au respectively. In addition, an electron density value less than 0.002 au at BCP can be treated as van der Waals interactions. It is to be noted that electron density at a bond critical point correlates well with the interaction energy of that bond linearly.

3). Laplacian of The Electron Density: The sign and magnitude of the Laplacian of the electron density is a characteristic of nature of a bond. In general, the closed-shell interactions (ionic bonds, hydrogen bonds and van der Waals interactions) have a negative value for the Laplacian. The shared-shell interactions (covalent or polar bonds) have a positive value for the Laplacian. For a bond to be a hydrogen bond this value lies between -0.15 to 0.02 au. Clearly, Koch and Popelier suggest that hydrogen bonding can happen with either closed shell or shared shell interaction.

4). Mutual Penetration: This criterion is not very much different from the classical detection of H-bond, wherein the sum of the van der Waals radii of the interacting atoms is compared with distance between the interacting atoms to distinguish an interaction from van der Waals interaction. However, AIM theory recognizes the fact

that atoms are not spherical. Hence, in AIM theory "non-bonded radii" similar to van der Waals radii and "bonded radii" are defined and calculated along the bond path. The non-bonded radius (r^0) for a given atom is defined as the distance from the nucleus to an electron density 0.001 au along the bond path without the interacting molecule. The bonded radius (r^b) for an atom in a molecule is defined as the distance from that atom to the bond critical point. The difference (r^0–r^b) gives the extent of penetration of the interacting atom. The extent of penetration for hydrogen atom is $\Delta r = r_H^0 - r_H^b$ and for the acceptor atom is, $\Delta r_A = r_A^0 - r_A^b$ and both of these should be positive for the penetration to occur. The following criteria are all invoking atomic properties which target the properties of hydrogen bonded hydrogen atom.

5). Loss of Charge of the Hydrogen Atom: This is computed by subtracting electronic population of the hydrogen atomic basin in the free monomer from the corresponding hydrogen in the complex. This quantity is denoted by ΔN and turns out to be negative. This can be explained with its experimental analogues, as the NMR shifts show the protons involving hydrogen bonding are descreened.

6). Energetic Destabilization of the Hydrogen Atom: This criterion requires that hydrogen atom in the complex should be destabilized, i.e. The hydrogen atom shows a loss in the total atomic energy in the complex. This is calculated as the difference between the total atomic energy of the hydrogen atom in the complex and in the monomer and is denoted by the symbol, ΔE(H).

7). Decrease Of Dipolar Polarization of the Hydrogen Atom: This criterion tells that the dipolar polarization of the hydrogen atom should decrease in the complex

compared to the hydrogen atom of the corresponding monomer. And this criterion asserts a reduction in polarization, which is primarily a result of the loss of the non-bonded density of the hydrogen atom.

8). Decrease of the Hydrogen Atom's Volume: This criterion requires that the volume of the hydrogen atom should decrease in the complex compared to the free monomer and is denoted by $\Delta V(H)$.

II. 7. References:

1. T. J. Balle, W. H.Flygare, *Rev. Sci. Instrum.,* **1981**, 52, 33.

2. Y. Xu, J. V. Wijngaarden, W. Jäger, *Int. Rev. Phys. Chem.,* **2005**, 24, 301.

3. E. Arunan, S. Dev, P. K. Mandal, *Appl. Spec. Rev.,* **2004**, 39, 131.

4. E. Arunan, A. P. Tiwari, P. K. Mandal, P. C. Mathias, *Curr. Sci.,* **2002**, 82, 533.

5. P. K. Mandal, J. D. J. Ramdass, E. Arunan, *Phys. Chem. Chem. Phys.*, **2005**, *7*, 2740.

6. J. Kraitchman, *American Journal of Physics,***1953**, *21(1),* 17.

7. J. C. Cramer, *Essentials of Computational Chemistry*. Chichester, John Wiley & Sons, Ltd **(2002)**.

8. M. Head-Gordon, J. A. Pople, *Chem Phys. Lett*., **1988**, *153(6),* 503 and the references therein.

9. S. B. Boys, F. Bernardi, *Mol. Phys.,* **1970**, *19*, 553.

10. M.J Frisch, G. W. Trucks, H. B Schlegel, G. E. Scuseria, M. A.Robb, J. R.Cheeseman, J. A. Montgomery Jr., T. Vreven, K. N. Kudin, J. C. Burant, J. M. Millam, S. S. Iyengar, J. Tomasi, V. Barone, B. Mennucci, M. Cossi, G. Scalmani, N. Rega, G. A Petersson, H. Nakatsuji, M. Hada, M. Ehara, K. Toyota, R. Fukuda, J. Hasegawa, M. Ishida, T. Nakajima, Y. Honda, O. Kitao, H. Nakai, M. Klene, X. Li, J. E. Knox, H. P. Hratchian, J. B.Cross, C. Adamo, J. Jaramillo, R. Gomperts, R. E. Stratmann, O. Yazyev, A. J. Austin, R. Cammi, C. Pomelli, J. W. Ochterski, P. Y. Ayala, K. Morokuma, G. A. Voth, P. Salvador, J. J. Dannenberg, V. G. Zakrzewski, S. Dapprich, A. D. Daniels, M. C. Strain, O. Farkas, D. K. Malick, A. D. Rabuck, K. Raghavachari, J. B. Foresman, J. V. Ortiz, Q. Cui, A. G. Baboul, S. Clifford, J.

Cioslowski, B. B. Stefanov, G. Liu, A. Liashenko, P. Piskorz, I. Komaromi, R. L. Martin, D. J. Fox, T. M. Keith, A. Al-Laham, C. Y. Peng, A. Nanayakkara, M. Challacombe, P. M. W. Gill, B. Johnson, W. Chen, M. W. Wong, C. Gonzalez, J. A. Pople, *Gaussian03*, Revision C-02; Gaussian, Inc. Wallingford CT, **2004**

11. R. F. W. Bader, *Atoms in Molecules: A quantum theory,* Clarendon Press, Oxford, **1990**.

12. R. F. W. Bader, *Chem. Rev.,* **1991,** 91, 893.

13. P. L. A Popelier, *Atoms in Moleculer: An Introduction*, Pearson Education Limited **2000**, Edinburgh gate, Harlow, England.

14. U. Koch, P. L. A. Popelier, *J. Phys. Chem.* **1995**, *99*, 9747.

CHAPTER III

Rotational Spectroscopic and Theoretical Investigations on $CH_4 \cdots H_2S$ complex

III. 1. Introduction:

According to the new IUPAC definition, "The hydrogen bond is an attractive interaction between a hydrogen atom from a molecule or fragment X–H in which X is more electronegative than H, and an atom or a group of atoms in the same or a different molecule or fragment in which there is evidence of bond formation"[1]. Unlike the earlier definitions, where the hydrogen bond acceptors were atoms with higher electronegativity, this one does not put any conditions on the nature of the acceptor. One good example of nonconventional hydrogen bond acceptor is a hydrocarbon. In most of the unsaturated hydrocarbons, the delocalized π electrons are the hydrogen bond acceptors. Many such systems have been studied using rotational spectroscopy. Microwave spectroscopic studies give valuable information about the structure as well as the dynamics of these complexes in the supersonic beam. Some of the examples are C_6H_6-H_2O[2, 3], C_6H_6-H_2S[4], C_6H_6-HCN[5], C_2H_4-H_2O[6,7], C_2H_4-HF[8],C_2H_4-HCl[9], C_2H_4-H_2S[10], C_2H_2-HCl[11]. All these complexes have the hydrogen bond donor (H_2O, H_2S or HCN) positioned above the plane of the hydrocarbon and the H pointing towards the π cloud except for benzene-water. In C_6H_6-H_2O complex, H_2O is nearly a free rotor with both hydrogen atoms pointing towards the π cloud.

What about saturated hydrocarbons?? Compared to hydrocarbons having delocalized π electrons taking part in hydrogen bonding, less volume of work has been done for saturated hydrocarbons. Among this the complexes of methane are extensively studied. Methane, the major component of natural gas is a potential green house gas with high global warming potential. Hence, it is very important to understand the nature of intermolecular interaction of methane with other molecules in the atmosphere to understanding how the impurities in natural gas affect the

properties of methane, the main concern being the acidic and basic nature of methane. Whether methane will act as a proton donor or proton acceptor??

Microwave spectroscopy has confirmed the structures of CH_4-HF/HCl[12], CH_4-HBr[13], CH_4-H_2O[14] and CH_4-HCN[15]. All these complexes have geometries in which methane is the hydrogen bond acceptor. The hydrogen atom of the donor interacts with methane along any of the four tetrahedron faces of CH_4. In all the above CH_4 complexes, the fact that methane is the acceptor can be well understood by looking at the electronegativities of carbon and the X of H-X. The electronegativity[16] of carbon is 2.55 where as that of F is 3.98, Cl is 3.16, Br is 2.96 and O is 3.44. There is considerable difference in the electronegativity and hence the hydrogen attached to Y will be more acidic than the methane hydrogen.

The main objective of the present investigation is to examine the probability of CH_4 acting as a hydrogen bond donor/acceptor. Methane is a spherical top molecule. It has a charge distribution similar to Ar. The lowest non-vanishing multipole moment in methane is an octapole moment. It has symmetrically distributed four positive and four negative charges in the molecule. Is it possible for these positive centers to attract more electronegative atom? Theoretical investigations have shown that methane can form hydrogen bonded complexes with HF, HCl, H_2O and H_2S where CH_4 plays the role of a hydrogen bond donor[17, 18].However these are results of looking at the static minimum structure. Goswami and Arunan[19] have suggested a dynamic criterion. According to this criterion, formation of hydrogen bond is possible only if the zero point energy along the torsional coordinate that can break the H-bond is below the barrier along the coordinate**.**

In the current study interaction of CH_4 with H_2S is studied. The electronegativity of S is 2.58[16], which is comparable to that of carbon, 2.55. Both CH_4

and H_2S will have equal tendency to act as hydrogen bond donor. H_2S is a moderate acceptor of hydrogen bonds as well as donor, but has always been regarded as a weaker donor and acceptor of hydrogen bonds compared to H_2O. H_2S acts as a hydrogen bond donor in its complexes with benzene and ethylene. Nature of interaction of H_2O and H_2S under the same conditions shows considerable difference. Experimentally determined structure of CH_4–H_2O[14] has hydrogen of H_2O interacting with the tetrahedron face of methane. In C_6H_6-H_2O[2,3] complex both hydrogen of H_2O interact with the π cloud while in C_6H_6-H_2S[4] one of the S-H bond is pointing towards the π cloud to form hydrogen bonded system. But the complexes, C_2H_4-H_2O[6,7] and C_2H_4-H_2S[10], have similar geometries; the O-H and S-H hydrogen interact with the π cloud of ethylene. Complexes of phenyl acetylene with H_2O and H_2S gave entirely different geometries. Phenylacetylene –H_2O[20] has a nearly planar structure where the H_2O is donating its hydrogen to acetylenic π cloud forming O–H···π bond and the ortho C–H group of phenylacetylene forms a C–H···O hydrogen bond with the H_2O oxygen. Whereas in phenylacetylene-H_2S[21] complex has a structure in which H_2S is located over the phenyl ring π cloud. Also the H_2S unit is shifted from the phenyl ring center towards the acetylene group. Hence it is difficult to assume the nature of interaction and geometry of CH_4-H_2S complex.

The interaction of CH_4 with H_2S is studied using rotational spectroscopy and a detailed analysis of the nature of interaction is done using theoretical methods such as *ab initio*, AIM and NBO analysis.

III. 2. Experimental Details:

The rotational spectra of CH_4-H_2S and its isotopomers were recorded with the home-built Pulsed Nozzle Fourier Transform Microwave Spectrometer described in

detail in chapter II and the references therein. 1-2 % of CH_4 and H_2S were seeded into argon and the mixture was expanded from a backpressure of 0.5 atm to undergo supersonic expansion. At the pulsed nozzle, under the ambient conditions the complex of CH_4 and H_2S was formed. This sample was polarized using a microwave pulse of duration 1.5 μs. 1000 shots of gas pulses were averaged to get a reasonable signal to noise ratio. The signals were checked for the component dependence by running the experiments in the absence of CH_4 and H_2S and the signals did not appear in absence of either. To rule out any probability of the signal being dependent on the carrier gas, Ar, the signals were again recorded with He as the carrier gas. All the signal could be observed by using helium as a carrier gas, at a higher back pressure (~1.2 atm). CH_4-HDS/D_2S signals were observed by passing H_2S through HDO/D_2O. For this H_2S was passed through several bubblers placed sequentially which is filled with D_2O. The identity of the D_2S signals were confirmed by passing H_2S through a mixture of 50% H_2O/D_2O, which diminished the CH_4-D_2S signal significantly because of the relative higher concentration of HDS in the expansion. The relative increase in HDS concentration was confirmed by monitoring the Ar-HDS and Ar-D_2S signals[22]. The samples e.g. Ar (99.999%), CH_4 (99.9%) and H_2S (99.5%) were obtained from Bhuruka Gases Ltd and were used without any further purification. D_2O (99.95 atom% D) was obtained from Sigma- Aldrich.

III. 3. Results and Discussions:

III. 3. A. Search and Assignment:

Complexes of CH_4 with first-row hydrides, CH_4-HF[12] and CH_4-H_2O[14] have similar rotational constants, B = 4238.5328 MHz and 4346.7202MHz respectively. Hence, it can be expected that the second-row hydrides also will be having similar

rotational constants, i.e. CH_4-H_2S will have rotational constant similar to that of CH_4-HCl, but on the lower side. The J=1← 0 transition of CH_4-HCl is at 5815.8202 MHz. The search for CH_4-H_2S signal was started from 5800 MHz downwards. The first transition of the complex was observed at 5365.827 MHz. CH_4 can have nuclear spin states, I= 0, 1, 2 and for H_2S, I=0, 1. Depending on the coupling, a large number of states can be present. The search was continued further down from 5365.827 MHz. The frequency domain signal for the particular transition is shown in Figure. III. 1. The next signal was observed at 5186.105 MHz. A total of 8 transitions were observed in the initial search. Two transitions were observed for $J_{1\leftarrow0}$ and three transitions each for $J_{2\leftarrow1}$ and $J_{3\leftarrow2}$. The 8 transitions observed were assigned to three different progressions and each progression could be fitted independently to a linear top. The observed transitions are listed in Table. III. 1. Transitions at 5365.827 MHz, 10729.387 MHz and 16088.437 MHz were assigned to one progression; Progression I. Progression II has transitions at 10583.405 MHz and 15870.149 MHz. The transitions at 5186.105 MHz, 10372.485 MHz and 15559.236 MHz were assigned to Progression III. Progression I and Progression III have all the three $J_{1\leftarrow0}$, $J_{2\leftarrow1}$ and $J_{3\leftarrow2}$ transitions. But Progression II has only $J_{2\leftarrow1}$ and $J_{3\leftarrow2}$ transitions The fitted parameters are given in Table. III. 2. The rotational transitions for CH_4•••HDS and CH_4•••D_2S were also recorded. The transitions are listed from Table. III. 3 and the fitted parameters in Table. III. 4. For both the isotopomers, all the three transitions corresponding to the Progression I was obtained. Only one of the two transitions corresponding to Progression II could be observed. The search for lines of Progression III did not give any results. The $J_{1\leftarrow0}$ line of CH_4•••D_2S shows a hyperfine structure. This hyperfine structure arises due to the quadrupole coupling of the deuterium nucleus present and is shown in Figure. III. 2. At higher J transitions these

hyperfine splitting could not be resolved. A later search for $J_{4\leftarrow3}$ transitions succeeded in observing two more transitions for CH_4•••H_2S complex, each one belonging to Progression I (21440.744 MHz) and progression II (21244.323 MHz). Due to low sensitivity of the spectrometer in this region, an extensive search could not be carried out.

Fitting of the lines in Progression I of the parent compound gave the rotational constant, B = 2683.097 MHz and the distortion constant, D_J = 0.0939 MHz. Progression II and III lines on fitting gave a rotational constant, B=2638.2575 MHz and 2593.05 MHz respectively. The fitting gave a surprising value for the distortion constant as, D_J = -0.5209 MHz for Progression II and D_J = -0.0089 MHz for progression III. This negative distortion constant implies rotational-vibrational coupling present in the complex. The progression arises from some excited internal rotor/torsional state. The rotational constant obtained from Progression I transitions, 2683.097 MHz is the ground state rotational constant. The ground state rotational constant of the isotopomer, CH_4•••HDS is B = 2658.48 MHz and the D_J is 0.0899 MHz. Similarly for CH_4•••D_2S, B = 2625.04 MHz and D_J = 0.0479 MHz.

Figure III.1. Frequency domain signal of CH_4-H_2S at 5365.827 MHz (offset 126.9531 kHz)

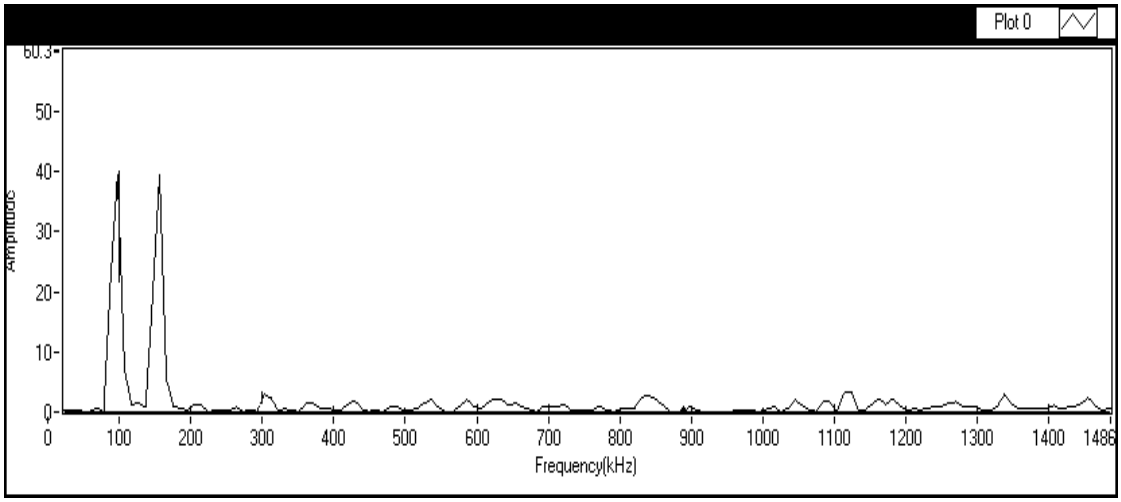

Table. III. 1: Experimentally observed rotational transitions of CH_4•••H_2S complex in MHz.

	Progression I	*Progression II*	*Progression III*
$J_{1\leftarrow0}$	5365.827	-----	5186.105
$J_{2\leftarrow1}$	10729.387	10583.405	10372.485
$J_{3\leftarrow2}$	16088.437	15870.149	15559.236
$J_{4\leftarrow3}$	21440.744	21244.323	------

Table. III. 2: Fitted Rotational Constant (B), Distortion Constant (D_J) for CH_4•••H_2S complex.

	Progression I	*Progression II*	*Progression III*
B (MHz)	2683.097(1)	2638.2575	2593.05(1)
D_J (MHz)	0.09390(7)	-0.5209	-0.0089(7)

Table. III. 3: Experimentally observed rotational transitions of CH_4•••HDS and CH_4•••D_2S complex in MHz.

	CH_4•••HDS		*CH_4•••D_2S*	
	Progression I	*Progression II*	*Progression I*	*Progression II*
$J_{1\leftarrow0}$	5316.4234	----	5249.839 5249.881	----
$J_{2\leftarrow1}$	10631.1755	10278.2462	10498.663	10157.9088
$J_{3\leftarrow2}$	15941.1215	----	15745.0489	----

Table. III. 4: Fitted Rotational Constant (B), Distortion Constant (D_J) of CH_4•••HDS and CH_4•••D_2S complexes.

	CH_4•••HDS	*CH_4•••D_2S*
B (MHz)	2658.48(8)	2625.04 (1)
D_J (MHz)	0.0899(5)	0.0479(9)

Figure. III. 2: Frequency domain signal of CH_4-D_2S $J_{1\leftarrow0}$ transition

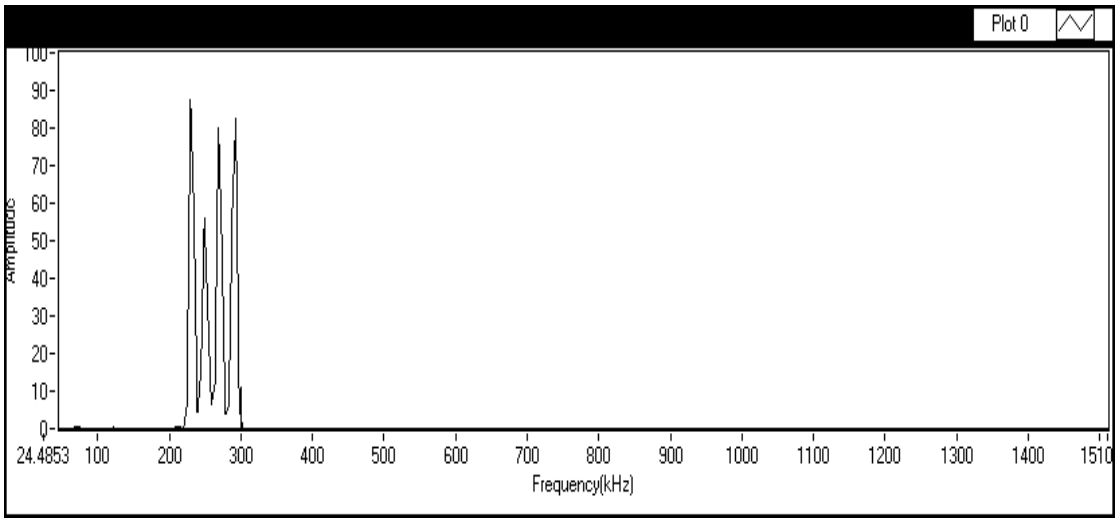

III. 3. B. Structure from rotational spectrum:

A comparison of the three progressions given in Table. III. 1. show that the Progression I and Progression III have $J_{1\leftarrow0}$ transitions as the lowest transition. The case is different in Progression II and it has its lowest transition from $J_{2\leftarrow1}$. From this observation it can be concluded that the lines assigned to Progression I and Progression III are due to transitions with internal angular momentum, m=0. The absence of $J_{1\leftarrow0}$ transition in Progression II confirms that the transitions belonging to this progression is due to transitions with higher internal angular momentum, m=1. From this it is evident that in the complex the monomers undergo internal rotation. The fact that the transitions could be fitted to linear top indicates that the two monomers can be considered as two interacting spheres. If it is so, then the monomers can undergo free rotation with respect to the other. As discussed in the previous section, the rotational constant obtained by fitting Progression I defines the ground

state structure of the CH_4•••H_2S complex. Similar is the case with the isotopomers, CH_4•••HDS and CH_4•••D_2S.

Considering CH_4 and H_2S as two spherical units, the intermolecular separation can be calculated from the ground state rotational constant, B.

$$\mu = \frac{m_1 m_2}{m_1 + m_2} \quad \text{---------- (1)}$$

$$I = \mu r^2 \quad \text{---------- (2)}$$

$$B = \frac{h}{8\pi^2 I} \quad \text{---------- (3)}$$

Here 'm_1' and 'm_2' are the total masses of the monomers CH_4 and H_2S respectively. 'μ' is the reduced mass of the whole system. 'r' is the distance between the center of mass of CH_4 and H_2S units. From equations (2) and (3), the 'r' value comes out to be 4.136 Å. Similar analysis for CH_4•••HDS and CH_4•••D_2S gave the intermolecular separation as 4.161 Å and 4.168 Å respectively. The ratio of the distance of center of mass of CH_4 and H_2S from the centre of mass of the molecule is roughly 2:1. Since the intermolecular separation is 4.136 Å the distance of CH_4 and H_2S from the center of mass of the molecule will be 2.811 Å and 1.325 Å respectively. This is possible if the sulphur is close to the center of mass of the molecule, or sulphur is pointing towards CH_4.

For a linear top, the distance of the substituted atom from the center of mass of the molecule is given by

$$|z| = \left[\frac{1}{\mu}(I_y' - I_y)\right]^{\frac{1}{2}} \quad \text{---------- (4)}$$

$$\mu = \frac{M * \Delta m}{M + \Delta m} \quad \text{---------- (5)}$$

I_y is the moment of inertia of the parent molecule (CH_4•••H_2S) and I'_y that of the substituted molecule (CH_4•••HDS). '*M*' is the mass of the parent isotopomers and '*Δm'* the difference in the isotopic mass, $\Delta m = m_D - m_H$. Using the above equations for single isotopic substitution, the distance of the substituted atom from the center of mass is found to be 1.3299 Å. For structure I in Figure. III. 3. the center of mass of the molecule coincides with the position of hydrogen in H_2S. Hence this structure is not possible since the distance of the hydrogen from the center of mass of the molecule is 1.3299 Å. In structure II (Figure. III. 3.) the center of mass of the molecule is close to the sulphur atom. This again supports the geometry in which sulphur is close to CH_4, since the distance of hydrogen from the center of mass of the molecule should be 1.3299 Å.

Figure . III. 3:

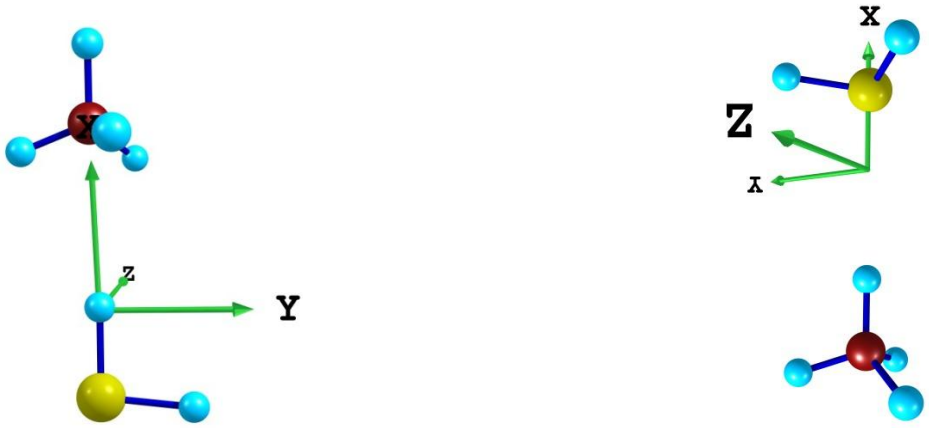

Structure I Structure II

From the experimental rotational transitions, the S of H_2S is close to CH_4 and CH_4 is the hydrogen bond donor in the CH_4-H_2S complex. To verify whether there is orientational preference or is the molecule really hydrogen bonded, the barrier for

internal rotation, the zero point energy along the torsional mode and AIM analysis have been carried out.

III. 4. Computational Methods:

Geometry optimizations using Gaussian 03[23] quantum chemical package were carried out on the different orientations for the complexes possible between CH_4 and H_2S to obtain the minimum energy structure. All calculations were done at MP2(full) level of theory at different basis sets, 6-311++G**, Aug-cc-pVDZ and Aug-cc-pVTZ. Frequency calculations were carried to ensure that the optimized geometries obtained were true minima. The frequency shifts on complex formation were also calculated. Bader's Atoms in Molecules theory[24] was used to obtain the electron densities and Laplacian of electron density and the other different properties of atomic basin required to shed more light on the nature of interaction. AIM2000 package[25] was used to get the properties of the atoms. Molecular electrostatic potential maps were obtained using Gauss View[26].

III. 4. A. Results and Discussion:

The molecular electrostatic potential map of CH_4 shown in Figure. III. 4, reveals the electron rich regions in the molecule. The blue color represents regions of positive potential and the regions of negative potential are denoted by red color. The centre of the tetrahedron face and the edges are having negative charges, the centre of the face being the more negative region. The hydrogen bond donors can approach CH_4 molecule along both the edge and face centre to form a hydrogen bond complex. The positive charge around the hydrogen atoms of CH_4 suggests a different donor-acceptor interaction, where CH_4 can act as the hydrogen bond donor. Same can be

reasoned for H_2S molecule. H_2S can donate the hydrogen to act as a hydrogen bond donor or the sulfur can accept a hydrogen atom. Since CH_4 can act as hydrogen bond donor as well as acceptor and similarly H_2S can be hydrogen bond donor or acceptor, different geometric orientations are possible for the complex between CH_4 and H_2S.

Figure. III. 4: The Molecular Electrostatic Map of CH_4 molecule:

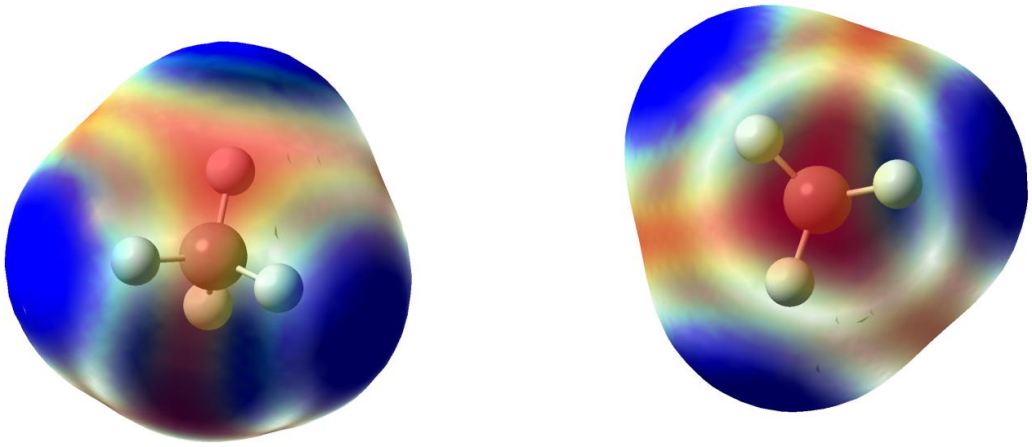

III. 4. A. 1. Results from *ab initio* calculations:

Three possible interactions between CH_4 and H_2S were considered: 1) H_2S as the hydrogen bond donor, 2) CH_4 as the hydrogen bond donor and 3) van der Waals complex of CH_4 and H_2S, showing C···S interaction.

For CH_4 acting as hydrogen bond acceptor, denoted as CH_4···HSH, two initial geometries were considered. One in which H-S bond is interacting with the tetrahedron face centre of CH_4 molecule and the second orientation in which the H-S bond of H_2S approaches CH_4 along the edge of CH_4 molecule.

In order to verify the probability of the edge of CH_4 acting as hydrogen bond acceptor, geometric optimization and frequency calculations have been carried out using different basis sets. Frequency calculations showed that the geometries obtained at 6-311++G** and Aug-cc-pVDZ basis sets are saddle points. Aug-cc-pVTZ gave a minimum energy structure, with $R_{C\cdots H}$ distance 2.8 Å and ∠CHS 177.43°. But in this minimum geometry H-S interacts with CH_4 through the tetrahedral face centre. This is because of the internal rotation of CH_4 molecule. The electron density at the edges of the CH_4 monomer is not sufficient to form a bound state or it is the transition state. This is clear from the potential energy surface obtained for the internal rotation of CH_4 molecule, Figure. III. 5. Interaction of S-H with the edge of CH_4 is a saddle point between the two minima where S-H interacts with the face centre. The energy difference between the minima and the saddle point is 0.06 kcal mol^{-1}.

Optimized geometries obtained at MP2(full) level with basis sets 6-311++G**, Aug-cc-pVDZ and Aug-cc-pVTZ for face centre of CH_4 acting as the hydrogen bond acceptor are minima energy structures as confirmed by the frequency calculations. The van der Waals radii of H, C and S are 1.2, 1.7 and 1.85 Å respectively. $R_{C\cdots H}$, the distance between S-H hydrogen and the carbon of CH_4, angle, ∠SHC, change in the S-H bond length, Δr_{S-H}, shift in H-S symmetric and asymmetric stretching frequencies upon complex formation, $\Delta\nu_S$ and $\Delta\nu_A$ and the interaction energies, ΔE at different basis sets are given in Table. III. 5. $R_{C\cdots H}$ is 2.604Å at MP2(full)/Aug-cc-pVTZ, which is less than the sum of the van der Waals radii of H and C. The bond angle, ∠SHC at the same level is 177.54°. ∠SHC is very close to linearity, characteristic of a hydrogen bond. From Table. III. 5 it is clear that there is not much change in the H-S bond length upon complex formation and the shift in the stretching frequency is negligible. Even though the numerical values of Δr_{S-H} and $\Delta\nu_{S-}$

$_H$ imply a very weak complex formation between CH_4 and H_2S, the interaction energy is quite significant. ΔE at MP2(full)/Aug-cc-pVTZ is -1.64 kcal $mol^{-1}$and the BSSE corrected interaction energy at the same level is -0.7 kcal mol^{-1}. The optimized geometries are shown is Figure. III. 6 (a).

Optimized geometries at different basis sets for the complex in which CH_4 acts as hydrogen donor and S of H_2S as the acceptor, $CH_3H\cdots SH_2$, is shown in Figure. III. 7 (a). The H-S distance, $R_{H\cdots S}$ is 3.026 Å at MP2(full)/Aug-cc-pVTZ. This distance is less than the sum of the van der Waals radii of H and S. The ∠CHS in CH_3-$H\cdots SH_2$ interaction is 179.8°. All geometric parameters and shift in C-H bond lengths, $\Delta r_{C\text{-}H}$ and the frequency shifts, $\Delta\nu_{C\text{-}H}$ at various basis sets are given in Table . III. 6. The shift in bond length and frequency are very small. Interaction energies from Table. III. 6 show that the complex is stable and has stabilization energy -1.18 kcal mol^{-1} at MP2(full)/Aug-cc-pVTZ level and the BSSE corrected interaction energy at the same level is -0.33 kcal mol^{-1}.

CH_4 and H_2S can interact in a third manner which is purely van der Waals or there is no hydrogen bond formation involved. The optimized geometry is shown in Figure. III. 8 (a) and geometric parameters in, Table. III. 7. The distance between S and C is 4.018 Å and the interaction energy is -0.85 kcal mol^{-1} at MP2(full)6-311++G**. This structure, stabilized by dispersive forces is interesting. Further analysis in the next section using atoms in molecules theory shows a direct interaction between C and S. Scheiner has studied complexes where phorphorous and nitrogen from two different monomers are directly interacting[27,28]. Here the electronegativity difference between P and N is large. Electronegativity[16] of P is 2.19 and that of N is 3.04. The electronegativities of C and S are 2.55 and 2.58. The fact that the interaction is between atoms with comparable electronegativity and more importantly it is the

carbon of CH_4, a spherical top molecule, directly taking part in the long range interaction makes it more interesting.

A comparison of Table. III. 5 and Table. III. 6 shows that the shift in the S-H bond length upon CH_4···H-SH formation and the shift in the C-H bond length upon CH_3-H···SH_2 complexation and the corresponding shift in the stretching frequencies are comparable. Even though the magnitude of the frequency shift is comparable, there is a striking difference in the nature of the shift. Complex in which H_2S is the hydrogen bond donor, both the symmetric and asymmetric stretching frequencies upon complexation show a blue shift. Where as in the complex having CH_4 as the hydrogen bond donor, the C-H stretching frequency shows a red shift on complexation. Interaction energies of the two complexes are also comparable. CH_4···H-SH has more stabilization energy than CH_3-H···SH_2. From *ab initio* calculations of the various interactions that are feasible between CH_4 and H_2S, CH_4 is a better acceptor of hydrogen bond than donor or H_2S has a greater tendency to donate hydrogen bond than accepting the bond.

The molecular electrostatic potential plots of the three above discussed geometries are given in Figure. III. 6 (b), 7 (b) and 8 (b). From the plots it is clear that in all the three cases, there is hardly any accumulation of electron density between CH_4 and H_2S. The bond lengths, bond angles and dihedral angles of the possible three structures optimized at various basis sets are given in Tables. III. 8 and Table. III. 9 have the normal mode vibrations of the complexes and are given at the end of this chapter.

Figure. III. 5: Potential Energy Surface for the internal rotation of CH_4 molecule

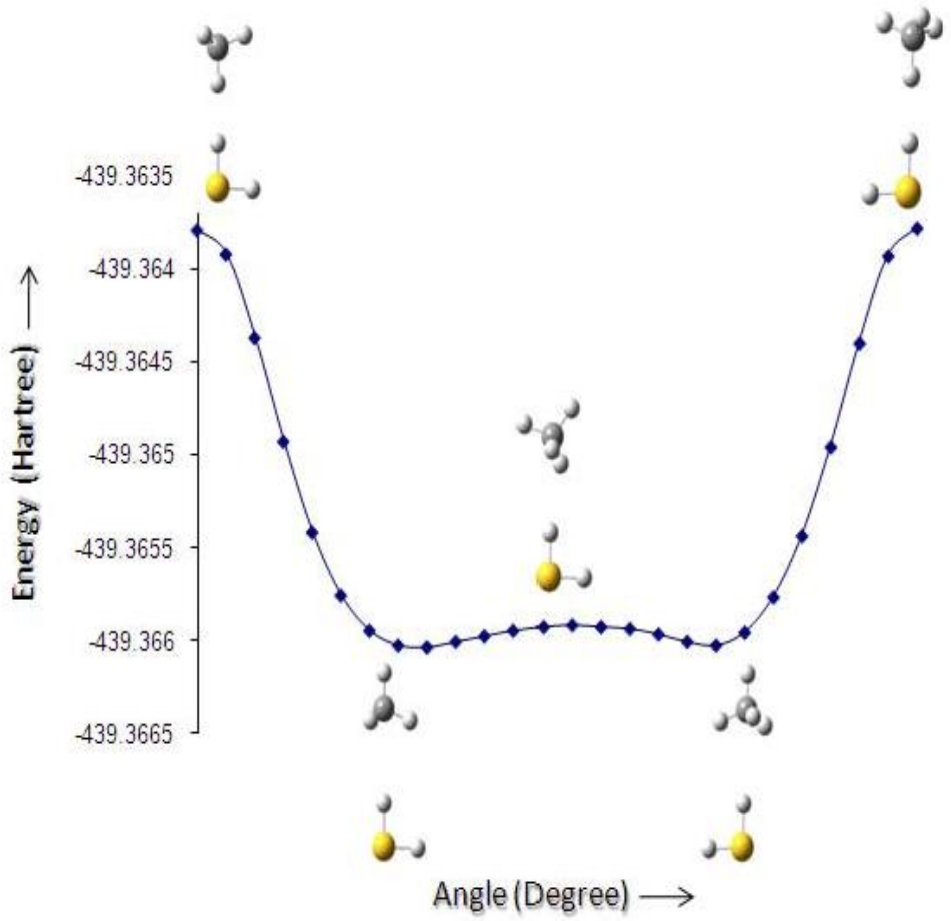

Figure. III. 6:

a) Optimized geometries of CH_4···HSH Complex at MP2(full)

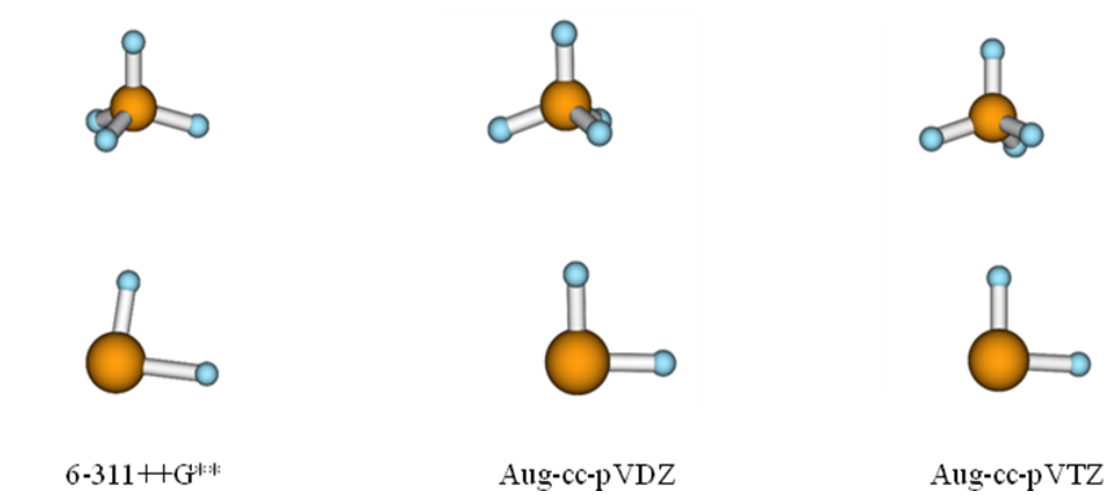

b) Molecular Electrostatic Plot of CH_4···HSH Complex at MP2(full)

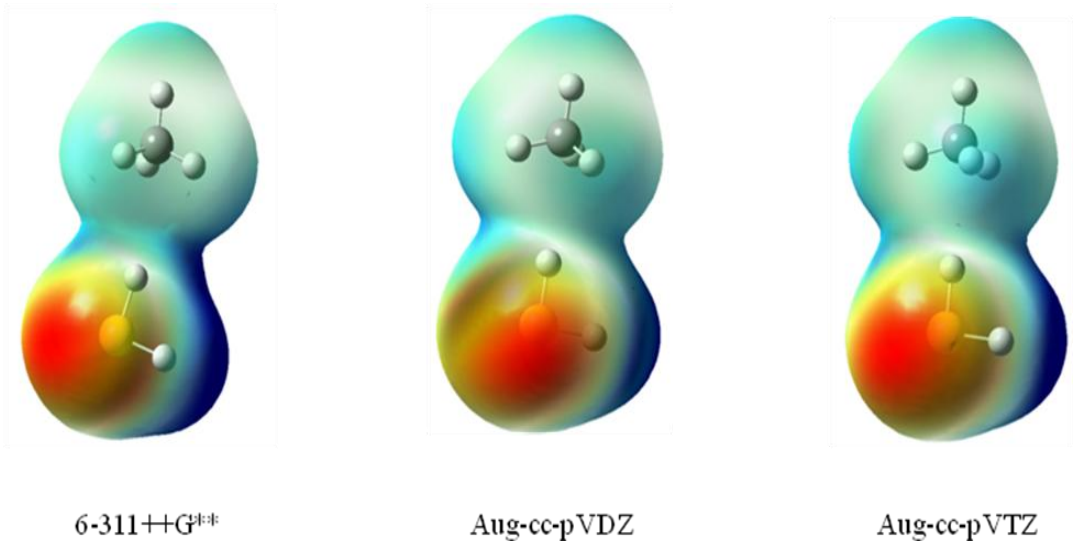

Figure. III. 7:

a) Optimized geometries of CH_3H···SH_2 Complex at MP2(full)

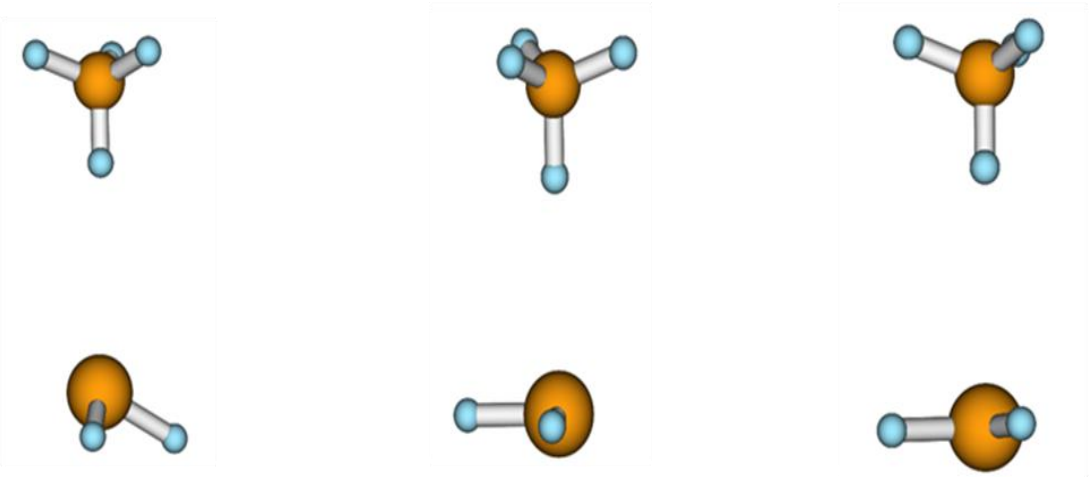

b) Molecular Electrostatic Plot of CH_3H···SH_2 Complex at MP2(full)

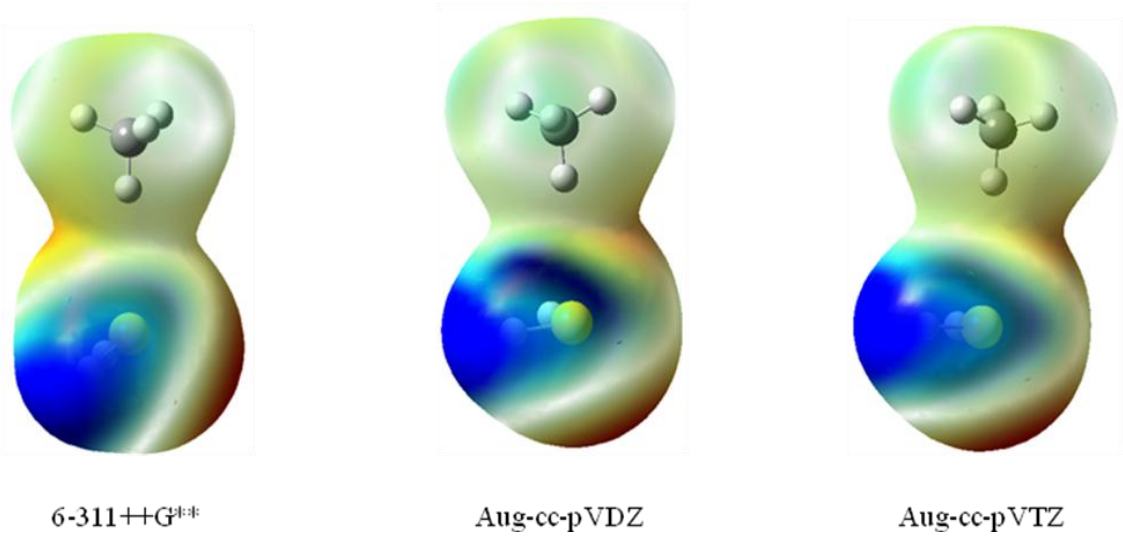

Figure. III. 8:

a) Optimized geometries and the Molecular Electrostatic Plot of H_4C···SH_2 Complex at MP2(full) /6-311++G**

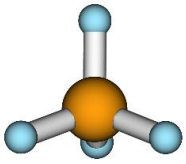

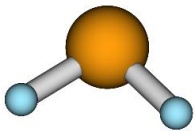

b) Molecular Electrostatic Plot of H_4C···SH_2 Complex at MP2(full) /6-311++G**

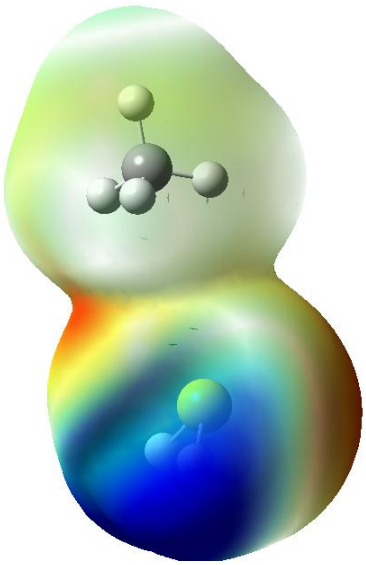

Table. III. 5: Optimized Bond lengths (Å), Bond angle (°), Shift in S-H bond length, Δr_{S-H} (Å), Shift in S-H Stretching Frequency $(\Delta\nu)^{\#}$ (cm^{-1}) and Interaction Energy ΔE (kcal mol^{-1}) of CH_4···HSH at MP2(full):

	$R_{C\cdots H}$	R_{S-H}	∠SHC	Δr_{S-H}	$\Delta\nu_s$	$\Delta\nu_A$	ΔE
6-311++G**	2.881	1.333	156.4	0.0003	3.87	3.78	-0.99
Aug-cc-pVDZ	2.697	1.348	177.7	0.0*	1.28	0.89	-1.45
Aug-cc-pVTZ	2.604	1.332	177.5	-0.0002	0.09	6.04	-1.64

*→ the difference in Δr is in the fifth decimal (-1E-05)

Table . III. 6: Optimized Bond lengths (Å), Bond angle (°), Shift in C-H bond length, Δr_{C-H} (Å), Shift in C-H Stretching Frequency $(\Delta\nu)^{\#}$ (cm^{-1}) and Interaction Energy ΔE (kcal mol^{-1}) of CH_3-H···SH_2 MP2(full):

	$R_{H\cdots S}$	R_{C-H}	∠CHS	Δr_{C-H}	Δν	ΔE
6-311++G**	3.083	1.089	178.1	-0.0004	-2.68	-0.97
Aug-cc-pVDZ	3.042	1.097	177.9	-0.0005	-0.20	-1.06
Aug-cc-pVTZ	3.026	1.084	179.8	0.0003	-6.35	-1.18

$^{\#}\Delta\nu = \nu$ (compex) – ν (monomer)

Table. III. 7: Optimized Bond lengths (Å), Bond angle (°) and Interaction Energy ΔE (kcal mol^{-1}) of $H_4C···SH_2$ MP2(full):

	$R_{C···S}$	∠SCH	ΔE
*6-311++G***	4.018	175.9	-0.85

III. 4. A. 2. Frequency Analysis:

The experimental data support the internal rotation of the monomers in the CH_4•••H_2S complex. *Ab initio* results support the formation of a hydrogen bonded complex whether it is CH_4•••HSH or CH_3H•••H_2S. Both the optimized structures have six intermolecular normal mode vibrations. If there is any normal mode in the molecule having zero point energy greater than the potential energy barrier along that coordinate, then the molecule can have free rotation.

The intermolecular vibrations in the CH_4•••HSH geometry at MP2(full)/Aug-cc-pVTZ are 25.80, 84.39, 98.75, 111.96, 117.29 and 150.91 cm^{-1}. Among these vibrations none of the modes can be explicitly assigned as intermolecular stretching. Vibration at 84.39 cm^{-1} is a intermolecular stretching mode slightly coupled with the rotation of H_2S about the c-axis of H_2S monomer. Rest of the five modes are due to internal rotation, mostly hindered. Vibration at 25.80 cm^{-1} is due to a hindered rotation of both CH_4 and H_2S, here the hydrogen of H_2S away from CH_4 undergo a large amplitude motion. 98.75 cm^{-1} corresponds to a rotation of H_2S about its c-axis. This motion can break the hydrogen bond, if it has zero point energy above the barrier for free rotation. 111.96 cm^{-1} is due to torsional motion of CH_4. Mode at 117.29 cm^{-1} has rotation of H_2S about the c-axis of H_2S monomer and 150.91 cm^{-1} has rotation of

H_2S along its C_2 axis. Vibration at 150.91 cm^{-1} involves a large amplitude wagging motion of the H_2S hydrogen close to the CH_4. This can again result in the breaking of the hydrogen bond, provided it has sufficient energy to cross the barrier. From these intermolecular vibrational frequencies it can be concluded that the interaction between CH_4 and H_2S is very weak. This is evident from the very small shift in the S-H stretching frequency listed in Table. III. 5. The shift in the symmetric stretching frequency upon complex formation is 0.09 cm^{-1} and that of the asymmetric stretch is 6.04 cm^{-1}.

Another interesting feature is the symmetric and asymmetric stretching modes of H_2S in CH_4•••HSH. The displacement of the atoms in the normal S-H stretching mode for the CH_4•••HSH complex and the H_2S monomer are shown in Table. III. 10. a and Table. III. 10. b respectively. From the table, it is clear that during symmetric and asymmetric stretch, the hydrogen atoms of H_2S undergo displacement of different magnitude in the complex compared to its displacement in the free monomer. This shows the presence of an interaction between H_2S and CH_4. In the complex, the two H_2S hydrogen behave differently during symmetric and asymmetric stretch. The difference in the displacement of the two hydrogen atoms along the X-axis of the complex, which is the direction in which the hydrogen bond is formed, is larger during the asymmetric stretch. This observation point that one mode is dominated by the stretch of bonded hydrogen while the other mode is dominated by the non-hydrogen bonded stretch.

Table. III. 10. a: Displacement of the atoms in the normal S-H stretching modes for the CH_4•••HSH at MP2(full)/Aug-cc-pVTZ level.

	Symmetric stretch			*Asymmetric stretch*		
	X	Y	Z	X	Y	Z
C	0 .00	.00	0.00	0.00	0.00	0.00
S	-0.01	-0.03	0.00	0.03	-0.01	0.00
H	0.00	0.00	0.00	0.00	0.00	0.00
H	0.00	0.00	0.00	0.00	0.00	0.00
H	0.00	0.00	0.00	0.00	0.00	0.00
H	0.00	0.00	0.00	0.00	0.00	0.00
H	*0.47*	*0.00*	*0.00*	*-0.88*	*-0.04*	*0.00*
H	-0.09	0 .88	0.00	-0.03	0.46	0.00

Table. III. 10. b: Displacement of the atoms in the normal S-H stretching modes of H_2S at MP2(full)/Aug-cc-pVTZ level.

	Symmetric stretch			*Asymmetric stretch*		
	X	Y	Z	X	Y	Z
S	0.00	0.03	0.00	0.03	0.00	0.00
H	0.52	-0.48	0.00	-0.51	0.49	0.00
H	-0.52	-0.48	0.00	-0.51	-0.49	0.00

Normal mode analysis of CH_3H•••H_2S complex (CH_4 is the hydrogen bond donor) shows similar trend. 10.98, 69.98, 71.28, 76.78, 137.41 and 147.32 cm^{-1} are the intermolecular vibrations. Unlike the intermolecular modes in CH_4•••HSH, in CH_3H•••H_2S one of the intermolecular vibration is purely due to intermolecular stretching, vibration at 71.28 cm^{-1}. 10.98 cm^{-1} has a torsional motion of CH_4 and hindered rotation of H_2S about c-axis of H_2S whereas at 69.98 cm^{-1}, H_2S rotation is about the C_2 axis of H_2S and CH_4 undergoes rotation about one of C_2 axis of the monomer, here both rotations are hindered. Vibration at 76.78 cm^{-1} is also similar except that the rotation of H_2S is about the monomers b-axis. 137.41 cm^{-1} mode has same vibrations as at 76.78 cm^{-1}. 147.32 cm^{-1} has a torsional motion of CH_4 and hindered rotation of H_2S about the C_2 axis of H_2S monomer. Here the intermolecular interaction is not strong enough to affect the normal modes of the CH_4 monomer.

The displacement of the atoms in the normal C-H stretching modes for the CH_3H•••SH_2 complex and the CH_4 monomer are shown in Table. III. 11. a and Table. III. 11, b respectively. The hydrogen bonded hydrogen shows same displacement during the C-H symmetric stretch in the complex as it has in the free monomer. The hydrogen retains its identity in complex and this indicates a weak interaction. The asymmetric stretch shows a difference in the displacement of hydrogen in the complex and in the monomer. C-H bond shows a slight red shift of 6.4 cm^{-1}, Table. III. 6, upon complex formation, which is a negligible shift to be listed as a unique feature of hydrogen bond. The hindered rotations in the complex indicated localized interaction which is very weak to perturb the normal mode of the monomer.

Table. III. 11. a: Displacement of the atoms in the normal C-H stretching modes for CH_3H•••SH_2 at MP2(full)/Aug-cc-pVTZ level.

	Symmetric			*Asymmetric*		
	X	Y	Z	X	Y	Z
C	0.0	0.0	0.0	-0.09	0.00	-0.01
H	0.16	0.41	-0.25	0.06	0.20	-0.12
H	0.16	-0.42	-0.24	0.06	-0.20	-0.12
H	0.18	0.01	0.47	0.10	0.01	0.32
H	*-0.48*	*0.0*	*0.01*	*0.87*	*0.00*	*-0.02*
S	0.0	0.0	0.0	0.0	0.0	0.0
H	0.0	0.0	0.0	0.0	0.0	0.0
H	0.0	0.0	0.0	0.0	0.0	0.0

Table. III. 11. b Displacement of the atoms in the normal C-H stretching modes for the CH_4 monomer at MP2(full)/Aug-cc-pVTZ level.

	Symmetric stretch			*Asymmetric stretch*		
	X	Y	Z	X	Y	Z
C	0.00	0.00	0.00	-0.04	0.02	-0.08
H	0.09	-0.42	-0.26	0.34	-0.04	-0.05
H	0.19	0.39	-0.25	-0.04	0.16	0.08
H	0.21	-0.03	0.45	-0.14	-0.26	0.15
H	*-0.49*	*0.06*	*0.05*	*0.36*	*-0.05*	*0.77*

Among the six intermolecular vibrations of the pure van der Waals complex of CH_4-H_2S obtained at MP2(full)6-311++G** level, two modes, 39.38 and 44.14 cm^{-1}, correspond to intermolecular stretch. The modes at 24.97, 85.35, 100.10, 131.54 cm^{-1} correspond to hindered rotation of CH_4 and H_2S in the complex. The S-H bond shows a slight red shift of 3.94 cm^{-1} in the asymmetric and 4.17 cm^{-1} symmetric stretching frequencies on complex formation. The red shift in the symmetric stretching frequency of C-H bond is negligible, 0.55 cm^{-1}.

III. 4. A. 3. Potential Energy Surface

The potential energy surface for various internal rotations of CH_4 and H_2S in the CH_4-H_2S were obtained to calculate the barrier height and to study which motions can break the hydrogen bond interaction.

In CH_4•••HSH, since H_2S is the hydrogen bond donor, internal rotation of the H_2S monomer can break the hydrogen bond interaction. From the frequency analysis it is clear that most of the intermolecular vibrational modes have contribution from the rotation of H_2S about its C_2 axis or about the c-axis of the monomer. Potential energy surface for the C_2 rotation and rotation about the c-axis of H_2S in CH_4•••HSH have been calculated at MP2(full)/Aug-cc-pVTZ level and are shown in Figure. III. 9 and Figure. III. 10 respectively. The energy barrier at this level for the rotation of H_2S about its C_2 axis is 0.69 kcal mol^{-1} (244.092 cm^{-1}). If the intermolecular vibration has energy greater than 244.092 cm^{-1}, then the hydrogen bond interaction can be broken and there will not be any orientational preference. For the rotation of H_2S about the c-axis, the barrier for rotation is 0.81 kcal mol^{-1} (282.55 cm^{-1}). The zero pint energy along the coordinate for rotation of H_2S about its C_2 axis and c- axis are 0.22 and 0.17

kcal mol^{-1} respectively, Table. III. 12. This energy is less than the barrier for free rotation. Hence there will be orientational preference.

Complex with CH_4 as the hydrogen bond donor, can have rotation about the C_3 axis and C_2 axis of CH_4 resulting in the breaking of the hydrogen bond. Potential energy surface obtained for the C_3 rotation of CH_4 in CH_3H•••SH_2 at MP2(full)/Aug-cc-pVTZ level and are shown in Figure. III. 11. The energy barrier is 0.47 kcal mol^{-1} (164.611 cm^{-1}). Similarly, the potential energy surface for the rotation of CH_4 about its C_2 axis gave an energy barrier of 0.42 kcal mol^{-1} (147.81 cm^{-1}). The potential energy surface is shown in Figure. III. 12. If any normal mode of CH_4 having energy greater than the barrier, it can result in the free rotation of the monomer. The zero pint energy along the coordinate for rotation of CH_4 about its C_3 axis and C_2 axis are 0.20 and 0.21 kcal mol^{-1} respectively, Table. III. 13. This energy is less than the barrier for free rotation. Hence there will be orientational preference.

Table. III. 12: The energy barrier and zero point energy in kcal mol^{-1} for CH_4•••HSH

Axis	***Barrier***	***ZPE***
C_2	0.69	0.22
c	0.81	0.17

Table. III. 13: The energy barrier and zero point energy in kcal mol^{-1} for CH_3H•••SH_2

Axis	***Barrier***	***ZPE***
C_3	0.47	0.20
C_2	0.42	0.21

Figure. III. 9: Potential Energy Surface for the rotation of H_2S about its C_2 axis in CH_4•••HSH

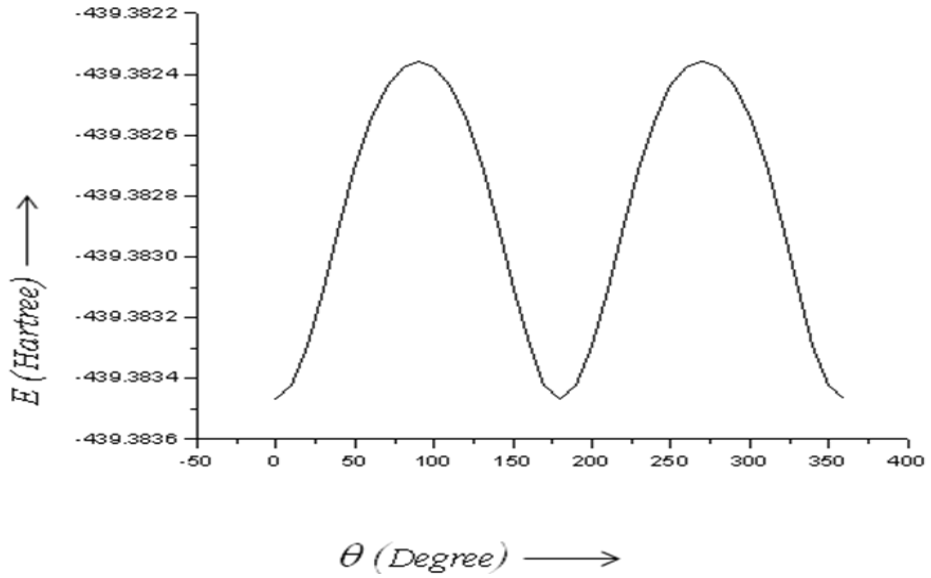

Figure .III. 10: Potential Energy Surface for the rotation of H_2S about its c-axis in CH_4•••HSH

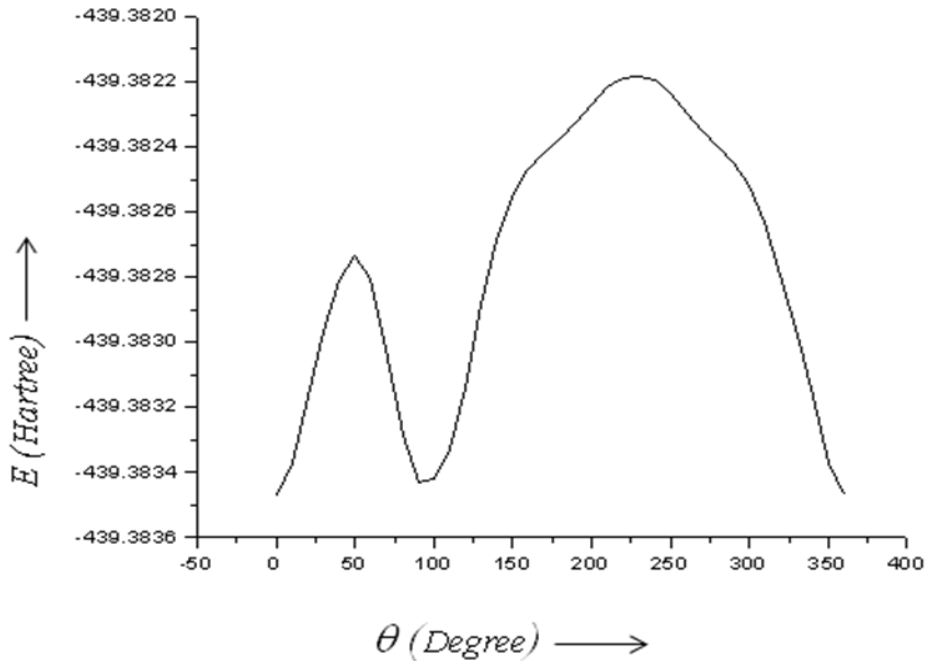

Figure. III. 11: Potential Energy Surface for the rotation of CH_4 about its C_3 axis in CH_3H•••SH_2

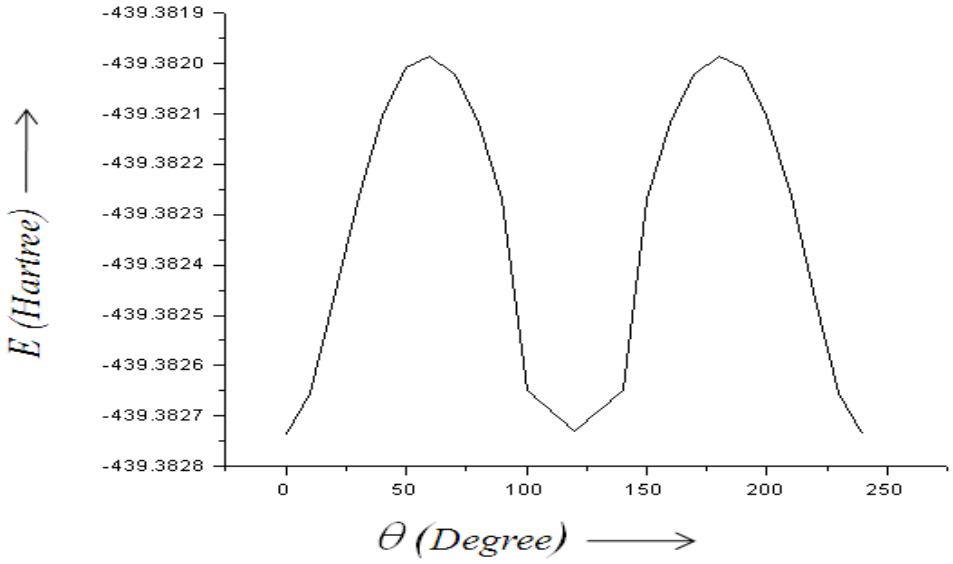

Figure. III. 12: Potential Energy Surface for the rotation of CH_4 about its C_2 axis in CH_3H•••SH_2

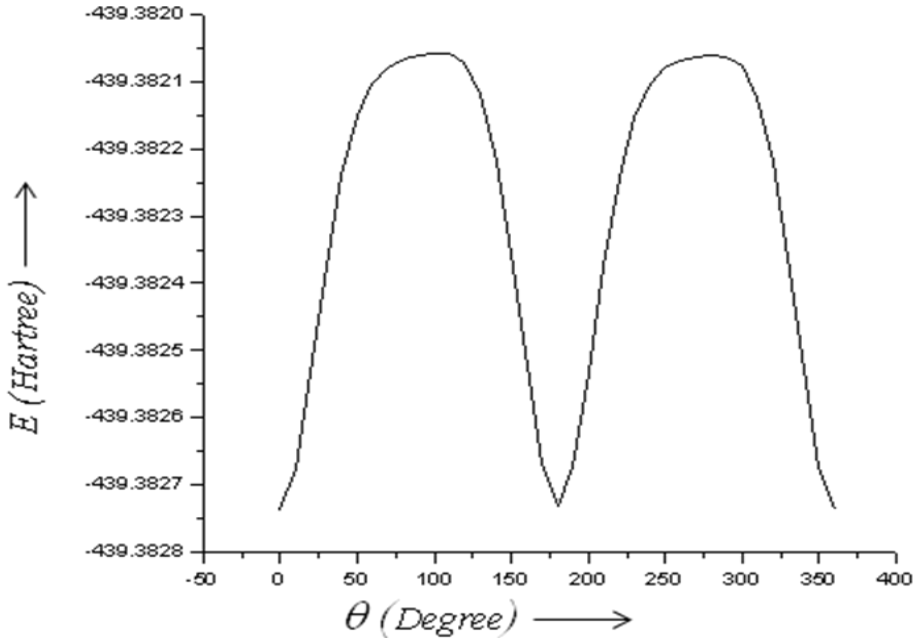

III. 4. B. Results from AIM calculations:

Atoms in molecules study of all the different minima obtained for the complex formed between CH_4 and H_2S have been carried out using AIM 2000 software[25]. The bond critical point or (3,-1) critical point between two interacting atoms and the presence of a bond path connecting the two interacting atoms are the necessary and sufficient condition to ascertain that the two atoms are bonded according to Bader[24]. Koch and Popelier[29,30] have suggested eight criteria on the basis of AIM theory which should be satisfied for a bond to be called as a hydrogen bond. According to Koch and Popelier, mutual penetration of H and acceptor atoms is the necessary and sufficient condition.

The eight criteria suggested by Koch and Popelier have been analyzed for both the geometries in with (a) methane and (b) H_2S act as the hydrogen bond acceptors. To verify the consistency of the results with basis sets, all the properties are analyzed at three different basis set level, 6-311++G**, Aug-cc-pVDZ and Aug-cc-pVTZ.

1) Topology: According to this criterion there should be a bond critical point, (3, -1), between interacting hydrogen atom and the acceptor atom and bond path passing through the BCP should connect both the interacting atoms. In CH_4•••HSH a bond critical point is present between CH_4 and H of H_2S. The bond path connects carbon of CH_4 and hydrogen of H_2S through the bond critical point and the bond path is linear. Hence from the topology analysis, the interaction is between carbon and hydrogen. Bond critical point is present between H of CH_4 and S of H_2S in CH_3H•••SH_2. The bond path connects hydrogen of CH_4 and sulphur of H_2S through the bond critical point and the bond path is linear. Hence from the topology analysis the interaction is between sulphur and hydrogen.

2) The Electron Density at the Bond Critical Point (ρ): For hydrogen bond the value of the electron density at the bond critical point proposed by the criterion lies between 0.002 to 0.04 au. Value of electron density at the bond critical point connecting C and H in CH_4•••HSH, ρ (bcp) is 0.004, 0.006 and 0.007 au at the basis sets 6-311++G**, Aug-cc-pVDZ and Aug-cc-pVTZ respectively. The charge density at the hydrogen bond critical point between H of CH_4 and S of H_2S in CH_3H•••SH_2 obtained at basis sets 6-311++G**, Aug-cc-pVDZ and Aug-cc-pVTZ are 0.0051, 0.0059 and 0.0061 au respectively. In both the cases values of ρ(bcp) at all basis sets are within the range suggested by Koch and Popelier. The electron densities are given in Table . III. 14. a.

3) The Laplacian of the charge density at the bond critical point (L): The Laplacian (L) for a hydrogen bond should be between -0.15 to 0.02 au. CH_4•••HSH has the value of L at hydrogen bond BCP as -0.004 (6-311++G**), -0.005 (Aug-cc-pVDZ) and -0.007 (Aug-cc-pVTZ) au. And the values of L for CH_3H•••SH_2 are -0.0039 (6-311++G**), -0.0043 (Aug-cc-pVDZ) and -0.0045 (Aug-cc-pVTZ) au. These values of L are within the range suggested by Koch and Popelier for a system to be called hydrogen bonded. The values of ρ(bcp) and L at various basis sets are given in Table.III. 14. a.

4) Mutual Penetration of Hydrogen and Acceptor Atom (Δr): Analysis at 6-311++G**, Aug-cc-pVDZ and Aug-cc-pVTZ gives a positive Δr value for penetration for hydrogen atom and the acceptor atom. The extent of mutual penetration of H and C in CH_4•••HSH are 0.47, 0.65 and 0.69Å and 0.52, 0.56 and 0.6Å for H and S in CH_3H•••SH_2 at 6-311++G**, Aug-cc-pVDZ and Aug-cc-pVTZ respectively. Hence

the criteria of mutual penetration are satisfied. The values of Δr at various basis sets are given in Table.III. 14. b.

5) Loss of charge of hydrogen atom (ΔN): The fifth criteria suggest a decrease in population of the hydrogen atom upon complex formation. From the calculations at all three basis sets the hydrogen atom of H_2S interacting with CH_4, in CH_4•••HSH suffers a loss of electron charge upon complexation. The extent of loss at 6-311++G**, Aug-cc-pVDZ and Aug-cc-pVTZ are -0.0005, -0.1217 and -0.00003 au respectively. In CH_3H•••SH_2, the difference in the population of the hydrogen of CH_4 involved in bonding at 6-311++G**, Aug-cc-pVDZ and Aug-cc-pVTZ are -0.0102, -0.0131 and -0.0125 au respectively. i.e. the H suffers a loss of population and hence follows the criteria. The values of ΔN at various basis sets are given in Table.III. 14. c.

6) Change in atomic energy (ΔE): The sixth criteria deals with destabilization of hydrogen atom. The H atom involved in bonding is destabilized by 0.0047, 0.0566 and 0.0038 a.u. at basis sets 6-311++G**, Aug-cc-pVDZ and Aug-cc-pVTZ respectively in the CH_4•••HSH complex. Similar to the hydrogen bonded hydrogen in the previous case, in CH_3H•••SH_2, the hydrogen of CH_4 also gets destabilized upon complex formation with H_2S. The magnitude of destabilization are 0.0092, 0.0099 and 0.0093 a.u. at 6-311++G**, Aug-cc-pVDZ and Aug-cc-pVTZ respectively. The values of ΔE at various basis sets are given in Table.III. 14. d.

7) Change in atomic first moment (ΔM): The dipolar polarization of the hydrogen atom should decreases on complex formation. The difference in the atomic first moment of the S-H hydrogen in CH_4•••HSH complex and H_2S monomer is -0.0103, -0.1031 and -0.0205 and that of C-H hydrogen in CH_3H•••SH_2 and CH_4 monomer is -0.0113, -0.0118, -0.0118 au at 6-311++G**, Aug-cc-pVDZ and Aug-cc-pVTZ

respectively. Hence, in all cases the complexation decreases the atomic first moment of hydrogen. The values of ΔM at various basis sets are given in Table.III. 14. e.

8) Change in atomic volume (ΔV): This criterion demands a decrease in the volume of the hydrogen bonded hydrogen upon complex formation. The difference in the atomic volume of H in the complex and in the monomer at 6-311++G**, Aug-cc-pVDZ and Aug-cc-pVTZ basis sets are -0.555, -3.1188 and -2.2367 au respectively in CH_4•••HSH complex. The extent of decrease in the H volume in CH_3H•••SH_2 at various basis sets are -0.0703 (6-311++G**), -0.5440 (Aug-cc-pVDZ) and -0.8051 (Aug-cc-pVTZ). The hydrogen atom, participating in the hydrogen bond formation in both cases follows the criteria; the volume of the hydrogen atom in the complexes is less than that in the monomer. The values of ΔV at various basis sets are given in Table.III. 14. f.

The hydrogen atoms involved in bonding in both geometries of CH_4-H_2S satisfies all the eight criteria by Koch and Popelier for a bond to be identified as hydrogen bond and are consistent with the basis sets.

Geometry optimization at MP2(full) with basis set 6-311++G** gave one more minimum energy structure (discussed in the previous section). AIM analysis carried out on the minima energy structure showed a bond critical point between CH_4 and H_2S. The interesting observation is that, the bond path passing through this critical point connects the carbon and sulphur. Hence from AIM analysis this complex formation between CH_4 and H_2S is due to the interaction between C and S and there is no hydrogen bonding in this structure. The electron density at the C-S bond critical point is 0.0024 au and the Laplacian at the bond critical point is -0.002 au. The bonded radius of carbon, r_C is 1.87Å and that of sulphur, r_S is 2.15Å.The non bonded radii are $r°_C$ and $r°_S$ are 2.07 and 2.26 Å. The extent of penetration, Δr, is positive and

the value is 0.31 Å. The penetration in this geometry is less than that in structures having hydrogen bond. The penetration reconfirms the C···S interaction. Figure. III. 13, (a), (b) and (c) shows bond critical points along with the bond path calculated using AIM theory for complexes, CH_4•••HSH, CH_3H•••SH_2 and H_4C•••SH_2 respectively.

Figure . III. 13 (a): CH_4···HSH Complex

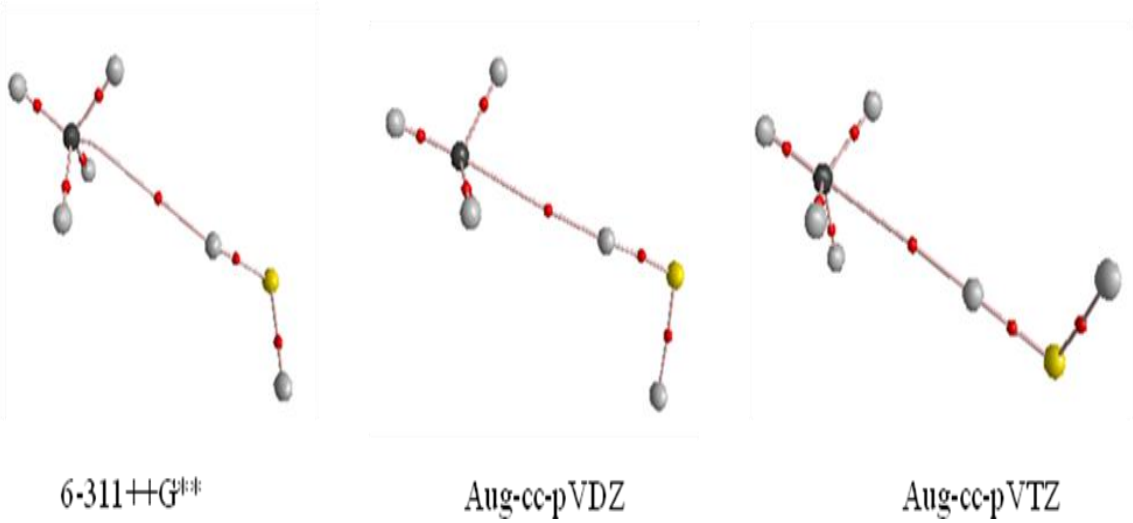

Figure III. 13 (b): CH_3H···SH_2 Complex

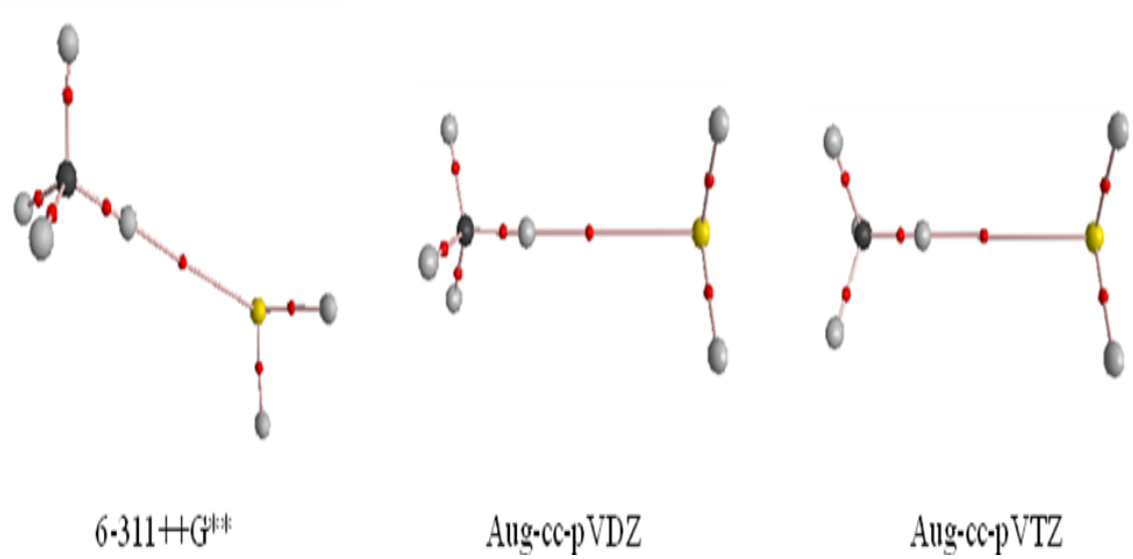

Figure III. 13 (c): H_4C···SH_2 Complex

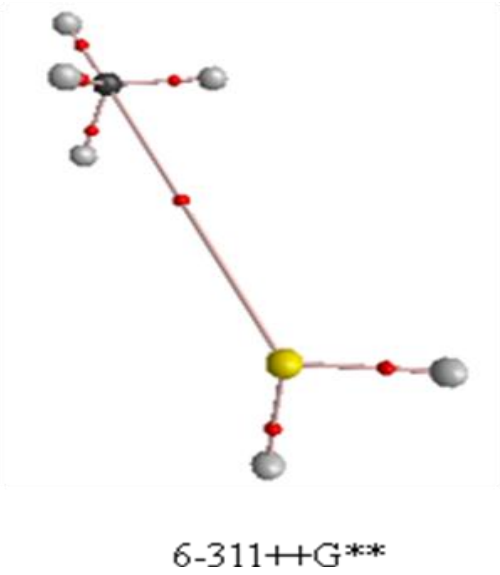

Table . III. 14: AIM analysis of the CH_4•••HSH, H_3CH•••SH_2 and H_4C•••SH_2 complexes

Table . III. 14. a: Electron density, ρ and Laplacian of electron density, L:

	*6-311++G***		*Aug-cc-pVDZ*		*Aug-cc-pVTZ*	
	ρ	L	ρ	L	ρ	L
CH_4•••HSH	0.0042	-0.0035	0.0056	-0.0053	0.0069	-0.0072
H_3CH•••SH_2	0.0051	-0.0039	0.0059	-0.0043	0.0061	-0.0045
H_4C•••SH_2	0.0024	-0.002	---	---	---	---

Table . III. 14. b: Penetration: Bonded (*r*b) and Nonbonded (*r*°) Radii (in Angstroms) and Penetration, Δr, Defined as the Sum of the Differences in Bonded and Nonbonded Radii of C/S and H.

Complex	*Basis set*	$r°_{C/S}$	$r^b_{C/S}$	$\Delta r_{c/s}$	$r°_H$	r^b_H	$\Delta r_{c/s}$	$\Delta r_{c/s}+\Delta r_{c/s}$
CH_4•••HSH	*6-311++G***	2.07	1.72	0.35	1.30	1.18	0.12	0.47
	Aug-cc-pVDZ	2.02	1.60	0.42	1.32	1.09	0.23	0.65
	Aug-cc-pVTZ	2.0	1.58	0.42	1.30	1.03	0.27	0.69
H_3CH•••SH_2	*6-311++G***	2.26	1.95	0.31	1.34	1.13	0.21	0.52
	Aug-cc-pVDZ	2.27	1.93	0.34	1.33	1.11	0.22	0.56
	Aug-cc-pVTZ	2.27	1.90	0.37	1.33	1.10	0.23	0.6

Table . III. 14. c: Change in the atomic population of the hydrogen atom (ΔN):

Complex	*Basis set*	$N(H)_{comp}$	$N(H)_{mono}$	ΔN
CH_4•••HSH	6-311++G**	1.0622	1.0627	-0.0005
	Aug-cc-pVDZ	1.1668	1.2885	-0.1217
	Aug-cc-pVTZ	1.03076	1.03079	-0.00003
H_3CH•••SH_2	*6-311++G***	0.9960	1.0062	-0.0102
	Aug-cc-pVDZ	1.0353	1.0484	-0.0131
	Aug-cc-pVTZ	1.0015	1.0140	-0.0125

*ΔN= $N(H)_{comp}$- $N(H)_{mono}$

Table . III. 14. d: Change in atomic energies of the H-bonded hydrogen (ΔE):

Complex	*Basis set*	$E(H)_{comp}$	$E(H)_{mono}$	Δ E
CH_4•••HSH	*6-311++G***	-0.6333	-0.6380	0.0047
	Aug-cc-pVDZ	-0.6682	-0.7248	0.0566
	Aug-cc-pVTZ	-0.6181	-0.6219	0.0038
H_3CH•••SH_2	*6-311++G***	-0.6164	-0.6256	0.0092
	Aug-cc-pVDZ	-0.6259	-0.6358	0.0099
	Aug-cc-pVTZ	-0.6249	-0.6342	0.0093

*ΔE= $E(H)_{comp}$- $E(H)_{mono}$

Table . III. 14. e: Change in atomic first moment of the H-bonded hydrogen (ΔM):

Complex	*Basis set*	$M(H)_{comp}$	$M(H)_{mono}$	ΔM
CH_4•••HSH	*6-311++G***	0.0333	0.0436	-0.0103
	Aug-cc-pVDZ	0.0771	0.1802	-0.1031
	Aug-cc-pVTZ	0.0294	0.0499	-0.0205
H_3CH•••SH_2	*6-311++G***	0.1194	0.1307	-0.0113
	Aug-cc-pVDZ	0.0909	0.1027	-0.0118
	Aug-cc-pVTZ	0.1145	0.1263	-0.0118

*ΔM= $M(H)_{comp}$- $M(H)_{mono}$

Table . III. 14. f: Change in atomic volume of the H-bonded hydrogen (ΔV):

Complex	*Basis set*	$V(H)_{comp}$	$V(H)_{mono}$	**ΔV**
CH_4•••HSH	*6-311++G***	54.9168	55.4723	-0.5555
	Aug-cc-pVDZ	57.4809	60.5997	-3.1188
	Aug-cc-pVTZ	50.5322	52.7689	-2.2367
H_3CH•••SH_2	*6-311++G***	51.0362	51.1065	-0.0703
	Aug-cc-pVDZ	52.4465	52.9905	-0.5440
	Aug-cc-pVTZ	50.2670	51.0721	-0.8051

*ΔV= $V(H)_{comp}$- $V(H)_{mono}$

III. 5. Discussion:

Three progressions were obtained for the CH_4•••H_2S complex. The progressions were independently fitted to a linear top Hamiltonian. Absence of $J_{1\leftarrow 0}$ transition in Progression II confirms the presence of higher internal angular momentum state, m=1. This also confirms the internal rotation of the monomers in the complex. Progressions II and III have negative centrifugal distortion constants. Hence both the states are from some excited internal rotation/torsional motion. Structural parameters obtained from the experimental rotational constant confirm the structure in which sulphur of H_2S is close to CH_4. This also supports the structure in which CH_4 is the hydrogen bond donor, if such an interaction is present. The *ab initio* results show that CH_4•••HSH interaction is more favorable than CH_3H•••SH_2, the energy difference between the two structures being 0.46 kcal mol^{-1} at MP2(full)/Aug-cc-pVTZ level. The shift in the H-X stretching frequency is a signature of hydrogen bond. The shift in the S-H and C-H stretching frequencies in CH_4•••HSH and CH_3H•••SH_2 are negligible to consider it as a hydrogen bond. In addition to these two possible interactions calculations at MP2(full)/6-311++G** gave a third minimum energy structure where there is direct interaction between carbon and sulphur. Potential energy surface for the various possible internal rotations that can break the hydrogen bond interaction were obtained at MP2(full)/Aug-cc-pVTZ level to very if there is orientational preference and therefore hydrogen bonding. In all the possibilities, the zero point energy along the torsional coordinate that can break the hydrogen bond interaction is less than the barrier along that coordinate. Hence there is orientational preference and the nature of interaction is hydrogen bonded. To further verify the hydrogen bond interaction Atoms In Molecules analysis is carried out. The three optimized structures show a bond critical point connecting the atoms in both the

monomers. The hydrogen atom involved in the intermolecular interaction in both cases, CH_4•••HSH and CH_3H•••SH_2, satisfy all the eight criteria proposed by Koch and Popelier for a bond to be called H-bond. The third possible geometry shows a bond critical point between C and S and the both path connects the bond critical point and the two atoms, C and S.

III. 6. Conclusions:

Rotational spectrum confirms the formation of CH_4•••H_2S complex. It also confirms the presence higher internal angular momentum states. *Ab initio* results show that CH_4•••HSH interaction is more favorable than CH_3H•••SH_2. In both cases, the zero point energy along the torsional coordinate is lower than the barrier for free internal rotation along that coordinate. Even though the shift in S-H stretching frequency in CH_4•••HSH is small, the displacement of hydrogen during the stretch in the complex and in the monomer shows large difference. Similarly, C-H stretching frequency in CH_3H•••SH_2 does not undergo much shift on complexation. But the displacement the hydrogen atom undergoes during the stretch in the complex is larger than that it undergoes in the free monomer. The hydrogen atom involved in the intermolecular interaction in both cases, CH_4•••HSH and CH_3H•••SH_2, satisfy all the eight criteria proposed by Koch and Popelier for a bond to be called H-bond. Theoretical calculations gave a third minimum where there is direct interaction between carbon and sulphur. This C···S interaction is further confirmed by AIM analysis which shows a bond critical point between C and S. This structure is more interesting since the electronegativities of C and S are comparable. Fitting of the rotational transitions gives the structure in which sulphur of H_2S is pointing towards the methane molecule. The rotational spectrum also confirms internal rotation and the

floppy nature of the complex. Hence, there is unlikely to be any orientational preference, found in hydrogen bond and dispersion is the dominant force present in the complex.

III. 7. References:

1) E. Arunan, G. R. Desiraju, R. A. Klein, J. Sadlej, S. Scheiner, I. Alkorta, D. C. Clary, R. H. Crabtree, J. J. Dannenberg, P. Hobza, H. G. Kjaergaard, A. C. Legon, B. Mennucci, D. J. Nesbitt, *Pure Appl. Chem.,* **2011**, *83*,1637.

2) S. Suzuki, P. G. Green, R. E. Bumgarner, R. D. Suenram, S. Dasgupta, W. A. Godderd III , G. A. Blake, *Science*, **1992**, *257*, 942.

3) H. S. Gutowsky, T. Emilsson, E. Arunan, *J. Chem. Phys.,* **1993,** *99*, 4883.

4) E. Arunan, T. Emilsson, H. S. Gutowsky, G. T. Fraser, G. de. Oliveria, C. E. Dykstra, *J. Chem. Phys.,* **2002**, *117* ,9766

5) H. S. Gutowsky, E. Arunan, T. Emilsson, S.L Tschopp, C. E. Dykstra, *J. Chem. Phys.*, **1995**, *103*, 3917.

6) K. I. Peterson, W.Klemperer, *J. Chem. Phys.,* **1986**, *85*, 725.

7) A. M. Andrews, R.L. Kuczkowski, *J. Chem. Phys.,* **1993**, *98*, 791.

8) J. A. Shea, W. H. Flygare, *J. Chem. Phys.,* **1982,** 76, 4857.

9) P. D. Aldrich, A. C. Legon, W. H. Flygare, *J. Chem. Phys.*, **1981**, *75*, 2126.

10) M. Goswami, P. K. Mandal, D. J. Ramdass, E. Arunan, *Chem. Phys. Lett*, **2004**, *393*, 22.

11) A. C. Legon, P. D. Aldrich, W. H. Flygare, *J. Chem. Phys*,**1981**, *75*, 625.

12) A. C. Legon, B.P. Roberts, A.L. Wallwork, *Chem. Phys. Lett*., **1990**, *173(1)*, 170.

13) M. J. Atkins, A.C. Legon, A.L. Wallwork, *Chem. Phys. Lett*., 1992, 192, 368.

14) R. D. Suenram, G. T. Fraser, F. J. Lovas, Y. Kawashima, *J. Chem. Phys.*, **1994**, *101(9)*, 7230.

15) A. C. Legon, A. L. Wallwork, *J. Chem. Soc. Faraday Trans*., **1992**, *88(1)*, 1.

16) A.L. Allred, *J. Inorg. Nucl. Chem.*, **1961**, *17*, 215.

17) B. Raghavendra, E. Arunan, *Chem. Phys. Lett.*, **2008**, *467*, 37.

18) C. Rovira, J. J. Novoa, *Chem. Phys. Lett.*, **1997**, *279*, 140.

19) M. Goswami, E. Arunan, *Phys. Chem. Chem. Phys*, **2009**, *11*, 8974.

20) M. Goswami, E. Arunan, *Phys. Chem. Chem. Phys*., **2011**, *13*, 14153.

21) M. Goswami, E. Arunan, *J. Mol. Spect.,* **2011**, *268*, 147.

22) H. S. Gutowsky, T. Emilsson, E. Arunan, *J. Chem. Phys*., **1997**, *106*, 5309.

23) M. J. Frisch, G. W. Trucks, H. B Schlegel, G. E. Scuseria, M. A.Robb, J. R.Cheeseman, J. A. Montgomery Jr., T. Vreven, K. N. Kudin, J. C. Burant, J. M. Millam, S. S. Iyengar, J. Tomasi, V. Barone, B. Mennucci, M. Cossi, G. Scalmani, N. Rega, G. A Petersson, H. Nakatsuji, M. Hada, M. Ehara, K. Toyota, R. Fukuda, J. Hasegawa, M. Ishida, T. Nakajima, Y. Honda, O. Kitao, H. Nakai, M. Klene, X. Li, J. E. Knox, H. P. Hratchian, J. B.Cross, C. Adamo, J. Jaramillo, R. Gomperts, R. E. Stratmann, O. Yazyev, A. J. Austin, R. Cammi, C. Pomelli, J. W. Ochterski, P. Y. Ayala, K. Morokuma, G. A. Voth, P. Salvador, J. J. Dannenberg, V. G. Zakrzewski, S. Dapprich, A. D. Daniels, M. C. Strain, O. Farkas, D. K. Malick, A. D. Rabuck, K. Raghavachari, J. B. Foresman, J. V. Ortiz, Q. Cui, A. G. Baboul, S. Clifford, J. Cioslowski, B. B. Stefanov, G. Liu, A. Liashenko, P. Piskorz, I. Komaromi, R. L. Martin, D. J. Fox, T. M. Keith, A. Al-Laham, C. Y. Peng, A. Nanayakkara, M. Challacombe, P. M. W. Gill, B. Johnson, W. Chen, M. W. Wong, C. Gonzalez, J. A. Pople, *Gaussian03*, Revision C-02; Gaussian, Inc. Wallingford CT, **2004**

24) R. F. W. Bader, *Atoms in Molecules: A Quantum Theory;*Clarendon Press: Oxford, **1990**.

25) F. Biegler-Konig, J. Schonbohm, R Derdau, D Bayles, R. F. W Bader, *AIM 2000*, version 1; Bu¨ro fu¨r Innovative Software: Bielefeld, Germany, **2000**.

26) R. Dennington II., T. Keith, J.Millam, K. Eppinnett, W. L. Hovell, R. Gilliland, *GaussView*, Version 3.09; Semichem, Inc.: Shawnee Mission, KS, **2003**.

27) M. Solimannejad, M. Gharabaghi, S. Scheiner, *J. Chem. Phys.*, **2011**, *134*, 024312.

28) S. Scheiner, *J. Chem. Phys.*, **2011**, *134*, 164313.

29) P. L. A. Popelier, *Atoms in Molecules. An Introduction* (Prentice Hall, **2000**).

30) U. Koch, P.L. A. Popelier *J. Phys. Chem.,* **1995**, *99*, 9747.

Appendix:

Table. III. 8. Geometric Parameters:

a) Geometric Parameters of H_3C-H•••SH_2

Position of the atoms	Coordinates (in Å, deg)	MP2(FULL)/6-311++G**	MP2(FULL)/aug-cc-pVDZ	MP2(FULL)/aug-cc-pVTZ
C1	R(2-1)	1.090	1.098	1.085
H2	R(3-1)	1.090	1.098	1.085
H3	R(4-1)	1.090	1.098	1.085
H4	R(5-1)	1.089	1.097	1.084
H5	R(6-5)	3.083	3.042	3.026
S6	R(7-6)	1.333	1.348	1.332
H7	R(8-6)	1.333	1.348	1.332
H8	A(3-1-2)	109.34	109.31	109.36
	A(4-1-2)	109.38	109.32	109.36
	A(5-1-2)	109.62	109.70	109.62
	A(6-5-1)	178.07	177.88	179.84
	A(7-6-5)	117.09	92.83	92.87
	A(8-6-7)	92.07	92.50	91.916
	D(4-1-2-3)	-119.73	-119.58	-119.73
	D(5-1-2-3)	120.14	120.23	120.20
	D(6-5-1-2)	179.65	-42.21	117.08
	D(7-6-5-1)	126.39	77.34	-130.09
	D(8-6-7-5)	-122.04	91.83	92.98

b) Geometric Parameters of CH_4•••HSH

Position of the atoms	Coordinates (in Å, deg)	MP2(FULL)/6-311++G**	MP2(FULL)/aug-cc-pVDZ	MP2(FULL)/aug-cc-pVTZ
C1	R(2-1)	4.137	4.044	3.935
S2	R(3-1)	1.090	1.098	1.085
H3	R(4-1)	1.090	1.098	1.084
H4	R(5-1)	1.090	1.098	1.085
H5	R(6-1)	1.090	1.098	1.085
S6	R(7-2)	1.333	1.348	1.332
H7	R(8-2)	1.333	1.348	1.332
H8	A(3-1-2)	67.00	72.02	72.09
	A(4-1-2)	175.66	178.72	178.62
	A(5-1-2)	74.30	70.11	70.07
	A(6-1-2)	70.85	70.11	70.07
	A(7-2-1)	16.21	1.51	1.63
	A(8-2-1)	98.01	93.99	93.58
	D(4-1-2-3)	63.53	-179.80	180.00
	D(5-1-2-4)	179.09	60.46	60.49
	D(6-1-2-5)	-117.46	119.54	-120.99
	D(7-2-1-3)	93.15	179.99	180.00
	D(8-2-1-3)	135.96	180.00	180.00

c) Geometric Parameters of $H_4C{\bullet\bullet\bullet}SH_2$

Position of the atoms	Coordinates (in Å, deg)	MP2(FULL)/6-311++G**
C1	R(2-1)	1.090
H2	R(3-1)	1.090
H3	R(4-1)	1.090
H4	R(5-1)	1.090
H5	R(6-1)	4.018
S6	R(7-6)	1.333
H7	R(8-6)	1.333
H8	A(3-1-2)	109.19
	A(4-1-2)	109.65
	A(5-1-2)	109.37
	A(6-1-4)	175.89
	A(7-6-1)	125.855
	A(8-6-7)	92.00
	D(4-1-2-3)	-120.18
	D(5-1-2-3)	119.59
	D(6-1-4-3)	-121.86
	D(7-6-1-3)	4.99
	D(8-6-7-1)	-127.37

Table. III. 9. Normal mode vibrational frequencies

a) Normal mode vibrations of CH_4···HSH complex at MP2(full)

6-311++G**	Aug-cc-pVDZ	Aug-cc-pVTZ
26.53	11.78	25.80
42.40	65.59	84.39
58.42	79.23	98.75
64.45	94.85	111.96
99.87	109.32	117.29
166.83	139.86	150.91
1239.42	1199.68	1234.46
1359.80	1324.81	1362.91
1363.35	1329.70	1364.82
1366.94	1331.18	1365.17
1566.98	1556.67	1598.82
1572.57	1557.33	1599.86
2820.23	2765.63	2784.58
2840.27	2791.56	2805.35
3076.62	3062.28	3078.55
3211.05	3205.38	3198.36
3215.68	3205.76	3298.82
3217.90	3213.00	3200.81

b) Normal mode vibrations of H_3C-H···SH_2 complex at MP2(full)

6-311++G**	Aug-cc-pVDZ	Aug-cc-pVTZ
23.08	6.01	10.98
57.09	60.45	69.98
62.76	63.25	71.28
101.23	73.83	76.78
125.13	124.46	137.41
162.52	133.97	147.32
1230.55	1198.34	1228.52
1358.78	1321.09	1355.90
1370.33	1331.72	1369.74
1371.11	1332.02	1371.30
1573.91	1557.35	1602.58
1575.24	1557.86	1603.04
2817.59	2761.81	2782.62
2837.41	2788.28	2798.00
3077.73	3062.70	3076.46
3212.51	3205.96	3197.62
3212.79	3206.88	3198.62
3225.24	3213.43	3203.12

c) Normal mode vibrations of H_4C···SH_2 complex

MP2(full)/6-311++G**	
24.97	1362.35
39.83	1363.88
44.14	1365.17
85.35	1569.99
100.10	1570.77
131.54	2816.95
1230.71	2836.63
1362.35	3079.86
1363.88	3215.61

CHAPTER IV

Rotational Spectroscopic and Theoretical Investigations on Benzene-Ethylene Complex

IV. 1. Introduction:

Complexes of hydrocarbons containing π-system are very interesting to study since the fundamental question often asked is whether they will act as proton donor or acceptor in complexes. CH/π interactions have been the topic of broad interest among researchers for the last few decades due to their ubiquity in biological and chemical processes. It is the interaction between C-H and π - electron cloud of aromatic system or double/triple bonds. These interactions were first proposed by Nishio and coworkers[1] to explain some specific orientation in the systems having C-H and aromatic rings in close contacts. These interactions play an important role in controlling molecular recognition processes, in folding and unfolding of proteins and in crystal packing[2-4]. According to the recently recommended definition of hydrogen bond by IUPAC[5] these interactions are characterized as hydrogen bonds. These are one of the weakest H-bonds yet reported. These are interaction between a soft acid and a soft base. In case of C-H···π bonds involving sp2/sp3 C-H bond as donor, stabilization comes mainly due to dispersion and electrostatic interaction has almost negligible contribution (typically interaction energy varies from 1.5 to 2.5 kcal mol^{-1}). On the other hand in case of C-H···π interactions involving sp hybridized C-H bond or C-H bond in which carbon is attached with highly electronegative atoms such as in F_3CH···π, electrostatic interaction plays major role in the stabilization of the resulting complexes. Energy range for the C-H···π interactions covers *ca.* 1-7 kcal mol^{-1}.

Other interaction of prime interest is π-π interaction. Interaction between heterocyclic bases in DNAs and RNAs mainly involves H-bonding and stacking interactions (stacking). Nature and energetics of H- bonding involved in these base pairs are well known and with the help of most of the available quantum chemical

methods structure and energy of the system can be predicted. But in case of π-π stacking interactions, calculations do not give very accurate result. Indeed HF and DFT level calculations completely fail to reproduce/predict the structure and energetics of stacked systems. However, higher level calculations like CCSD(T)[6] with extended basis set do offer reliable results. The two interactions, CH-π and π--π have been studied though various theoretical and experimental methods[7-10]

In case of benzene dimer many structures are possible and the potential energy curve turns out to be very shallow and thus there is a possibility of interconversion among several possible structures. Most of the theoretical calculations done by now predict parallel-displaced structure (π-π interaction) to be global minimum for the dimer. But rotational spectroscopic experiments confirm T-shape structure of benzene dimer[11]which involves C-H···π interaction and to the best of our knowledge there have been no direct experimental evidence for π-stacked structure. π- stacked or parallel displaced geometries of benzene dimer do not have a permanent dipole moment and hence cannot be observed using rotational spectroscopy.

If we replace one of the benzene with ethylene, the resulting complex will have a net dipole moment in the π-stacked geometry and can be studied in the gas phase using microwave spectroscopic technique. In addition to the π-π interaction there can be C-H···π interaction between benzene and ethylene where the C-H of C_6H_6 can interact with the π-electron cloud of C_2H_4 or the C-H of C_2H_4 can interact with the π-cloud of C_6H_6. Thus, benzene-ethylene complex forms an ideal system to study the C-H···π interaction and the π-π interaction and the competition between the two. Considering the various ways in which benzene and ethylene can interact, the question addressed in the present work is 1) whether benzene and ethylene can have a

π - π interaction to give a stacked structure? 2) If the interaction is through hydrogen bond formation, which of the hydrocarbon will donate the C-H bond?

IV. 2. Computational Methods:

Geometry optimizations of the various possible interactions between benzene and ethylene were carried out to obtain the structural parameters and interaction energies. All calculations were done using Gaussian 03[12] quantum chemical package. Higher level *ab initio* calculations were done at MP2(full) using basis sets 6-311G** and 6-311++G**. The frequency shifts on complex formation were also calculated, since they are signatures for hydrogen bond formation. Bader's[13] Atoms in Molecules theory was used to obtain the electron densities and Laplacian of electron density and the other different properties of atomic basin required to shed more light on the nature of interaction. The properties of atoms were calculated using AIM2000[14] package. Molecular electrostatic potential maps were obtained using Gauss View[15].

IV. 3. Results from *ab initio* calculations:

Interaction of benzene with ethylene can result in complexes having entirely different nature. For example, benzene and ethylene can form π stacked or hydrogen bonded complex. Both benzene and ethylene have C-H group and π electron cloud. Two possible ways of interaction are 1) benzene C-H interacting with π electron cloud of C_2H_4, 2) C-H group of C_2H_4 can interact with the π electron cloud of C_6H_6, resulting in hydrogen bonded complex. Earlier theoretical analysis shows a strong interaction between ethylene C-H and benzene π-cloud[16]. The possible orientations of C_6H_6•••C_2H_4 complex were optimized at MP2(full) level of theory using basis sets 6-311G** and 6-311++G** using Gaussian 03. For that the monomer geometries were

optimized at the same level of theory and the structural parameters from these calculations are supplied as the input during the geometry optimization of the complex. All these structures turned out to be true minima. The binding energies were calculated using supermolecular approach. Optimized structures of these three possible geometries at MP2(full)/6-311++G** are shown in Figure. IV. 1. For the π-stacked geometry, structure I, the spacing between the two monomers, center of mass - centre of mass distance, at MP2(full) level using basis sets 6-311G** and 6-311++G** are 3.1922 and 3.2845 Å respectively. The corresponding interaction energies are -2.48 and -3.06 kcal mol^{-1}. The BSSE corrected interaction energy at MP2(full)/6-311++G** is -0.75 kcal mol^{-1}. Structure II, where C_2H_4 is placed above the benzene plane at an angle, the distance of the ethylene H interacting with the π cloud from the center of mass of C_6H_6 is 2.4855 and 2.5664 Å and the corresponding interaction energies are -2.57 and -4.07 kcal mol^{-1} at basis sets 6-311G** and 6-311++G** respectively. The BSSE corrected interaction energy at MP2(full)/6-311++G** is -1.41 kcal mol^{-1}. The change in the C-H bond length of the hydrogen bonded C-H group is 0.0081 and 0.008Å and the C-H bond show a large red shift in the stretching frequency of 66.61 and 37.79 cm^{-1}. The geometry in which C_6H_6 is the hydrogen bond donor, structure III, at MP2(full) basis set 6-311G** level gave the distance of the centre of mass of C_2H_4 to the hydrogen of C_6H_6 as 2.8787Å and 6-311++G** gave a distance of 2.8009Å. The benzene C-H bond shows lengthening of 0.0073Å in the bond length and the corresponding red shift in the C-H stretching frequency is 65.1cm^{-1}. Here the interaction energy is much less compared to the other two structures and it is -0.78 and -1.10 kcal mol^{-1} respectively at basis sets 6-311G** and 6-311++G**. These large red shifts may be contrasted to the small blue shift

predicted early for the T-shaped benzene dimer. However, even for benzene dimer, experiment showed a small red shift of ~ 3 cm^{-1}.[17,18]

To obtain a rotational spectrum, the system should have a permanent dipole moment. The calculated dipole moment, μ in Debye, along with the rotational constants of the three optimized structures, π stacked (structure 'I'), C_2H_4 as hydrogen bond donor (structure 'II') and C_6H_6 as hydrogen bond donor (structure 'III') are given in Table. IV. 1. The rotational constants of the structures are significantly different. Hence the rotational spectrum can be used to obtain the structure unambiguously. The optimized geometric parameters are given in Table. IV. 11. at the end of the chapter.

Table. IV. 1: Dipole moment and Rotational constants at MP2(full)/6-311++G**

	I	**II**	**III**
μ (D)	0.2201	0.2777	0.3337
A (GHz)	2.5453	2.7809	4.5679
B (GHz)	1.5705	1.2832	0.7380
C (GHz)	1.5076	1.2723	0.6635

Figure. IV. 1:

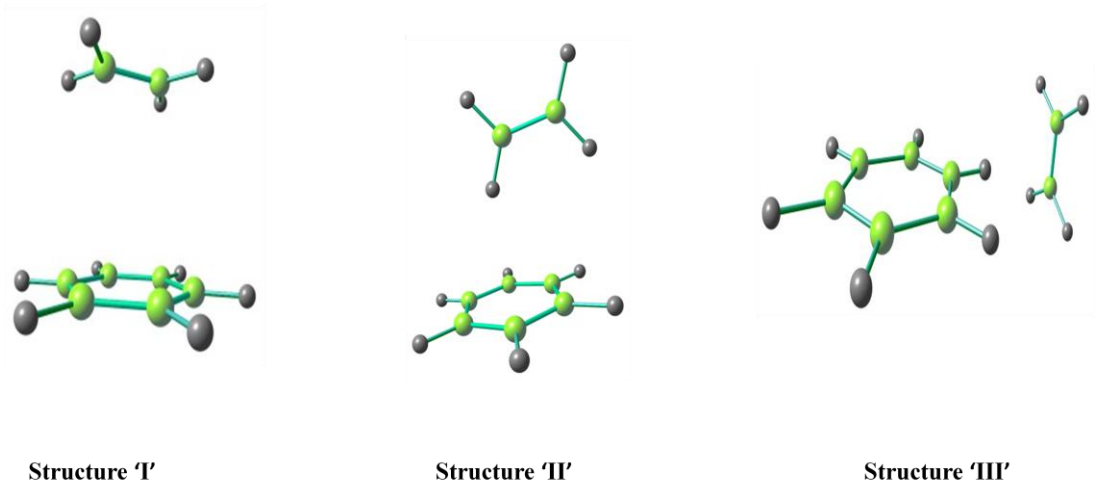

Structure 'I' Structure 'II' Structure 'III'

IV. 4. Experimental Details:

Home-built Pulsed Nozzle Fourier Transform Microwave Spectrometer, described in detail in chapter II and the references therein, is used to obtain the rotational spectrum of C_6H_6-C_2H_4 complex. Helium is used as the carrier gas during the experiment. C_6H_6 being in liquid state, to inject into the cavity, He at a rate of 5.0 SCCM is bubbled through the C_6H_6 sample taken in a bubbler. 1.0 SCCM of C_2H_4 is used. Since He is the carrier gas, back pressure of 1.2 atm is used for the supersonic expansion of the mixture. To maintain this back pressure the flow rate of He is kept at 200.0 SCCM. At the pulsed nozzle, the complex of C_6H_6-C_2H_4 is formed in a supersonic expansion. This sample is polarized using a microwave pulse of duration 1.5 μs. About 1500-2000 shots of gas pulses are averaged to get a reasonable signal to

noise ratio. The signals are checked for the component dependence by running the experiments in the absence of C_6H_6 and C_2H_4 and the signals did not appear in the absence of either. The signals are checked in Ar as carrier gas. The samples e.g. He (99.999%) and C_2H_4 (99.9%) were obtained from Bhuruka Gases Ltd and were used without any further purification. C_6H_6 (99.7%) was obtained from Sisco Research Laboratories Pvt. Ltd.

IV. 5. Search and Assignment:

Since there is no gas phase evidence for π stacked structure, the primary aim of this work was to obtain the C_6H_6-C_2H_4 π stacked structure. The search was started on the basis of the predicted rotational transitions made for π stacked structure. The predicted $J_{3\leftarrow2}$ transitions (3_{12} - 2_{11}) for the geometry is at 9326.523 MHz. The scan was started at 9500.0MHz and a downward search with a step size of 0.3MHz was performed. The first transition was observed at 7260.6737 MHz. All the three structures are nearly prolate top and the search was continued on the basis of modified predicted transitions. 24 transitions were observed during the search. All the lines could not be assigned to one structure. Of the 24 transitions, 20 transitions could be fitted to one of the optimized structures. Four transitions could not be assigned to any of the structures. Presence of these four transitions which are dependent on both benzene and ethylene suggests the existence of some other C_6H_6-C_2H_4 interaction. For a particular J, K can have the values 0, ±1, ±2…±J. For $J_{2\leftarrow1}$, both K=0 and K=1 transitions were observed. Similarly K=0 and K=1 transitions have been recorded for J"= 1→5. But the search did not give any higher K transitions. At all the Js' K=0 lines

show splitting. The transitions are listed in Table. IV. 2 and the unassigned lines in Table. IV. 3.

To obtain the rotational constants and distortion constants spectral fitting have been carried out where three plausible fitting of transitions are considered, i.e., along with K=1 transitions, in Fit I the higher component of the K=0 transitions is used, in Fit II the line centre of K=0 transitions are used and in Fit III the lower component of the K=0 transitions is used. Seven parameters could be obtained from the fitting of the transitions. The rotational constants obtained by Fit I are A=2.66(1) GHz, B=1223.717(4) MHz and C=1208.642(4) MHz. The standard deviation of the fit is 8.1 kHz. Fit I gives reasonable value for the rotational constants but the D_{JK} obtained is fairly large, 2.3241(1) MHz**.** Rotational constants for Fit II are A=5.4(1) GHz, B=1221.879(3) MHz and C=1206.794(4) MHz. Rotational constant A has high dependence on K=2 transition. The large uncertainty in A, in the order of MHz, is due to absence of higher K lines in the fitting. The fit has a standard deviation of 7.9 kHz. Fit III gives a very high value for the standard deviation, 8173.951 kHz and hence is not considered. The fitted parameters and the standard deviation are given in Table. IV. 4.

Table. IV. 2: Experimentally Observed Transitions, Assignments and their Residue

Transition	Frequency (MHz)	Line center of K=0	Res. Fit I	Res. Fit II
$1_{11}\rightarrow2_{12}$	4840.4016		-0.0030	-0.0125
$1_{01}\rightarrow2_{02}$	4849.8937	4857.2193	-0.0106	
$1_{01}\rightarrow2_{02}$	4864.5449			-0.0058
$1_{10}\rightarrow2_{11}$	4870.3145		-0.0146	-0.0127
$2_{12}\rightarrow3_{13}$	7260.6737		0.0050	-0.0000
$2_{02}\rightarrow3_{03}$	7274.7706	7285.6029	-0.0040	
$2_{02}\rightarrow3_{03}$	7296.4351			-0.0038
$2_{11}\rightarrow3_{12}$	7305.0982		-0.0057	-0.0055
$3_{13}\rightarrow4_{14}$	9680.9903		-0.0035	0.0018
$3_{03}\rightarrow4_{04}$	9699.5528	9713.7128	0.0094	
$3_{03}\rightarrow4_{04}$	9727.8728			0.0074
$3_{12}\rightarrow4_{13}$	9739.4313		0.0073	0.0065
$4_{14}\rightarrow5_{15}$	12101.3745		-0.0005	0.0118
$4_{04}\rightarrow5_{05}$	12124.1964	12141.4386	0.0076	
$4_{04}\rightarrow5_{05}$	12158.6807			0.0091
$4_{13}\rightarrow5_{14}$	12173.1683		0.0137	0.0145
$5_{15}\rightarrow6_{16}$	14521.7797		0.0013	-0.0068
$5_{05}\rightarrow6_{06}$	14548.6509	14568.6902	-0.0071	
$5_{05}\rightarrow6_{06}$	14588.7295			-0.0019
$5_{14}\rightarrow6_{15}$	14606.1567		-0.0085	-0.0093

Table. IV. 3: Unassigned lines

Frequency MHz
7323.7922
7321.2977
7345.0307
9709.4883

Table. IV. 4: Fitted Parameters for C_6H_6-C_2H_4 Complex

Parameters	**Fit I**	**Fit II**
A(GHz)	**2.66(1)**	**5.4(1)**
B(MHz)	**1223.717(4)**	**1221.879(3)**
C(MHz)	**1208.642(4)**	**1206.794(4)**
d_1(kHz)	**-3.71(9)**	**-3.84(7)**
d_2(kHz)	**-7(2)**	**-29(4)**
D_J(kHz)	**1.56(2)**	**2.31(4)**
D_{JK}(MHz)	**2.3241(1)**	**0.476(2)**
Sd(kHz)	**8.1**	**7.9**

IV. 6. Structure from rotational spectrum:

A comparison of the experimentally observed rotational constants (Table. IV. 4) with the rotational constants from the calculations (Table. IV. 1) reveal that the fitting of K=1 lines along with the higher component of K=0 transition of the benzene-ethylene complex, Fit I, gives rotational constants A=2.66(1) GHz, B=1223.717(4) MHz and C=1208.642(4) MHz which are close to the rotational constants predicted at MP2(full)/6-311++G** for the structure 'II' in which C_2H_4 is the hydrogen bond donor and the hydrogen of C_2H_4 interacts with the π-cloud of the C_6H_6 ring.

The B and C rotational constants obtained by Fit II for the benzene-ethylene complex are reasonably accurate compared to the A rotational constant. Comparison of Table. IV. 4 and Table. IV. 1 show that the experimental B and C, 1221.879(3)MHz and 1206.794(4) MHz are close to the one predicted for the structure 'II' in which C_2H_4 is the hydrogen bond donor than the π stacked geometry. The B and C of structure 'II' at MP2(full)/6-311++G** are 1283.2 MHz and 1272.3 MHz. From this comparison, the C_6H_6-C_2H_4 complex has a geometry in which the C-H bond of C_2H_4 is interacting with the π electron cloud of benzene, C-H/π interaction. The experimentally observed A, 5.4(1) GHz, has larger uncertainty in the fit. The experimentally observed A rotational constant of the C_6H_6•••C_2H_4 complex is close to the A rotational constant of benzene, 5.6 GHz. However it is very different from the calculated value for this structure. For A of the complex to be equal to the A of C_6H_6 monomer, C_2H_4 should approach benzene along it's 'a' axis. Also C_2H_4 should be a free rotor. Various plausible geometries were considered and the corresponding rotational constants were obtained. Benzene being an oblate top, the rotational

constants A and B are equal. Various geometrics are considered in which C_2H_4 approaches C_6H_6 along the 'a' and 'b' axis of C_6H_6. The various possibilities are shown in the Figure. IV. 2.

Structures A1, A2 and A3 have C_2H_4 approaching benzene along its a-axis. Structures A1 and A2 have the a-axis of C_6H_6 passing through the C-C bond of ethylene. Optimized geometries could not be obtained for these structures at MP2 (full) level using both the basis sets. A scan by varying 'r' gave minimum energy for these structures at r=3.0391Å and r=3.0537Å, where 'r' is the distance of the carbon of C_2H_4 from H of benzene interacting with ethylene. The rotational constants of structure A1 are A=5.40GHz, B=0.68GHz and C=0.60GHz. The rotational constants of structure A2 are A=5.46GHz, B=0.56GHz and C=0.51GHz. Structure A3 has the C-H of benzene interacting with the π cloud of C_2H_4. Here the plane of C_6H_6 and C_2H_4 are perpendicular to each other. The optimized geometry at MP2(full)/6-311++G** gave the distance of the benzene C-H hydrogen to the centre of mass of C_2H_4, r= 2.8009Å and the rotational constants as, A=4.57 GHz, B=0.74GHz and C=0.6 GHz. Calculations with basis set 6-311G** at MP2(full) gave 'r' as 0.8787Å and A, B and C as 4.57GHz, 0.72GHz and 0.65GHz.

Structures B1, B2, B3 and B4 have C_2H_4 approaching benzene along its b-axis. Structures B1 and B2 have the b-axis of C_6H_6 passing through the C-C bond of ethylene. In the optimized geometry B1, the distance of ethylene carbon from the center of the benzene C-C bond is, r= 3.6708Å and A, B and C are 5.467, 0.68 and 0.61 GHz. An optimized geometry could not be obtained for structure B2, since the monomers were drifting away with SCF iteration. The A, B and C at r=2.4294Å were 5.49, 1.04 and 0.87GHz and at r=4.8205Å, 5.46, 0.49 and 0.45GHz respectively.

Ethylene dimer[19] has a geometry in which both the C-C bonds of the monomers are perpendicular to each other. A similar geometry has been considered for C_6H_6•••C_2H_4 complex. Here, the ethylene C-C bond or the π-cloud of ethylene is perpendicular to the benzene C-C bond and the b-axis of benzene passes through the center of mass of ethylene. Two possibilities were examined, which differs in the orientation of C_2H_4 hydrogens with respect to benzene. Structure B3, has r=3.7265Å, distance of the center of mass of C_2H_4 from the center of C_6H_6 C-C bond, and rotational constants, A=4.62, B=0.83 and 0.74 GHz. Structure B4 gave r=3.6867Å and rotational constants as A=4.620, B=0. 8299 and C=0.7382 GHz

In all the above discussed geometries, even though the A rotational constant is close to the experimentally observed A, the B and C obtained theoretically and experimentally show a huge difference. Hence the possibility of C_2H_4 approaching C_6H_6 along its a-axis is rules out.

Figure. IV. 2:

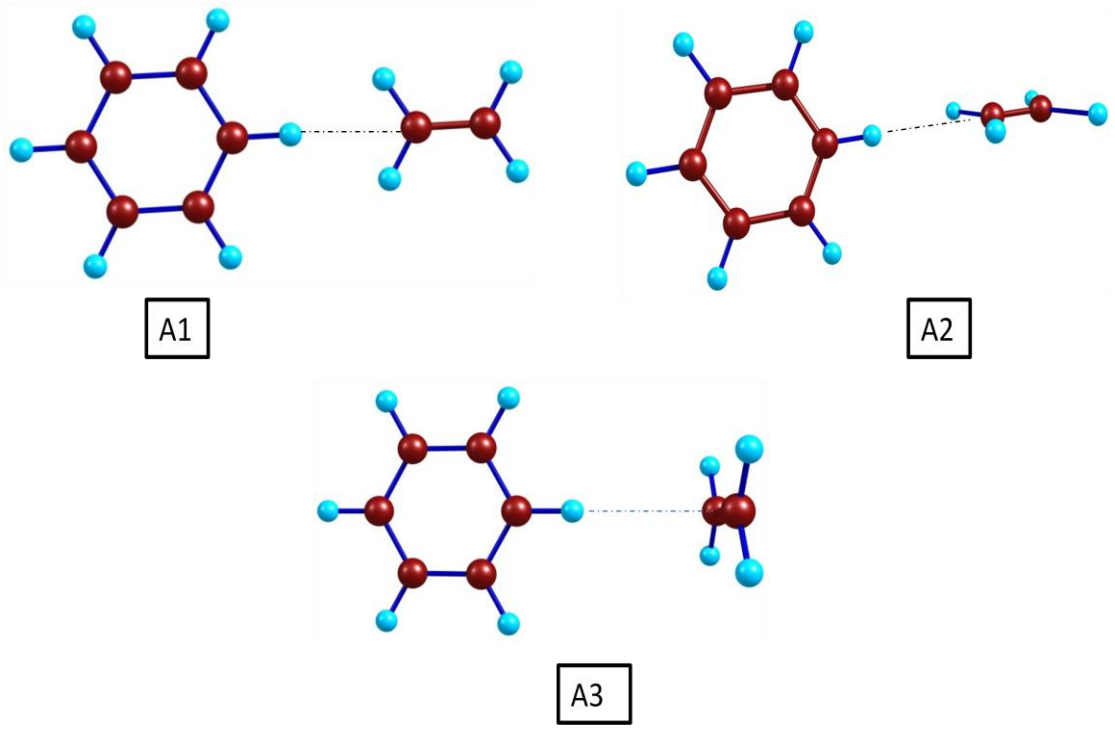

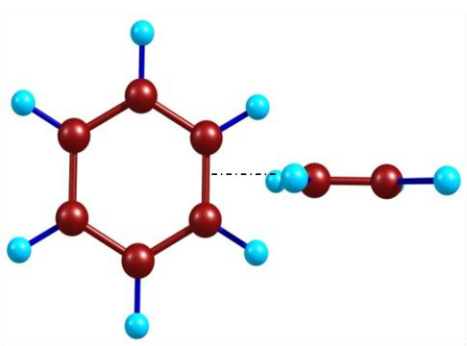

B1

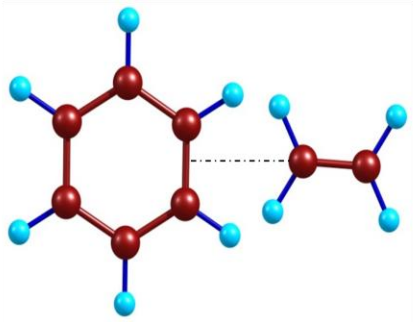

B2

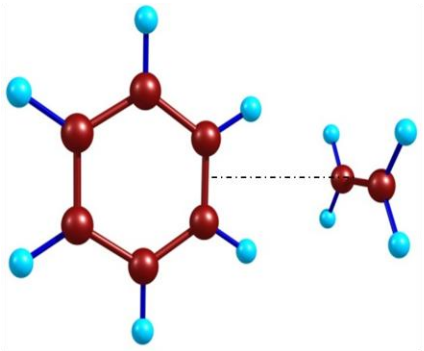

B3

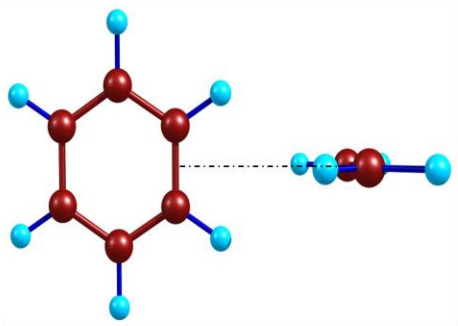

B4

Among the complexes of benzene with H_2O, H_2S and SO_2, C_6H_6-H_2O and C_6H_6-H_2S are symmetric top complexes where as $C_5{}^{13}CH_6$-H_2O[20] and $C_5{}^{13}CH_6$-H_2S[21] are asymmetric tops. The complex C_6H_6-SO_2[22] is also an asymmetric top complex. The rotational constants for $C_5{}^{13}CH_6$-H_2O and $C_5{}^{13}CH_6$-H_2S are 2.83[23] GHz and 2.84 GHz respectively. Both H_2O and H_2S are free rotors in the respective complexes with benzene and hence H_2O and H_2S do not contribute to the rotational constant about the axis. Hence the rotational constant in both the cases have major contribution from the benzene molecular frame and the rotational constant of the frame is 2.84 GHz which is close to the experimentally observed A rotational constant of $C_5{}^{13}CH_6$-H_2O and $C_5{}^{13}CH_6$-H_2S. The rotational constants A, B and C are 9031.936, 963.9484 and

892.568 MHz for C_6H_6-SO_2. Here the A rotational constant of the complex is close to the constant for free SO_2 perpendicular to its C_2 axis (8799.65 MHz). This is due to an internal rotation or tunneling motion between benzene and SO_2. Here benzene undergoes a free rotation about its C_6 axis and does not contribute to the moment of inertia of the molecular frame. For the rigid structure, the A should have been ~2240MHz, dramatically different from experimental value. C_6H_6-C_2H_4 may also be having a similar situation where C_2H_4 is having free rotation. That may be the reason for the difference in the experimentally observed A rotational constant (5.4(1) GHz) and the theoretically calculated (2.8 GHz).

The experimentally observed transitions for a particular rotational level fall in the same region as the predicted transitions for the structure 'II'. Table. IV. 5 list the experimental transitions along with the calculated transitions for the three optimized geometries. The line center for the K=0 transition is given in the table. Hence on the basis of the experimentally observed transitions, rotational constants obtained from Fit I and Fit II and its comparison with the theoretical results, it is concluded that benzene - ethylene interaction is an example of C-H/π interaction, where C-H group of C_2H_4 interacts with the benzene π-cloud. The question whether the complex is hydrogen bonded or is it pure van der Waals complex remains. To verify the possibility of the complex being hydrogen bonded AIM analysis has been done and is discussed in the next section.

Table. IV. 5: Transition Frequencies for Structures I, II and III and the Experimentally Observed Transitions

Transitions	*I*	*II*	*III*	*Experiment*
$2_{12} \rightarrow 3_{13}$	9137.910	7650.248	3990.676	7260.6737
$2_{02} \rightarrow 3_{03}$	9222.317	7666.412	4093.453	7285.60285
$2_{11} \rightarrow 3_{12}$	9326.523	7682.978	4202.738	7305.0982

IV. 7. Results from Atoms In Molecules Analysis:

AIM analysis of the benzene-ethylene complex, with ethylene C-H pointing towards the π-electron cloud of benzene shows interesting results. Two bond critical points are present between benzene and ethylene. Here bond path connects two ethylene hydrogens to C_6H_6 as shown is Figure. IV. 3.

Figure. VI. 3: Optimized geometry with bond critical point and bond path calculated using AIM theory of C_6H_6-C_2H_4 having C_2H_4 as H-donor.

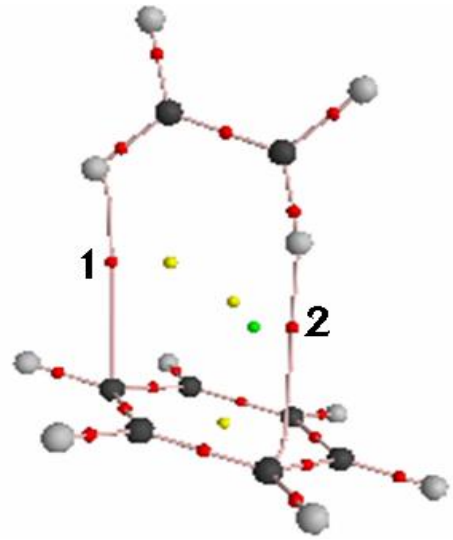

In addition to bond critical points, ring and cage critical points are also present between benzene and ethylene. The electron densities at both the bond critical points, ρ and its Laplacian of electron density, L are with the range suggested by Koch and Popelier[24,25] for hydrogen bond interaction. The ρ and L calculated at MP2(full) level with basis sets 6-311G** and 6-311++G** are given in Table. IV. 6.

Table. IV. 6: The electron densities at both the bond critical points, ρ and its Laplacian of electron density calculated using AIM theory

	MP2(full)/6-311G**		MP2(full)/6-311++G**	
	1	2	1	2
ρ(BCP)	0.0059	0.0072	0.004	0.0063
L	-0.0045	-0.0055	-0.0031	-0.0052

To analyze it further the atomic basin properties were considered. According to Koch and Popelier, on bond formation they suggest a decrease in population (ΔN) of the hydrogen atom, destabilization of hydrogen atom (ΔE), decrease in the dipolar polarization (ΔM) of the hydrogen atom and decrease in the volume (ΔV) of hydrogen atom. At MP2(full)/6-311G**, the hydrogen, H1, shows an increase in the population of the hydrogen atom on complex formation whereas the criteria demands a decrease. The criteria of destabilization of hydrogen atom and decrease in the atomic moment on complexation are satisfied by H1. But the hydrogen atom shows an increase in the volume of the hydrogen atom in the complex instead of a decrease as suggested. So H1 does not satisfy all the criteria proposed by Koch and Popelier. The hydrogen H2, shows a decrease in the population, ΔN= -0.0242 au, destabilization of hydrogen atom

on complex formation, ΔE=0.0184 au, decrease in the dipolar polarization of the hydrogen atom in the complex, ΔM=-0.0211 au and also the volume of the hydrogen atom decreases upon complex formation, ΔV=-7.2019 au. Hence H2 satisfies all the criteria for the hydrogen to be hydrogen bonded. Table. IV. 7 list the basis properties of hydrogen in the free monomer, in the complex and the difference. Same trends in the basis properties are obtained at MP2(full)/6-311++G** and are given in Table. IV. 8. From the AIM analysis, only one of the hydrogen atom of the ethylene forms hydrogen bond with the benzene π-cloud. Looking at the H···π distance, this is not surprising.

Table. IV. 7: AIM analysis at MP2(full)/6-311G**

H1	**Com**	**Mono**	**Diff**
N	0.9878	0.9778	0.01
E	-0.6143	-0.6165	0.0022
M	0.1192	0.1226	-0.0034
V	50.4272	49.7982	0.629

H2	**Com**	**Mono**	**Diff**
N	0.9536	0.9778	-0.0242
E	-0.5981	-0.6165	0.0184
M	0.1015	0.1226	-0.0211
V	42.5963	49.7982	-7.2019

Table. IV. 8: AIM analysis at MP2(full)/6-311++G**

H1	Com	Mono	Diff
N	0.9890	0.9751	0.0139
E	-0.6181	-0.6147	-0.0034
M	0.1236	0.1243	-0.0007
V	51.4114	49.8674	1.5440

H2	Com	Mono	Diff
N	0.9652	0.9751	-0.0099
E	-0.6071	-0.6147	0.0076
M	0.1026	0.1243	-0.0217
V	43.6065	49.8674	-6.2609

AIM analysis of the geometries in which benzene and ethylene are π- stacked and the one in which benzene is the hydrogen bond donor have been carried out at both MP2(full)/6-311G** and MP2(full)/6-311++G** since *ab initio* calculations show that they are minima energy structures.

Atoms In Molecules analysis of the π-stacked structure at MP2(full) with basis sets 6-311G** and 6-311++G** showed the presence of bond critical point between the two monomers, confirming possible interaction and is shown in Figure. IV. 4. There are two bond critical points connecting the two monomers. In addition to bond critical points, both ring critical point and cage critical point are present in the system between the two monomers. The presence of ring and cage critical points

between benzene and ethylene planes indicates the depletion of electron density between the plane of the monomers which indicates a weak interaction. The absolute value of electron density at the bond critical points 1 and 2 are same and is 0.0066 au and the Laplacian of electron density at the bond critical point is -0.0045 au.

Figure. IV. 4: Optimized geometry of π-stacked structure with bond critical point and bond path calculated using AIM theory.

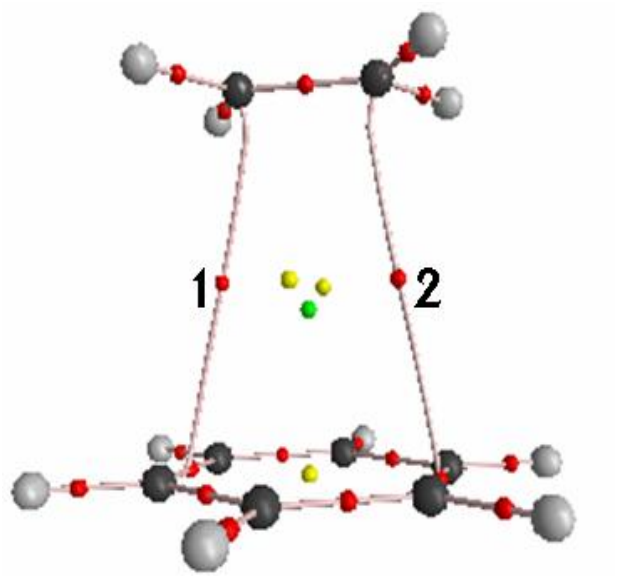

For the complex with benzene as the hydrogen donor, AIM analysis shows a bond critical point between the hydrogen of C_6H_6 and C_2H_4 and the bond path passing through the bond critical point connects the hydrogen to the centre of the ethylene C-C double bond and is shown in Figure. IV. 5. The electron density at the bond critical point is 0.0066 au and its Laplacian is -0.0039 au at 6-311++G** and is given in Table. IV. 9.

Figure . IV. 5:

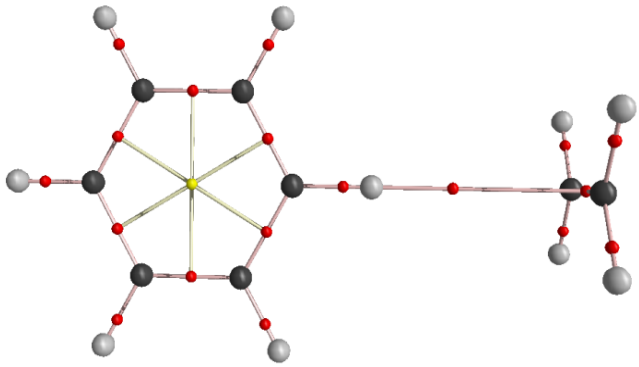

Table. IV. 9:

	MP2(full)/6-311G**	MP2(full)/6-311++G**
ρ(BCP)	0.0059	0.0066
L	-0.0033	-0.0039

The atomic basin properties have also been analyzed at both the basis sets. The hydrogen atom undergoes depletion in population on complex formation and ΔN is -0.0142 au. The next criterion is destabilization of the hydrogen atom. From Table. IV. 10, it is clear that the hydrogen atom gets destabilized on complexation and ΔE is 0.0090 au. The dipolar polarization of the hydrogen atom is less in the complex than in the monomer and ΔM is -0.0088 au. The hydrogen atom also shows a decrease in its volume in the complex, ΔV is -0.8476 au. The hydrogen atom satisfies all the criteria proposed by Koch and Popelier.

Table. IV 10. a: AIM analysis at MP2(full)/6-311G**

	Com	**Mono**	**Diff**
N	0.9635	0.9832	-0.0197
E	-0.6032	-0.6196	0.0164
M	0.1142	0.1203	-0.0061
V	49.8152	50.9524	-1.1372

Table. IV. 10. b: AIM analysis at MP2(full)/6-311++G**

	Com	**Mono**	**Diff**
N	0.9631	0.9773	-0.0142
E	-0.6081	-0.6171	0.0090
M	0.1134	0.1222	-0.0088
V	48.8999	49.7475	-0.8476

IV. 8. Conclusions:

Rotational spectroscopy confirms the formation of benzene-ethylene complex. *Ab initio* calculations predict three minima energy structures for benzene-ethylene complex. The experimentally obtained rotational constants confirm the presence of C-H/π interaction in benzene-ethylene complex, where C_2H_4 is the hydrogen bond donor. Experimental rotational constants A, B and C obtained by Fit I where K=1 lines along with the higher component of K=0 transition are used, unambiguously confirm this structure. Even though Fit II where the K=1 lines are fitted along with

the line centre of K=0 lines, gives reasonable value for the standard deviation, the rotational constants are not physically consistent with any of the structures. To ascertain hydrogen bond interaction AIM analysis has been carried out. The results show hydrogen bonding where one of the C_2H_4 hydrogen interacts with the benzene. Even though the aim was to get the π-stacked geometry, it could not be obtained. However *ab initio* and AIM theory support the formation of π-stacked complex.

IV. 9. References:

1) Y. Kodama, K. Nishihata, M. Nishio, N. Nakagawa, *Tetrahedron Lett.* **1977**, 2105.

2) G. R. Desiraju, T. Steiner, *The Weak Hydrogen Bond: In Structural Chemistry and Biology*, Oxford University Press, Oxford, **1999**.

3) S. Scheiner, *Hydrogen Bonding*: *A TheoreticalPperspecitive*; Oxford University Press: Oxford, NY, **1997**.

4) M. Brandl , M. S. Weiss, *J. Mol. Biol.*, **2001**, *307*, 357.

5) E. Arunan et al. *Pure Appl. Chem*., **2011**, *83*, 1637.

6) M. O. Sinnokrot et al. *J. Am. Chem. Soc*. **2002**, *124*, 10887.

7) A. C. Legon, P. D. Aldrich, W. H. Flygare, *J. Chem. Phys*., **1981**, 75, 625.

8) N. W. Howard, A. C. Legon, *J. Chem. Phys*., 1988, 88, 6793.

9) C. W. Gillies, J. Z. Gillies, F. J. Lovas, R. D. Suenram, *J. Am. Chem. Soc*., **1993**, *115*, 9253.

10) H. O. Leung, M. D. Marshall, *J. Chem. Phys*., **2006**, *125*, 154301.

11) E. Arunan, H. S. Gutowsky , *J. Chem. Phys.*, **1993**, *98*,4294.

12) M. J. Frisch, G. W. Trucks, H. B Schlegel, G. E. Scuseria, M. A.Robb, J. R.Cheeseman, J. A. Montgomery Jr., T. Vreven, K. N. Kudin, J. C. Burant, J. M. Millam, S. S. Iyengar, J. Tomasi, V. Barone, B. Mennucci, M. Cossi, G. Scalmani, N. Rega, G. A Petersson, H. Nakatsuji, M. Hada, M. Ehara, K. Toyota, R. Fukuda, J. Hasegawa, M. Ishida, T. Nakajima, Y. Honda, O. Kitao, H. Nakai, M. Klene, X. Li, J. E. Knox, H. P. Hratchian, J. B.Cross, C. Adamo, J. Jaramillo, R. Gomperts, R. E. Stratmann, O. Yazyev, A. J. Austin, R. Cammi, C. Pomelli, J. W. Ochterski, P. Y.

Ayala, K. Morokuma, G. A. Voth, P. Salvador, J. J. Dannenberg, V. G. Zakrzewski, S. Dapprich, A. D. Daniels, M. C. Strain, O. Farkas, D. K. Malick, A. D. Rabuck, K. Raghavachari, J. B. Foresman, J. V. Ortiz, Q. Cui, A. G. Baboul, S. Clifford, J. Cioslowski, B. B. Stefanov, G. Liu, A. Liashenko, P. Piskorz, I. Komaromi, R. L. Martin, D. J. Fox, T. M. Keith, A. Al-Laham, C. Y. Peng, A. Nanayakkara, M. Challacombe, P. M. W. Gill, B. Johnson, W. Chen, M. W. Wong, C. Gonzalez, J. A. Pople, *Gaussian03*, Revision C-02; Gaussian, Inc. Wallingford CT, **2004.**

13) R. F. W. Bader, *Atoms in Molecules: A quantum theory,* Clarendon Press, Oxford, **1990**.

14) F.Biegler-Konig, J.Schonbohm, R. Derdau, D. Bayles, R. F. W Bader, *AIM 2000*, version 1; Bu¨ro fu¨r Innovative Software: Bielefeld, Germany, **2000**.

15) R. Dennington II; T.Keith, J. Millam, K. Eppinnett, W. L. Hovell, R. Gilliland, *GaussView*, Version 3.09; Semichem, Inc.: Shawnee Mission, KS, **2003.**

16) S. Tsuzuki, K. Honda, T. Uchimaru, M. Mikami, K. Tanabe, *J. Am. Chem. Soc.* **2000**, *122*, 3746.

17) R. H. Page, Y. R. Shen,Y. T. Lee, *J. Chem. Phys*., **1988**, *88 (8),* 4621.

18) V. Chandrasekaran, L. Biennier, E. Arunan, D. Talbi, R. Georges, *J. Phys. Chem. A,* **2011**, *115*, 11263.

19) M. C. Chan, P. A. Block, R. E. Miller, *J. Chem. Phys.,***1995**, *102,* 3993.

20) H. S. Gutowsky, T. Emilsson, E. Arunan, J. *Chem. Phys*., 1**993**, *99*, 4883.

21) E. Arunan, T. Emilsson, H. S. Gutowsky, G. T. Fraser, G. de Oliveira, C. E. Dykstra, *J. Chem. Phys.,***2002**, *117*, 9766.

22) A. Taleb-Bendiab, K. W. Hillig II, R. L. Kuczkowski, *J. Chem. Phys*, **1992**, 97, 2996.

23) B. R. Prasad, M. S. Krishnan, E. Arunan, *J. Mol. Spect*., **2005**, *232*, 308.

24) P.L. A. Popelier, *Atoms in Molecules. An Introduction* (Prentice Hall, 2000).

25) U. Koch, P. L. A. Popelier, *J. Phys. Chem.,***1995**, *99*, 9747.

Appendix:

Table. IV. 11. Geometric Parameters of C_6H_6-C_2H_4 Optimized at Various Basis Sets:

a) π-stacked (Structure I)

	*B3LYP/ 6-311G***	*B3LYP/ 6-311++G***
$R(C_B\text{-}C_B)$	1.397	1.399
$R(C_B\text{-}H_B)$	1.086	1.087
$R(C_E\text{-}C_E)$	1.337	1.339
$R(C_E\text{-}H_E)$	1.085	1.085
$A(C_B\text{-}C_B\text{-}C_B)$	119.99	120.00
$A(C_B\text{-}C_B\text{-}H_B)$	120.01	120.00
$A(H_E\text{-}C_E\text{-}C_E)$	121.40	121.36
$D(C_B\text{-}C_B\text{-}C_B\text{-}C_B)$	0.00	0.00
$D(C_B\text{-}C_B\text{-}C_B\text{-}H_B)$	179.79	-180.00
$D(H_E\text{-}C_E\text{-}C_E\text{-}H_E)$	0.00	0.023
$D(H_E\text{-}C_E\text{-}C_E\text{-}H_E)$	180.00	179.28

b) C_2H_4 as H-bond donor (Structure II)

	*B3LYP/ 6-311G***	*B3LYP/ 6-311++G***
R(C-C)	1.4066	1.3992
R(C-H)	1.0932	1.0864
R(C_1-C_2)	1.3483	1.3389
R(C_1-H_3)	1.0922	1.0842
R(C_1-H_4)	1.0922	1.0860
R(C_2-H_5)	1.0922	1.0854
R(C_2-H_6)	1.0922	1.0857
A(C-C-C)	120.00	120.00
A(C-C-H)	120.00	120.00
A(H_3-C_1-C_2)	121.30	121.23
A(H_4-C_1-C_2)	188.70	121.15
A(H_5-C_2-C_1)	121.30	120.93
A(H_6-C_2-C_1)	121.30	121.69
D(C-C-C-C)	0.00	0.00
D(C-C-C-H)	180.00	180.00
D(H_3-C_1-C_2-H_5)	0.00	-0.04
D(H_3-C_1-C_2-H_6)	180.00	-179.99

c) C_6H_6 as H-donor (Structure III)

	*B3LYP/ 6-311G***	*B3LYP/ 6-311++G***
$R(C_B\text{-}C_B)$	1.407	1.407
$R(C_B\text{-}H_B)$	1.093	1.093
$R(C_E\text{-}C_E)$	1.348	1.348
$R(C_E\text{-}H_E)$	1.092	1.092
$A(C_B\text{-}C_B\text{-}C_B)$	120.00	120.00
$A(C_B\text{-}C_B\text{-}H_B)$	120.00	120.00
$A(H_E\text{-}C_E\text{-}C_E)$	120.00	120.00
$D(C_B\text{-}C_B\text{-}C_B\text{-}C_B)$	0.00	0.00
$D(C_B\text{-}C_B\text{-}C_B\text{-}H_B)$	180.00	180.00
$D(H_E\text{-}C_E\text{-}C_E\text{-}H_E)$	0.00	0.00
$D(H_E\text{-}C_E\text{-}C_E\text{-}H_E)$	180.00	180.00

Table. IV. 12. Normal mode vibrations of benzene-ethylene complex with C_2H_4 as H-bond donor (Structure II)

*B3LYP/ 6-311G***	*B3LYP/ 6-311++G***
89.76	22.71
97.40	56.16
107.71	59.18
131.51	77.36
193.99	113.26
292.72	121.18
402.61	367.64
406.50	377.30
467.36	479.37
612.02	609.53
612.26	609.99
717.23	668.57
860.91	828.52
868.30	834.80
870.20	837.93
925.14	892.56
926.40	907.92
929.32	924.45

940.78	938.11
986.33	971.24
991.18	1010.98
1010.35	1012.62
1055.14	1061.13
1055.52	1061.40
1090.81	1067.43
1181.07	1174.31
1199.82	1199.16
1200.70	1199.43
1249.90	1237.34
1365.55	1368.17
1374.86	1378.02
1417.86	1457.17
1475.68	1474.32
1500.87	1505.97
1501.10	1506.27
1615.77	1638.86
1615.92	1638.98
1648.31	1671.00
3116.75	3177.52
3131.04	3193.94

3141.46	3201.26
3151.42	3211.17
3152.02	3212.38
3166.54	3226.73
3167.08	3228.21
3176.06	3236.95
3212.23	3270.60
3240.67	3298.76

CHAPTER V

CF_3 radical as Hydrogen, Lithium and Chlorine Bond Acceptor: *Ab initio*, AIM and NBO Study

V. 1. Introduction

According to the new definition of hydrogen bond by IUPAC[1], hydrogen bond can be denoted as Z-A···H-Y and A can be an atom or molecule having lone pair of electrons, unpaired electron, sigma bonding electrons, A-Z π bond, hydride ions etc [2-14]. The red shift of the H-Y stretching frequency is a well established signature of 'hydrogen-bond' formation and has been known for long. But, it has been observed that there are hydrogen bonds which cause a blue shift of the H-Y stretching frequency. Recently the existence of blue shifted hydrogen bonds gained immense popularity [15,16].

Hydrogen bonds are very sensitive to the environment and hence by varying the fragments a variety of non conventional hydrogen bond donors and acceptors can be obtained. Interaction of H-Y with a series of fluorine substituted acceptors has been examined by Alkorta et al.[17]. Sathyamurthy and coworkers[18] have studied the interaction of benzenoid rings with different hydrogen bond donors. H_2O can interact with C_6H_6 either through oxygen or through O-H bond to give different geometries. But the minimum energy structure is the one in which the O-H of H_2O interacts with the π electron cloud of the benzene ring. In geometries where hydrogen of C_6H_6 is systematically substituted by fluorine, the orientation of the hydrogen bond donors with respect to that of hexafluorobenzene and 1,3,5-trifluorobenzene is very different. In case of C_6F_6, the geometry in which the oxygen of H_2O points towards the ring is the stable structure. This difference in the orientational preference can be attributed to the topological difference in the electron density distribution in C_6H_6 and C_6F_6. A negative region extends over the aromatic ring in C_6H_6 which favors an attractive interaction between the aromatic ring and an electron deficient species. This interaction results in the formation of hydrogen bonded complexes, with the π cloud

of C_6H_6 as the hydrogen bond acceptor. On the contrary, C_6F_6 due to high electronegativity of fluorine has a positive region over the ring, which can attract electron donating groups. $C_6H_3F_3$ forms a six-membered ring with H_2O through F···H-O and C-H···O hydrogen bonds. Similarly HF interacts with C_6F_6, here F point towards the centre of the ring contrary to its minimum structure with C_6H_6, where H point towards the centre of the benzene ring. The change in the orientational preference upon fluorine substitution was well explained on the basis of the distributed point-multipole model. C_6H_6 and C_6F_6 have large negative and positive quadrupole moments respectively. Here dipole – quadrupole and quadrupole – quadrupole interactions of small units with C_6H_6 and C_6F_6 result in the specific relative orientation of the monomers in the complex.

Single electron hydrogen bonds are formed when unpaired electron of a radical molecule acts as an electron donor or proton acceptor. Among this kind of non-conventional hydrogen bond, methyl radical acting as hydrogen bond acceptor is well established[19]. Single electron lithium bonds were theoretically predicted and characterized by Li et al.[20]. Raghavendra and Arunan[13] have shown that CH_3 radical is a good acceptor of H bonds.

Li is analogous to H and can participate in three centre interactions like that of hydrogen. Li interacts with lone pair electrons, π electron cloud etc similar to hydrogen, forming Li bonds. Its existence was theoretically predicted by Kollman *et al.*[21]. Matrix isolation study carried out by Ault and Pimentel gave the first experimental evidence for the formation of 1:1 lithium bonded complex[22]. The stability and geometrical preference of lithium bonded complexes are different from that of the hydrogen bonded complexes. Because of the higher dipole moment of Li-Y bonds compared to H-Y bonds, lithium bonds are found to be much stronger than

hydrogen bonds. However, unlike in hydrogen bonded systems, one needs to be careful in interpreting the red and blue shift in lithium bonded systems. The frequency shift of lithium bond is much smaller than that observed in case of hydrogen bond. Lithium, congener of hydrogen can also show blue shift, giving rice to blue-shifted lithium bonds[23].

The halogen bond is the other non-covalent interaction which has recently gained immense attention[24,25,26]. Here a halogen atom interacts with a Lewis base. Halogen bonds are strong, specific and directional, hence give rise to well-defined structures and has application in biology and supramolecular chemistry to direct molecular conformation[27,28]. Among halogen bonds, the most popular is the chlorine bond. Using rotational spectroscopic technique, Klemperer and co-workers have solved the structure of HF…ClF[29] and HF…Cl_2[30] complexes, where chlorine is the halogen bond donor. Chlorine interacts with other atoms, lone pair electrons, sigma electrons, π electrons etc to form chlorine bonded complexes[13,24,31-36].

The main objective of this work is to find out whether the unpaired electron in CF_3 radical can form single electron bond with hydrogen, lithium and chlorine bond donors. CH_3 and CF_3 radicals are topologically opposite as in the case of C_6H_6 and C_6F_6. Will it be hydrogen or halogen of H-Y (Y=halogen) that will interact with the unpaired electron of CF_3 to give a stable structure? Other question we would like to address is, whether the fluorine substitution weakens the ability of the unpaired electron to act as H bond acceptor? Also will it be the carbon or the fluorine atom in CF_3 that will preferentially bond with the hydrogen? *Ab initio* and AIM studies have been carried out to explore the structure and properties of these complexes.

V. 2. Computational Methods:

Interaction of CF_3 radical with X-Y, X=H, Li, Cl and Y= F, Cl, Br, -CN have been considered to study the structural and energetic properties of H, Li and Cl bonded complexes. Geometries of all the complexes of CF_3 with H/Li/Cl bond donors were fully optimized at MP2(full) level of theory at different basis sets, 6-311G**, 6-311++G**, Aug-cc-pVDZ and Aug-cc-pVTZ. All calculations were done using Gaussian 03[37] and Gaussian 09[38] quantum chemical package. Frequency calculations were carried out for all the complexes at all basis sets to ascertain whether the geometries obtained were true minima or not. The frequency shifts on complex formation were also calculated. NBO analyses of the complexes were done using Gaussian 03. Bader's[39] Atoms In Molecules theory was used to obtain the electron densities and Laplacian of electron density and other different properties of atomic basin required to shed more light on the nature of interaction. AIM2000[40] package was used to get the properties of atoms. Also geometry optimizations and frequency calculations were carried out for similar complexes with CH_3 radical as the acceptor at MP2(full)/6-311++G** level of theory for comparison. Molecular electrostatic potential maps were obtained using Gauss View[41].

Bond lengths and bond angles are the two geometric parameters mainly used to characterize various interactions in the complexes. Non-covalent interactions can be generally depicted as Z-A···X-Y, where A is the acceptor moiety and X-Y the donor, Y being the more electro negative atom than X. Opposite to the concept that distance A-Y in a complex should be smaller than the sum of the van der Waals radii of A and Y, recent studies support the criteria of considering A-X distance to judge whether a bond is H/Li/Cl bond. Conventionally in isolated complexes, ∠YXA is expected to be 180°. In the present work CF_3 radical, the acceptor, is denoted by A

and H/Li/Cl by X. The van der Waals radii (in angstroms) for H, C, Cl and Li are 1.2, 1.7, 1.8 and 2.1Å respectively[42].

V. 3. Results and Discussion of CF_3 radial as Hydrogen bond acceptor:

V. 3. A. Results from *ab initio* calculations:

Optimized geometries of the hydrogen bonded complexes of CF_3 radical with HF, HCl, HBr and HCN at MP2(full)/6-311G** and MP2(full)/6-311++G** level are given in Figure. V. 1. Table. V. 1 lists the optimized bond distances, $R_{C\text{-}H}$ and bond angles, ∠YHC and the sum of the van der Waals radii of C and H. Table. V. 2 lists the change in H-Y bond length (Δr) and H-Y stretching frequency (Δν) and the interaction energies are given in Table. V. 3. Here Δr is the difference between the H-Y bond length in the complex and in the free monomer. Similarly Δν is the difference in the stretching frequency of H-Y bond in the complex and in the monomer.

From Figure. V. 1 and Table. V. 1, it can be observed that with basis set, 6-311G**, CF_3 interacts with all the four hydrogen donors to give almost linear hydrogen bonded complex. With a higher basis set, 6-311++G**, it is true only in the case of CF_3··HF and CF_3··HCN complexes. Complexes of CF_3 with HCl and HBr give entirely different geometries, where HCl gave two different minima with slightly different stabilization energies.

From the frequency analysis at the 6-311G** level, except CF_3··HF, all the optimized geometries are true minima. So, at this level CF_3 radical acts as a good acceptor of hydrogen bond. All the five geometries (complex with HCl gave two different orientations) obtained at 6-311++G** are true minima. At 6-311G** basis

set, ∠ClHC, ∠BrHC and ∠CHC are 178.8°, 178.8° and 179.3° respectively. R_{A-X} in all the three minima is slightly greater than the sum of the respective van der Waals radii. The results obtained at 6-311++G** basis set are much more complicated than 6-311G**. Here also the R_{A-X} is greater than the sum of the van der Waals radii. van der Waals radii is arbitrary and a better approach would be using Koch and Popelier's[42] criteria of mutual penetration of the electron cloud of the acceptor and the hydrogen atom which can be calculated using the nonbonded and bonded radii. This analysis is described in the next section along with the results from AIM theoretical calculations. At MP2(full)/6-311++G**, ∠FHC of CF_3-HF is 180.0°, perfectly linear and ∠CHC of CF_3-HCN is 179.176°, very close to linearity. Complexs 'a' and 'b' of CF_3-HCl give ∠ClHC as 83.497° and 153.355° respectively and ∠BrHC in CF_3-HBr is 91.493°. In complex 'a' of CF_3-HCl, the distance from carbon to hydrogen is 3.4747Å, fluorine to hydrogen 2.8047 Å and carbon to chlorine is3.5629 Å. In complex 'b' the carbon to hydrogen distance is 3.6038Å, fluorine to hydrogen is 2.2938 Å and carbon to chlorine is 4.7763 Å. In CF_3-HBr complex carbon to hydrogen distance is 3.4792Å, fluorine to hydrogen is 2.7692 Å and carbon to bromine is 3.7881 Å. From The distance between carbon and the hydrogen in CF_3-HCl and CF_3-HBr, at 6-311++G**, are too far to form a hydrogen bonded complex. Complex 'b' of CF_3-HCl has F-H distance as 2.2938 Å and ∠ClHF angle 151.46°. The F-H distance is less than the sum of the van der Waals radii of F (1.4 Å) and H (1.2 Å) and hence results in a $CF_2F\cdots HCl$ hydrogen bonded complex. AIM analysis, discussed in the coming section, also shows a bond critical point between the F and H. The F-H distance in complex 'a' of CF_3-HCl (2.8047 Å) and CF_3-HBr (2.769 Å) are greater than the sum of the van der Waals radii of F and H. From the geometry of

these two complexes, shown in Figure. V. 1, there can be dipole-dipole interaction between C and F of CF_3 with Cl/Br and H respectively of HCl and HBr. This dipole-dipole interaction stabilizes these two structures. Hence at this level, MP2(full)/6-311++G**, CF_3 acts as an acceptor of hydrogen bond only for HF and HCN.

The interaction energies listed in Table. V. 3 establish how weak all the four complexes are. This is reflected in the change in H-Y bond length upon complex formation and the frequency shifts. The interaction energy of CF_3···HCl at 6-311G** basis set is nearly zero. The minima energy geometries obtained for all the other complexes at both basis sets, 6-311G** and 6-311++G**, are of bound states. CF_3···HCl and CF_3···HBr shows negligible change in the H-Cl and H-Br bond length on complex formation and a very small shift in the H-Cl and H-Br stretching frequency to the red side at MP2(full)/6-311G**. Calculations at the same level for CF_3···HCN gave a blue shift. At MP2(full)/6-311++G**, CF_3···HF, CF_3···HCl(a) and CF_3···HBr show slight red shift upon complex formation. There is no change in the H-F bond length on complexation and the red shift observed is quite small, 2.55 cm^{-1}. On the contrary, a blue shift is observed for CF_3···HCl(b) and CF_3···HCN complexes. C-H bond of H-C-N undergoes a shortening of 0.0004Å and shows a blue shift in the stretching frequency (6.62 cm^{-1}). It can be concluded that CF_3 at MP2(full)/6-311++G** level gives red shifted hydrogen bond with HF and blue shifted hydrogen bond with HCN.

From Figure. V. 1 and the geometric parameters listed in Table. V. 1 for CF_3-HY complexes, it is clear that the optimized geometries at 6-311G** and 6-311++G** are very different. In an attempt to explain the change in the geometries of CF_3···HCl and CF_3···HBr with basis sets, we carried out geometry optimizations and frequency calculations of all the H bond complexes at MP2(full)/Aug-cc-pVDZ and

MP2(full)/Aug-cc-pVTZ levels. Calculations at both the basis sets gave geometries similar to the geometry obtained at MP2(full)/6-311G** for all the eight complexes. From frequency analysis all optimized geometries are minima except HCN complex at Aug-cc-pVDZ. Geometry obtained for CF_3···HCN at MP2(full)/Aug-cc-pVDZ is a transition state.

The R_{C-H} distances and ∠YHC angles are listed in Table. V. 1. Calculations at MP2(full)/Aug-cc-pVDZ and MP2(full)/Aug-cc-pVTZ levels give R_{C-H} distances which are less than the sum of the van der Waals radii. R_{C-H} distances at Aug-cc-pVTZ basis sets are 2.355, 2.321, 2.196 and 2.524Å for CF_3 HF/Cl/Br/CN respectively. The ∠YHC angles are close to 180.0° at both the levels. The change in H-Y bond length, the shift in H-Y stretching frequency and interaction energy for the complexes are listed in Table. V. 2 and Table. V. 3. The change in H-Y bond length (Δr) for CF_3···H-Y (Y=F,Cl,Br) at MP2(full)/Aug-cc-pVTZ are 0.0022, 0.0035 and 0.0073Å respectively and that for CF_3···H-CN is -0.0008 Å. Except for CF_3···H-CN, there is an elongation in the H-Y bond length on complex formation. This is reflected in the change in the H-Y stretching frequency. CF_3···H-Y (Y=F,Cl,Br) shows a red shift in the H-Y stretching frequency where as CF_3···H-CN gives a blue shift. The displacements of the atoms in the normal H-Y stretching modes in the complex and in the monomer are given in Table. V. 4 (a) and Table. V. 4 (b) respectively at MP2(full)/Aug-cc-pVTZ. On comparing the tables, the displacement of H-Y in the complex during the H-Y stretch is found to be the same as the displacement it undergoes during the H-Y stretch in the free monomer. And the atoms of CF_3 radical do not undergo any displacement in the complex during the stretch. This shows how weak the interaction of H-Y is with the CF_3 radical. Since there is no mode coupling

between CF_3 radical and H-Y, during H-Y stretch, the criterion of using the shift in frequency to evaluate the bond strength is valid.

V. 3. B. Results from AIM analysis:

AIM studies have been carried out on the various CF_3···HX/LiX/ClF complexes using AIM 2000 software[40]. According to Bader the presence of (3,-1) critical point or bond critical point (BCP), along the bond path connecting the two interacting atoms is a necessary and sufficient condition to ascertain that the two atoms are bonded. Koch and Popelier[43,44] have suggested a set of criteria on the basis of AIM theory which should be satisfied for a bond to be called as a hydrogen bond.

In this section the necessary and sufficient criteria are examined to classify the bonding between CF_3 radical and the hydrogen bond donors. The criteria considered are 1) Topology: the presence of a bond critical point between the hydrogen atom and the acceptor atom and a bond path connecting the two, 2) The charge density at the Bond Critical Point: According to Koch and Popelier the range for the charge density at the BCP for a bond to be classified as hydrogen bond is between 0.002 and 0.4 au. 3) The Laplacian of the charge density (L) at the bond critical point: the range suggested by Koch and Popelier for L is -0.15 to 0.02 au., 4) Mutual penetration of hydrogen and acceptor atom.

All the complexes show the presence of a bond critical point between the monomers and is shown in Figure. V. 2. Calculations with the three basis sets 6-311G**, Aug-cc-pVDZ and Aug-cc-pVTZ show the presence of bond critical point between the carbon atom and the hydrogen atom and a bond path connecting the atoms in all the complexes, CF_3···HY(Y=F,Cl,Br,CN). The values of electron density and the Laplacian of electron density calculated at different basis sets, listed in Table.

V. 5, fall in the range suggested for hydrogen bonded complexes. AIM studies give interesting results at 6-311++G**. AIM calculations show the presence of bond critical point between carbon and hydrogen in CF_3-HF and CF_3···HCN. The values of electron density and its Laplacian show that it is hydrogen bonded. AIM calculation of the complex 'a' of CF_3···HCl shows a bond critical point between the two monomers CF_3 and HCl along the bond path connecting fluorine and chlorine. In case of complex 'b', CF_3 acts as an acceptor of hydrogen bond, but the bond critical point is between the fluorine and hydrogen, it is the fluorine of CF_3 not the carbon which acts as the hydrogen bond acceptor. Same is the case with CF_3···HBr, the bond critical point connects the fluorine and the hydrogen atom.

Among the criteria, the mutual penetration of hydrogen atom and the acceptor atom is the necessary and sufficient condition. The distance from the nucleus of the atom to the contour where the electron density is 0.001au is defined as the nonbonded radius, r° and the distance from the nucleus to the bond critical point is defined as the bonded radius, r^b. The difference between the two radius, bonded and nonbonded, give the extent of penetration. If there is penetration of electron cloud of the hydrogen atom and the acceptor atom, Δr is positive and results in the formation of a bond. The importance of using separate nonbonded and bonded radii for atoms instead of van der Waals radii is discussed by Raghavendra and Arunan [13]. Table. V. 6 lists the r° and r^b of carbon and hydrogen in all CF_3···HY complexes. In case of complexes of CF_3 with HF/Cl/Br, at all basis sets, the numerical value of r° is greater than that of r^b for both C and H and hence shows mutual penetration.

Mutual penetration (Δr) of hydrogen and acceptor atom can be considered as a criterion to determine how strong a bond is. A comparison of the radius of carbon at MP2(full)/Aug-cc-pVTZ, Table. V. 6, shows that in the bonded state the carbon

radius, i.e. distance between carbon nuclei and the bond critical point, decreases as the H bond donor varies from HF to HCl to HBr. The radius can be interpreted as a consequence of the extent of penetration. A decrease in the radius indicates more penetration and hence a stronger interaction. Among the halogens, the polarizability increases down the group. The most polar H bond donor, HBr, interacts strongly to give maximum penetration resulting in the largest decrease in the carbon radius. The bonded carbon radii are 1.54, 1.48 and 1.40 Å for CF_3···HF, CF_3···HCl and CF_3···HBr respectively and the corresponding penetration of carbon atom ($r_C^{\circ} - r_C^{b}$) in the complexes are 0.41, 0.47and 0.55 Å. Similarly for hydrogen, the bonded radii are 0.84, 0.83 and 0.79 Å for HF, HCl and HBr and the corresponding penetration of the hydrogen atom in the complexes are 0.25, 0.39 and 0.48 Å. The bonded radii of hydrogen are quite different from the hydrogen bond radii reported for several conventional hydrogen bonded complexes. They have the trend HF < HCl ≤ HBr. Extent of mutual penetration at MP2(full)/Aug-cc-pVTZ level for CF_3···HY, are 0.66Å for CF_3···HF, 0.86Å for CF_3···HCl and 1.03Å for CF_3···HBr. Mutual penetration increases from CF_3···HF to CF_3···HBr. Here, Δr follows the same trend as ΔE (Table. V. 3), i. e. interaction energy is directly proportional to the mutual penetration of the interacting atoms.

Comparisons of the nonbonded radii in various non-conventional hydrogen bonds have been done. The nonbonded radius of carbon,, $r_C°$ in CF_3 is 1.95Å. $r_C°$ in CH_3 is 2.25Å. Similarly the nonbonded radius of hydrogen for H-F, H-Cl and H-Br are 1.09, 1.22 and 1.27 Å. Depending on the environment, the nonbonded radii of the elements vary. These values of r°are greater than the van der Waals radii of the elements (H=1.2, C=1.7 Å). This shows the importance of using separate nonbonded

and bonded radii for atoms instead of van der Waals radii. An important observation is that, the bonded radii are similar in CF_3 and CH_3 radicals. For carbon the bonded radii are 1.54Å and 1.47Å in CF_3···HF and CH_3···HF respectively.

Figure. V. 1: Optimized geometries of CF_3···HY complexes

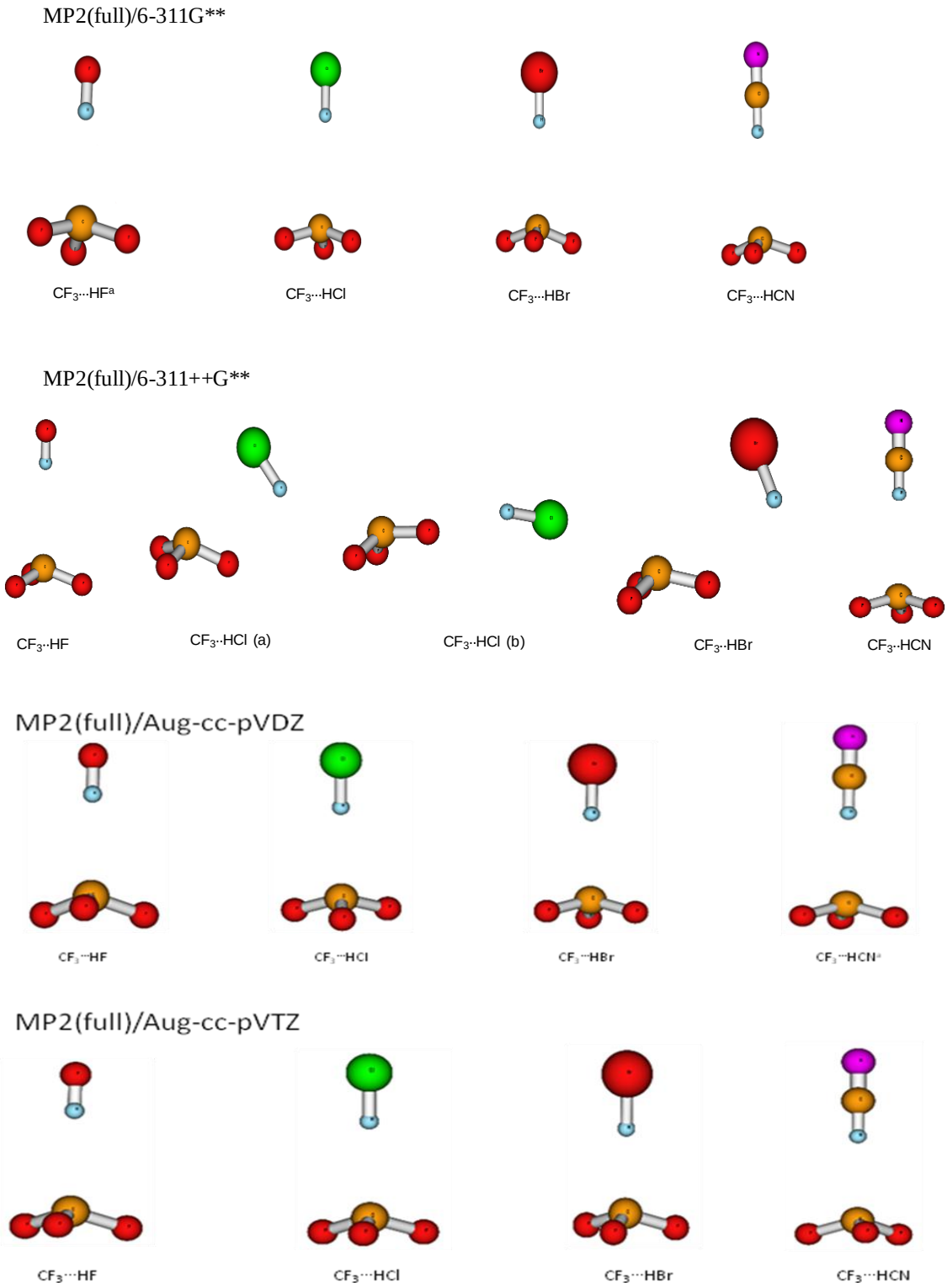

Table. V. 1: C-H Bond Distances R_{C-H} (Å) and Bond angles ∠YHC (°) at MP2(full)

	Sum of van der Waals radii	*6-311G***		*6-311++G***	
		R_{C-H}	∠YHC	R_{C-H}	∠YHC
CF_3···HF	2.9	2.5001*	179.999	3.0462	180.000
CF_3···HCl	2.9	3.0629	178.833	a)3.4747	83.4970
				b)3.6038	153.355
CF_3···HBr	2.9	3.0681	178.822	3.4792	91.439
CF_3···HCN	2.9	3.1745	179.252	3.2127	179.176

*→Transition state

	Sum of van der Waals radii	*Aug-cc-pVDZ*		*Aug-cc-pVTZ*	
		R_{C-H}	∠YHC	R_{C-H}	∠YHC
CF_3···HF	2.9	2.4973	179.998	2.3547	179.978
CF_3···HCl	2.9	2.5045	179.211	2.3206	179.615
CF_3···HBr	2.9	2.4903	179.999	2.1955	179.846
CF_3···HCN	2.9	2.739*	179.912	2.5244	179.991

Table. V. 2: Change in H-Y Distance (Δr) in Å and Shift in H-Y Stretching Frequency ($\Delta\nu$)* in cm^{-1}.

	*MP2(full)/ 6-311G***		*MP2(full)/ 6-311++G***		*MP2(full)/ Aug-cc-pVDZ*		*MP2(full)/ Aug-cc-pVTZ*	
	Δr	*$\Delta\nu$*	*Δr*	*$\Delta\nu$*	*Δr*	*$\Delta\nu$*	*Δr*	*$\Delta\nu$*
CF_3···HF	---	---	0.0	-2.6	0.0013	-41.2	0.0022	-75.5
CF_3···HCl	0.0002	-3.7	0.0008 0.0002	-5.4 5.0	0.0011	-28.7	0.0035	-65.8
CF_3···HBr	0.00001	-2.2	0.0007	-3.5	0.0012	-30.3	0.0073	-116.1
CF_3···HCN	-0.0001	0.2	-0.0004	6.6	---	---	-0.0008	48.9

*($\Delta\nu = \nu_{complex} - \nu_{monomer}$)

Table. V. 3: Interaction Energy CF_3•••H-Y complex, ΔE (kcal mol^{-1})

	*MP2(full)/ 6-311G***	*MP2(full) 6-311++G***	*MP2(full)/ Aug-cc-pVDZ*	*MP2(full)/ Aug-cc-pVTZ*
CF_3···HF	---	-0.06	-0.38	-1.36
CF_3-···HCl	$8.79x10^{-4}$	-1.63[a] -1.51[b]	-0.86	-1.51
CF_3···HBr	-0.09	-1.38	-1.19	-2.38
CF_3···HCN	-0.05	-0.06	---	-1.51

*[a, b] → ΔE of 'a' and 'b' geometries of CF_3-···HCl

Table. V. 4 (a): Displacement of the atoms in the normal H-Y(Y=F/Cl/Br/CN) stretching modes for the CF_3•••H-Y complex at MP2(full)/Aug-cc-pVTZ level.

	CF_3•••H-F			*CF_3•••H-Cl*			*CF_3•••H-Br*			*CF_3•••H-CN*		
	X	*Y*	*Z*	*X*	*Y*	*Z*	*X*	*Y*	*Z*	*X*	*Y*	*Z*
C	0.00	0.00	0.00	0.00	0.00	0.00	0.00	0.00	0.00	0.00	0.00	0.00
H	1.00	0.00	0.00	1.00	0.00	0.00	1.00	0.00	0.00	0.00	0.00	0.99
F	0.00	0.00	0.00	0.00	0.00	0.00	0.00	0.00	0.00	0.00	0.00	0.00
F	0.00	0.00	0.00	0.00	0.00	0.00	0.00	0.00	0.00	0.00	0.00	0.00
F	0.00	0.00	0.00	0.00	0.00	0.00	0.00	0.00	0.00	0.00	0.00	0.00
Y	-0.05	0.00	0.00	-0.03	0.00	0.00	-0.01	0.00	0.00	0.00	0.00	-0.11
N	---	---	---	---	---	---	---	---	---	0.00	0.00	0.03

Table. V. 4 (b): Displacement of the atoms in the normal H-Y(Y=F/Cl/Br/CN) stretching modes for monomer at MP2(full)/Aug-cc-pVTZ level.

	H-F			*H-Cl*			*H-Br*			*H-CN*		
	X	*Y*	*Z*	*X*	*Y*	*Z*	*X*	*Y*	*Z*	*X*	*Y*	*Z*
H	1.00	0.00	0.00	1.00	0.00	0.00	1.00	0.00	0.00	0.00	0.00	0.99
Y	-0.05	0.00	0.00	-003	0.00	0.00	-0.01	0.00	0.00	0.00	0.00	-0.11
N	---	---	---	---	---	---	---	---	---	0.00	0.00	0.03

Table. V. 5: Electron Densities (ρ, au.) and the Laplacian (*L, au.*)

Complex	*MP2(full)/6-311G***		*MP2(ful)/6-311++G***	
	ρ	*L*	*ρ*	*L*
CF_3···HF	---	---	0.0084	-0.0058
CF_3···HCl	0.0033	-0.0019	0.0052	-0.0057
CF_3···HBr	0.0035	-0.0019	0.0049	-0.0053
CF_3···HCN	0.0025	-0.0015	0.0023	-0.0015

Complex	*MP2(full)/Aug-cc-pVDZ*		*MP2(full)/Aug-cc-pVTZ*	
	ρ	*L*	*ρ*	*L*
CF_3···HF	0.0069	-0.0053	0.0094	-0.0087
CF_3···HCl	0.0088	-0.0061	0.0146	-0.0093
CF_3···HBr	0.0098	-0.0066	0.0202	-0.0111
CF_3···HCN	---	---	0.0084	-0.0063

Table. V. 6: Bonded (r^b) and Nonbonded ($r°$) Radii (in Angstroms) of Acceptor (C) and Donor (H) Atoms and Penetration, Δ*r*, Defined as the Sum of the Differences in Bonded and Nonbonded Radii of C and H at MP2(full)/Aug-cc-pVTZ level.

Complex	$r°$ *(C)*	r^b *(C)*	$r° - r^b$ *(C)*	$r°$ *(H)*	r^b *(H)*	$r° - r^b$ *(H)*	*Δr*
CF_3···HF	1.95	1.54	0.41	1.09	0.84	0.25	0.66
CF_3···HCl	1.95	1.48	0.47	1.22	0.83	0.39	0.86
CF_3···HBr	1.95	1.40	0.55	1.27	0.79	0.48	1.03
CF_3···HCN	1.95	1.58	0.37	1.21	0.94	0.27	0.64

Figure. V. 2.: AIM analysis of CF_3···HY showing Bond Critical Points and Bond Paths

Figure. V. 2. a): MP2(full)/6-311G**

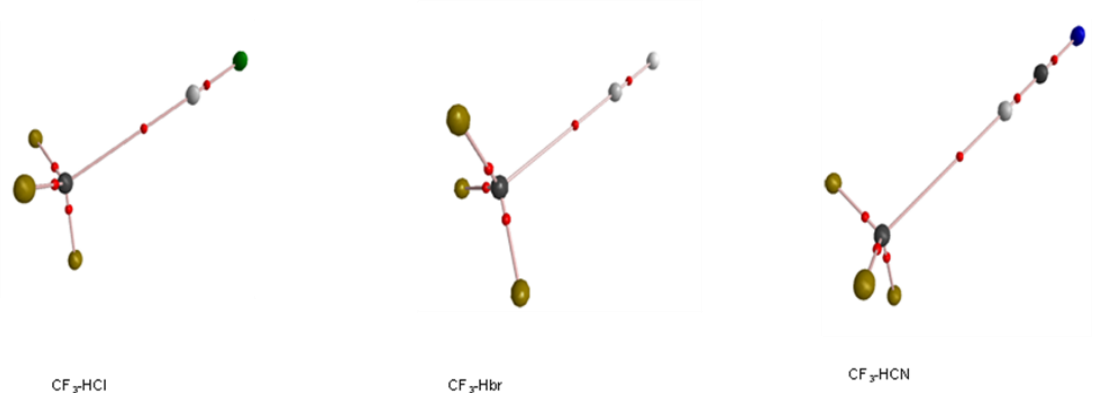

Figure. V. 2. b): MP2(full)/6-311++G**

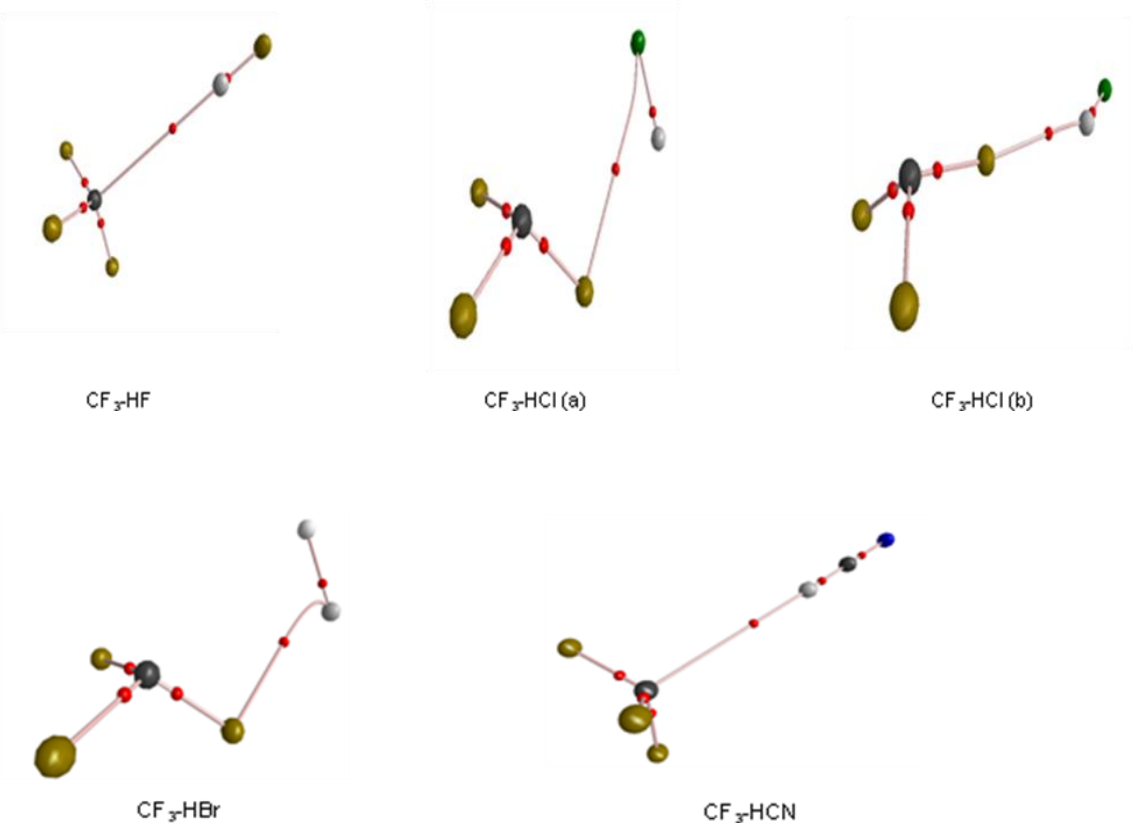

Figure. V. 2. c): MP2(full)/Aug-cc-pVDZ

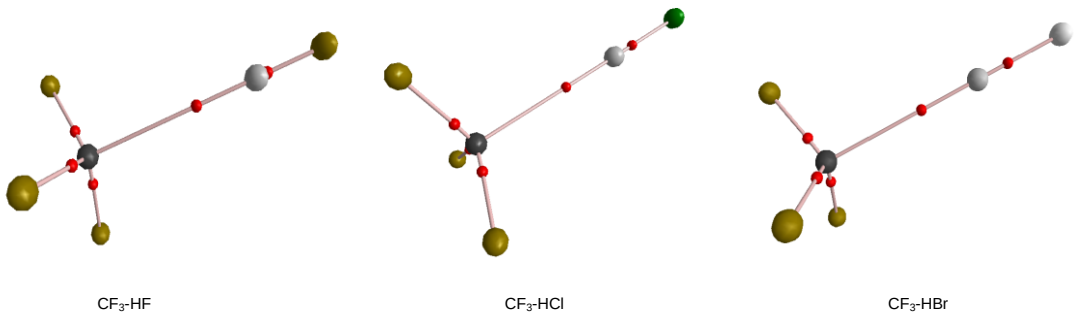

Figure. V. 2. d): MP2(full)/Aug-cc-pVTZ

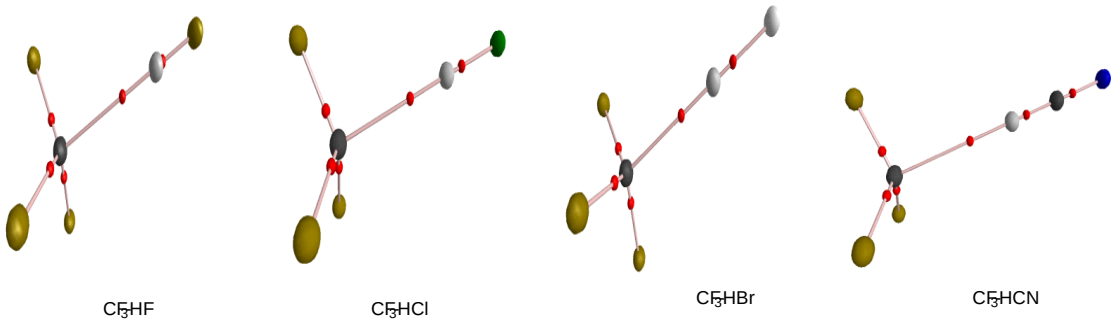

V. 4. Results and Discussion of CF_3 radial as lithium bond acceptor:

V. 4. A. Results from *ab initio* calculations:

Coming to lithium bonds, Gaussian calculations show that the complexes of CF_3 radical with LiF/Cl/Br are true minima at both 6-311G** and 6-311++G** level except CF_3···LiF at 6-311G**. The distance between C and Li and the ∠YLiC bond angles are given in Table. V. 7. In all the lithium complexes the R_{Li-C} distances are less than the sum of the van der Waals radii. At MP2(full)/6-311++G**, the C-Li distances are 2.7317, 2.6373 and 2.6641 Å for CF_3···LiF, CF_3···LiCl and CF_3···LiBr respectively The ∠YLiC angles for the optimized geometries are linear. ∠FLiC, ∠ClLiC and ∠BrLiC are 179.760°, 179.844° and 179.780° respectively at

MP2(full)/6-311++G**. The interaction energies are very low and the change in LiF/Cl/Br bond lengths upon complex formation is negligible. The optimized geometric parameters, frequency shifts and interaction energies obtained for Li complexes using Dunning basis sets, Aug-cc-pVDZ and Aug-cc-pVTZ, follow the same pattern obtained at 6-311G** and 6-311++G** basis sets. The optimized geometries at MP2(full)/Aug-cc-pVTZ are shown in Figure. V. 3. The changes in Li-Y bond lengths and frequency shifts in Li-Y stretching frequencies and the interaction energies are given in Table. V. 8 and Table. V. 9 respectively. All the three complexes give blue shifted Li bonds, which is a common feature of Li bond.

In CF_3···LiY complexes, none of the modes can be explicitly assigned to the change in the Li-Y stretching frequency. Li-Y vibrations are coupled to other vibrations in the complex. The displacements of the atoms in the normal Li-Y stretching modes in the complex and in the monomer are given in Table. V. 10 (a) and Table. V. 10 (b) respectively at MP2(full)/Aug-cc-pVTZ. The displacement of Li and Y(H/Cl/Br) atoms during Li-Y stretch in CF_3···Li-Y complex and Li-Y monomer is compared. The atoms of Li-Y undergo the same amplitude of displacement in both complex and monomer, i.e. it retains its identity. But, unlike in CF_3···H-Y complex, in CF_3···Li-Y the atoms of CF_3 radical also show displacement during the Li-Y stretching vibration in the complex. In CF_3···H-Y, atoms of CF_3 have zero displacement during the H-Y stretch in the complex. This observation points towards a stronger interaction between CF_3 and LiY, than CF_3 and HY. But, since none of the modes can be explicitly assigned as Li-Y stretching mode, the concept of using shift in the bond length and shift in the stretching frequency as a criteria to estimate the strength of the noncovalent interaction is not valid.

Figure. V. 3: Optimized geometries of CF_3···LiY complexes at MP2(full)/Aug-cc-pVTZ

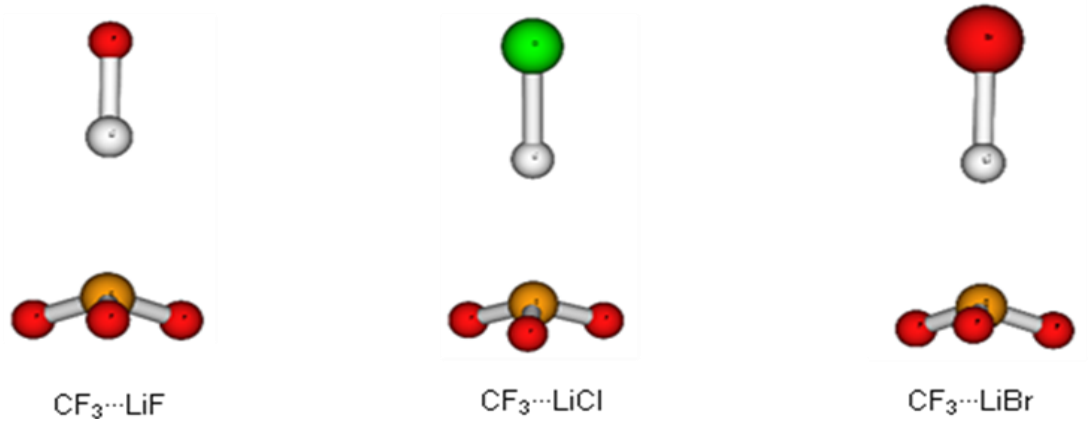

V. 4. B. Results from AIM analysis:

For the AIM analysis of lithium bond, no criterion has been yet suggested to ascertain the bond to be lithium bond as in the case of hydrogen bond. So the presence of bond critical point, bond path and mutual penetration remain the main parameters to characterize Li bonds. AIM analysis shows the presence of bond critical point between carbon and Li in all the three CF_3-LiY complexes. And a bond path passing through the bond critical point connects the carbon atom to Li and is shown in Figure. V. 4. The criteria of mutual penetration between lithium and the acceptor atom, carbon are also satisfied in all the cases. Table. V. 11 lists the electron density at the lithium bond critical point and its Laplacian of electron density. Table. V. 12 lists the nonbonded and bonded radii of C and Li and the mutual penetration of C and Li atoms

The bonded radius of carbon (Table. V. 12) decreases as the polarizbility of the LiY bond increases. The bonded radius of carbon varies as 1.71, 1.68 and 1.65 Å

and the penetration as 0.24, 0.27 and 0.30 Å when the electronegative atom attached to lithium varies from F to Cl to Br. Similarly in CF_3···LiF, CF_3···LiCl and CF_3···LiBr, the bonded radii of lithium are 0.94, 0.91 and 0.89 Å and the penetration in the respective cases are 0.08, 0.09 and 0.10 Å. The extents of mutual penetration are 0.32, 0.36 and 0.40 Å. Hence, for Li bonded complexes also the mutual penetration increases as the lithium bond donor varies from LiF to LiCl to LiBr. Li bonded complexes show similar behaviour as H bonded complexes; interaction energy is directly proportional to the extent of mutual penetration. The decrease in the bonded radii of C and Li, the increase in the penetration and the increase in the interaction energy as Y(F, Cl, Br) changes can be ascribed to the polarizability of the halogen atom, which increases down the group in the periodic table of elements. As larger electron cloud has a greater polarizability, it results in stronger London forces.

Figure. V. 4: AIM analysis of CF_3···LiY showing Bond Critical Points and Bond Paths

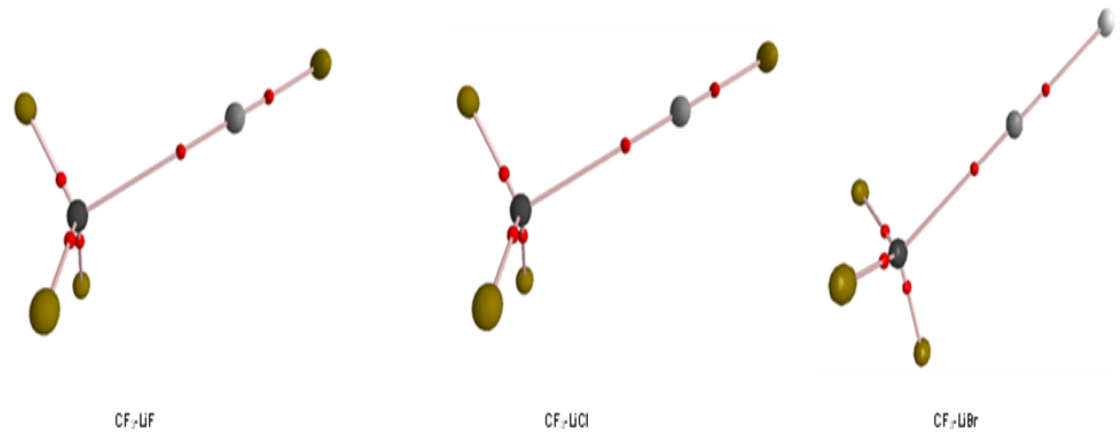

Table. V. 7: C-Li Bond Distances $R_{C\text{-}Li}$ (Å) and Bond angles ∠YLiC (°) at MP2(full)

	Sum of van der Waals radii	*6-311G***		*6-311++G***	
		$R_{C\text{-}Li}$	*∠YLiC*	$R_{C\text{-}Li}$	*∠YLiC*
CF_3···LiF	3.8	2.5559*	131.033	2.7317	179.760
CF_3···LiCl	3.8	2.5215	179.921	2.6373	179.844
CF_3···LiBr	3.8	2.5267	179.900	2.6641	179.780

*→Transition state

	Sum of van der Waals radii	*Aug-cc-pVDZ*		*Aug-cc-pVTZ*	
		$R_{C\text{-}Li}$	*∠YLiC*	$R_{C\text{-}Li}$	*∠YLiC*
CF_3···LiF	3.8	2.6396	179.859	2.6446	179.849
CF_3···LiCl	3.8	2.5257	179.904	2.5971	179.875
CF_3···LiBr	3.8	2.4538	179.931	2.5430	179.816

Table. V. 8: Change in Li-Y Distance (Δr) in Å and Shift in Li-Y Stretching Frequency (Δν) in cm^{-1} at MP2(full)

	*63-11G***		*6-311++G***		*Aug-cc-pVDZ*		*Aug-cc-pVTZ*	
	Δr	*Δv*	*Δr*	*Δv*	*Δr*	*Δv*	*Δr*	*Δv*
CF_3···LiF	---	---	-0.001	4.2	-0014	25.3	-0.0027	8.8
CF_3···LiCl	0.0005	14.5	-0.0016	9.3	-0.0181	43.5	0.0012	12.2
CF_3···LiBr	-0.0007	20.6	-0.0011	11.0	-0.0328	61.0	-0.0047	17.1

Table. V. 9: Interaction Energy of CF_3•••Li-Y complex, ΔE (kcal mol^{-1})

	*MP2(full)/ 6-311G***	*MP2(full) 6-311++G***	*MP2(full)/ Aug-cc-pVDZ*	*MP2(full)/ Aug-cc-pVTZ*
CF_3···LiF	---	-0.3	-1.5	-1.4
CF_3···LiCl	-2.6	-0.8	-1.6	-2.1
CF_3···LiBr	-2.4	-0.6	-2.0	-3.0

Table. V. 10 (a): Displacement of the atoms in the normal Li-Y(Y=F/Cl/Br) stretching modes for the CF_3•••Li-Y complex at MP2(full)/Aug-cc-pVTZ level.

	CF_3•••Li-F			*CF_3•••Li-Cl*			*CF_3•••Li-Br*		
	X	*Y*	*Z*	*X*	*Y*	*Z*	*X*	*Y*	*Z*
C	0.02	0.00	0.00	0.09	0.00	0.00	0.07	0.00	0.00
F	-0.01	0.00	-0.03	-0.02	0.04	0.00	-0.02	0.02	-0.01
F	-0.01	0.03	0.02	-0.02	-0.02	0.04	-0.02	0.00	0.03
F	-0.01	-0.03	0.01	-0.02	-0.02	-0.04	-0.02	-0.02	-0.02
Li	0.94	0.00	0.00	0.97	0.00	0.00	0.99	0.00	0.00
Y	-0.34	0.00	0.00	-0.19	0.00	0.00	-0.08	0.00	0.00

Table. V. 10 (b): Displacement of the atoms in the normal Li-Y(Y=F/Cl/Br) stretching modes for monomer at MP2(full)/Aug-cc-pVTZ level.

	Li-F			*Li-Cl*			*Li-Br*		
	X	*Y*	*Z*	*X*	*Y*	*Z*	*X*	*Y*	*Z*
Li	0.94	0.00	0.00	0.98	0.00	0.00	1.00	0.00	0.00
Y	-0.35	0.00	0.00	-0.20	0.00	0.00	-0.09	0.00	0.00

Table. V. 11: Electron Densities (ρ, au.) and the Laplacian (*L, au.*)

Complex	*MP2(full)/6-311G***		*MP2(ful)/6-311++G***	
	ρ	*L*	*ρ*	*L*
CF_3···LiF	---	---	0.0058	-0.0055
CF_3···LiCl	0.0093	-0.0094	0.0071	-0.0071
CF_3···LiBr	0.0091	-0.0093	0.0066	-0.0067

Complex	*MP2(full)/Aug-cc-pVDZ*		*MP2(full)/Aug-cc-pVTZ*	
	ρ	*L*	*ρ*	*L*
CF_3···LiF	0.0055	-0.0075	0.0064	-0.0084
CF_3···LiCl	0.0073	-0.0106	0.0072	-0.0098
CF_3···LiBr	0.0087	-0.0132	0.0082	-0.0113

Table. V. 12: Bonded (r^b) and Nonbonded ($r°$) Radii (in Angstroms) of Acceptor (C) and Donor (Li) Atoms and Penetration, Δr, Defined as the Sum of the Differences in Bonded and Nonbonded Radii of C and Li at MP2(full)/Aug-cc-pVTZ level.

Complex	$r°$ *(C)*	r^b *(C)*	$r° - r^b$ *(C)*	$r°$ *(Li)*	r^b *(Li)*	$r° - r^b$ *(Li)*	Δr
CF_3···LiF	1.95	1.71	0.24	1.02	0.94	0.08	0.32
CF_3···LiCl	1.95	1.68	0.27	1.00	0.91	0.09	0.36
CF_3···LiBr	1.95	1.65	0.30	0.99	0.89	0.10	0.40

V. 5. Results and Discussion of CF_3 radial as chlorine bond acceptor:

V. 5. A. Results from *ab initio* calculations:

To explore whether CF_3 radical can act as chlorine bond acceptor interaction of CF_3 with Cl-F is studied. Like hydrogen and lithium, chlorine also interacts with CF_3 radical to give very weak chlorine bond. Here $R_{C\text{-}Cl}$ distance is 3.203 Å and 3.314Å at MP2(full)/6-311G** and MP2(full)/6-311++G** respectively and the ∠FClC angles at both the levels are 179.556° and 179.310°. The $R_{C\text{-}Cl}$ distances at both levels are less than the sum of van der Waals radii (3.5Å). The interaction energies are -0.50 and -0.52 kcal mol^{-1} at 6-311G** and 6-311++G** respectively. The change in Cl-F bond length at both basis sets is negligible (-0.0037Å and -0.0008Å). The shift in Cl-F stretching frequencies, 93.7 and 43.6 cm^{-1}, show that CF_3 radical interacts with ClF to form a blue shifted chlorine bonded complex. The optimized geometric parameters, frequency shifts and interaction energies obtained for the CF_3···ClF complexes using basis sets Aug-cc-pVDZ and Aug-cc-pVTZ follow

the same pattern obtained at 6-311G** and 6-311++G** basis sets. The optimized geometry at MP2(full)/Aug-cc-pVTZ is shown in Figure. V. 5. The geometric parameters, shift in the Cl-F bond length, shift in the Cl-F stretching frequency and interaction energies are given in Table. V. 13. The Dunning basis set gave a shorter C-Cl distance and higher interaction energy, similar to hydrogen bonded complexes of CF_3. The C-Cl distance at Aug-cc-pVDZ and Aug-cc-pVTZ are 2.9834 and 2.6920 Å respectively and the corresponding interaction energies are -1.34 and -2.28 kcal mol^{-1}. Upon complexation the Cl-F bond undergoes a shortening and the Cl-F stretching frequency shows a blue shift. But, frequency analysis shows that, like Li bond complexes, there is mode mixing in CF_3···ClF too and none of the modes can be explicitly assigned as Cl-F stretching. The displacements of the atoms in the normal Cl-F stretching modes in the monomer and in the complex at MP2(full)/Aug-cc-pVTZ are given in Table. V. 14. Cl-F atoms show similar amplitude of displacement in the monomer and in the complex. The displacement of atoms of CF_3 is larger in CF_3···ClF compared to CF_3···LiY. Here again, as in case of lithium bonded complexes, for chlorine bonded complexes the shift in bond length and change in the stretching frequency cannot be used as a tool to judge the strength of the interaction.

Figure. V. 5: Optimized Geometry of CF_3···ClF at MP2(full)/Aug-cc-pVTZ

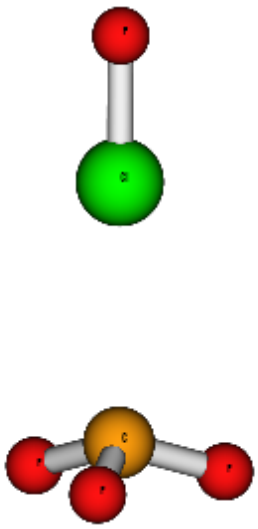

V. 5. B. Results from AIM analysis:

Similar to Li bonds, presence of bond critical point, bond path and concept of mutual penetration of interacting atoms, acceptor and chlorine, are the AIM parameters that can be used to characterize chlorine bond. AIM analysis at MP2(full) level with different basis sets showed the presence of a bond critical point between C and Cl and a bond path passing through the BCP connects the two atoms. The structure of CF_3•••Cl-F with bond critical points and bond path is shown in Figure. V. 6. The electron density at the chlorine bond critical point at MP2(full)/Aug-cc-pVTZ is 0.0229 au. On bonding the radius of carbon atoms reduces by 0.58 Å and the hydrogen atom radii by 0.45Å. Δr is positive and the extent of mutual penetration is 1.03Å. AIM analysis shows a strong interaction between C and Cl in CF_3•••Cl-F complex. The electron density at the chlorine bond critical point and its Laplacian obtained at different basis sets are given in Table. V. 15. The bonded and nonbonded radii of C and Cl are given in Table. V. 16.

Figure. V. 6: AIM analysis of CF_3···ClF showing Bond Critical Points and Bond Paths

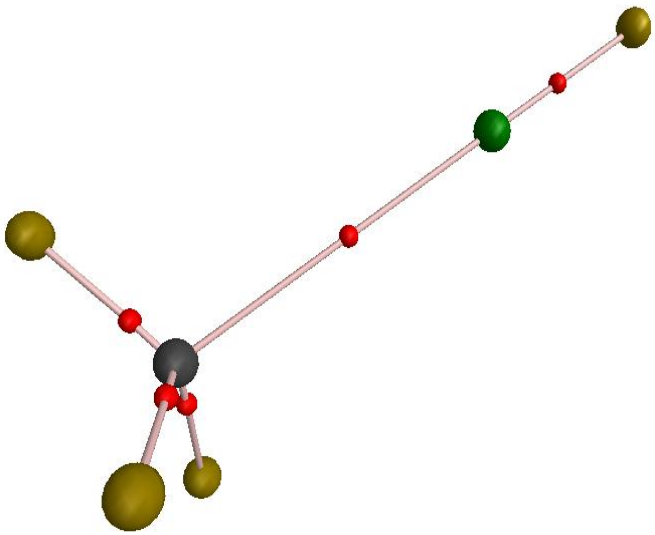

Table. V. 13: Bond length, bond angle, shift in Cl-F bond length and Cl-F stretching frequency and interaction energy at MP2(full)

	*6-311G***	*6-311++G***	*Aug-cc-pVDZ*	*Aug-cc-pVTZ*
$R_{C\text{-}Cl}$ (Å)	3.2030	3.3136	2.9834	2.692
∠FClC (°)	179.6	179.3	179.7	179.9
Δr (Å)	-0.0037	-0.0008	-0.0041	-0.001
Δν (cm^{-1})	93.7	43.6	126.6	110.7
ΔE (kcal mol^{-1})	-0.5	-0.5	-1.3	-2.3

Table. V. 14: Displacement of the atoms in the normal Cl-F stretching modes for the CF_3•••Cl-F complex and the monomer at MP2(full)/Aug-cc-pVTZ level.

	CF_3•••ClF				*Cl-F*		
	X	*Y*	*Z*		*X*	*Y*	*Z*
C	0.08	0.00	0.00	Cl	0.48	0.00	0.00
F	-0.02	-0.08	0.00	F	-0.88	0.00	0.00
F	-0.02	0.04	-0.07				
F	-0.02	0.04	0.07				
Cl	0.47	0.00	0.00				
F	-0.86	0.00	0.00				

Table. V. 15: Electron Densities (ρ, au.) and the Laplacian (*L, au.*)

Complex	*MP2(full)/Aug-cc-pVDZ*		*MP2(full)/Aug-cc-pVTZ*	
	ρ	*L*	*ρ*	*L*
CF_3···ClF	0.0106	-0.0103	0.0229	-0.0175

Complex	*MP2(full)/6-311G***		*MP2(ful)/6-311++G***	
	ρ	*L*	*ρ*	*L*
CF_3···ClF	0.0076	-0.0064	0.0063	-0.0050

Table. V. 16: Bonded (r^b) and Nonbonded ($r°$) Radii (in Angstroms) of Acceptor (C) and Donor (Cl) Atoms and Penetration, Δr, Defined as the Sum of the Differences in Bonded and Nonbonded Radii of C and Cl at MP2(full)/Aug-cc-pVTZ level.

Complex	$r°$ *(C)*	r^b *(C)*	$r° - r^b$ *(C)*	$r°$ *(Cl)*	r^b *(Cl)*	$r° - r^b$ *(Cl)*	Δr
$CF_3\cdots ClF$	1.95	1.37	0.58	1.77	1.32	0.45	1.03

Table. V. 17 list the geometric parameters and Table. V. 18 the rotational constants of all the complexes at MP2(full) level with basis sets at 6-311G**, 6-311++G**, Aug-cc-pVDZ and MP2(full)/Aug-cc-pVTZ. From the values of A, B and C rotational constants, CF_3 radical forms symmetric top complexes with HF, HCl, HBr, HCN, LiF, LiCl, LiBr, ClF. The only exceptions are $CF_3\cdots$HCl and $CF_3\cdots$HBr at MP2(full)/6-311++G** level.

The normal mode vibrational frequencies of all the complexes and the monomers are listed in Table. V. 19. Frequency analysis shows that the normal modes of the CF_3 radical in the complex show a slight shift upon complex formation, which is negligible. Hence it can be concluded that the monomer geometry is not affected by the complexation, which reconfirms the nature of interaction between the monomers a very weak one. In case of Li and Cl bond complexes there is mode mixing which is not found in case of hydrogen bond complexes. Table. V. 17, Table. V. 18 and Table. V. 19 are given at the end of the chapter.

V. 6. Comparison of the nature of hydrogen, lithium and chlorine bonds formed by CF_3 radical:

The carbon of CF_3 radical acts as an acceptor of hydrogen, lithium and chlorine bonds. From the results obtained using different basis sets, 6-311G**, 6-311++G**, Aug-cc-pVDZ and Aug-cc-pVTZ, at MP2(full) level, it can be observed that the optimized geometries of the complexes do not change with the expansion of Dunning basis sets but it changes with Pople basis sets.

A comparison of the interaction energies of the hydrogen bonded and lithium bonded complexes show that the lithium bonds are stronger than the corresponding hydrogen bonds. At MP2(full)/Aug-cc-pVTZ, the interaction energies for CF_3-HF, CF_3-HCl and CF_3-HBr are -1.36, -1.51 and -2.38 kcal mol^{-1} and -1.44, -2.07 and -3.05 kcal mol^{-1} for $CF_3\cdots$LiF, $CF_3\cdots$LiCl and $CF_3\cdots$LiBr complexes respectively. This is due to the high dipole moment of Li-F/Cl/Br compared to the corresponding H-F/Cl/Br. The dipole moments of Li-F, Li-Cl and Li-Br are 6.5D, 7.3D and 7.4D and that of H-F, H-Cl and H-Br are 1.9D, 1.2D and 0.9D respectively. Here we can observe a trend in the bond strength with the bond donors. For H bond complexes the interaction energy and dipole moment shows a reverse trend. Interaction energy increases in the order $CF_3\cdots$HF< $CF_3\cdots$HCl< $CF_3\cdots$HBr, where as dipole moment of the H bond donor decreases in the order HF > HCl >HBr. The trend is different in case of Li bond complexes. Here the dipole moment increases from LiF< LiCl< LiBr and interaction energy follows the same pattern, i.e. interaction energy of the lithium bonded complexes are directly proportional to the dipole moment of the Li bond donor. The strength of HF, LiF and ClF complexes with CF_3 can also be compared in a similar fashion, $CF_3\cdots$HF (-1.36) < $CF_3\cdots$LiF (-1.44) < $CF_3\cdots$ClF (-2.28). The dipole

moment of Cl-F is 1. 1D, i.e., the dipole moment increases in the order, Cl-F< H-F< Li-F. For complexes of CF_3 with various donors, the comparison of interaction energy and dipole moment of the H/L/Cl bond donors give the following conclusions, 1) for hydrogen bond complexes interaction energy increases as the dipole moment of the hydrogen bond donor decreases ($\Delta E\alpha\ \mu^{-1}$), 2) for lithium bond complexes interaction energy increases as the dipole moment of the lithium bond donor increase ($\Delta E\alpha\ \mu$) and 3) $CF_3\cdots HF$, $CF_3\cdots LiF$ and $CF_3\cdots ClF$ do not follow any trend. On the basis of the above observation, it is worth mentioning that the bond strength of complexes of CF_3 radical with H, Li and Cl cannot be explained only on the basis of dipole-dipole interaction. These trends are discussed further in the following section on the basis of NBO analysis.

Many groups have tried to explain the geometry of the complexes on the basis of the molecular electrostatic potential of the monomers. The electrostatic potential maps of CF_3 radical obtained at all the four different basis sets are shown in Figure. V. 7. The blue color represents regions of positive potential and the regions of negative potential are denoted by red color. The isosurface maps of CF_3 radical at all the basis sets are similar. It seems that electrostatic potential of CF_3 radical does not play a major role in the determination of the structure of the complex. The molecular electrostatic maps of the complexes at MP2(full)/Aug-cc-pVTZ is shown in Figure. V. 8. The change in the electron density at the CF_3 radical on complex formation is very obvious from the comparison of the potential at CF_3 radical (Figure. V. 7) with the potential at the CF_3 radical in the complex (Figure. V. 8). It is the H, Li and Cl bond donors which determines the nature of interaction and the structure of the complex. Higher interaction energy of Li bonds compared to H bonds can also be explained using the isosurface maps. In H bond complexes, the potential around the

CF_3 radical is more negative than the corresponding Li bond complexes. In another way, in the complex more charge transfer occurs to LiY from CF_3 radical than from CF_3 to HY. There is not much variation in the potential at the F in CF_3 in all the three CF_3···HY complexes. But it is not the same for Li complexes. In Li complexes the potential at the F of CF_3 is more positive at CF_3···LiBr than CF_3···LiCl and least positive or comparatively more negative in CF_3···LiF. i.e., charge transfer from CF_3 to lithium bond donor is maximum in CF_3···LiBr complex. From the molecular electrostatic potential, the extent of charge transfer can be represented as CF_3···LiBr > CF_3···LiCl > CF_3···LiF, which is reflected in the trend in the interaction energy. Clearly, induction and dispersion (dipole-induced dipole, induced dipole-induced-dipole etc) play an important role in the determination of the structure of the complexes.

The absolute values of electron density at the hydrogen and lithium bond critical point and the extent of mutual penetration obtained using AIM analysis reveal interesting trends. At MP2(full)/Aug-cc-pVTZ the value of ρ for the hydrogen bonded complexes are 0.0094, 0.0146 and 0.0202 au and that of lithium bonded complexes are 0.0064, 0.0072 and 0.0082 au when the donor varies as X-F, X-Cl and X-Br (X=H, Li). From the values of ρ, it is clear that there is more accumulation of electron density between C and X in hydrogen bonded complexes than lithium bonded complexes. Hence hydrogen bonded complexes have more covalent nature. For chlorine bonded complex, CF_3···ClF, ρ is 0.0229 au. The nature of chlorine bond is similar to that of hydrogen bond.

Figure. V. 7: Molecular electrostatic potential isosurface of CF_3 radical

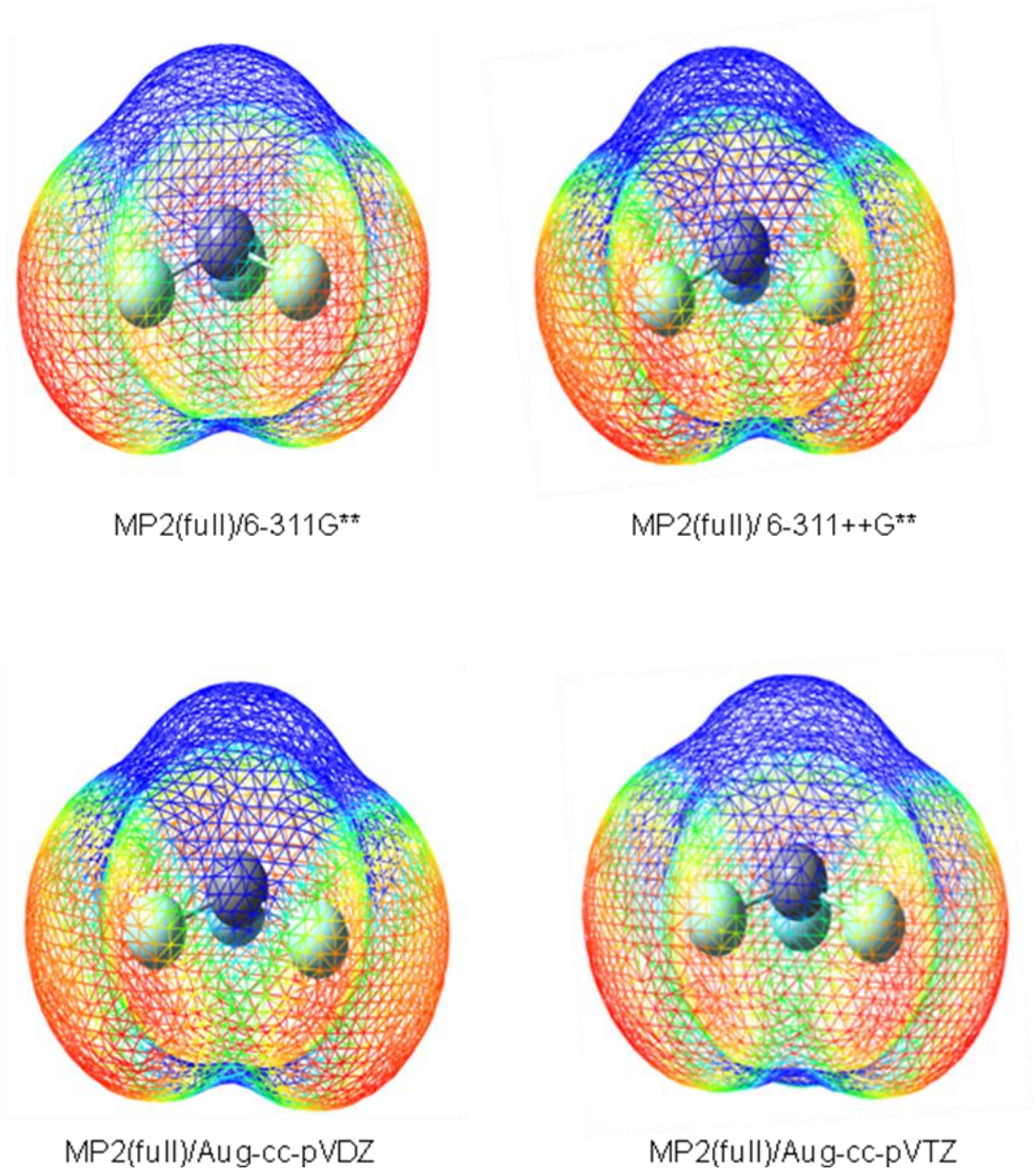

Figure. V. 8: Molecular Electrostatic Potential Map of CF_3···XY complexes at MP2(full)/Aug-cc-pVTZ.

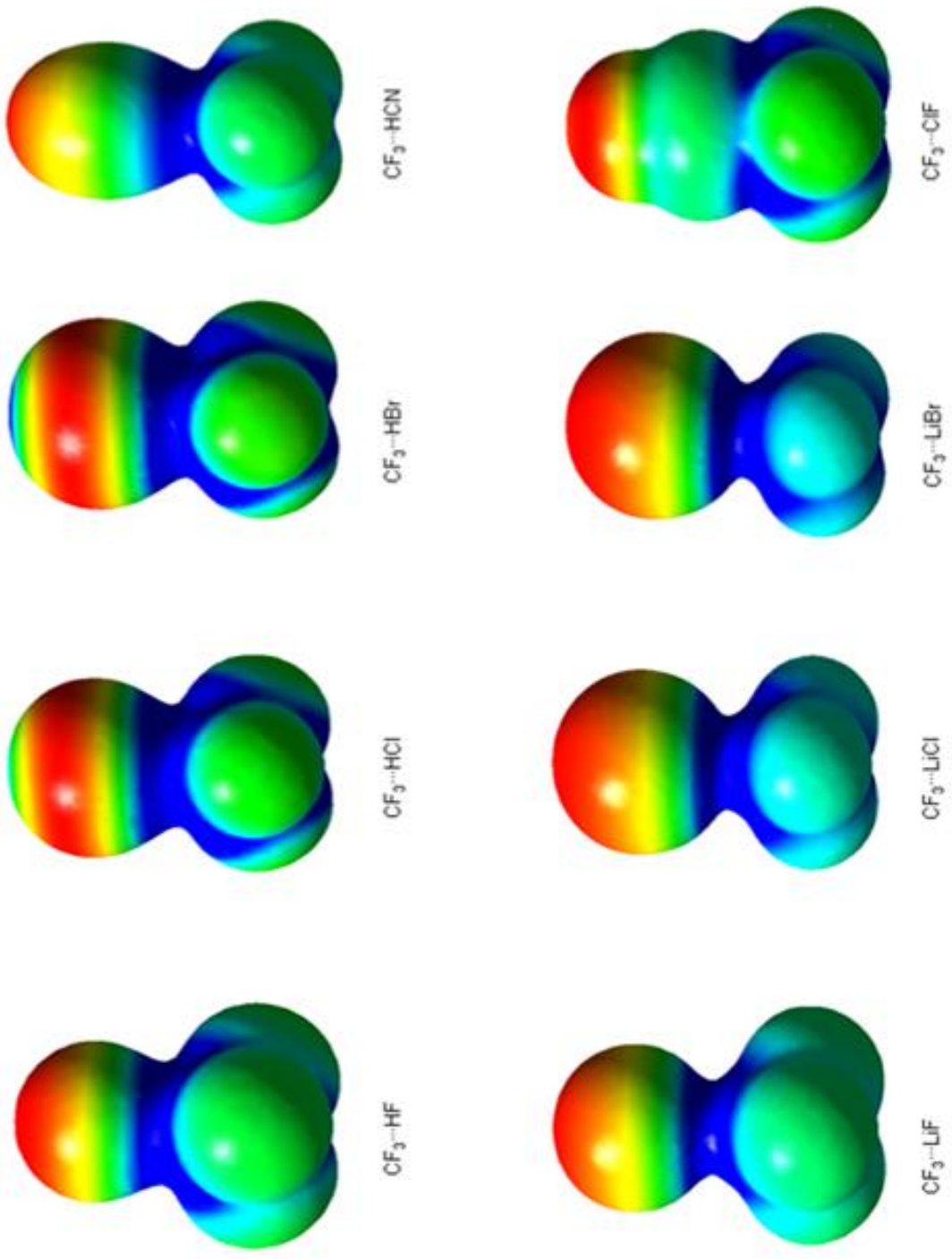

V. 7. NBO analysis

NBO analysis of all the complexes of CF_3 with hydrogen, lithium and chlorine bond donors at MP2(full) level with basis set Aug-cc-pVTZ has been carried out. The charge on the atoms and the difference, ΔQ (e) is given in Table. V. 20. The charges on each of the atoms of all the complexes are given in Table. V. 21, at the end of the chapter. On comparison of the charge on the carbon and fluorine atoms of CF_3 in CF_3···HF/Cl/Br/CN, the extent of charge transfer is more from carbon and the values varies with the hydrogen bond donor. The charge on fluorine is same for CF_3···HCl/Br/CN (-0.370 e) complexes and it is -0.367 e for CF_3···HF complex. This is visible in the isosurface maps of CF_3···HY complexes in Figure. V. 8. The scenario is different when Li bond complexes are considered. The charge on the carbon atom is 1.095 e for CF_3···LiF and it is 1.102 e for both CF_3···LiCl and CF_3···LiBr complexes. From LiF to LiBr the charge on fluorine decreases as -0.358 e (CF_3···LiF), -0.355 e (CF_3···LiCl) and -0.353 e (CF_3···LiBr). This explains the maximum positive potential at fluorine atom in CF_3···LiBr complexes (Figure. V. 8). In all the complexes the values of ΔQ is positive, i.e. charge is transferred from the CF_3 radical to the H/Li/Cl bond donors. There is more charge transfer occurring in lithium bonded complexes than in hydrogen bonded complexes.

The trends observed in the interaction energies of various H/Li/Cl bond donors can be further evaluated using the NBO analysis. CF_3···HF/Cl/Br complexes showed an increase in interaction energy from CF_3···HF to CF_3···HCl to CF_3···HBr. For these complexes ΔQ also varies in the same order, $\Delta Q_{(CF_3\cdots HF)}$ (0.013) < $\Delta Q_{(CF_3\cdots HCl)}$ (0.020) < $\Delta Q_{(CF_3\cdots HBr)}$ (0.028). Li bond complexes show similar trend for both interaction

energy and ΔQ, $\Delta E_{(CF_3\cdots LiF)} < \Delta E_{(CF_3\cdots LiCl)} < \Delta E_{(CF_3\cdots LiBr)}$ and $\Delta Q_{(CF_3\cdots LiF)}$ (0.020) < $\Delta Q_{(CF_3\cdots LiCl)}$ (0.036) < $\Delta Q_{(CF_3\cdots LiBr)}$ (0.042). The ΔQ for $CF_3\cdots ClF$ (0.031) is greater than that of $CF_3\cdots HF$ and $CF_3\cdots LiF$. The higher interaction energy of $CF_3\cdots ClF$ than $CF_3\cdots LiF$ may be because of the higher charge transfer occurring from CF_3 to ClF. Charge transfer plays a major role in the stability of the complexes of CF_3 radical.

Table. V. 20:Natural Atomic Charge on each atom and the charged transferred (ΔQ,e) at MP2(full)/Aug-cc-pVTZ

	$q_{(C)}$	$q_{(F)}$	ΔQ
CF_3	1.138	-0.379	-
$CF_3\cdots HF$	1.115	-0.367	0.013
$CF_3\cdots HCl$	1.131	-0.370	0.020
$CF_3\cdots HBr$	1.139	-0.370	0.028
$CF_3\cdots HCN$	1.130	-0.370	0.019
$CF_3\cdots LiF$	1.095	-0.358	0.020
$CF_3\cdots LiCl$	1.102	-0.355	0.036
$CF_3\cdots LiBr$	1.102	-0.353	0.042
$CF_3\cdots ClF$	1.136	-0.368	0.031

V. 8: Correlation of interaction energy with charge transfer and electron density at the bond critical point:

Figure. V. 9 shows the plot of interaction energy as a function of charged transferred. In both hydrogen bonded (Figure. V. 9. a) and lithium bonded complexes (Figure. V. 9. b) there is a direct correlation between interaction energy and the extent of charge transfer from CF_3 to H/Li bond donor. ΔE is in kcal mol^{-1} and ΔQ in e (extent of charge transferred).

Figure. V. 9. a: Plot of interaction energy as a function of charge transferred for hydrogen bonded complexes

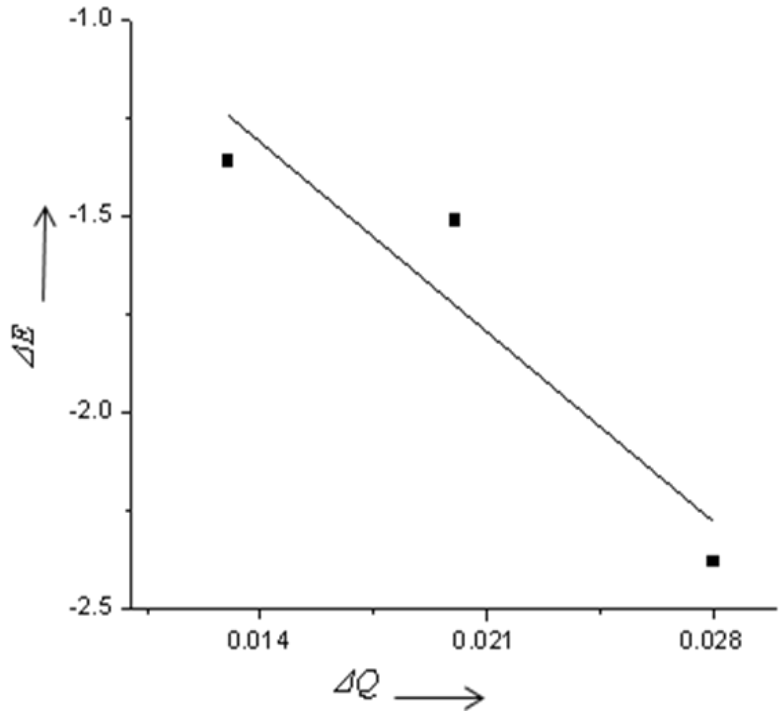

Figure. V. 9. b: Plot of interaction energy as a function of charge transferred for lithium bonded complexes

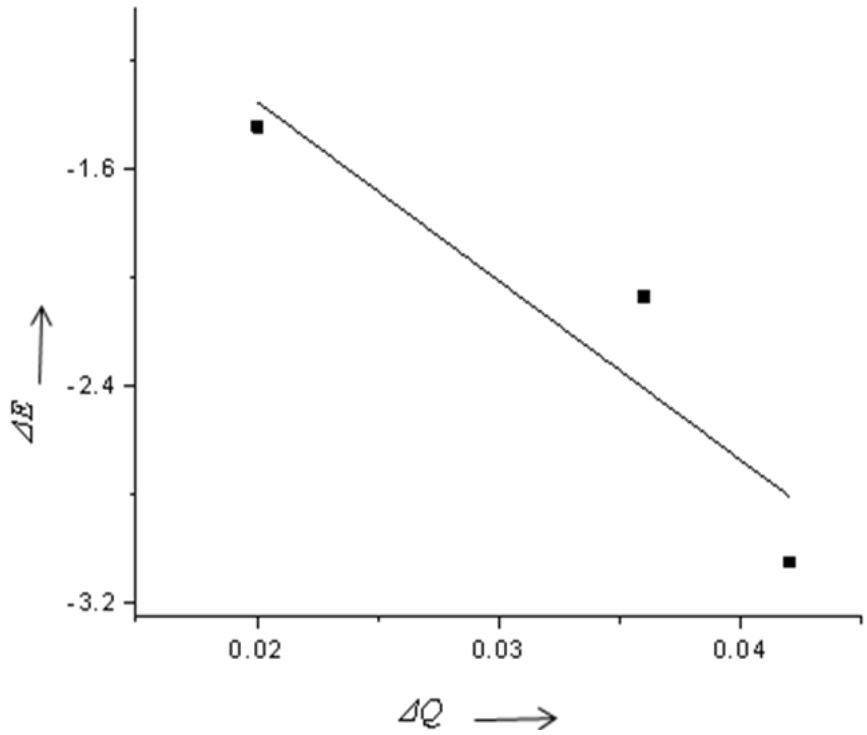

A plot of interaction energy as a function of electron density at the bond critical point can reveal a lot about the strength and nature of the interaction. Correlation between electron density and interaction energy is shown in Figure. V. 10. a. for hydrogen and Figure. V. 10. b. for lithium bonded complexes. Here the hydrogen bond acceptor is the same and the donor varies. The correlation is better for Li bonded complex (R=-0.99) than H bonded complex (R= -0.93). The slope of the linear fit gives an idea about the electron density distribution between atoms A and X. A higher value of slope indicates less accumulation of electron density between A and X. Hence a plot with higher slope indicates an interaction which is dominated by electrostatic forces. A covalent interaction where there is more accumulation of

electron density at the BCP or between A and X gives a linear fit with smaller value of slope.

Figure. V. 10. a) : Plot of interaction energy as a function of electron density at the bond critical point for H-bonded complex:

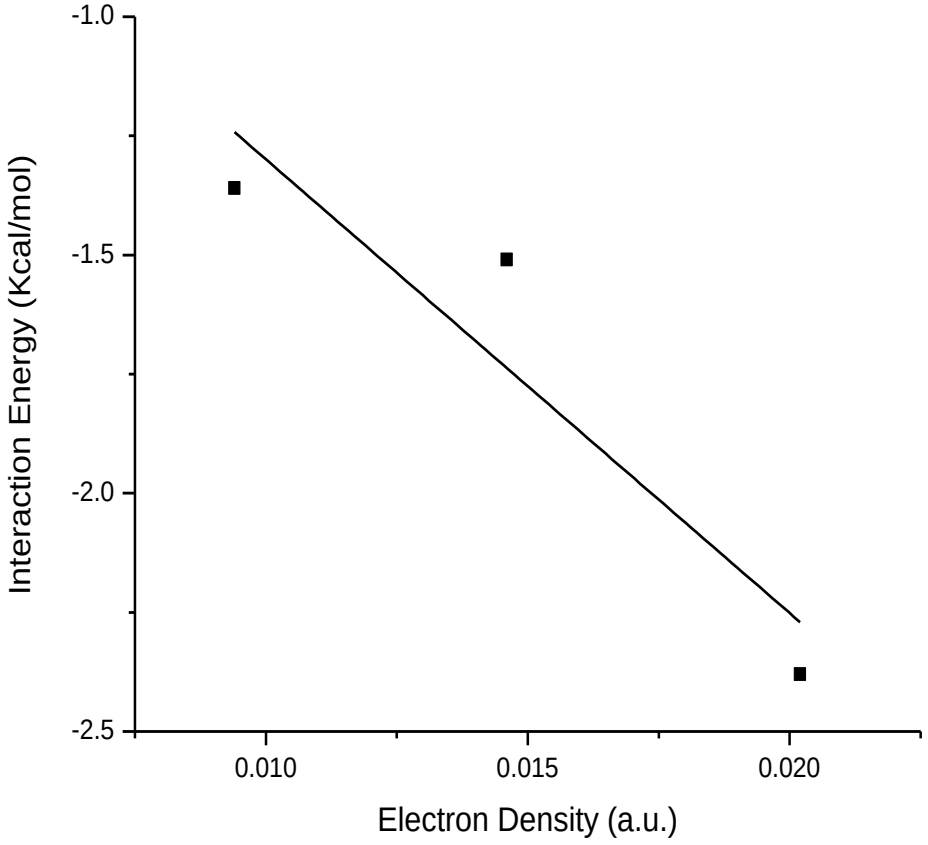

Figure. V. 10. b) : Plot of interaction energy as a function of electron density at the bond critical point for Li-bonded complex:

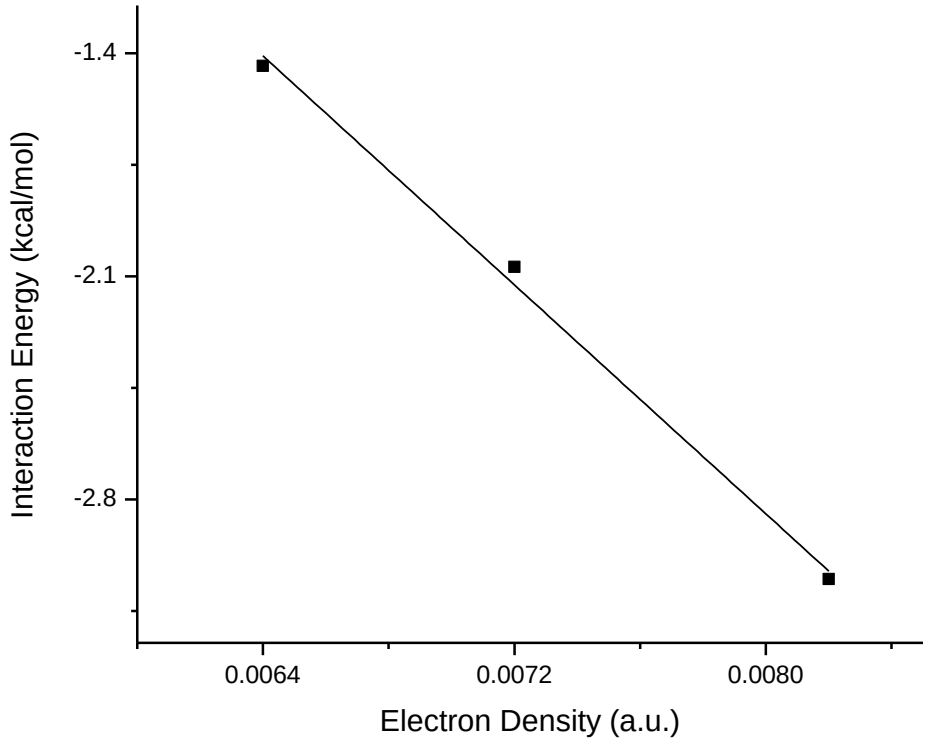

The ΔE obtained from the linear fit for H and Li bonded complexes are

ΔE= (-95.22)*ρ -0.35 (H-bond)

ΔE= (-897.95)*ρ + 4.34 (Li-bond)

The value of slope for H–bonded complex is much low compared to that obtained for Li-bonded complex. This indicates more accumulation of electron density between the atoms in case of hydrogen bonded complex than lithium bonded complex. Hence H-bonded complex has more covalent nature and the major force acting in case of Li-bonded complex is electrostatic.

In the previous work done by Raghavendra and Arunan[13], for HF as hydrogen bond donor with various acceptors, the slope obtained was -263.2 and for Li bond the

slope is -769.2. Similar results are obtained in the present work. Hydrogen bonds are more covalent in nature and lithium bonds more electrostatic.

V. 9. Comparison of CF_3 radical with CH_3 radical:

Figure. V. 11 shows the molecular electrostatic potential maps of CF_3 and CH_3 radicals at 6-311++G** level.

Figure. V. 11:

CF_3 radical **CH_3 radical**

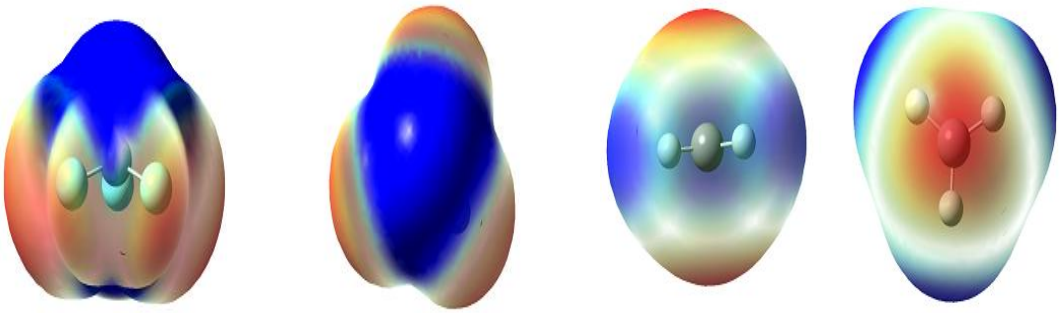

From the electrostatic potential map, it is clear that the behaviour of CH_3 radical and CF_3 radical will be opposite to each other. In case of CH_3 radical, since carbon is more electro negative than hydrogen the electron density is concentrated over the carbon atom. There is a depletion of electron density at the carbon atom in CF_3 radical, since the carbon is attached to more electro negative fluorine atom. Here the electron cloud is pulled towards the three fluorine atoms. This is same as the electron density distribution difference observed in C_6H_6 and C_6F_6[18]. In case of C_6H_6, the hydrogen of HX interacts with the centre of the π cloud to form a stable complex. On the contrary, the interaction of hydrogen of HF with the centre of C_6F_6 ring does

not give a stable geometry. Instead fluorine of HF interacts with the ring to give a stable geometry. But CH_3 and CF_3 do not share this property. Geometric optimization of CF_3 with HF, HCl and HBr with the halogen atom interacting with the carbon had been carried out. The frequency calculations showed that the optimized geometries do not correspond to a minimum energy structure. i.e. the interaction of the halogen of H-Y with the carbon of CF_3 radical does not give a stable geometry, this is opposite to what has been reported in case of C_6F_6-HF complex.

Properties of the CF_3 radical are related more to the properties of CH_3 radical than C_6F_6. The carbon of CF_3 radical forms hydrogen bonded complex with HF at basis sets 6-311++G**, Aug-cc-pVDZ and Aug-cc-pVTZ, similar to CH_3. The geometry of the complexes of CF_3 with HY, LiY and ClF are similar to geometry of the complexes of CH_3 with same donors. But the stabilization energy of CF_3-HY/LiY/ClF complexes are much less compared to the corresponding complexes of CH_3. In the previous section on NBO analysis, it was shown that the ΔQ for CF_3···HF/Cl/Br increases in the order $\Delta Q_{(CF_3\cdots HF)} < \Delta Q_{(CF_3\cdots HCl)} < \Delta Q_{(CF_3\cdots HBr)}$ even though the dipole moment of the hydrogen bond donor shows the reverse trend. For complexes of CH_3 radical with HF, HCl and HBr, Table. V. 22, the value of ΔQ varies in the same order $\Delta Q_{(CH_3\cdots HF)} < \Delta Q_{(CH_3\cdots HCl)} < \Delta Q_{(CH_3\cdots HBr)}$. When hydrogen bonded complexes are considered, in CH_3···HY complexes, the interaction energy is proportional to the dipole moment of the hydrogen bond donor. Whereas in CF_3···HY the interaction energy is inversely proportional to the dipole moment of the hydrogen bond donor. The hydrogen formed in case of CH_3 radical is more of electrostatic in nature compared to the hydrogen bond formed by CF_3 radical, which is charge transfer assisted.

Table. V. 22: Natural Atomic Charge on each atom and the charged transferred (ΔQ) at MP2(full)/Aug-cc-pVTZ

	$q_{(C)}$	$q_{(H)}$	ΔQ
CH_3	-0.418	0.139	
CH_3···HF	-0.446	0.153	0.014
CH_3···HCl	-0.435	0.152	0.022
CH_3···HBr	-0.432	0.155	0.034
CH_3···HCN	-0.433	0.147	0.009

V. 10. Comparison of the nature of hydrogen, lithium and chlorine bonds formed by CF_3 radical with other non-conventional acceptors:

Interaction energies of complexes with CF_3 as H/Li/Cl-F bond acceptor are compared with various non-conventional acceptors at MP2(full)/Aug-cc-pVTZ in Table. V. 23. The various acceptors chosen from literature[13] are lone pair (H_2O), π-cloud (C_2H_4), unpaired (CH_3) electrons and σ (H_2) bonded pairs. For these acceptors the interaction energies of Li bond complexes are much larger compared to H and Cl bond complexes. CF_3 as acceptor shows a different order of stability of the complexes. CF_3 is a better acceptor of chlorine bond than hydrogen and lithium bonds.

Table. V. 23: Interaction Energy, ΔE (kcal mol^{-1})

	H_2O	*C_2H_4*	*CH_3*	*H_2*	*CF_3*
H-F	-9.4	-5.7	-3.3	-1.2	-1.4
Li-F	-18.4	-10.8	-7.1	-3.3	-1.4
Cl-F	-6.0	-8.0	-4.2	-1.2	-2.3

The electron density and its Laplacian at the H, Li and Cl bond critical point for different acceptors at MP2(full)/Aug-cc-pVTZ level have been compared. The value of electron density (ρ) at hydrogen bond critical point for HF as donor with various acceptors such as lone pair (H_2O), π (C_2H_4), unpaired (CH_3) electrons and σ (H_2) bonded pairs taken from literature[13] are 0.0436, 0.0225, 0.0196 and 0.0110 au respectively and its Laplacian are -0.0262, -0.0114, -0.0096 and -0.0087 au. For complex of HF with CF_3, ρ(HBCP) is 0.0094 au and L is -0.0087 au. The value of electron density of CF_3•••HF is much less than the ρ(HBCP) for HF-CH_3 complex and is comparable to the ρ for σ (H_2) bonded pairs as acceptors. Extending the comparison to Li bonds, the ρ(LiBCP) for CF_3•••LiF is 0.0064 au and L is -0.0084 au and ρ(LiBCP) for H_2O, C_2H_4, CH_3 and H_2 are 0.0298, 0.0151, 0.0123 and 0.0108 au respectively and its L are -0.0588, -0.0179, -0.0142 and -0.0150 au respectively. It can be observed that the capacity of CF_3 as Li bond acceptor is the least. In case of Cl bonds, ρ(ClBCP) for complexes of ClF with H_2O, C_2H_4, CH_3, CF_3 and H_2 are 0.0293, 0.0394, 0.0266, 0.0229 and 0.0106 au respectively and L are -0.0303, -0.0230, -0.0160, -0.0174 and -0.0108 respectively. In chlorine bond interaction, the value of

electron density at the bond critical point between CF_3 and ClF is comparable to ρ(ClBCP) of CH_3 and is greater than H_2 as Cl bond acceptors.

The nonbonded radius of carbon in CF_3 radical is 1.95 Å, whereas the nonbonded radius of carbon in CH_3 radical is 2.25Å, C_2H_4 is 2.34Å and CH_4 molecule is 2.0Å. Similarly the nonbonded radius of oxygen in H_2O is 2.04 Å and that of H_2 is 1.72Å. CF_3 radial is similar to CH_4 molecule than other non-conventional acceptors.

V. 11. Conclusions:

CF_3 radical acts as hydrogen, lithium and chlorine bond acceptor. Higher basis sets give better results since dispersion plays a major role in these weak interactions. CF_3 radical is a better acceptor of Li and Cl bonds than H bond. Frequency analysis shows mode mixing in CF_3···LiY and CF_3···ClF complexes, but mode mixing is absent in CF_3···HY complexes. Hence the criteria of using shift in X-Y bond length and shift in X-Y stretching frequency on complex formation to characterize the strength of the interaction is applicable only for hydrogen bonded complex. AIM calculations also support the fact that CF_3 can act as hydrogen, lithium and chlorine bond acceptor. Molecular electrostatic potential maps and the NBO analysis confirm that charge is transferred from the CF_3 radical to the H/Li/Cl bond donors. The electron density at the bond critical point, mutual penetration, extent of charge transfer and interaction energy are inversely proportional to the dipole moment of the donor molecule for hydrogen bond complexes of CF_3 radical whereas all the parameters are proportional to the dipole moment of the donor in case of lithium bonded complexes . It is worth mentioning that H, Li and Cl bond strength cannot be explained only on the basis of dipole-dipole interaction. Even though the interaction is believed to be predominantly

electrostatic in nature, charge transfer interactions are also important. The hydrogen bond formed by CF_3 radical is charge transfer assisted. Geometries of the hydrogen, lithium and chlorine bonded complexes of CF_3 radical is similar to hydrogen, lithium and chlorine bonded complexes of CH_3 radical , even though they are topologically different.

V. 12. References:

1) E. Arunan et al. *Pure Appl. Chem.,* **2011***, 83,* 1637;

http://ipc.iisc.ernet.in/_arunan/iupac/

(2) S. Scheiner, *Hydrogen Bonding*: *A TheoreticalPperspecitive*; Oxford University Press: Oxford, NY, **1997**.

(3) G. R. Desiraju, T. Steiner, *The Weak Hydrogen Bond: In Structural Chemistry and Biology*; Oxford University Press: Oxford, NY, **1997**.

4) L. Pauling, *The Nature of the Chemical Bond;* Cornell University Press: Ithaca, NY, **1960**.

5) E. Y Misochko, V. A , Benderskii, A. U Goldshleger, A. V Akimov,. A. F Shestakov, *J. Am. Chem. Soc.* **1995**, *117*, 11997

6) I. Alkorta,I. Rozas, J. F. Elguero, *Ber. Bunsen.-Ges. Phys. Chem.,* **1998**, *102*, 429.

7) J. J Szymczak, S. J Grabowski, S. Roszak, J. Leszczynski, *Chem. Phys. Lett.,* **2004**, *393*, 81.

8) S. J. Grabowski, W. A.Sokalski, J Leszczynski, *Chem. Phys. Lett.,* **2006**, *432*, 33.

9) D. Wu, Z-R. Li, X. Y. Hao, A. F Jalbout, L . Adamowicz, R. J. Li, C-C. Sun,. *J. Chem. Phys.,* **2004**, *120*, 1330.

10) I. Alkorta, I. Roza, J. Ekguero, *Chem. Soc. Rev.,* **1998**, *27*, 163.

11) J. J.Sczymczak, S. J. Grabowski,. S. Roszak, J. Leszczynski, *Chem. Phys Lett.,* **2004**, *393*, 81.

12) T. F. Koetzle, O. Eisenstein, A. L. Rheingold, R. H. Crabtree, *Angew. Chem., Int. Ed. Engl*., **1995**, *34*, 2507.

13) B. Raghavendra, E. Arunan, *J. Phys. Chem. A*., **2007**, *111*, 9699.

14) B. Raghavendra, E. Arunan, *Chem. Phys. Lett.,* **2008**, *467*, 37.

15) P. Hobza, Z. Havlas, *Chem. Rev.,* **2000**, *100*, 4253

16) X. Li, L. Liu, H. B. Schlegel, *J. Am. Chem. Soc.,* **2002**, *124*, 9639.

17) I. Alkorta, I Rozas, J. Â Elguero, *Journal of Fluorine Chemistry*., **2000**, *101*, 233.

18) B. K. Mishra , N. Sathyamurthy, *J. Phys. Chem. A.,* **2007**, *111,* 2139.

19) B. Q. Wang, Z-R. Li ,D Wu, Xi. Y. Hao, R. J. Li, C-C. Sun, *Chemical Physics Letters*., 2003, 375 ,91.

20) Y. Li, D Wu, Z-R. Li, W. Chen, C.-C. Sun, *J. Chem. Phys*, **2006**, 125, 084317.

21) P. A. Kollman, J. F. Liebman, L. C. Allen. *J. Am. Chem. Soc*., **1970**, *92*, 1142.

22) B. S. Ault, G. C. Pimentel, *J. Phys. Chem*., **1975**, *79*, 621

23) Y. Feng, L. Liu, J. T. Wang, X. S. Li, Q. X. Guo,*Chem. Commun*. , 2 0 0 4, 8 8 – 8 9.

24) A. C. Legon, *Phys. Chem. Chem. Phys*., **2010**, *12*, 7736.

25) P. Politzer, P. Lane, M. C. Concha, Y. Ma, J. S. Murray*, J. Mol. Model*., **2007**, *13*, 305.

26) J. Nancy, M. Amezaga, S. C. Pamies,N. M. Peruchena, G. L. Sosa, *J. Phys. Chem. A,* **2010**, *114,* 552.

27) A. Brisdon, *Annu Rep Prog Chem Sect A.* **2002***, 98*, 107.

28) A. R. Voth, F. A. Hays, P. S. Ho, *PNAS*. **2007**, *104*, 6188.

29) S. E. Novick, K. C. Janda, W. Klemperer, *J. Chem. Phys*., **1976**, *65*, 5115.

30) F. A. Baiocchi, T. A. Dixon, W. Klemperer, *J. Chem. Phys*., **1982**, *77*, 1632.

31) R.-Y. Li, Z.-R. Li. D.Wu, Y. Li, W. Chen, C.-C. Sun, *J. Phys.Chem.* **2005**, *109*, 2608.

32) A. C. Legon, *Angew. Chem., Int. Ed*., **1999**, *38*, 2686.

33) P. Metrangalo, G. Resnati, *Chem.-Eur. J*., **2001**, *7*, 2511.

34) W. Wang, N.-B. Wong, W. Zheng, A. Tian, *J. Phys. Chem. A*., **2004**, *108*, 1799.

35) A. C. Legon, *Chem. Eur. J*.,**1998**, *4*, 1890.

36) A. C. Legon, *Chem. Phys. Lett*., **1997**, *279*, 55.

37) M. J. Frisch, G. W. Trucks, H. B Schlegel, G. E. Scuseria, M. A.Robb, J. R.Cheeseman, J. A. Montgomery Jr., T. Vreven, K. N. Kudin, J. C. Burant, J. M. Millam, S. S. Iyengar, J. Tomasi, V. Barone, B. Mennucci, M. Cossi, G. Scalmani, N. Rega, G. A Petersson, H. Nakatsuji, M. Hada, M. Ehara, K. Toyota, R. Fukuda, J. Hasegawa, M. Ishida, T. Nakajima, Y. Honda, O. Kitao, H. Nakai, M. Klene, X. Li, J. E. Knox, H. P. Hratchian, J. B.Cross, C. Adamo, J. Jaramillo, R. Gomperts, R. E. Stratmann, O. Yazyev, A. J. Austin, R. Cammi, C. Pomelli, J. W. Ochterski, P. Y. Ayala, K. Morokuma, G. A. Voth, P. Salvador, J. J. Dannenberg, V. G. Zakrzewski, S. Dapprich, A. D. Daniels, M. C. Strain, O. Farkas, D. K. Malick, A. D. Rabuck, K. Raghavachari, J. B. Foresman, J. V. Ortiz, Q. Cui, A. G. Baboul, S. Clifford, J. Cioslowski, B. B. Stefanov, G. Liu, A. Liashenko, P. Piskorz, I. Komaromi, R. L. Martin, D. J. Fox, T. M. Keith, A. Al-Laham, C. Y. Peng, A. Nanayakkara, M. Challacombe, P. M. W. Gill, B. Johnson, W. Chen, M. W. Wong, C. Gonzalez, J. A. Pople, *Gaussian03*, Revision C-02; Gaussian, Inc. Wallingford CT, **2004.**

38) M. J. Frisch, G. W. Trucks, H. B. Schlegel, G. E. Scuseria, M. A. Robb, J. R. Cheeseman, G. Scalmani, V. Barone, B. Mennucci, G. A. Petersson, H. Nakatsuji, M. Caricato, X. Li, H. P. Hratchian, A. F. Izmaylov, J. Bloino, G. Zheng, J. L. Sonnenberg, M. Hada, M. Ehara, K. Toyota, R. Fukuda, J. Hasegawa, M. Ishida, T. Nakajima, Y. Honda, O. Kitao, H. Nakai, T. Vreven, J. A. Montgomery, Jr., J. E. Peralta, F. Ogliaro, M. Bearpark, J. J. Heyd, E. Brothers, K. N. Kudin, V. N. Staroverov, R. Kobayashi, J. Normand, K. Raghavachari, A. Rendell, J. C. Burant, S. S. Iyengar, J. Tomasi, M. Cossi, N. Rega, J. M. Millam, M. Klene, J. E. Knox, J. B. Cross, V. Bakken, C. Adamo, J. Jaramillo, R. Gomperts, R. E. Stratmann, O. Yazyev, A. J. Austin, R. Cammi, C. Pomelli, J. W. Ochterski, R. L. Martin, K. Morokuma, V.

G. Zakrzewski, G. A. Voth, P. Salvador, J. J. Dannenberg, S. Dapprich, A. D. Daniels, Ö. Farkas, J. B. Foresman, J. V. Ortiz, J. Cioslowski, D. J. Fox, Gaussian, Inc., Wallingford CT, **2009**.

39) R. F. W Bader, *Atoms in Molecules: A Quantum Theory;*Clarendon Press: Oxford, **1990**.

40) F. Biegler-Konig, J. Schonbohm, R. Derdau, D. Bayles, R. F. W Bader, *AIM 2000*, version 1; Bu¨ro fu¨r Innovative Software: Bielefeld, Germany, **2000**.

41) R. II Dennington, T. Keith, J. Millam, K. Eppinnett, W. L. Hovell, R. Gilliland, *GaussView*, Version 3.09; Semichem, Inc.: Shawnee Mission, KS, **2003**.

42) S. S. Batsanov, *Russian Journal of Inorganic Chemistry*, **1991**, *36*, 3015.

43) U. Koch; P. L. A. Popelier. *J. Phys. Chem.,* **1995**, *99*, 9747.

44) P. L. A. Popelier, *Atoms in Molecules. An Introduction* (Prentice Hall, **2000**)

Appendix:

Table. V. 17: Geometric Parameters:

1) **Geometric parameter of CF_3•••HF:**

Position of the Atoms	*Coordinates (in Å, deg)*	*MP2(FULL)/ 6-311G***	*MP2(FULL)/ 6-311++G***	*MP2(FULL)/ Aug-cc-pVDZ*	MP2(FULL)/ Aug-cc-pVTZ
C1	R(2-1)	2.5	3.05	2.497	2.355
H2	R(3-1)	1.314	1.316	1.330	1.309
F3	R(4-1)	1.314	1.316	1.330	1.309
F4	R(5-1)	1.314	1.316	1.330	1.309
F5	R(6-2)	0.913	0.916	0.926	0.922
F6	A(3-1-2)	107.06	107.27	107.14	107.02
	A(4-1-2)	107.07	107.27	107.15	107.03
	A(5-1-2)	107.07	107.27	107.15	107.04
	A(6-2-1)	179.99	180.00	179.99	179.98
	D(4-1-2-3)	119.99	90.00	119.99	119.99
	D(5-1-2-3)	-119.99	90.00	-119.99	-119.99
	D(6-2-1-3)	-42.44	90.00	-119.043	-88.06

2) **Geometric parameter of CF_3•••HCl:**

Position of the atoms	*Coordinates (in Å, deg)*	*MP2(FULL)/ 6-311G***	*MP2(FULL)/ 6-311++G*** a	b	*MP2(FULL)/ Aug-cc-pVDZ*	MP2(FULL)/ Aug-cc-pVTZ
C1	R(2-1)	3.063	3.475	3.604	2.504	2.32
H2	R(3-1)	1.315	1.319	1.325	1.331	1.310
F3	R(4-1)	1.315	1.319	1.316	1.331	1.310
F4	R(5-1)	1.315	1.319	1.314	1.331	1.310
F5	R(6-2)	1.274	1.274	1.274	1.288	1.274
Cl6	A(3-1-2)	107.05	49.544	6.92	108.02	107.04
	A(4-1-2)	107.21	152.70	108.32	107.48	107.40
	A(5-1-2)	107.62	94.99	117.82	106.30	107.02
	A(6-2-1)	178.83	83.497	153.36	179.21	179.62
	D(4-1-2-3)	-119.82	51.66	114.21	120.52	120.07
	D(5-1-2-3)	120.05	-113.61	-13.73	-119.88	-119.87
	D(6-2-1-3)	-128.43	-117.30	65.11	149.27	164.34

3) **Geometric parameter of CF_3•••HBr:**

Position of the atoms	*Coordinates (in Å, deg)*	*MP2(FULL)/ 6-311G***	*MP2(FULL)/ 6-311++G***	*MP2(FULL)/ Aug-cc-pVDZ*	MP2(FULL)/ Aug-cc-pVTZ
C1	R(2-1)	3.068	3.479	2.479	2.195
H2	R(3-1)	1.315	1.318	1.331	1.130
F3	R(4-1)	1.315	1.316	1.331	1.130
F4	R(5-1)	1.315	1.323	1.331	1.130
F5	R(6-2)	1.409	1.410	1.421	1.406
Br6	A(3-1-2)	107.75	148.54	107.30	107.13
	A(4-1-2)	107.61	99.13	107.31	107.14
	A(5-1-2)	106.61	47.77	107.312	107.15
	A(6-2-1)	178.82	91.49	179.99	179.85
	D(4-1-2-3)	120.39	-166.68	119.99	119.99
	D(5-1-2-3)	-119.84	-56.39	-119.99	-119.99
	D(6-2-1-3)	156.26	-122.41	-175.47	179.04

4) **Geometric parameter of CF_3•••HCN:**

Position of the atoms	*Coordinates (in Å, deg)*	*MP2(FULL)/ 6-311G***	*MP2(FULL)/ 6-311++G***	*MP2(FULL)/ Aug-cc-pVDZ*	*MP2(FULL)/ Aug-cc-pVTZ*
C1	R(2-1)	3.175	3.213	2.739	2.524
H2	R(3-1)	1.315	1.317	1.331	1.311
F3	R(4-1)	1.315	1.317	1.331	1.311
F4	R(5-1)	1.315	1.317	1.331	1.311
F5	R(6-2)	1.067	1.067	1.077	1.057
C6	R(7-6)	1.170	1.171	1.179	1.162
N7	A(3-1-2)	107.40	107.45	107.29	107.20
	A(4-1-2)	107.16	107.21	107.32	107.18
	A(5-1-2)	107.30	107.34	107.32	107.19
	A(6-2-1)	179.25	179.18	179.91	179.99
	A(7-6-2)	179.81	179.79	179.96	179.99
	D(4-1-2-3)	119.99	119.99	119.99	119.99
	D(5-1-2-3)	-120.07	-120.07	-119.99	-120.00
	D(6-2-1-3)	167.99	167.68	156.32	-123.72
	D(7-6-2-1)	140.53	139.66	124.62	169.89

5) **Geometric parameter of CF_3•••LiF:**

Position of the atoms	*Coordinates (in Å, deg)*	*MP2(FULL)/ 6-311G***	*MP2(FULL)/ 6-311++G***	*MP2(FULL)/ Aug-cc-pVDZ*	*MP2(FULL)/ Aug-cc-pVTZ*
C1	R(2-1)	2.556	2.732	2.640	2.645
Li2	R(3-1)	1.311	1.312	1.327	1.307
F3	R(4-1)	1.311	1.312	1.327	1.307
F4	R(5-1)	1.311	1.312	1.327	1.307
F5	R(6-2)	1.567	1.594	1.582	1.579
F6	A(3-1-2)	105.34	106.36	106.41	106.45
	A(4-1-2)	107.31	106.80	106.86	106.78
	A(5-1-2)	106.65	106.45	106.49	106.51
	A(6-2-1)	131.03	179.76	179.86	179.85
	D(4-1-2-3)	119.97	120.05	120.05	120.03
	D(5-1-2-3)	-119.65	-119.87	-119.86	-119.89
	D(6-2-1-3)	-49.04	-16.92	-2.06	-0.23

6) **Geometric parameter of CF_3•••LiCl**:

Position of the atoms	*Coordinates (in Å, deg)*	*MP2(FULL)/ 6-311G***	*MP2(FULL)/ 6-311++G***	*MP2(FULL)/ Aug-cc-pVDZ*	*MP2(FULL)/ Aug-cc-pVTZ*
C1	R(2-1)	2.522	2.637	2.526	2.597
Li2	R(3-1)	1.310	1.311	1.326	1.306
F3	R(4-1)	1.310	1.311	1.326	1.306
F4	R(5-1)	1.310	1.311	1.326	1.306
F5	R(6-2)	2.017	2.015	2.032	2.028
Cl6	A(3-1-2)	106.02	106.23	106.23	106.30
	A(4-1-2)	106.33	106.64	106.59	106.60
	A(5-1-2)	106.09	106.30	106.35	106.37
	A(6-2-1)	179.92	179.84	179.90	179.88
	D(4-1-2-3)	120.03	120.04	120.02	120.04
	D(5-1-2-3)	-119.91	-119.88	-119.89	-119.92
	D(6-2-1-3)	-27.94	-26.10	-46.82	-25.75

7) **Geometric parameter of CF_3•••LiBr:**

Position of the atoms	*Coordinates (in Å, deg)*	*MP2(FULL)/ 6-311G***	*MP2(FULL)/ 6-311++G***	*MP2(FULL)/ Aug-cc-pVDZ*	*MP2(FULL)/ Aug-cc-pVTZ*
C1	R(2-1)	2.527	2.664	2.454	2.543
Li2	R(3-1)	1.310	1.311	1.325	1.306
F3	R(4-1)	1.310	1.311	1.325	1.306
F4	R(5-1)	1.310	1.311	1.325	1.306
F5	R(6-2)	2.177	2.178	2.176	2.164
Br6	A(3-1-2)	106.01	106.22	106.12	106.05
	A(4-1-2)	106.32	106.64	106.43	106.63
	A(5-1-2)	106.08	106.30	106.39	106.46
	A(6-2-1)	179.90	179.78	179.93	179.82
	D(4-1-2-3)	120.03	120.05	119.97	119.96
	D(5-1-2-3)	-119.91	-119.87	-119.95	-119.87
	D(6-2-1-3)	-41.78	-41.69	-52.22	-46.89

8) **Geometric parameter of CF_3•••ClF:**

Position of the atoms	*Coordinates (in Å, deg)*	*MP2(FULL)/ 6-311G***	*MP2(FULL)/ 6-311++G***	*MP2(FULL)/ Aug-cc-pVDZ*	*MP2(FULL)/ Aug-cc-pVTZ*
C1	R(2-1)	3.203	3.314	2.983	2.692
Cl2	R(3-1)	1.315	1.316	1.330	1.308
F3	R(4-1)	1.315	1.316	1.330	1.308
F4	R(5-1)	1.315	.316	1.330	1.308
F5	R(6-2)	1.669	1.671	1.671	1.636
F6	A(3-1-2)	106.97	106.93	106.94	106.87
	A(4-1-2)	107.73	107.72	107.66	107.03
	A(5-1-2)	107.12	107.16	107.04	106.90
	A(6-2-1)	179.56	179.31	179.72	179.89
	D(4-1-2-3)	120.03	120.06	120.09	120.03
	D(5-1-2-3)	-119.87	-119.76	-119.76	-119.96
	D(6-2-1-3)	5.92	30.21	33.13	42.50

Table. V. 18: Rotational constants (GHz) at MP2(full):

	Rotational Constants	*6-311G***	*6-311++G***	*Aug-cc-pVDZ*	*Aug-cc-pVTZ*
CF_3•••HF	A	----	5.6126	5.4892	5.6571
	B	----	1.5501	1.9381	2.0876
	C	----	1.5501	1.9381	2.0876
CF_3•••HCl	A	5.6220	a)7.7719 b) 10.7077	5.4904	5.6568
	B	0.9129	1.3242 0.8896	1.1401	1.2527
	C	0.9129	1.2383 0.8269	1.1400	1.2527
CF_3•••HBr	A	5.6236	7.4828	5.4893	5.6574
	B	0.5643	0.7906	0.7162	0.8255
	C	0.5643	0.7619	0.7162	0.8255
CF_3•••HCN	A	5.6218	5.6119		5.6531
	B	0.8881	0.8756		1.1368
	C	0.8881	0.8756		1.1368
CF_3•••LiF	A	----	5.6052	5.4824	5.6512
	B	----	1.2847	1.3329	1.3393
	C	----	1.2847	1.3329	1.3393
CF_3•••LiCl	A	5.6033	5.6041	5.4821	5.6477
	B	0.8432	0.8054	0.8331	0.8145
	C	0.8432	0.8054	0.8331	0.8145
CF_3•••LiBr	A	5.6031	5.6039	5.4816	5.6480
	B	0.5218	0.4945	0.5349	0.5206
	C	0.5218	0.4945	0.5349	0.5206
CF_3•••ClF	A	5.6212	5.6129	5.4910	5.6602
	B	0.8529	0.8133	0.9329	1.0806
	C	0.8529	0.8133	0.9329	1.0806

Table. V. 19: Normal mode vibrational frequencies

1) Normal mode vibrational frequencies of CF_3···HF

*MP2(full)/ 6-311G***	*MP2(full)/ 6-311++G***	*MP2(full)/ Aug-cc-pVDZ*	*MP2(full)/ Aug-cc-pVTZ*
-129.60	18.08	19.67	37.68
-129.60	20.15	19.72	37.69
38.79	20.15	48.07	66.80
48.49	96.41	157.55	279.13
48.49	96.41	157.57	279.14
521.74	518.50	493.81	517.35
521.74	518.50	493.81	517.35
721.85	714.18	689.52	723.46
1124.70	1108.35	1076.81	1123.92
1314.23	1282.27	1247.73	1298.54
1314.23	1282.27	1247.76	1298.55
4236.41	4198.03	4041.47	4066.85

2) Normal mode vibrational frequencies of CF_3···HCl

*MP2(full)/ 6-311G***	*MP2(full)/ 6-311++G***		*MP2(full)/ Aug-cc-pVDZ*	*MP2(full)/ Aug-cc-pVTZ*
	a	*b*		
13.26	21.30	13.74	14.14	30.48
13.42	33.19	18.30	14.57	30.70
19.41	65.48	45.68	45.06	55.83
44.65	71.73	47.70	153.72	225.88
45.88	134.90	144.23	153.99	226.23
520.79	517.42	515.29	493.32	516.40
520.82	518.00	519.12	493.39	513.43
718.83	710.56	711.13	688.24	720.94
1122.82	1104.13	1104.40	1074.07	1119.92
1307.96	1269.57	1257.15	1243.92	1293.86
1308.18	1271.78	1287.77	1244.00	1293.87
3081.87	3079.75	3090.07	2999.81	2992.97

3) Normal mode vibrational frequencies of CF_3···HBr

*MP2(full)/ 6-311G***	*MP2(full)/ 6-311++G***	*MP2(full)/ Aug-cc-pVDZ*	*MP2(full)/ Aug-cc-pVTZ*
11.04	13.26	14.67	37.41
11.64	22.20	14.69	37.43
16.58	57.00	37.59	46.80
48.82	67.68	155.42	316.18
50.92	126.78	155.43	316.33
520.83	517.06	493.26	517.15
520.86	517.86	493.26	517.16
718.57	710.42	687.81	720.26
1122.19	1103.54	1072.59	1117.66
1307.43	1262.42	1242.70	1294.54
1307.44	1279.37	1242.70	1294.60
2742.43	2738.86	2700.01	2676.22

4) Normal mode vibrational frequencies of CF_3···HCN

*MP2(full)/ 6-311G***	*MP2(full)/ 6-311++G***	*MP2(full)/ Aug-cc-pVDZ*	*MP2(full)/ Aug-cc-pVTZ*
10.82	17.01	-24.73	24.09
10.98	17.04	-24.72	24.12
25.03	22.04	51.45	76.83
34.06	53.11	55.33	124.76
34.20	53.25	55.38	124.76
520.78	517.95	492.69	515.21
520.79	517.95	492.70	515.22
718.72	713.08	687.57	719.79
773.84	751.80	760.55	785.01
773.85	751.86	760.56	785.02
1122.51	1107.50	1074.68	1121.36
1308.10	1279.96	1242.12	1291.47
1308.15	1280.03	1242.15	1291.48
2037.90	2028.93	2779.91	2160.95
3499.39	3491.72	3536.59	3541.54

5) Normal mode vibrational frequencies of CF_3···LiF

*MP2(full)/ 6-311G***	*MP2(full)/ 6-311++G***	*MP2(full)/ Aug-cc-pVDZ*	*MP2(full)/ Aug-cc-pVTZ*
-39.29	22.99	17.06	32.11
-28.52	23.29	18.67	32.68
12.59	30.98	82.22	68.78
37.28	32.47	99.06	69.03
130.67	60.36	99.09	77.08
518.56	519.03	494.00	516.90
522.04	519.09	494.06	516.94
726.93	721.12	696.79	727.57
965.62	889.81	964.75	900.52
1128.01	1114.06	1085.79	1128.65
1318.08	1298.27	1261.41	1307.37
1322.12	1298.33	1261.47	1307.41

6) Normal mode vibrational frequencies of CF_3···LiCl

*MP2(full)/ 6-311G***	*MP2(full)/ 6-311++G***	*MP2(full)/ Aug-cc-pVDZ*	*MP2(full)/ Aug-cc-pVTZ*
10.65	18.84	22.40	35.77
12.02	19.26	23.44	36.35
58.15	42.15	53.85	72.90
58.59	43.34	54.02	80.90
86.65	63.68	65.89	81.14
520.58	519.14	494.24	516.61
520.71	519.22	494.29	516.86
672.07	672.82	663.04	655.38
735.23	726.19	703.89	732.11
1129.37	1114.86	1085.79	1128.03
1326.48	1301.40	1265.67	1310.50
1326.56	1301.47	1265.72	1310.65

7) Normal mode vibrational frequencies of CF_3···LiBr:

*MP2(full)/ 6-311G***	*MP2(full)/ 6-311++G***	*MP2(full)/ Aug-cc-pVDZ*	*MP2(full)/ Aug-cc-pVTZ*
14.63	8.42	18.12	34.60
15.70	9.34	18.69	35.03
49.47	40.71	50.98	66.00
49.91	41.87	73.19	78.22
69.99	49.64	73.36	78.78
520.69	519.23	494.07	516.84
520.82	519.32	494.23	516.92
594.71	585.15	590.62	598.50
732.84	724.30	701.94	732.66
1128.83	1114.16	1087.26	1129.40
1326.63	1301.39	1267.19	1311.50
1326.71	1301.47	1267.30	1311.98

8) Normal mode vibrational frequencies of CF_3···ClF:

*MP2(full)/ 6-311G***	*MP2(full)/ 6-311++G***	*MP2(full)/ Aug-cc-pVDZ*	*MP2(full)/ Aug-cc-pVTZ*
13.29	11.45	21.77	50.76
13.97	11.73	22.09	51.06
42.34	32.54	55.48	65.29
45.98	41.38	69.35	115.18
46.08	41.53	69.54	115.22
521.09	518.55	493.65	518.62
521.10	518.56	493.66	518.73
720.15	714.36	689.08	724.65
829.16	778.35	909.53	917.25
1122.53	1106.99	1074.49	1119.33
1310.54	1281.72	1245.15	1301.33
1310.55	1281.74	1245.16	1301.39

9) Normal mode vibrational frequencies of the monomers:

Monomers	*MP2(full)/ 6-311G***	*MP2(full)/ 6-311++G***	*MP2(full)/ Aug-cc-pVDZ*	*MP2(full)/ Aug-cc-pVTZ*
CF_3	520.04	517.43	491.11	514.75
	520.04	517.43	491.11	514.75
	716.55	711.64	682.59	713.37
	1123.47	1106.58	1071.34	1115.44
	1302.02	1274.73	1232.51	1279.08
	1302.02	1274.73	1232.51	1279.08
HF	4253.15	4200.58	4082.63	4142.31
HCl	3085.60	3085.11	3028.55	3058.80
HBr	2744.62	2742.31	2735.57	2792.35
HCN	764.67	735.98	709.04	704.61
	764.67	735.98	709.04	704.61
	2026.51	2020.76	1995.39	2047.94
	3499.16	3489.10	3463.02	3492.63
LiF	963.69	885.61	939.50	891.76
LiCl	657.55	663.54	619.55	643.17
LiBr	574.10	574.19	529.59	573.42
ClF	735.48	734.80	782.92	806.46

Table. V. 21: NBO Analysis: Charge on each of the atoms at MP2(full)/Aug-cc-pVTZ level.

1) CF_3···HF

Atom	*Complex*	*Monomer*	$D_{(C-M)}$
C	1.115	1.138	-0.023
F	-0.367	-0.379	0.012
F	-0.367	-0.379	0.012
F	-0.367	-0.379	0.012
H	0.545	0.558	-0.013
F	-0.558	-0.558	0.000

2) CF_3···HCl

Atom	*Complex*	*Monomer*	$D_{(C-M)}$
C	1.131	1.138	-0.007
F	-0.370	-0.379	0.009
F	-0.370	-0.379	0.009
F	-0.370	-0.379	0.009
H	0.226	0.250	-0.024
Cl	-0.246	-0.250	0.004

3) CF_3···HBr

Atom	*Complex*	*Monomer*	$D_{(C-M)}$
C	1.139	1.138	0.001
F	-0.370	-0.379	0.009
F	-0.370	-0.379	0.009
F	-0.370	-0.379	0.009
H	0.136	0.172	-0.036
Br	-0.164	-0.172	0.008

4) CF_3···HCN

Atom	*Complex*	*Monomer*	$D_{(C-M)}$
C	1.130	1.138	-0.008
F	-0.370	-0.379	0.009
F	-0.370	-0.379	0.009
F	-0.370	-0.379	0.009
H	0.198	0.221	-0.023
C	0.115	0.119	-0.004
N	-0.332	-0.340	0.008

5) CF_3···LiF

Atom	*Complex*	*Monomer*	$D_{(C-M)}$
C	1.095	1.138	-0.043
F	-0.358	-0.379	0.021
F	-0.358	-0.379	0.021
F	-0.358	-0.379	0.021
Li	0.957	0.982	-0.025
F	-0.979	-0.982	0.003

6) CF_3···LiCl

Atom	*Complex*	*Monomer*	$D_{(C-M)}$
C	1.102	1.138	-0.036
F	-0.355	-0.379	0.024
F	-0.355	-0.379	0.024
F	-0.355	-0.379	0.024
Li	0.893	0.950	-0.057
Cl	-0.931	-0.950	0.019

7) CF_3···LiBr

Atom	*Complex*	*Monomer*	$D_{(C-M)}$
C	1.102	1.138	-0.036
F	-0.353	-0.379	0.026
F	-0.353	-0.379	0.026
F	-0.353	-0.379	0.026
Li	0.867	0.923	-0.056
Br	-0.910	-0.923	0.013

8) CF_3···ClF

Atom	*Complex*	*Monomer*	$D_{(C-M)}$
C	1.136	1.138	-0.002
F	-0.368	-0.379	0.011
F	-0.368	-0.379	0.011
F	-0.368	-0.379	0.011
Cl	0.370	0.395	-0.025
F	-0.402	-0.395	-0.007

CHAPTER VI

Stabilizing The Square Pyramidal $Fe(CO)_5$ Through

Hydrogen and Chlorine Bonding

VI. 1. Introduction:

In order to extend the concept of non conventional hydrogen bond acceptors, in this chapter the potential of transition metals to take part in hydrogen bond interaction is explored. Application of transition metals to organic synthesis is one of the most active research areas in organic chemistry. The transition metal can get involved in the three-centre interactions. Some transition metals show properties similar to classical hydrogen bond acceptors, generating nonclassical or nonconventional hydrogen bonds. Interaction of metals with hydrogen to form hydrogen bond complex was first demonstrated by Trifan and Bacskai[1]. Interaction of transition metal centers with hydrogen atom is a widely studied topic[2-7] and the common metals which act as hydrogen bond acceptors are Au, Co, Ni, Pt, Ir, Ru, Os etc.

The ability of transition metals Co and Ni to form hydrogen bonded complexes were studied by Alkorta et al.[8] using $(CO)_4Co^-$ and $(CO)_4Ni$ as hydrogen bond acceptors. $(CO)_4Co^-$ forms a strong hydrogen bond complex whereas $(CO)_4Ni$ is a very poor acceptor of hydrogen bonds. The difference in the behavior of the two carbonyls was attributed to the presence of the charge on Co in $(CO)_4Co^-$. The lack of charge on the metal in $(CO)_4Ni$ made it a weak acceptor of hydrogen bond.

In the present work, the focus is on transition metal as hydrogen bond acceptor, with iron pentacarbonyl as the model system. Iron pentacarbonyl is a neutral transition metal complex. It is a yellow, oily liquid which is pyrophoric in air and burns to Fe_2O_3 and decomposes by light to $Fe_2(CO)_9$ and CO. Theoretically trigonal bipyramid (D_{3h}) is the most stable geometry of iron pentacarbonyl. $Fe(CO)_5$ is a fluxional molecule and in the gas phase it can exist in both trigonal bipyramid and square pyramidal geometry, the energy separation between D_{3h} and C_{4v} geometries

being very small. In the gas phase, square pyramidal geometry exists as a transition state during the Berry pseudorotation[9]. This square pyramidal geometry can be further stabilized by a sixth ligand. Interaction of metal with hydrogen in alpha-metallocenylcarbinols (M=Fe, Ru, Os) showed no evidence of Fe forming a hydrogen bond where as Ru and Os did show[10]. The reason was attributed to steric factors. On the other hand Rose-Petruck et al[11] have observed $Fe(CO)_5\cdots C_6H_6$ complex in solution, where benzene coordinates to iron with one of its aryl hydrogen instead of with its π-system. Another study by the same group[12] has shown that when $Fe(CO)_5$ is solvated in alcohols, it forms a weak complex with a single solvent molecule. There is no bond formation between the two interacting moieties. The study reported transfer of electron density from the alcohol to the organometallic system in the complex. To the best of our knowledge, there is no direct observation of $Fe(CO)_5$ interacting with a ligand in isolation.

Interaction of $Fe(CO)_5$ with different halides, HX (X=F, Cl, Br), are considered to explore whether $Fe(CO)_5$ can act as hydrogen bond acceptor. In these complexes the hydrogen of the hydrogen halide interacts with Fe through the sixth coordination site. Characterization of whether Fe can act as hydrogen bond acceptor or not is done by DFT calculations where the geometric parameters, frequency shift and interaction energies are considered. A detailed analysis have been carried out using Atoms In Molecules theory and NBO analysis to ascertain whether the bond formed between Fe and the hydrogen of HX can be classified as a hydrogen bond interaction or not.

VI. 2. Computational Methods:

Both square pyramidal and trigonal bipyramid structures of iron pentacarbonyl were optimized using Gaussian 03[13] at B3LYP level of theory using different basis sets. Geometry optimizations for the interaction of HX(X=F,Cl,Br) with the square pyramidal structure of $Fe(CO)_5$ have been done. The geometries of the complexes are optimized using Gaussian 03 at B3LYP level of theory with different basis sets, 6-311++G**, Aug-cc-pVDZ and Aug-cc-pVTZ. For all the calculations basis set 6-311++G** has been assigned to Fe. Frequency calculations are carried out for all the complexes at all the above mentioned basis sets to ascertain whether the geometries obtained were true minima. Bader's[14] Atoms in Molecules theory is used to obtain the electron densities and Laplacian of electron density and the other different properties of atomic basin required to shed more light on the nature of interaction. AIM2000[15] package is used to get the properties of the atoms. NBO analyses of the complexes are done and by using Gauss View[16] the molecular electrostatic potential maps are obtained.

VI. 3. Results and discussion:

VI. 3. A. Geometric Parameters, Frequency shift and Interaction Energies: Results from DFT calculations

The molecular electrostatic potential map of $Fe(CO)_5$ at B3LYP/Aug-cc-pVTZ is shown in Figure. VI. 1. The blue color represents region of positive potential and the region of negative potential is denote by red color. The intermediate values of electrostatic potential is represented other colors, green and yellow etc. From the figure, the electron rich region in the molecule is at the sixth coordination site of iron.

So any electron deficient species will tend to approach $Fe(CO)_5$ along this site to form weak or strong complex.

Figure. VI. 1: Molecular electrostatic potential map of $Fe(CO)_5$ at B3LYP/Aug-cc-pVTZ

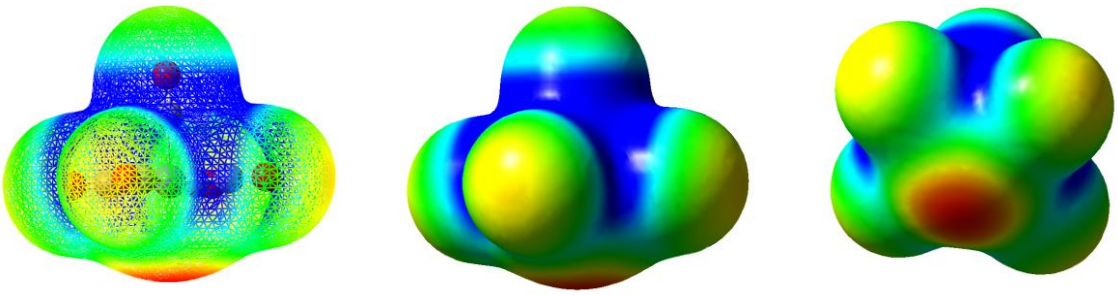

Geometry optimizations and frequency calculations show that $Fe(CO)_5$ can forms complex with HX (X=F, Cl, Br). The structure in which Fe interacts with the hydrogen of the HX resulting in octahedral type geometry is a minimum. Various interactions in a complex can be characterized on the basis of bond lengths, bond angles and interaction energies. The main geometric parameters under consideration in weak complexes in isolation are the penetration of the electron of the interacting atoms (bond length) and the bond angle. When it comes to hydrogen bond complexes, directionality is a unique feature. Conventionally in strong hydrogen bond complexes, X-H···A-Z, distance between H and acceptor A should be less than the sum of the van der Waals radii of H and A and ∠XHA is expected to be 180° or almost linear. The distance between iron and hydrogen, the change in the H-X bond length upon complex formation and the shift in the H-X stretching frequencies are given in Table.

VI. 1. The van der Waals radii of Fe and H are 2.0 Å and 1.2 Å respectively. The covalent radius of Fe is 1.27 Å. From Table. VI. 1 the Fe-H distance at B3LYP/Aug-cc-pVTZ level for $Fe(CO)_5$ ···HF/HCl/HBr are 2.39, 2.50, 2.46 Å respectively. These values are less than the sum of the van der Waals radii of Fe and H. By comparing the Fe···H distance with the covalent and van der Waals radii of Fe, it is apparent that the interaction is non-covalent**.** Optimized geometries at all the levels for the complexes of $Fe(CO)_5$ with HF, HCl and HBr gives ∠XHFe to be 180.0°, indicating a strong hydrogen bond formation. The optimized geometries and the electrostatic potential maps of the complexes of $Fe(CO)_5$ with HF, HCl and HBr obtained at B3LYP/Aug-cc-pVTZ are shown in Figure. VI. 2 and Figure. VI. 3.

The shift in H-X frequency upon complex formation is a crucial criteria used to ascertain the strength of hydrogen bond. Table. VI. 2 compare the change in H-X bond length, $\Delta R_{H\text{-}X}$, and the frequency shift in the H-X stretching mode, $\Delta\nu$ following the complex formation. The H-F bond length in $Fe(CO)_5$ ···HF is 0.9419, 0.9453 and 0.9434 Å at the basis sets 6-311++G**, Aug-cc-pVDZ and Aug-cc-pVTZ respectively and the extend of bond elongation ($\Delta R_{H\text{-}F}$) on complex formation at the three basis sets are 0.0197, 0.0196 and 0.0193 Å. All basis sets give consistent data and gives a large red shift of 457.58(6-311++G**), 474.72(Aug-cc-pVDZ) and 452.05(Aug-cc-pVTZ) cm^{-1}.. The $\Delta R_{H\text{-}F}$ and the frequency shift ($\Delta\nu$) is similar to the one observed for strong hydrogen bond complexes. e.g. the $\Delta R_{H\text{-}F}$ and $\Delta\nu$ observed for H_2O···HF at B3LYP/6-311++G** is 0.019 Å and 422.3 cm^{-1} respectively. Similar red shift has been observed in complex of HF with Au[10]. $Fe(CO)_5$ ···HCl and $Fe(CO)_5$ ···HBr complexes show the same trend. In $Fe(CO)_5$ ···HCl, the $\Delta R_{H\text{-}Cl}$ values are

0.0314(6-311++G**), 0.0325(Aug-cc-pVDZ) and 0.0294(Aug-cc-pVTZ) Å and the corresponding $\Delta\nu$ are 439.52, 444.15 and 421.02 cm^{-1}. Similarly the $\Delta R_{H\text{-}Br}$ and $\Delta\nu$ computed for $Fe(CO)_5$ ···HBr at 6-311++G**, Aug-cc-pVDZ and Aug-cc-pVTZ levels are 0.0423, 0.0468 and 0.0389 Å and 415.89, 425.95 and 448.47 cm^{-1} respectively. The complexes of HCl and HBr with $Fe(CO)_5$ also show strong red shift usually observed for strong hydrogen bonded complexes.

Interaction energies (ΔE), BSSE corrected interaction energies (ΔE_{BSSE}), Zero point energies (ΔE_{ZPE}), BSSE corrected zero point energies ($\Delta E_{ZPE(BSSE)}$) of $Fe(CO)_5$ ···HX complexes are given in Table . VI. 3. The interaction energies at B3LYP/Aug-cc-pVTZ level are -5.6, -3.6 and -3.3 kcal mol^{-1} for $Fe(CO)_5$ ···HF, $Fe(CO)_5$ ···HCl , $Fe(CO)_5$ ···HBr respectively. A comparison of the binding energies of $Fe(CO)_5$ ···HX, shows highest binding energy for $Fe(CO)_5$ ···HF and at all basis sets the binding energy follows the pattern $Fe(CO)_5$ ···HF > $Fe(CO)_5$ ···HCl > $Fe(CO)_5$ ···HBr. At B3LYP/Aug-cc-pVTZ, the dipole moments of H-F, H-Cl and H-Br are 1.8D, 1.1D and 0.8D. The binding energies are directly proportional to the dipole moments of the hydrogen bond donors.

A comparative study of the interaction energy of $Fe(CO)_5$ as H bond acceptor with standard acceptors have been done at B3LYP/6-311++G** level. The various acceptors chosen from literature[14] are lone pair (H_2O), π (C_2H_4), unpaired (CH_3) electrons and σ (H_2) bonded pairs. HF is the hydrogen bond donor in all the cases. The interaction energies are -10.1, -4.5, -3.3 and -0.9 kcal mol^{-1} for H_2O···HF, C_2H_4···HF, CH_3···HF and H_2···HF respectively. The interaction energy of $Fe(CO)_5$ ···HF (-6.6) falls between that of H_2O···HF and C_2H_4···HF. Coming to $(CO)_4Co^-$ and

$(CO)_4Ni$[23], complexes of these two transition metal compounds with HF gives interaction energies -11.90 and -1.23 kcal mol^{-1} respectively. From the stabilization energies of all the complexes, it can be concluded that $Fe(CO)_5$ forms strong hydrogen bonded complex. It acts as a strong hydrogen bond acceptor even being a neutral compound.

In weak complexes the monomers retain their geometry. The geometric parameters of $Fe(CO)_5$ does not vary much on complex formation. This variation in the geometric parameters is only in the bond length, which is negligible and the molecules retain its monomer bond angles. The numerical values of bond lengths, bond angles and dihedral angles are given in Table. VI. 8. Table. VI. 9 lists the rotational constants of all the complexes at B3LYP level with basis sets at 6-311++G**, Aug-cc-pVDZ and Aug-cc-pVTZ. From the values of A, B and C rotational constants, the complex of $Fe(CO)_5$ with HF, HCl and HBr are all symmetric tops. The normal mode vibrational frequencies of the complexes at all the basis sets are listed in Table. VI. 10. (Table. VI. 8. Table. VI. 9 and Table. VI. 10. are listed at the end of this chapter)

Table. VI. 1 : Bond length (Å) and bond angle (°)

Complex	*B3LYP/ 6-311++G***		*B3LYP/ Aug-cc-pVDZ*		*B3LYP/ Aug-cc-pVTZ*	
	R_{Fe-H}	∠FeHX	R_{Fe-H}	∠FeHX	R_{Fe-H}	∠FeHX
$Fe(CO)_5\cdots HF$	2.376	180.0	2.372	179.9	2.391	180.0
$Fe(CO)_5\cdots HCl$	2.448	180.0	2.468	180.0	2.501	180.0
$Fe(CO)_5\cdots HBr$	2.412	180.0	2.395	180.0	2.46	180.0

Table. VI. 2: Change in H-X bond length (Å) and shift in the H-X stretching frequency (cm^{-1})

Complex	*B3LYP/ 6-311++G***		*B3LYP/ Aug-cc-pVDZ*		*B3LYP/ Aug-cc-pVTZ*	
	Δr	Δν	Δr	Δν	Δr	Δν
$Fe(CO)_5\cdots HF$	0.0197	457.6	0.0196	474.7	0.0193	452.1
$Fe(CO)_5\cdots HCl$	0.0314	439.5	0.0325	444.2	0.0294	421.0
$Fe(CO)_5\cdots HBr$	0.0423	415.9	0.0468	426.0	0.0389	448.5

Table. VI. 3: Interaction Energy (Δ E), BSSE corrected Interaction Energy (ΔE_{BSSE}), Zero Point corrected Interaction energy with ($\Delta E_{ZPE\ (BSSE)}$) and without BSSE correction (ΔE_{ZPE}) (kcal mol^{-1})

$Fe(CO)_5$···HF

	*B3LYP/6-311++G***	*B3LYP/Ag-cc-pVDZ*	*B3LYP/Ag-cc-pVTZ*
Δ E	-6.55	-6.09	-5.58
ΔE_{BSSE}	-5.84	-5.46	-3.83
ΔE_{ZPE}	-5.08	-5.65	-5.27
$\Delta E_{ZPE\ (BSSE)}$	-4.27	-5.02	-3.51

$Fe(CO)_5$···HCl

	*B3LYP/6-311++G***	*B3LYP/Ag-cc-pVDZ*	*B3LYP/Ag-cc-pVTZ*
Δ E	-4.58	-4.20	-3.58
ΔE_{BSSE}	-3.70	-3.70	-3.39
ΔE_{ZPE}	-3.35	-3.26	-2.64
$\Delta E_{ZPE\ (BSSE)}$	-2.46	-2.76	-2.45

$Fe(CO)_5$···HBr

	*B3LYP/6-311++G***	*B3LYP/Ag-cc-pVDZ*	*B3LYP/Ag-cc-pVTZ*
Δ E	-4.08	-4.01	-3.26
ΔE_{BSSE}	-3.45	-3.70	-1.57
ΔE_{ZPE}	-3.06	-3.14	-2.38
$\Delta E_{ZPE\ (BSSE)}$	-2.43	-2.82	-0.69

Figure. VI. 2.: Optimized geometries of $Fe(CO)_5$---HX at B3LYP/Aug-cc-pVTZ

Figure. VI. 3.: Molecular Electrostatic Potential Map of $Fe(CO)_5$---HX at B3LYP/Aug-cc-pVTZ

VI. 3. B. Atoms In Molecules Analysis

A detailed AIM analysis have been carried out on all the three $Fe(CO)_5\cdots HX$ complexes to study the nature of the bond formed between iron and the hydrogen using AIM 2000 software. According to Bader the presence of (3,-1) critical point or bond critical point (BCP), along the bond path connecting the two interacting atoms is a necessary and sufficient condition to ascertain that the two atoms are bonded. Koch and Popelier[17] have suggested eight criteria on the basis of AIM theory, which should be satisfied for a bond to be called hydrogen bond. These criteria were suggested for weak hydrogen bond interactions on the basis of C-H···O contacts. Among the eight criteria, according to them, the mutual penetration of hydrogen atom and the acceptor atom is a sufficient condition.

Electron density at the bond critical point, its Laplacian and the penetration criteria are mainly used to identify and differentiate the type of bond formed between Fe and H. All the complexes gave a (3,-1) critical point along the bond path connecting the iron and the hydrogen atom. The eight criteria for the $Fe(CO)_5\cdots HX$ complexes at different basis set are given in Table. VI. 4. The numerical values of the electron density, $\rho(r_c)$ and Laplacian of the electron density, L at the bond critical point falls in the range suggested by Koch and Popelier for the formation of a hydrogen bond. So, all the (3,-1) critical points between Fe and H correspond to hydrogen bond critical point. Each of the eight criteria has been analyzed in detail.

Criteria for hydrogen bonding

1) **Topology:** in all the complexes there is the presence of a bond critical point between the hydrogen atom and the acceptor atom Fe. And both the atoms are linked by a bond path. In all the complexes the bond path is linear (distance between H and

Fe is equal to the sum of the distances of Fe to BCP and H to BCP), no ellipticity is observed. The geometry of the complexes with bond critical points and bond baths are shown in Figure. VI. 4.

2) **The charge density at the Bond Critical Point (ρ):** Koch and Popelier have proposed a range for the charge density at the BCP for a bond to be classified as hydrogen bond. It ranges from 0.002 to 0.04 au. At B3LYP/Aug-cc-pVTZ level of calculation the values of ρ (bcp) (Table. VI. 4. a.) are 0.0199, 0.0177 and 0.0194au for complexes of $Fe(CO)_5$ with HF, HCl and HBr respectively. The ρ(bcp)s along the hydrogen bond in all the complexes are within the range suggested by Koch and Popelier. The values of ρ for the different complexes are given in Table. VI. 4. a.

3) **The Laplacian of the charge density at the bond critical point (L):** The third criterion is about the Laplacian of the charge density at the hydrogen bond critical point. The range suggested by Koch and Popelier for laplacian is -0.15 to 0.02 au. From Table. VI. 4.a. the L values are -0.0060, -0.0059 and -0.0060 au for the complexes $Fe(CO)_5\cdots HF$, $Fe(CO)_5\cdots HCl$ and $Fe(CO)_5\cdots HBr$ respectively at B3LYP/Aug-cc-pVTZ level. The negative sign of L implies a closed-shell interaction, expected for typical hydrogen bond.

4) **Mutual Penetration of Hydrogen and Acceptor Atom:** The distance from the nucleus to the electron density contour 0.001au is defined as the nonbonded radius, r° and the distance from the nucleus to the bond critical point is defined as the bonded radius, r^b. The difference between the bonded and nonbonded gives the extent of penetration. If there is penetration of electron cloud of the hydrogen atom and the acceptor atom, Δr will be positive and it indicates bond formation. The values of r°, r^b and Δr for $Fe(CO)_5\cdots HX$(X=F, Cl, Br) at different basis sets are given in Table. VI. 4.

b. All the complexes show mutual penetration of the electron cloud of hydrogen atom and the Fe atom. The extent of mutual penetration for $Fe(CO)_5\cdots HF$, $Fe(CO)_5\cdots HCl$ and $Fe(CO)_5\cdots HBr$ at B3LYP/Aug-cc-pVTZ are 1.1792, 1.1820 and 1.2613 Å respectively. The extent of penetration increases as the polarizability of the hydrogen bond donor increases.

5) **Loss of charge of hydrogen atom (ΔN):** There should be a decrease in population of the hydrogen atom upon complex formation according to the fifth criteria proposed by Koch and Popelier. $Fe(CO)_5\ldots HBr$ is in agreement with the criteria proposed. At B3LYP/Aug-cc-pVTZ, the decrease in population is 0.0007 au. However, there is an increase in the population of the hydrogen upon complex formation in of $Fe(CO)_5\cdots HF$ and $Fe(CO)_5\cdots HCl$ and the increase is 0.0579 and 0.0226 au respectively at B3LYP/Aug-cc-pVTZ. Analyses at different basis sets show the same trend and are given in Table. VI. 4. c.

6) **Change in atomic energy (ΔE):** The sixth criteria deals with destabilization of hydrogen atom. This is due to the decrease in the total atomic energy of the hydrogen atom in the hydrogen bonded complex compared to that in the monomer. The hydrogen atom shows a loss in the total atomic energy in the complex in for $Fe(CO)_5\cdots HCl$ and $Fe(CO)_5\cdots HBr$. At B3LYP/Aug-cc-pVTZ, the extend of destabilization of the hydrogen atoms are 0.0229 and 0.0342 au respectively. However it, shows an increase in stability in $Fe(CO)_5\cdots HF$ complex, i.e. the hydrogen of HF on interaction with $Fe(CO)_5$ gets more stabilized, against the expected behavior or the suggested criterion. The magnitude of stabilization of H on complexation is 0.0037au at B3LYP/Aug-cc-pVTZ. The ΔE obtained at different basis sets for all the complexes are given in Table. VI. 4. d.

7) **Change in atomic first moment (ΔM):** The dipolar polarization of the hydrogen atom decreases on complex formation due to the loss of non-bonding density of hydrogen. Hydrogen in the complexes, $Fe(CO)_5$···HF, $Fe(CO)_5$···HCl, $Fe(CO)_5$···HBr, show an increase in the dipolar polarization on formation of hydrogen bond. At Aug-cc-pVTZ, the change in atomic first moments for the hydrogen bond donors HF, HCl and HBr are 0.0258, 0.0151 and 0.0187au respectively. ΔM calculated at different basis sets show the same trend and are given in Table. VI. 4. e.

8) **Change in atomic volume (ΔV):** The eigth criterion demands a decrease in the volume of the hydrogen atom upon complex formation. The hydrogen atom, participating in the hydrogen bond formation in all the three complexes follow this criteria, the volume of the hydrogen atom in the complexes is less than that in the monomer. This decrease in the volume of hydrogen on complex formation is observed at all the three basis sets. The ΔV values are given in Table. VI. 4. f.

From the AIM analysis of the eight criteria proposed by Koch and Popelier to characterize hydrogen bond, complexes of $Fe(CO)_5$ with HF, HCl and HBr do not follow all the criteria. The necessary and sufficient criteria such as presence of bond critical point, bond path connecting the interacting atoms, value of electron density and its Laplacian at the bond critical point and mutual penetration are followed by all the complexes at the three different basis sets. But among the basin properties only the criterion which demands a reduction in the atomic volume of hydrogen on complex formation is followed by all the complexes. The criteria proposed by Koch and Popelier to characterize hydrogen bonds, on the basis of C-H---O interaction, cannot be applied to characterize hydrogen bonding in $Fe(CO)_5$.

A plot of interaction energy as a function of electron density at the bond critical point can reveal a lot about the strength and nature of the interaction. The nature of interaction is covalent, if there is more electron density at the bond critical point connecting H and Fe and the value of the slope of the plot is less. A significantly large value of slope indicates less accumulation of electron density between the interacting atoms and hence the nature of interaction will be electrostatic. Plot of electron density as a function of interaction energy is shown in Figure. VI. 5. for $Fe(CO)_5\cdots HX$ complexes. The correlation is poor and the correlation coefficient is 0.6.

The ΔE obtained from the linear fit is

$$\Delta E = (-632.21)*\rho + 7.87$$

The slop of the plot is significantly large which shows strong interaction between Fe and H. The slope obtained is similar to lithium bonding condition which is electrostatic in nature. From the value of the slope the nature of interaction between Fe and H should be electrostatic. But the absolute value of electron density at the bond critical point,ρ, given in Table. VI. 4. a., is similar to ρ obtained for conventional hydrogen bond acceptors. However, the correlation coefficient is very small and it may not be proper to make serious conclusions from this.

Figure. VI. 4: AIM analysis of $Fe(CO)_5$···HX showing Bond Critical Points and Bond Path at B3LYP level with different basis sets

6-311++G**	Aug-cc-pVDZ	Aug-cc-pVTZ

$Fe(CO)_5$···HF

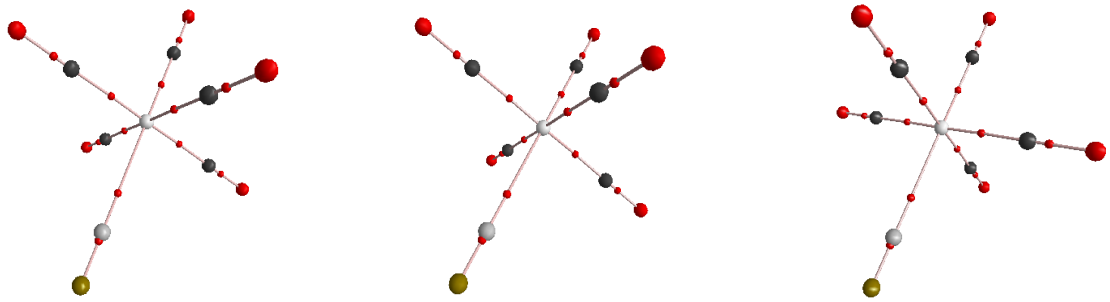

$Fe(CO)_5$···HCl

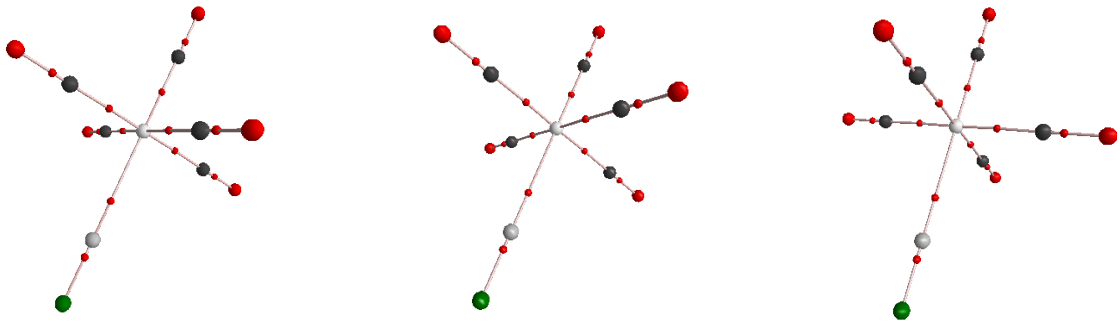

$Fe(CO)_5$···HBr

Figure. VI. 5: Plot of interaction energy as a function of electron density at the BCP

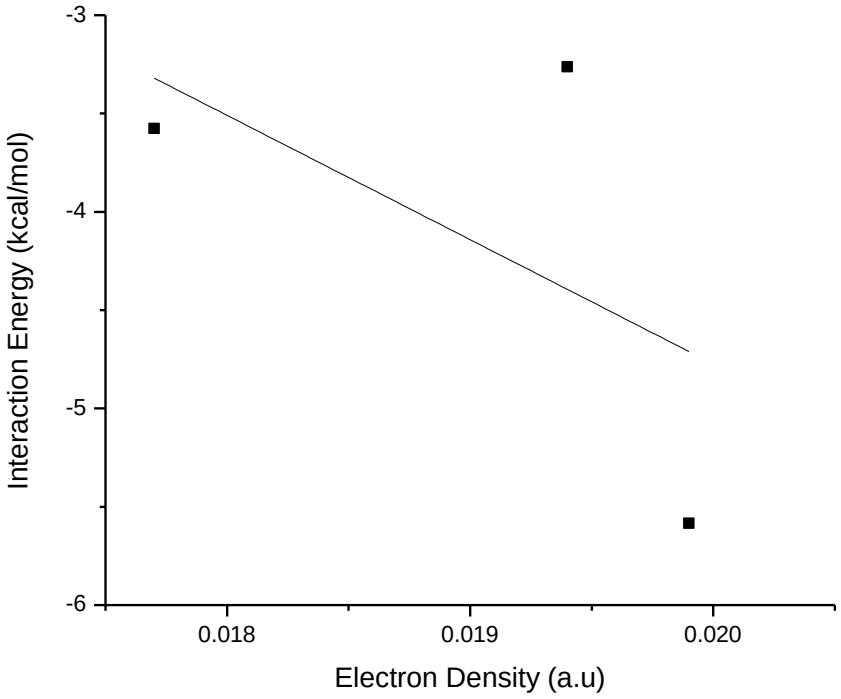

Table. VI. 4:

a) Electron density, ρ (a.u) and laplacian of electron density, L (a.u):

Complex	*B3LYP/ 6-311++G***		*B3LYP/ Ag-cc-pVDZ*		*B3LYP/ Aug-cc-pVTZ*	
	ρ(bcp)	***L***	***ρ(bcp)***	***L***	***ρ(bcp)***	***L***
$Fe(CO)_5$···HF	0.0197	-0.0074	0.0198	-0.0065	0.0199	-0.0060
$Fe(CO)_5$···HCl	0.0191	-0.0066	0.0187	-0.0054	0.0177	-0.0059
$Fe(CO)_5$···HBr	0.0207	-0.0065	0.0221	-0.0055	0.0194	-0.0060

b) Penetration: Bonded (*r*b) and Nonbonded (*r*°) Radii (in Angstroms) of Acceptor (Fe) and Donor (H) Atoms and Penetration, Δr, Defined as the Sum of the Differences in Bonded and Nonbonded Radii of Fe and H

$Fe(CO)_5$···HF

Basis set	$r°_{Fe}$	r^b_{Fe}	$r°_{Fe}-r^b_{Fe}$	$r°_H$	r^b_H	$r°_H-r^b_H$	Δr
6-311++G**	2.3987	1.6077	0.7910	1.1594	0.7936	0.3658	1.1568
Ag-cc-pVDZ	2.3996	1.6102	0.7894	1.1983	0.8129	0.3854	1.1748
Aug-cc-pVTZ	2.4324	1.5899	0.8425	1.1676	0.8309	0.3367	1.1792

$Fe(CO)_5$···HCl

Basis set	$r°_{Fe}$	r^b_{Fe}	$r°_{Fe}-r^b_{Fe}$	$r°_H$	r^b_H	$r°_H-r^b_H$	Δr
6-311++G**	2.3987	1.6078	0.7909	1.3049	0.8605	0.4444	1.2353
Ag-cc-pVDZ	2.3996	1.6089	0.7907	1.2829	0.8860	0.3969	1.1876
Aug-cc-pVTZ	2.4324	1.6200	0.8124	1.2667	0.8971	0.3696	1.1820

$Fe(CO)_5$···HBr

Basis set	$r°_{Fe}$	r^b_{Fe}	$r°_{Fe}-r^b_{Fe}$	$r°_H$	r^b_H	$r°_H-r^b_H$	Δr
6-311++G**	2.3987	1.5763	0.8224	1.3399	0.8566	0.4833	1.3057
Ag-cc-pVDZ	2.3996	1.5516	0.8480	1.3127	0.8639	0.4488	1.2968
Aug-cc-pVTZ	2.4324	1.5851	0.8473	1.3102	0.8962	0.4140	1.2613

c) Change in the atomic population (a.u):

Complex	***Basis set***	***$N(H)_{mono}$***	***$N(H)_{comp}$***	***ΔN***
$Fe(CO)_5\cdots HF$	*6-311++G***	0.2938	0.3460	-0.0522
	Ag-cc-pVDZ	0.2850	0.3429	-0.0579
	Aug-cc-pVTZ	0.2628	0.3207	-0.0579
$Fe(CO)_5\cdots HCl$	*6-311++G***	0.7245	0.7411	-0.0166
	Ag-cc-pVDZ	0.7086	0.7255	-0.0169
	Aug-cc-pVTZ	0.7109	0.7335	-0.0226
$Fe(CO)_5\cdots HBr$	*6-311++G***	0.8991	0.8918	0.0073
	Ag-cc-pVDZ	0.9010	0.8907	0.0103
	Aug-cc-pVTZ	0.8828	0.8821	0.0007

***** $\Delta N = N(H)_{mono} - N(H)_{comp}$

d) Change in atomic energies (a.u):

Complex	***Basis set***	***$E(H)_{mono}$***	***$E(H)_{comp}$***	**Δ E**
$Fe(CO)_5\cdots HF$	*6-311++G***	-0.3050	-0.3054	0.0004
	Ag-cc-pVDZ	-0.2852	-0.2909	0.0057
	Aug-cc-pVTZ	-0.2728	-0.2765	0.0037
$Fe(CO)_5\cdots HCl$	*6-311++G***	-0.4942	-0.4681	-0.0261
	Ag-cc-pVDZ	-0.4684	-0.4459	-0.0225
	Aug-cc-pVTZ	-0.4899	-0.4670	-0.0229
$Fe(CO)_5\cdots HBr$	*6-311++G***	-0.5464	-0.5072	-0.0392
	Ag-cc-pVDZ	-0.5319	-0.4948	-0.0371
	Aug-cc-pVTZ	-0.5387	-0.5045	-0.0342

***** $\Delta E = E(H)_{mono} - E(H)_{comp}$

e) Change in atomic first moment (a.u):

Complex	***Basis set***	M_{mono}	M_{comp}	**ΔM**
$Fe(CO)_5\cdots HF$	*6-311++G***	0.1300	0.1489	-0.0189
	Ag-cc-pVDZ	0.1325	0.1503	-0.0178
	Aug-cc-pVTZ	0.1265	0.1523	-0.0258
$Fe(CO)_5\cdots HCl$	*6-311++G***	0.1336	0.1396	-0.0060
	Ag-cc-pVDZ	0.1378	0.1526	-0.0148
	Aug-cc-pVTZ	0.1336	0.1487	-0.0151
$Fe(CO)_5\cdots HBr$	*6-311++G***	0.0721	0.0838	-0.0117
	Ag-cc-pVDZ	0.0737	0.0939	-0.0202
	Aug-cc-pVTZ	0.0859	0.1046	-0.0187

***** $\Delta M = M_{mono} - M_{comp}$

f) Change in atomic volume (a.u):

Complex	*Basis set*	$V(H)_{mono}$	$V(H)_{comp}$	**ΔV**
$Fe(CO)_5\cdots HF$	*6-311++G***	16.5089	14.5453	1.9636
	Ag-cc-pVDZ	16.2733	14.4531	1.8202
	Aug-cc-pVTZ	15.3511	14.1356	1.2155
$Fe(CO)_5\cdots HCl$	*6-311++G***	40.3947	37.1762	3.2185
	Ag-cc-pVDZ	38.7815	37.2474	1.5341
	Aug-cc-pVTZ	38.2168	36.8795	1.3373
$Fe(CO)_5\cdots HBr$	*6-311++G***	48.4491	44.6607	3.7884
	Ag-cc-pVDZ	49.0948	44.4482	4.6466
	Aug-cc-pVTZ	48.3074	44.7189	3.5885

***** $\Delta V = V(H)_{mono} - V(H)_{comp}$

VI. 3. C. NBO analysis

To probe whether there is any charge transfer occurring between $Fe(CO)_5$ and the hydrogen bond donor and if, then to estimate the amount of charge transfer occurred between the monomers during complexation a detailed NBO analysis of $Fe(CO)_5\cdots HX$(X=F, Cl, Br) at B3LYP level with basis sets 6-311++G**, Aug-cc-pVDZ and Aug-cc-pVTZ have been carried out . Table. VI. 5. lists the charge on each of the atom and the difference, i.e. charge transferred, ΔQ at B3LYP/Aug-cc-pVTZ level.

NBO analysis at all the three different basis sets at B3LYP levels show that there is charge transfer between the organometallic complex, $Fe(CO)_5$ and HX(F, Cl, Br). The values of ΔQ show that the charge is transferred from the organometallic system to the hydrogen bond donor. ΔQ is 0.041, 0.058 and 0.08 e for $Fe(CO)_5 \cdots$ HF/HCl/HBr respectively at Aug-cc-pVTZ level. In the previous chapter (Chapter V) a comparison of dipole moment of the hydrogen bond donors with the interaction energies and charge transferred, ΔQ, for the hydrogen bonded complexes had showed that the interaction energies and charge transfer decreases as the dipole moment of the hydrogen bond donors increases. In $Fe(CO)_5\cdots HX$ the extend of charge transfer increases in the order $Fe(CO)_5\cdots HF < Fe(CO)_5\cdots HCl < Fe(CO)_5\cdots HBr$ and the interaction energies shows a decrease from $Fe(CO)_5\cdots HF$(-3.9) to $Fe(CO)_5\cdots HCl$(-3.4) to $Fe(CO)_5\cdots HBr$(-1.6). In $Fe(CO)_5\cdots HX$ complexes, the interaction energy is directly proportional to the dipole moment of the hydrogen bond donor and the net charge transferred is inversely proportional to the dipole moment of the hydrogen bond donor. Hence in $Fe(CO)_5 \cdots$ HX complexes, the stabilization of the complex is due to electrostatic forces. $Fe(CO)_5 \cdots$ HX is not a charge transfer assisted hydrogen bond. In

the previous chapter, $CF_3\cdots HX$, hydrogen bond was found to be charge transfer assisted. This is evident from the slope (-632.21) obtained for the plot of interaction energy as a function of the electron density at the hydrogen bond critical point discussed in the previous section. In case of $CF_3\cdots HX$, the slope is less (-95.22), which indicates more electron accumulation between the interacting atoms.

Table. VI. 5: Natural Atomic Charge on each atom and the charged transferred (ΔQ,e) at B3LYP/Aug-cc-pVTZ

	$q_{(Fe)}$	$q_{(C)eq}$	$q_{(C)ax}$	$q_{(O)eq}$	$q_{(O)ax}$	$q_{(H)}$	ΔQ
$Fe(CO)_5$	-0.466	0.549	0.519	-0.449	-0.454	---	----
$Fe(CO)_5\cdots HF$	-0.554	0.563	0.529	-0.436	-0.443	0.541	0.041
$Fe(CO)_5\cdots HCl$	-0.535	0.563	0.534	-0.437	-0.446	0.252	0.058
$Fe(CO)_5\cdots HBr$	-0.533	0.567	0.544	-0.438	-0.448	0.167	0.080

VI. 4. $Fe(CO)_5$ as chlorine bond acceptor:

The similarities in the behavior of hydrogen and the halogens are discussed in the previous chapters. Halogen bonds have recently gained immense popularity and among halogen bonds, chlorine bond is the most popular. Since Fe is a good acceptor of hydrogen bonds like the conventional hydrogen bond acceptors, we wanted to verify whether Fe can take part in chlorine bonding. ClF and HCl were chosen as the chlorine bond donors and their interaction with $Fe(CO)_5$ was studied. Geometry optimization were done at B3LYP level using basis sets 6-311G** and 6-311++G**. In the optimized geometries chlorine interacts with Fe in the same way as hydrogen,

i.e. along the sixth coordination site. From frequency calculations, $Fe(CO)_5\cdots ClF$ at both basis sets were true minima. But for $Fe(CO)_5\cdots ClH$ optimization at B3LYP/6-311G**gave minimum energy structure.

In $Fe(CO)_5\cdots ClF$ the R_{Fe-Cl} distances are 2.59 Å and 2.53 Å and Fe-Cl-F bond angles are 179.974° and 179.983° at 6-311G** and 6-311++G** respectively. The corresponding change in Cl-F bond lengths are 0.21 and 0.27 Å. Due to mode mixing, none of the normal mode vibrations in the complex can be assigned to Cl-F stretching. The complex has very high interaction energy, -17.49 kcal mol^{-1} and -20.42 kcal mol^{-1}. The high stabilization can be explained using Atoms In Molecules analysis. AIM analysis of $Fe(CO)_5\cdots ClF$ shows a bond critical point between Fe and Cl and bond path connects the two atoms. The electron density at the bond critical point (ρ) between Fe and Cl is 0.0427 au and its laplacian (L) is -0.0139 au at 6-311G** and at 6-311++G** ρ is 0.0497 au and L is -0.0148 au. The electron density at bond critical point is much higher than what is usually obtained for noncovalent interactions. The high electron density indicates more electron accumulation between Fe and Cl and hence a strong covalent like interaction. This is reflected in the mutual penetration of Fe and Cl atoms. The penetration of Fe at 6-311G** and 6-311++G** are 0.9643 and 1.0178Å respectively and that of Cl are 0.4923 and 0.5138 Å. The mutual penetrations at both the basis sets are 1.4566 and 1.5316Å. The bonded radius of Fe is 1.2778Å which is very close to the covalent radius of Fe, 1.27Å. Hence in $Fe(CO)_5\cdots ClF$, Fe---Cl interaction has a strong covalent nature. The bonded and nonbonded radii of Fe and Cl are given in Table. VI. 6. The optimized geometries and structure from AIM figure having bond critical point and bond path are shown in Figure. VI. 6.

Table. VI. 6: Penetration: Bonded (r^b) and Nonbonded ($r°$) Radii (in Angstroms) of Acceptor (Fe) and Donor (Cl) Atoms and Penetration, Δr, Defined as the Sum of the Differences in Bonded and Nonbonded Radii of Fe and Cl in $Fe(CO)_5\cdots ClF$

Basis set	$r°_{Fe}$	r^b_{Fe}	$r°_{Fe}-r^b_{Fe}$	$r°_{Cl}$	r^b_{Cl}	$r°_{Cl}-r^b_{Cl}$	Δr
6-311G**	2.2421	1.2778	0.9643	1.8098	1.3175	0.4923	1.4566
6-311++G**	2.3987	1.2243	1.0178	1.8189	1.3051	0.5138	1.5316

Figure. VI. 6: Optimized Geometry and AIM analysis of $Fe(CO)_5\cdots ClF$ showing Bond Critical Points and Bond Path at B3LYP/6-311G**

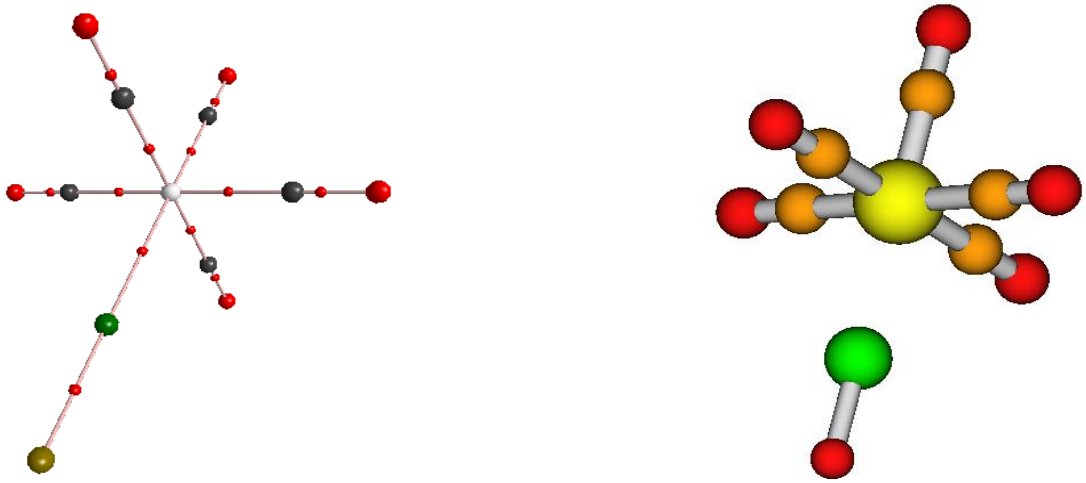

At B3LYP/6-311G**, Fe-Cl distance (R_{Fe-Cl}) in $Fe(CO)_5\cdots ClH$ is 3.72 Å and H-Cl-Fe bond angle is 179.349°. The change in the Cl-H bond length, Δr is 0.003 Å and the shift in the Cl-H stretching frequency is 40.89 cm^{-1}. $Fe(CO)_5\cdots ClH$ has a very low interaction energy, -0.75 kcal mol^{-1}, compared to the $Fe(CO)_5\cdots ClF$ complex. Here electron density at the bond critical point (ρ) between Fe and Cl is 0.0048 au and

its Laplacian (L) is -0.0036 au. The electron density at the bond critical point is one unit less than that for $Fe(CO)_5$···ClF complex. This explains the huge difference in the stabilization energy. Fe and Cl show mutual penetration at B3LYP/6-311G**. The penetration of Fe and Cl are 0.3099 and 0.1526Å respectively and the mutual penetration is 0.4625Å. The bonded radii of Fe and Cl are 1.9322 and 1.7878Å, close to the van der Waals radii of Fe (2.0 Å) and Cl(1.7 Å). In $Fe(CO)_5$···ClH, Fe---Cl interaction is very weak. The nonbonded and bonded radii of Fe and Cl are given in Table. VI. 7. The optimized geometries and structure from AIM figure having bond critical point and bond path are shown in Figure. VI. 7.

Table. VI. 7: Penetration: Bonded (r^b) and Nonbonded ($r°$) Radii (in Angstroms) of Acceptor (Fe) and Donor (Cl) Atoms and Penetration, Δr, Defined as the Sum of the Differences in Bonded and Nonbonded Radii of Fe and Cl in $Fe(CO)_5$···ClH

Basis set	r^o_{Fe}	r^b_{Fe}	r^o_{Fe}-r^b_{Fe}	r^o_{Cl}	r^b_{Cl}	r^o_{Cl}-r^b_{Cl}	Δr
6-311G**	2.2421	1.9322	0.3099	1.9404	1.7878	0.1526	0.4625

Figure. VI. 7: Optimized Geometry and AIM analysis of $Fe(CO)_5$···ClH showing Bond Critical Points and Bond Path at B3LYP/6-311G**

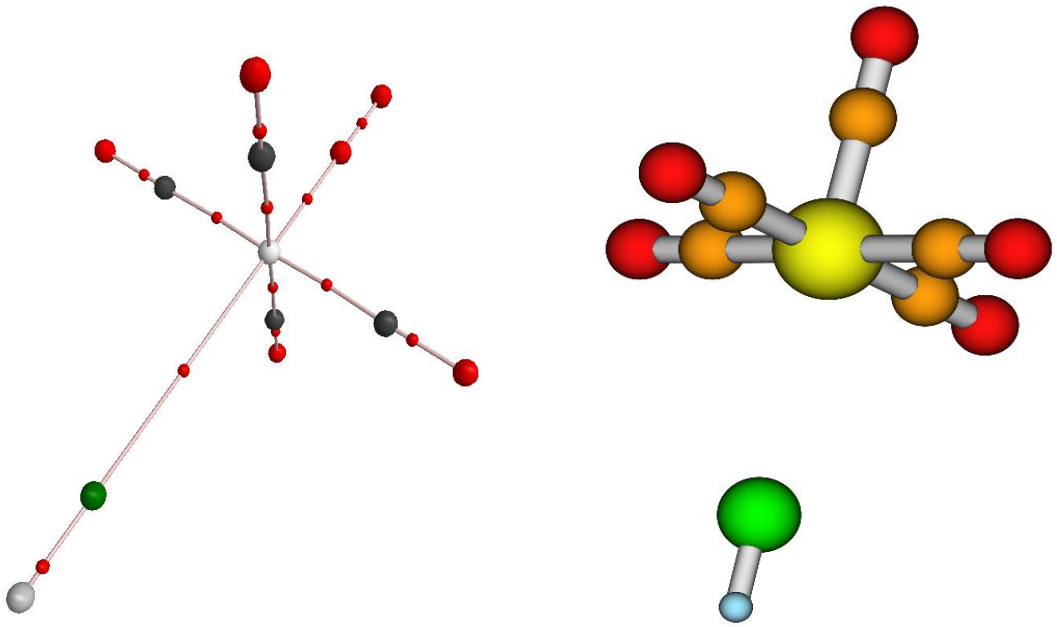

NBO analysis has been carried out to assay the influence of charge transfer on the stability of the complex. From the NBO analysis of $Fe(CO)_5$···ClF and $Fe(CO)_5$···ClH complexes at B3LYP/6-311G** level, the amount of charge transferred from $Fe(CO)_5$, ΔQ , is positive. This means, charge is transferred from the organometallic system to the chlorine bond donor. The amount of charge transferred from $Fe(CO)_5$ is 0.524e and 0.026e for $Fe(CO)_5$···ClF and $Fe(CO)_5$···ClH respectively. The ΔQ for $Fe(CO)_5$···ClH is comparable to that of for $Fe(CO)_5$···HX complexes, even though it is less compared to the latter. $Fe(CO)_5$···ClF shows a huge charge transfer from $Fe(CO)_5$ to the chlorine bond donor, which stabilizes the complex. Hence charge transfer is responsible for the dramatically high stability of $Fe(CO)_5$···ClF complex.

The difference in the stability between $Fe(CO)_5\cdots ClF$ and $Fe(CO)_5\cdots ClH$ is mainly due to the Cl bond donor. The high ΔE, ΔQ and ρ at the bond critical point between Fe and Cl in $Fe(CO)_5\cdots ClF$ complex can be explained on the basis of σ-hole concept[18]. The blue color denotes regions of strong positive potential and the red color denotes the regions of strong negative potential. The molecular electrostatic potential maps of ClF and ClH are shown in Figure. VI. 8. The positive potential around chlorine in ClF is much higher than that on chlorine in ClH, which is because of the higher electronegativity of F compared to that of H. Due to the presence of high positive potential on Cl in Cl-F, it interacts strongly with $Fe(CO)_5$. The higher charge transfer from $Fe(CO)_5$ to Cl-F is also obvious from the map. In $Fe(CO)_5\cdots ClF$, there is a huge depletion of negative potential at the oxygen atoms after complex formation. But in $Fe(CO)_5\cdots ClH$, even after complexation there is high negative potential around the oxygen atoms, since the charge transferred from $Fe(CO)_5$ to Cl-H is less.

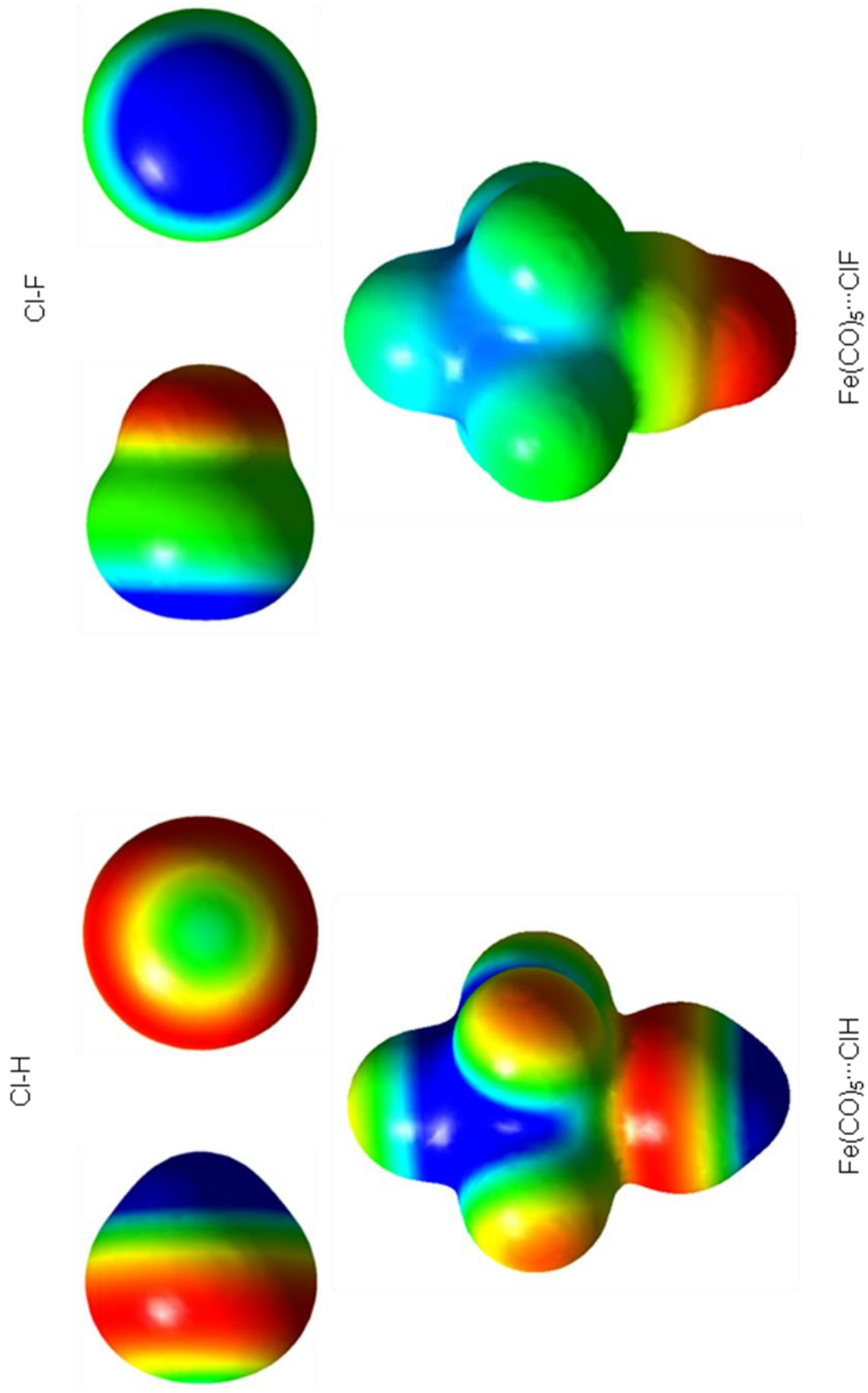

Figure. VI. 8: Molecular Electrostatic Potential of ClH, ClF, $Fe(CO)_5$···ClH and $Fe(CO)_5$···ClF at B3LYP/6-311G**

VI. 5. Hydrogen Bond Radius of Iron

From Table. VI. 4.1, Table. VI. 6 and Table. VI. 7, it is clear that the bonded radius of elements vary with the interacting partner. Hence it will not be appropriate to use the van der Waals radii for all interactions. In the books Hydrogen Bonding in Biological Structures[19] and The Weak Hydrogen Bond: In Structural Chemistry and Biology[20], the authors have talked about the inadequacy of van der Waals radii for identifying hydrogen bonding. In many cases, the non bonded radii are larger than the van der Waals radii. The radius of an atom for a particular interaction can be considered as the distance from the atom to the bond critical point, r_E. Raghavendra and Arunan[21] have calculated the hydrogen bond radii of various acceptors and donors using *ab initio* and AIM methods. From $Fe(CO)_5\cdots HX(X=F,Cl,Br)$ interactions, hydrogen bond radius of Fe can be defined. At B3LYP/Aug-cc-pVTZ, the distance of the hydrogen bond critical point from Fe for $Fe(CO)_5\cdots HF$, $Fe(CO)_5\cdots HCl$ and $Fe(CO)_5\cdots HBr$ are 1.5899, 1.6200 and 1.5851Å respectively. From the r_E obtained for different hydrogen bond donors the hydrogen bond radii of Fe is defined and is 1.60 (±0.02)Å. This may be compared with the van der Waals radius of Fe is 2.0Å and covalent radius of Fe is 1.27 Å.

VI. 6. Conclusions

Interaction of hydrogen halides, HX (X=F, Cl, Br), with the square pyramidal geometry of iron pentacarbonyl is studied. The hydrogen of HX interacts with Fe through the sixth co-ordination site. The stabilization energies of all the complexes show strong hydrogen bond interaction. The large red shift in H-X stretching frequency on complex formation supports this. QTAIM analysis of the complexes

show the presence of a bond critical point between the iron and the hydrogen of HX and hence bond formation. Moreover the numerical values of the electron density and Laplacian of the electron density at the hydrogen bond critical point confirms the bond formed between $Fe(CO)_5$ and HX to be a hydrogen bond. The complexes do not follow all the criteria proposed by Koch and Popelier for hydrogen bonding. In all the complexes Fe and H show mutual penetration and the criteria of decrease in the volume of H in the complex is followed. NBO analysis confirms charge transfer from the organometallic system to the hydrogen bond donor. The interaction energies are proportional to the dipole moment of the hydrogen bond donor and it is the dipole-induced dipole interaction which stabilizes the hydrogen bond than charge transfer. Choosing ClF and ClH as chlorine bond donors, the capability of Fe to act as chlorine bond acceptor is examined. Optimized geometries and the AIM analysis show that Fe can act as chlorine bond acceptor. The huge difference in the stabilization energy and charge transfer between $Fe(CO)_5\cdots$ClF and $Fe(CO)_5\cdots$ClH can be understood from the σ-hole concept. $Fe(CO)_5$ acts as a strong hydrogen and chlorine bond acceptor, even being a neutral compound. Hydrogen bonding and chlorine bonding can stabilize the square pyramidal geometry of iron pentacarbonyl. Hydrogen bond radius of Fe has been defined and is 1.60(±0.02)Å.

VI. 7.References:

1) D. S. Trifan, R. Bacskai, *J. Am. Chem. Soc.*, **1960**, *82*, 5010.

2) L. Brammer, D. Zhao, F. T. Ladipo, J. Braddock-Wilking; *Acta Cryst.,* **1995**. *B51*,632.

3) D. Braga, F. Grepioni, E. Tedesco, K.Biradha, G. R. Desiraju; *Organometallics,* **1997**, *16*,1846.

4) L. Brammer, *Dalton Trans.*, **2003** , 3145.

5) A. Martin, *J. Chem Ed.,* **1999**, *76*, 578.

6) E. S. Kryachko, A. Karpfen, F. Remacle, *J. Phys. Chem. A* **2005**, *109,* 7309.

7) D. Natale, J. C. Mareque-Rivas, *Chem. Commun*., **2008**, 425..

8) I. Alkorta, I. Rozas, J. Elguero, *J. Mol. Struct. (THEOCHEM)*, **2001**, *537* 139.

9) R. S. Berry, *J. Chem. Phys*., **1960**, *32*, 933.

10) G. Orlova, S. Scheiner, *Organometallics*, **1998**, *17*, 4362.

11) Y. Jiang; T. Lee; C. G. Rose-Petruck. *J. Phys. Chem. .A,* **2003**, *107*, 7524.

12) T. Lee , F. Benesch, Y. Jiang , C. G. Rose-Petruck, *Chem. Phys*., 2004, 299, 233.

13) M. J. Frisch, G. W. Trucks, H. B Schlegel, G. E. Scuseria, M. A.Robb, J. R.Cheeseman, J. A. Montgomery Jr., T. Vreven, K. N. Kudin, J. C. Burant, J. M. Millam, S. S. Iyengar, J. Tomasi, V. Barone, B. Mennucci, M. Cossi, G. Scalmani, N. Rega, G. A Petersson, H. Nakatsuji, M. Hada, M. Ehara, K. Toyota, R. Fukuda, J. Hasegawa, M. Ishida, T. Nakajima, Y. Honda, O. Kitao, H. Nakai, M. Klene, X. Li, J. E. Knox, H. P. Hratchian, J. B.Cross, C. Adamo, J. Jaramillo, R. Gomperts, R. E. Stratmann, O. Yazyev, A. J. Austin, R. Cammi, C. Pomelli, J. W. Ochterski, P. Y. Ayala, K. Morokuma, G. A. Voth, P. Salvador, J. J. Dannenberg, V. G. Zakrzewski, S. Dapprich, A. D. Daniels, M. C. Strain, O. Farkas, D. K. Malick, A. D. Rabuck, K. Raghavachari, J. B. Foresman, J. V. Ortiz, Q. Cui, A. G. Baboul, S. Clifford, J.

Cioslowski, B. B. Stefanov, G. Liu, A. Liashenko, P. Piskorz, I. Komaromi, R. L. Martin, D. J. Fox, T. M. Keith, A. Al-Laham, C. Y. Peng, A. Nanayakkara, M. Challacombe, P. M. W. Gill, B. Johnson, W. Chen, M. W. Wong, C. Gonzalez, J. A. Pople, *Gaussian03*, Revision C-02; Gaussian, Inc. Wallingford CT, **2004**

14) R. F. W Bader, *Atoms in Molecules: A Quantum Theory;*Clarendon Press: Oxford, **1990**.

15) F. Biegler-Konig, J. Schonbohm, R. Derdau, D. Bayles, R. F. W. Bader, *AIM 2000*, version 1; Bu¨ro fu¨r Innovative Software: Bielefeld, Germany, **2000**.

16) R. II. Dennington, T. Keith, J. Millam, K. Eppinnett, W. L. Hovell, R. Gilliland, *GaussView*, Version 3.09; Semichem, Inc.: Shawnee Mission, KS, **2003**.

17) U. Koch, P. L. A. Popelier, *J. Phys. Chem.,***1995**, *99*, 9747.

18) P. Politzer, P. Lane, M. C. Concha, Y. Ma, J. S. Murray, *J. Mol. Model.*, **2007**, *13*, 305.

19) G. A. Jeffrey, W. Saenger, *Hydrogen Bonding in Biological Structures*, Springer Verlag, Berlin, **1991.**

20) G. R. Desiraju, T. Steiner, *The Weak Hydrogen Bond: In Structural Chemistry and Biology*, Oxford University Press, Oxford, **1999**.

21) B. Raghavendra, P. K. Mandal, E. Arunan, *Phys. Chem. Chem. Phys*., **2006**, *8*, 5276.

Appendix:

Table. VI. 8: Geometric Parameters: Bond length (Å), Bond Angle (°) and Dihedral Angle (°)

i) Structure Of Monomers Optimized At Various Basis Sets:

Molecule		*B3LYP/ 6-311++G***	*B3LYP/ Aug-cc-pVDZ*	*B3LYP/ Aug-cc-pVTZ*
$Fe(CO)_5$	R(Fe-C)	1.8437	1.8434	1.8415
	R(C-O)	1.1414	1.1473	1.1394
	A(C-Fe-C)	90.00	90.00	90.00
	A(Fe-C-O)	180.00	180.00	180.00
	D(C-Fe-C-O)	90.00	90.00	90.00
HF	R(H-F)	0.9222	0.9257	0.9241
HCl	R(H-Cl)	1.2870	1.2950	1.2837
HBr	R(H-Br)	1.4266	1.4316	1.4239

Molecule		*B3LYP/ 6-311G***	*B3LYP/ 6-311++G***
Cl-H	R(Cl-H)	1.2871	1.2870
Cl-F	R(Cl-F)	1.6813	1.6789

ii) Structure Of $Fe(CO)_5$···HF Optimized At Various Basis Sets:

	*B3LYP/ 6-311++G***	*B3LYP/ Aug-cc-pVDZ*	*B3LYP/ Aug-cc-pVTZ*
R(Fe-C)	1.8437	1.8465	1.8437
R(C-O)	1.1413	1.1449	1.1413
R(Fe-H)	2.3804	2.3717	2.3908
R(H-F)	0.9419	0.9453	0.9434
A(C-Fe-C)	90.00	90.00	90.00
A(Fe-C-O)	180.00	180.00	180.00
A(C-Fe-H)	90.00	90.00	90.00
A(Fe-H-F)	180.00	179.998	180.00
D(C-Fe-C-O)	90.00	90.00	90.00
D(F-H-Fe-C)	90.00	90.00	90.00
D(F-H-Fe-C)	0.00	0.00	0.00

iii) Structure Of $Fe(CO)_5$···HCl Optimized At Various Basis Sets:

	*B3LYP/ 6-311++G***	*B3LYP/ Aug-cc-pVDZ*	*B3LYP/ Aug-cc-pVTZ*
R(Fe-C)	1.8437	1.8465	1.8447
R(C-O)	1.1413	1.1452	1.1375
R(Fe-H)	2.4539	2.4678	2.5009
R(H-Cl)	1.3184	1.3275	1.3131
A(C-Fe-C)	90.00	90.00	90.00
A(Fe-C-O)	180.00	180.00	180.00
A(C-Fe-H)	90.00	90.00	90.00
A(Fe-H-Cl)	180.00	180.00	180.00
D(C-Fe-C-O)	90.00	90.00	90.00
D(Cl-H-Fe-C)	90.00	90.00	90.00
D(Cl-H-Fe-C)	180.00	180.00	180.00

iv) Structure Of $Fe(CO)_5$···HBr Optimized At Various Basis Sets:

	*B3LYP/ 6-311++G***	*B3LYP/ Aug-cc-pVDZ*	*B3LYP/ Aug-cc-pVTZ*
R(Fe-C)	1.8437	1.8473	1.8437
R (C-O)	1.1413	1.1450	1.1413
R (Fe-H)	2.4211	2.3947	2.4685
R (H-Br)	1.4689	1.4784	1.4629
A(C-Fe-C)	90.00	90.00	90.00
A(Fe-C-O)	180.00	180.00	180.00
A(C-Fe-H)	90.00	90.00	90.00
A(Fe-H-Br)	180.00	180.00	180.00
D(C-Fe-C-O)	90.00	90.00	90.00
D(Br-H-Fe-C)	90.00	90.00	90.00
D(Br-H-Fe-C)	0.00	0.00	0.00

v) Structure Of $Fe(CO)_5$···ClH/F Optimized at Various Basis Sets:

	$Fe(CO)_5$···ClH		$Fe(CO)_5$···ClF	
	*B3LYP/ 6-311G***		*B3LYP/ 6-311G***	*B3LYP/ 6-311++G***
R(Fe-C)	1.8498	R(Fe-C)	1.8657	1.8437
R (C-O)	1.1343	R (C-O)	1.1334	1.1413
R (Fe-Cl)	3.7198	R (Fe-Cl)	2.5952	2.5300
R (Cl-H)	1.2902	R (Cl-F)	1.8882	1.9492
A(C-Fe-C)	90.00	A(C-Fe-C)	90.00	90.00
A(Fe-C-O)	180.00	A(Fe-C-O)	180.00	180.00
A(C-Fe-H)	90.00	A(C-Fe-H)	90.00	90.00
A(Fe-Cl-H)	180.00	A(Fe-Cl-F)	179.983	180.00
D(C-Fe-C-O)	90.00	D(C-Fe-C-O)	90.00	90.00
D(H-Cl-Fe-C)	90.00	D(F-Cl-Fe-C)	90.00	90.00
D(H-Cl-Fe-C)	0.00	D(F-Cl-Fe-C)	0.00	0.00

Table. VI. 9: Rotational constants (MHz)

Comples	Rotational Constants	6-311++G**	Aug-cc-pVDZ	Aug-cc-pVTZ
$Fe(CO)_5$●●●HF	A	689.24	686.47	689.24
	B	660.40	659.11	659.06
	C	660.40	659.11	659.06
$Fe(CO)_5$●●●HCl	A	689.24	686.40	690.11
	B	487.98	484.21	483.43
	C	487.98	484.21	483.43
$Fe(CO)_5$●●●HBr	A	689.24	686.01	689.24
	B	327.75	328.87	323.55
	C	327.75	328.87	323.55

Table. VI. 10: Normal mode vibrational frequencies (cm^{-1})

a) Monomers

	*B3LYP/ 6-311++G***	*B3LYP/ Aug-cc-pVDZ*	*B3LYP/ Aug-cc-pVTZ*
$Fe(CO)_5$	8.44	17.96	6.20
	85.04	83.75	83.99
	85.04	83.75	83.99
	96.60	94.25	95.41
	103.87	102.30	102.35
	104.11	102.30	103.52
	104.11	102.65	103.52
	295.10	293.52	302.50
	295.10	293.52	302.50
	322.74	321.72	327.85
	357.40	354.89	361.23
	387.52	391.33	389.80
	406.28	410.85	408.29
	414.12	416.28	416.30
	423.66	426.71	427.58
	423.66	426.71	427.58
	509.73	505.14	511.30
	509.73	505.14	511.30
	540.32	537.33	543.07
	618.67	619.67	624.55
	618.67	619.67	624.55

	653.88	651.20	656.59
	2075.88	2057.37	2076.36
	2075.88	2057.37	2076.36
	2078.92	2061.01	2079.10
	2081.86	2063.95	2082.88
	2166.60	2146.74	2165.21
HF	4096.00	4059.94	4070.20
HCl	2925.88	2912.58	2935.03
HBr	2598.64	2599.40	2624.57

	*B3LYP/ 6-311G***	*B3LYP/ 6-311++G***
ClH	2927.33	2925.88
ClF	734.90	739.62

b) $Fe(CO)_5$···HF

*B3LYP/6-311++G***	*B3LYP/Aug-cc-pVDZ*	*B3LYP/Aug-cc-pVTZ*
27.68	25.50	28.86
27.68	25.50	28.86
33.23	30.13	36.92
93.02	84.32	97.50
93.02	84.32	97.50
104.20	95.79	102.72
105.21	97.03	109.51
115.75	103.53	122.14
115.76	103.53	122.14
137.78	133.84	138.03
330.07	315.68	343.85
330.07	315.68	343.85
360.46	348.50	371.61
371.43	357.41	384.06
390.73	390.62	389.92
412.19	411.60	411.99
421.40	418.90	422.10
427.85	425.05	430.91
427.85	425.05	430.91
495.90	509.52	507.52
495.90	509.52	507.52
526.70	515.82	530.34
526.71	515.82	530.34
554.39	544.67	560.38
629.06	625.61	635.56

629.06	625.61	635.56
656.68	647.79	660.77
2078.28	2075.42	2063.02
2078.28	2075.42	2063.02
2081.42	2078.54	2066.42
2085.78	2083.40	2071.05
2163.85	2158.91	2417.30
3638.42	3585.22	3618.15

c) $Fe(CO)_5$···HCl

*B3LYP/6-311++G***	*B3LYP/Aug-cc-pVDZ*	*B3LYP/Aug-cc-pVTZ*
21.24	17.82	16.51
21.24	17.82	16.51
33.92	30.62	28.26
75.14	68.19	66.82
91.89	84.14	84.72
91.89	84.14	84.72
103.93	95.25	96.60
114.16	103.25	103.77
114.16	103.25	103.77
120.65	110.85	110.41
320.59	308.31	314.70
320.59	308.31	314.70
356.57	344.52	349.39
369.11	356.44	362.72
389.74	389.77	387.77

410.31	409.73	407.56
418.58	416.64	411.11
423.33	418.06	411.11
423.33	418.06	416.63
448.20	442.38	435.60
448.20	442.39	435.60
522.39	511.40	515.77
522.39	511.40	515.77
551.85	542.79	546.77
625.77	621.77	625.56
625.77	621.77	625.56
654.20	645.73	651.70
2077.57	2072.62	2090.47
2077.57	2072.62	2090.47
2081.09	2076.08	2094.18
2084.96	2080.53	2098.20
2158.67	2151.36	2170.20
2486.36	2468.43	2514.02

d) $Fe(CO)_5$···HBr

*B3LYP/6-311++G***	*B3LYP/Aug-cc-pVDZ*	*B3LYP/Aug-cc-pVTZ*
16.31	15.20	22.61
16.31	15.20	22.61
35.67	35.00	38.69
53.79	52.07	48.30

92.02	84.53	96.49
92.02	84.53	96.49
103.95	95.42	108.26
114.13	102.82	120.60
114.13	102.82	120.60
118.71	109.02	124.20
317.46	306.01	330.89
317.46	306.01	330.89
358.17	347.52	368.40
369.01	356.33	381.13
389.17	388.08	388.41
409.69	408.38	405.91
417.80	415.00	405.91
419.54	423.14	409.50
419.54	423.15	417.83
439.89	459.67	437.53
439.89	459.67	437.53
512.66	510.67	525.80
512.66	510.67	525.80
550.94	542.21	557.09
625.49	621.25	631.41
625.49	621.25	631.41
652.31	642.85	657.05
2054.79	2027.40	2062.06
2077.36	2073.43	2062.06
2077.36	2073.43	2065.51

2081.46	2077.43	2070.06
2084.85	2081.44	2088.26
2180.75	2173.46	2176.10

e) $Fe(CO)_5\cdots ClX(X=H,F)$

$Fe(CO)_5\cdots ClH$	***$Fe(CO)_5\cdots ClF$***	
B3LYP/6-311G**	B3LYP/6-311G**	B3LYP/6-311++G**
17.45	37.15	40.51
17.47	37.15	40.51
24.35	51.10	55.59
47.14	81.86	81.25
84.69	81.87	81.25
84.69	100.69	99.32
98.83	100.94	102.44
104.35	102.00	102.44
104.35	102.00	104.31
106.48	145.56	135.66
223.53	145.56	135.67
223.99	165.94	182.25
281.02	320.28	335.05
281.02	320.28	335.05
320.49	352.79	335.38
356.31	368.45	353.02
404.31	387.33	378.63
409.88	396.00	388.40

426.55	418.72	392.50
431.30	418.72	404.62
431.30	419.96	404.63
507.62	427.61	426.63
507.62	507.89	511.75
539.86	507.90	511.76
628.58	541.98	540.84
628.58	615.32	603.89
653.82	615.32	603.89
2087.97	635.53	629.76
2087.97	2136.57	2137.02
2088.13	2136.57	2137.02
2094.52	2138.02	2139.20
2175.04	2146.25	2147.14
2886.44	2203.96	2202.28

CHAPTER VII

Conclusions and Future Directions

VII. 1. Conclusions:

Pulsed Nozzle Fourier Transform Microwave Spectrometer and various theoretical methods such as *ab initio*, Density Functional Theory, Atoms In Molecules Theory and Natural Bond Orbital analysis are used to study the structure and dynamics and to characterize non-conventional hydrogen bonds.

The first system studied is the complex formed between CH_4 and H_2S. Both rotational spectroscopy as well as theoretical methods such as *ab initio*, Atoms In Molecules and Natural Bond Orbital analysis are employed to investigate the nature of interaction. Ab initio calculations are done at MP2(full) level and basis sets used are 6-311++G**, Aug-cc-pVDZ and Aug-cc-pVTZ. The rotational transitions belonging to three progressions could be obtained using the microwave spectrometer. The progressions were independently fitted to a linear top Hamiltonian. Absence of $J_{1\leftarrow 0}$ transition in Progression II confirms the presence of higher internal angular momentum state, m=1. This also confirms the internal rotation of the monomers in the complex. Progressions II and III have negative centrifugal distortion constants. Hence both the states are from some excited internal rotation/torsional motion with strong vibrational-rotational coupling. Only Progression I corresponds to transitions from ground state of the complex and hence the rotational constant obtained from this progression is the ground state rotational constant of CH_4-H_2S complex. The moments of inertia obtained from the experimental rotational constant confirm the structure in which sulphur of H_2S is close to CH_4. This also supports the structure in which CH_4 is the hydrogen bond donor, if such an interaction is present. Ab initio calculations show the presence of three minimum energy structures, 1) CH_4 as the hydrogen bond donor, 2) H_2S as the hydrogen bond donor and 3) van der Waals

complex. Comparison of the potential energy surface obtained for the various possible internal rotations of the monomers in the first two cases with the zero point energy along the torsional mode which can break the hydrogen bond interaction shows the orientational preference. The zero point energy is less than the barrier for internal rotation. AIM analysis also supports the presence of hydrogen bonding in this complex. The *ab initio* results show that CH_4•••HSH interaction is more favorable than CH_3H•••SH_2. *Ab initio* and AIM studies also gave a structure where there is direct interaction between C and S. This is interesting since the electronegativities of C and S are comparable. Experimentally obtained negative distortion constants for the other two states, confirm excited state rotational-vibrational coupling. The experimental data give a floppy structure having internal rotation.

The next complex chosen for investigation is benzene-ethylene. Experiments in condensed phase and theoretical works show evidence of π-stacking in benzene dimer, but there is no gas phase spectroscopic evidence available for the same. The lack of permanent dipole moment in the π-stacked geometry of benzene dimer is the hindrance in the experimental observation of the same using microwave spectroscopy. Substitution of one of the benzene with ethylene in the π-stacked structure will result in a complex having permanent dipole moment and can be studied using rotational spectroscopy. C_6H_6••• C_2H_4 complex can have, in addition to π-stacking, C-H/π interaction where there can be a competition between C_6H_6 and C_2H_4 about which of the two moieties will act as H-bond donor. *Ab initio* calculations at MP2 (full) level of theory using basis sets 6-311G** and 6-311++G** supports the existence of π-stacked structure. It also supports the formation of complexes CH-π complexes where C_2H_4 is the hydrogen bond donor and C_6H_6 the acceptor and the case in which C_6H_6 is

the hydrogen bond donor and C_2H_4 the acceptor. Experiments show the evidence of C-H/π interaction, where C_2H_4 is the hydrogen bond donor. To ascertain hydrogen bond interaction AIM analysis has been carried out. The results show C-H/π interaction, where one of the C_2H_4 hydrogen interacts with the benzene. Even though the aim was to get the π-stacked geometry, it could not be obtained. However theory and AIM supports the formation of π-stacked complex.

The ability of radicals as acceptor of H, Li and Cl bond is examined in the next chapter with CF_3 radical as the model system. H-Y(Y=F, Cl, Br, CN), Li-Y(Y=F, Cl, Br) and Cl-F are used as the H, Li and Cl bond donors respectively. As hydrogen bonds are highly sensitive to the environment, the effect of substitution of hydrogen by fluorine is also analyzed. Geometry optimizations are done at MP2(full) level. Both Pople (6-311G** and 6-311++G**) and Dunning (Aug-cc-pVDZ and Aug-cc-pVTZ) basis sets are used. *Ab initio* calculations support hydrogen bond formation between CF_3 radical and H-Y. AIM analysis of CF_3●●●HY satisfies all the eight criteria proposed by Koch and Popelier for hydrogen bonding. Here the hydrogen bond formed is charge transfer assisted. The interaction energies of the complexes are inversely proportional to the dipole moment of the hydrogen bond donors and are proportional to the charge transfer occurring in the complex. Interaction energies from *ab initio* calculations confirm complexation of CF_3 radical with LiX and ClF. AIM analysis of CF_3●●●LiY and CF_3●●●ClF complexes show a bond critical point between Li/Cl and the C of CF_3 and the condition of mutual penetration is also met. In CF_3●●●LiY complexes the interaction energies and charge transferred are directly proportional to the dipole moment of the Li bond donor. CF_3●●●LiY complexes are electrostatic in nature, evident from the higher value of slope obtained for the plot of

interaction energy as a function of electron density at the bond critical point. Even though CH_3 and CF_3 radicals are topologically different, they interact in a similar fashion.

In the last chapter in order to extend the concept of non conventional hydrogen bond acceptors to transition metals, complexes of Fe ($Fe(CO)_5$) with HX (X=F,Cl,Br) have been studied. DFT calculations show that the structure in which the hydrogen of HX interacting with Fe through the sixth co-ordination site is a stable geometry. AIM analysis shows the presence of a bond critical point between the iron and the hydrogen of HX and hence bond formation. ΔQ obtained from NBO analysis shows that there is charge transfer from the organometallic system to the hydrogen bond donor. However the interaction energies of the complexes are proportional to the dipole moment of the hydrogen bond donors and are inversely proportional to the charge transfer for these complexes. H-bonding leads to the stabilization of square pyramidal geometry. 'Hydrogen bond radius' of iron has also been defined. Studies on the interaction of $Fe(CO)_5$ with ClF and ClH showed that Fe can also act as a chlorine bond acceptor.

VII. 2. Future Directions

Scopes in further carrying out the research in this area are immense. We are planning to fabricate Broad Band Fourier Transform Microwave Spectrometer in our lab. This will help in solving the structure and dynamics of various complexes in a shorter duraction. By incorporating a stark cage to the present set up, the dipole moment of the complexes can also be obtained.

Three progressions were obtained for the CH_4- H_2S complex. Microwave studies on CH_4- H_2O complex showed the presence of ten progressions. Similarly there can be many more states present in the CH_4- H_2S complex too. Since a large region can be scanned at a time using Broad Band Fourier Transform Microwave Spectrometer, it can help in obtaining transitions which were not observed in the current work, if present.

Experiments on Ar-H_2O-H_2S trimer were carried out. The preliminary data obtained confirms the formation of the trimer. The splitting of some of the observed transitions indicates the presence of interesting dynamics. The transitions observed till now could not be assigned to one structure. Carrying out the research further for this trimer will help in solving the structure of the Ar-H_2O-H_2S trimer and also will help in understanding the dynamics.

Theoretical confirmation of the ability of $Fe(CO)_5$ to form hydrogen bond complex was discussed in the Chapter VI. To verify it experimentally, we had tried to obtain the rotational spectrum of $Fe(CO)_5$-H_2O. But the vapour pressure was not sufficient to carry $Fe(CO)_5$ from the sample holder to the vacuum chamber since the path length was too long. This problem can be solved by introducing the sample holder just after the nozzle. A similar situation was encountered when Bromobenzonitrile was studied, which is a solid. This is a very interesting system to study since it will give hyperfine spectra due to quadrupole splitting. The vapours of the samples were produced by slightly heating the sample. Here also the vapour pressure was not sufficient to carry bromobenzonitrile into the cavity. Modified sample holder can help in solving the structure of the monomer.

In Chapter V CF_3 radical as acceptor of H, Li and Cl was studied using theoretical methods. If CF_3 radicals can be produced, then hydrogen bonding in CF_3●●●HY complexes can be studied by rotational spectroscopy. CF_3 radicals can be produced from CF_3I by using a discharge nozzle or a heated nozzle. Hence by introducing a discharge or heated nozzle or by modifying the setup by integrating a laser source for producing CF_3 radical, complexes of CF_3 radical or any such radicals can be studied by microwave spectroscopic technique.